Thermal and Hydraulic Performance of Compact Brazed Plate Heat Exchangers Operating as Evaporators in Domestic Heat Pumps

JOACHIM CLAESSON

KTH Energy Technology

Doctoral Thesis
Stockholm, Sweden 2004

KTH Energy Technology

Thermal and Hydraulic Performance of Compact Brazed Plate Heat Exchangers Operating as Evaporators in Domestic Heat Pumps

Doctoral Thesis

by

Joachim Claesson

Division of Applied Thermodynamics
and Refrigeration
Department of Energy Technology
Royal Institute of Technology, KTH

TRITA REFR Report No 04/44
ISSN 1102-0245
ISRN KTH/REFR/04/44-SE
ISBN 91-7283-931-7

ABSTRACT

This thesis investigates the performance of compact brazed plate heat exchangers (CBE) operating as evaporator in heat pump applications. The thesis, and the performances investigated, has been divided into three main sections; One zone evaporator performance; Two zone evaporator performance; and finally Local performance.

The 'One zone evaporator performance' section considers the evaporator as one "black box". It was found that "approaching terminal temperatures" were obtained as low overall heat flux is employed. It was also found that the total area averaged film heat transfer coefficient was affected by changes of the brine mass flow rate. This indicates that the widespread Wilson plot method may not be used to determine flow boiling heat transfer coefficients. Further, it seems that co- and counter-current flow configuration performs equally well if the superheat is kept low. A numerical simulation of the above investigations indicates that a nucleate boiling model better predicts the performance compared to a convective evaporation model. Finally, the significant impact of the refrigerant inlet distributor design was illustrated using several CBEs with different inlet geometries but with identical heat transfer surfaces.

The 'Two zone evaporator performance section' considers the evaporator as two "black boxes", i.e. the boiling and superheating boxes. Thermochromic liquid crystals (TLC) was used to determine the boiling heat transfer area. The resulting flow boiling heat transfer coefficient was found to correlate with heat flux. The superheated heat transfer area was then estimated using single phase correlations. It was observed that the TLC measurements and the predicted superheating area did not agree. Possible causes for this deviation were discussed. The most likely explanation found was the presence of mist flow at the higher vapor quality range in the boiling section of the evaporator.

The 'Local Performance' section considers local pressure drop and flow boiling heat transfer. The Chisholm parameter was found not to be a constant and was found to correlate well with the kinetic energy per volume. The resulting predictions of the pressure drop were better than ± 10%.

The resulting local flow boiling heat transfer coefficient, at different vapor quality, mass flux and heat flux, was compared to flow boiling correlations available in the literature. It was found that the saturated nucleate pool boiling correlation by Cooper (1984) and narrow channel flow boiling correlations (Tran 1999, Lazarek and Black 1982) predicted the experimental data better than several traditional flow boiling correlations, developed for larger tubes.

Keywords: Plate heat exchanger, Evaporator, Heat pump, Flow boiling, Pressure drop

ACKNOWLEDGEMENT

I wish to thank all people who, in any way, have assisted me during the course of my Ph.D. studies. First of all, I would like to take the opportunity to sincerely thank my supervisor, Dr. Björn Palm, for his enormous patience with all my questions, wild ideas, reading thru half ready manuscript, etc. Your door is always open and you always take the time, even though time is short.

I would also like to thank my office-mate, Dr. Rahmatollah Khodabandeh, for, among other things, his patience with loud music disturbing him in his work.

Further, I wish to say thanks to Erik Björk, with whom I had many long discussions regarding all aspects of heat exchangers, two-phase flows and boiling, and not least domestic refrigerators!

Dr. Hans Jonsson (Dr. Flänsis) for sharing the same kind of music (partly) and to introduce me into the world of research at the department and always being able to answer questions regarding teaching and thermodynamics.

Peter, Martin, Jaime, Carina, Anders (Dr. Freon) and Fredrik (Dr. Flum) for all lunches and all nonsense discussions during eating.

Benny S, Benny A, Bosse and Jim for all the help in the workshop. Inga DuRietz for keeping us all in order, keep up the good work. Eric Granryd for the never ending base of knowledge and for employing me for this Ph.D. – project.

Klas Andersson and Jan-Erik Nowacki, for sharing the fun of discussing all crazy ideas, since no idea is crazy enough in your minds.

All other employees at the refrigeration department, for allowing me to walk around the lab and just being a pain in the ass with all my opinions.

Olivier Pelletier, SWEP International AB and Thermia Värme AB for financial support, ideas, discussions and for sharing non-public information with me, it saved me some extra years! Energimyndigheten (STEM) for financial support.

My parents, Hans and Gunilla, for all your support, love and believing in me during all these years.

To my beloved wife Åsa for all her love, patience with my lack of knowledge in housekeeping and who has sacrificed a lot in order for me to finalize this thesis.

Finally, all my love goes out to the person dearest to me, my daughter Moa.

PREFACE

As a young child, my interest was focusing on playing soccer and ice-hockey. School and studying was not for me, I was going professional as a soccer player and as a goal keeper in ice hockey. In the worst case, I would have settled as a professional in only one of the sports.

However, as time and hair went by, apparently no money was coming in from any sport clubs. At that time, I had the opportunity to move Lund and study Mechanical Engineering at Lunds Institute of Technology. At that time the main goal was to see were my capabilities in "advanced" studies would be insufficient. Lund had an ice hockey team in the lowest division, which indeed had use for a goalkeeper. However, as time is always running to fast, I had to choose; studying and try to make an income as a Mechanical Engineer or to make no money as a goalkeeper in the lowest division. What would you have chosen?

Well, I choose the other option, quit playing hockey.

In my final year of the studies at LTH my main interest was heat transfer and in particular numerical heat transfer (CFD). For the Master of Science thesis work I had the opportunity to numerically investigate single phase heat transfer and fluid flow in a unitary cell of a plate heat exchanger. After finalizing the master of science thesis, I started working at a company selling air handling systems for paper manufacturing machines. At that company we used software to size the heat exchangers. No time was available to fully understand the long forgotten software used.

I wanted to know more, and had still not found out were my skills in advanced studies ended. So, I had the opportunity to start a Ph.D. project at KTH, concerning boiling of refrigerant in plate heat exchangers.

Now, too long time has passed, but here it his, my thesis submitted for a Ph.D. degree, concerning boiling of refrigerants in plate heat exchangers.

PUBLICATIONS

The present thesis is based on several previously published articles. These are:

Journal Papers (Reviewed):

Claesson J., 2004a, The influence of brine flow on the flow boiling refrigerant heat transfer coefficient in a compact brazed plate heat exchanger, Accepted for publication in International Journal of Heat Exchangers.

Claesson J., 2004b, Correction of logarithmic mean temperature difference in compact brazed plate heat evaporator with heat flux governed flow boiling heat transfer coefficient, Accepted for publication in International Journal of Refrigeration, doi:10.1016/j.ijrefrig.2004.09.011.

Claesson J., 2004c, Theoretical study of a compact brazed plate heat exchanger operating as evaporator, Submitted for publication in the International Journal of Refrigeration.

Conference papers (Peer Reviewed):

Claesson J., Palm B., 1999, Boiling mechanism in a small compact brazed plate heat exchanger (CBE) determined by using thermochromic liquid crystals (TLC), 20th Int. Congr. of Refrigeration, IIR/IIF, Sydney, 1999, paper 117.

Claesson J., Forsén M., 2002, Capacity control of a domestic heat pump Part 1 – Performance of the heat pump and its components, IIR/IIF Zero Leakage – Minimum Charge, Efficient Systems for Refrigeration, Air Conditioning and Heat Pumps, August 26-28, Stockholm, Sweden, ISBN 2-913149-28-6, ISSN 0151-1637, paper M1.

Claesson J., Palm B., 2002, Discrepancy between calculated and measured superheated area in an evaporator plate heat exchanger, HEFAT 2002, 1st Int. Conf. on Heat Transfer, Fluid Mechanics and Thermodynamics, 8-12 April, Kruger Park, South Africa, vol. 1, pt. 2, pp. 1079-1086.

Claesson J., Afghani M., Palm B., 2003, Influence of large temperature difference in a compact brazed plate evaporator with low overall heat flux, in Proc. Eurotherm no. 72: Thermodynamics, Heat and Mass Transfer of Refrigeration machines and heat pumps, eds. J.M. Corberán, R. Royo, Valencia, Spain, March 31 – April 2, pp. 33-37.

Claesson J., Simanic B., 2003, Pressure drop and visualization of adiabatic R134a two-phase flow inside a chevron type plate heat exchanger, 21st Int. Congr. of Refrigeration, IIR/IIF, Washington D.C., USA, paper 314.

Claesson J., 2005, Thermal and hydraulic characteristics of brazed plate heat exchangers – Part I: Review of single- and two-phase adiabatic and flow boiling characteristics, Accepted for presentation and publication at the ASHRAE Winter Meeting, Orlando, Fl., USA, Feb. 5 – 10, 2005.

Claesson J., 2005, Thermal and hydraulic characteristics of brazed plate heat exchangers – Part II: Current research on evaporators at KTH, Accepted for presentation and publication at the ASHRAE Winter Meeting, Orlando, Fl., USA, Feb. 5 – 10, 2005.

Conference papers (Others):

Claesson J., Palm B., Pelletier O., 2001, On the influence of geometry on evaporation in compact brazed plate heat exchangers, ICMF-2001 4th International Conference on Multiphase Flow, E.E. Michaelides ed., May 27 to June 1, 2001, New Orleans, Louisiana, USA, paper 156.

Claesson J., Palm B., 2003, Performance of a compact brazed plate heat exchanger evaporator run in co-current and counter-current, in Proceeding 5th International Conference on Boiling Heat Transfer, Montego Bay, Jamaica, May 5 – May 8, Session VIII: Heat Transfer and Heater Characteristics, third paper.

CONTENTS

PART I

INTRODUCTION

This section of the thesis introduces the application of interest and the plate heat exchanger, defining the geometry at hand. The necessary correlations needed in the subsequent analysis is establish and finally some of the earlier published work found in the open literature is reviewed.

1 OBJECTIVE AND LIMITATIONS

The purpose of the present thesis is to investigate the evaporator, one of the heat exchangers, under conditions similar to those in domestic heat pumps. Even though several types of evaporators are available, this thesis limits itself to investigate the compact brazed plate heat exchanger operating as dry expansion (DX) evaporator. As such, the refrigerant has been in its superheated state upon leaving the evaporator.

The fluids tested have been limited to R134a and R22. In addition, the focus of the investigation has been of typical operating parameters for an ordinary commercial heat pump. Thus, the sizes of the evaporators have been chosen accordingly.

The brine side of the evaporator has not been investigated. Single phase heat transfer correlations have been obtained from the manufacturer. These correlations have been used "as is" in the present thesis. Water or water mixed with approximately 20% (by mass) ethanol has been used as brine fluid. The thermophysical properties of the brine have been evaluated using the equations from Melinder (1997) and for water the IAPWS-IF97 correlations (Wagner and Kruse 1998).

No information of the circulated amount of oil in the system has been available. Oil separators were present in the systems during the experiments. Oil separators are unfortunately not perfect, and an oil concentration less than 1 % may be expected in the circulating refrigerant. Still, all thermophysical properties of the refrigerant/oil mixture in the evaporator have been assumed equal to that of the pure refrigerant. The properties have been evaluated in MS Excel with the Refprop 6.01 code (NIST 1998), using an in-house developed xla-file.

The objective of the present thesis has been to determine and evaluate the performance of plate heat exchanger, operating as evaporator in domestic heat pump. The performances of the evaporator have been investigated using several different approaches, e.g. Black box of entire evaporator; Black box of two sections in the evaporator, boiling and superheated sections; and finally Local performance in the boiling section.

2 METHOD

In the present thesis, the performances of compact brazed plate heat exchangers are investigated. The investigations are both experimental and numerical, however, the focus is on the experimental part.

The purposes of the numerical parts are mainly to compare trends with experimental observations.

The accuracy of experimental data may always be debated. In this thesis, the experiments are conducted according classical experimental methods, i.e. measurements are conducted under “steady state”, using at least 100 readings for each measured point. This ensures a good estimation of the standard deviations of each measurement. The scan rate of the different experiments is different. For most of the experiments, the measurements are conducted for 20 minutes of more, with one exception, the TLC-measurements using 10 minutes.

Each point of the measurement is checked for steady state and the standard deviation should be sufficient small. If these requirements are fulfilled, the measurement is accepted as a measured “point”.

3 MOTIVATION

Small heat pumps increase their market share for heating one family houses. Heat pumps make use of the heat in the surroundings, i.e. air, water or ground. To be able to upgrade the low temperature heat in the surrounding to a higher temperature, which can be utilized to heat the house, the heat pump uses approximately 1/3 (of the total delivered energy) of compressor work. In these kinds of appliances, the compressor is usually electrically driven.

Many of the ground source heat pumps for domestic use in Sweden have compact brazed plate heat exchanger as evaporators and condensers. In many cases the evaporator and the condenser are of the same model and size.

In Sweden, there are approximately 1 500 000 single family houses exist (SCB, 2003). 566 000 of these had direct electrical heating or electrical heating distributed by water. 51 000[i] single family houses used heat pump utilizing heat from rock, ground or lake (SCB, 2003).

A rough estimate of decrease of energy consumption for compressor work in a heat pump is 2 %/K increase of evaporation temperature. The electrical energy consumption used for ground/rock/sea heat pumps reported by the Statistics Sweden (SCB, 2003) are 933 GWhr. Increasing the evaporation temperature (by increasing the efficiency of the evaporator) with, lets say, 1 K would save 18.7 GWhr, and assuming an electricity cost of 0.7 SEK/kWhr, would result in a saving in running costs of 13 100 000 SEK/year or 1 633 000 $US/year (assuming 8 SEK/$US).

The total usage of energy for direct electrical heating is approximately 24 000 GWhr. If all of these converted to heat pumps, the energy saving would be 12 800 GWhr, assuming 20 % of the present electrical usage still is required as supplementary heating for the coldest days. Again, assume an energy price of 0.7 SEK/kWhr, this alone corresponds to a capital saving of 8 938 000 000 SEK/year or 1 117 000 000 $US/year. Increasing the efficiency of the evaporator by 1 °C would further decrease the energy usage with 223 GWhr, corresponding to 156 400 000 SEK/year or 19 500 000 $US/year.

The discussion above applies for domestic heat pumps in Sweden. If also the refrigeration applications were included, the annual saving would increase considerably.

---

[i] However, according to statistics from SVEP (Forsén, 2004) the annual sale of ground source heat pumps are approximately 30 000 to 40 000. The official Swedish statistics from SCB (2003) seems to be rather low.

As may be seen, there is a large potential for energy saving, first of all converting direct electrically heated houses to heat pump, then also to increase the efficiency of the evaporator.

The present thesis has been a part of a larger government funded research program aiming at development of more efficient heat pump and refrigerating systems. The specific topic in the present thesis has been to investigate the compact brazed plate heat exchanger (CBE) from a heat pump system point of view, identifying the typical performance of CBE, determining performance of CBE with slightly different geometry and inlet distributors. In addition, investigations of refrigerant side heat transfer coefficients have been undertaken, based on total heat transfer area, boiling heat transfer area, and local heat transfer coefficients.

4 OVERVIEW OF THESIS

The compact brazed plate heat exchanger (CBE) has emerged as the preferred choice as evaporators and condensers in ground source domestic heat pumps on the Swedish market. This thesis investigates the performance of CBE operating as evaporator in heat pump applications. The thesis, and the performance investigated, has been divided into three main sections; One zone evaporator performance; Two zone evaporator performance; and finally Local performances. The three sections investigate the evaporator with increasingly refinement.

4.1 One zone heat exchanger

The purpose of this section is to investigate the evaporator from a heat pump perspective, considering the evaporator as one “black box”.

In order to obtain higher heat pump efficiency, the heat pump manufacturers select larger evaporator, decreasing the overall heat flux. Hence, the performance of low overall heat flux was investigated. It was found that in order to obtain efficient heat transfer, the brine mass flow rate and the heat exchanger size should be selected with care. For a given heat duty and superheat setting of the expansion device, the brine flow rate and heat exchanger size should be selected to meet the point indicated in Figure 19.

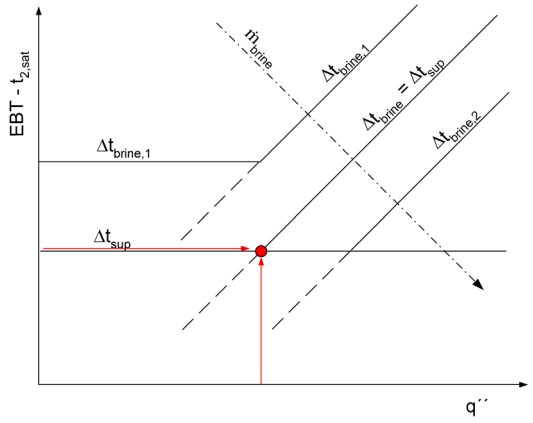

Figure 19: Schematic temperature lines as measured.

It was found that the brine mass flow rate affects the refrigerant side heat transfer coefficient. Thus, two separate investigations were conducted to establish the influence and to investigate whether co-current could be more efficient than counter-current. Surprisingly enough, no significant difference between the co- and counter-current cases could be established, see Figure 26.

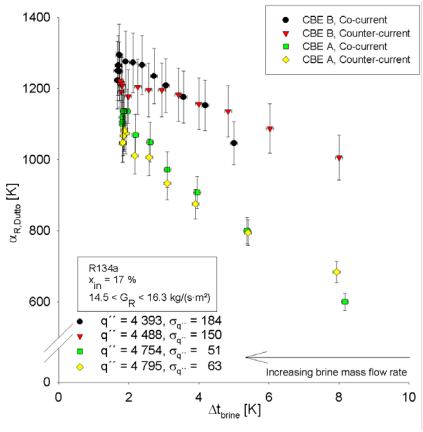

Figure 26: Refrigerant average heat transfer coefficient for different brine flows and configurations.

The performance of the evaporator was simulated, using two significantly different boiling models, and only marginal differences were found; except for the two investigated flow configurations. For the nucleate boiling model the performance did not change between co- and counter-current, which is in agreement with experimental results. However, the convective evaporation model predicted an opposite trend compared to the experimentally observed for the co-current case. This indicates that the nucleate boiling model better predicted the performance of the plate heat evaporator.

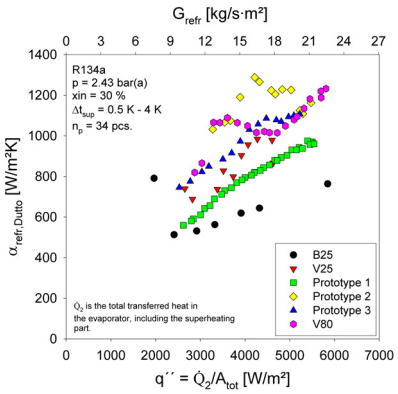

Figure 42: Total area averaged heat transfer coefficient at –5°C evaporation and 30 % inlet vapor quality for five identical heat exchangers (B25 to Prototype 3) with different distributor designs. V80 has a slightly different plate pattern. The wavy patterns of some of the heat exchangers have been verified in several tests.

Finally, the impact of different inlet refrigerant flow distributor designs on the evaporator performance was investigated. As the two-phase mixture should distribute evenly, both the gas and the liquid, among several parallel flow channels, inlet flow geometry may be expected to affect the overall performance. Indeed, the impact is significant. Rather different performances were observed for plate heat exchangers having identical heat transfer surface but with different inlet flow geometry, as seen in Figure 42.

4.2 Two zone heat exchanger

In this section of the thesis, the evaporator is considered as two "black boxes", one boiling "black box" and one superheating "black box". Thus, the respective heat transfer areas are needed. Two approaches have been used; Measuring the boiling heat transfer area and Estimating the superheating heat transfer area.

The first approach utilized Thermochromic Liquid Crystals (TLC, temperature sensitive paint) to determine the boiling heat transfer area. The resulting boiling area averaged flow boiling heat transfer coefficient could thus be determined. It was found that the boiling area averaged flow boiling coefficient well correlated with the boiling area based heat flux, see Figure 51. Thus, simply by adjusting the leading constant in the Cooper (1984) pool boiling to 1.5, good agreement was obtained.

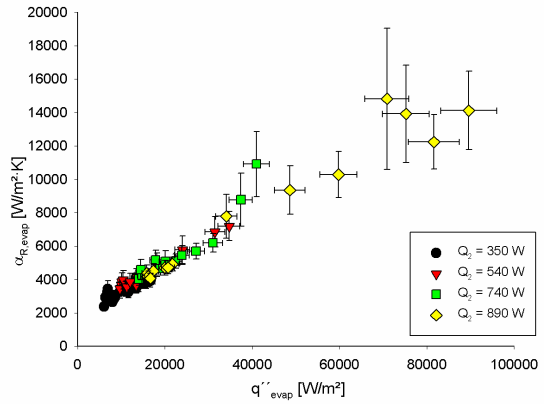

Figure 51: $\alpha_{R,evap}$ versus the boiling heat flux.

As the LMTD method was used in evaluating the temperature difference in the boiling section of the evaporator, the applicability of LMTD was investigated. As the flow boiling heat transfer was found to depend on heat flux, it should not be expected that the LMTD method applies. A numerical approach was employed, calculating the correction factor, F, required in order for the LMTD to be accurate. The correction factor was found to be sufficient close to one for

high LMTD. However, at low LMTD the correction factor may become rather low, see Figure 56, indicating that a correction of the LMTD may be necessary.

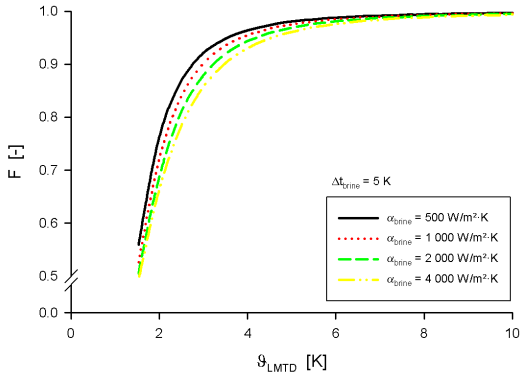

Figure 56:Correction factor when using LMTD for different α_{brine} at 5 K brine temperature drop.

In a subsequent test, the second approach (estimating the superheated area) was employed. It was observed that the obtained heat transfer area was not the same as measured with TLC. Possible reasons for this discrepancy were discussed, and the most likely reason found was the presence of mist flow. Assuming mist flow and that single phase gas heat transfer coefficient applies in the mist flow region, the dry-out quality could be estimated, see Figure 73. Assuming mist flow also implies a new leading constant of the Cooper correlation, as less heat is transferred.

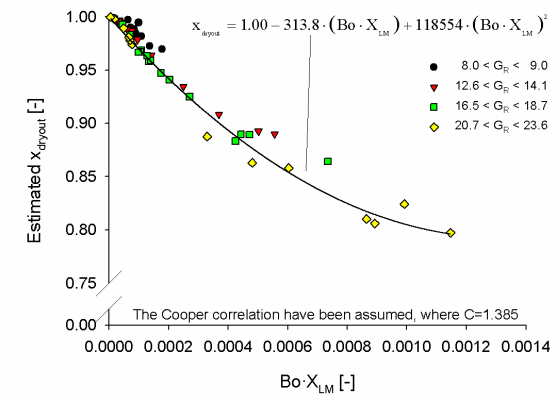

Figure 73: Estimated dry-out quality as a function of the local boiling number, estimated using the Cooper correlation with the new fitting constant, and the Lockhart-Martinelli parameter.

4.3 Local performance

In this last main section of the thesis, local thermal and hydraulic performances of the evaporator were investigated experimentally. The adiabatic pressure drop was experimentally determined for a wide range of mass flux, valid for domestic heat pumps, and for vapor fractions ranging from 10 % to 80 %. Best fit between experimental data and predicted data was obtained with the classical correlation by Chisholm (1967) if the Chisholm parameter was fitted with a new suggested correlation, using the kinetic energy per volume. The deviation from experiments is less than ± 10 % for all measured points, see Figure 78.

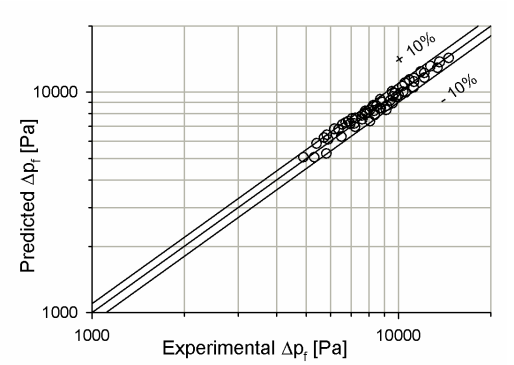

Figure 78: Predicted vs. experimental adiabatic two phase frictional pressure drop in a compact brazed plate heat exchanger.

Finally, the local flow boiling heat transfer coefficient was estimated using a novel technique for flow boiling in plate heat exchangers. The experimental local heat transfer coefficients were compared with several correlations from the literature. Best agreements were found with the pool boiling correlation by Cooper (1984) and the narrow channel flow boiling correlation by Tran (1999).

5 THE HEAT PUMP

As mentioned in chapter 3, the delivered heat to the house from a heat pump consists of energy from the surrounding and energy as work to the compressor. A relation between these was also given. However the actual relation between the heat from the surrounding and the work input depends on several parameters. In this section a brief introduction to heat pump theory is given.

5.1 Carnot heat pump

When investigating any machine, it is important to be able to answer the question: How efficient is the machine?

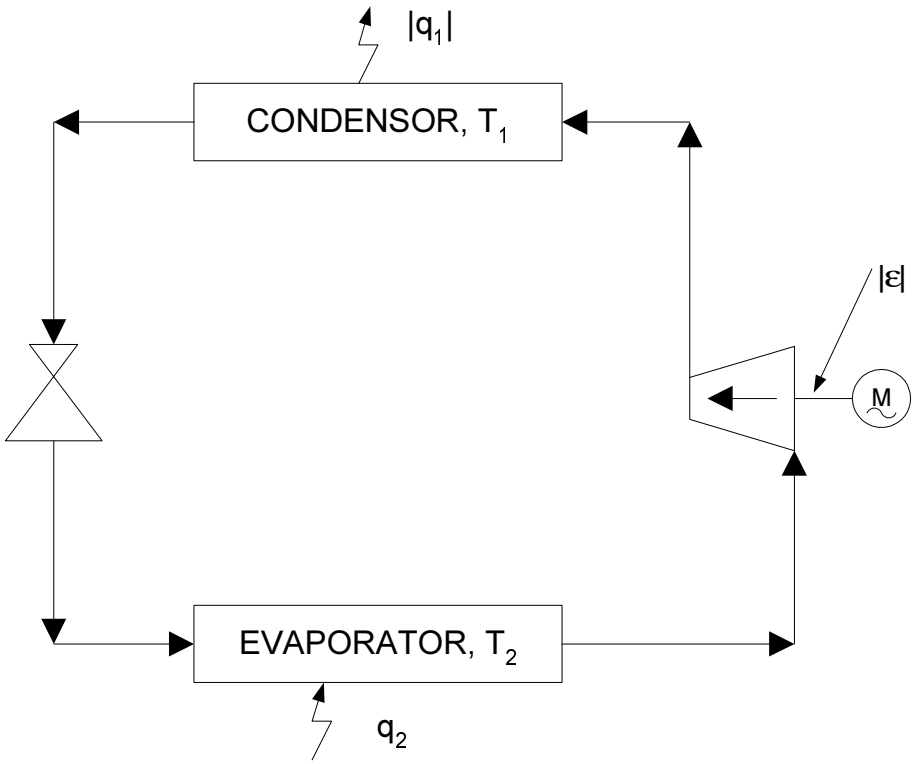

Figure 1: Simple Carnot Heat Pump.

To answer that question one must first know how efficient the machine can be ideally. One measure is the relation to the Carnot Engine. It can be shown that the Carnot Engine has the highest possible efficiency theoretically available for a machine operating between the temperatures T_1 and T_2.

For a Carnot heat pump, see Figure 1, the rejected heat to the heat sink (hot side) is

$$|q_1| = T_1 \cdot \Delta s_1 \tag{1}$$

and the heat obtained from the heat source (cold side) is

$$q_2 = T_2 \cdot \Delta s_2 \tag{2}$$

For a Carnot heat pump the entropy change over the low temperature equals the entropy change of the high temperature heat exchanger. The amount of heat given off by the heat pump compared to the amount of energy put into the compressor is called COP (Coefficient Of Performance). Index 1 and 2 are used to separate between heat pump and refrigeration duty. The COP_{1C}, Coefficient Of Performance for heat pump duty, is thus

$$COP_{1C} = \frac{|q_1|}{|\varepsilon|} = \frac{|q_1|}{|q_1| - q_2} = \frac{T_1}{T_1 - T_2} \tag{3}$$

In the same manner the COP_{2C} can be written. Index C is added to distinguish between the real world machine and the Carnot machine.

These two COPs are the highest theoretically obtainable a heat pump or a refrigerating machine can have. Inspecting eq. (3), one may see that the temperature difference, $T_1 - T_2$, should be kept as small as possible in order to obtain high COP. However, these temperatures depend on the specific task and may not be chosen freely.

5.2 The "real" heat pump

In any "real" world machine there exists losses (irreversibilities). For instance, friction between the moving parts in the compressor is one example. In addition, the real heat pump has temperature differences in the heat exchangers. Temperature differences in heat exchangers are necessary in order to have heat transfer between the surrounding and the heat pump. However, a temperature difference also introduces losses compared to the ideal machine.

These are examples to illustrate the fact that a real world heat pump does not have the same efficiency as an ideal one. Consequently, the COP_1 of a real heat pump is calculated as

$$COP_1 = \frac{|q_1|}{|\varepsilon|} \tag{4}$$

and for a refrigerating machine the COP_2 is calculated as

$$COP_2 = \frac{q_2}{|\varepsilon|} \tag{5}$$

The Carnot efficiency, a comparison between the ideal Carnot heat pump and the "real" world heat pump, is defined as

$$\eta_C = \frac{COP_2}{COP_{2C}} \tag{6}$$

If no information is available, a good estimate is 0.5 (Granryd et al. 2003, Spindler and Müller-Steinhagen 2003).

It is of course desirable to obtain as high COP as possible. However, the heat pump should solve a specific task, i.e. obtain heat from a surrounding at temperature T_2 and deliver heat to a surrounding at a temperature T_1. These temperatures are therefore fixed and given. To obtain high COP one should then keep temperature differences in the heat exchangers as small as possible. The reason for this is that the heat pump does not work with T_1 and T_2, but rather $T_1+\Delta T_1$ and $T_2-\Delta T_2$. Hence, decreasing ΔT_1 and ΔT_2 increases the COP. One should also make the compressor as efficient as possible, to keep the compressor work as small as possible.

6 HEAT EXCHANGER THEORY

The temperature difference in heat exchangers may be reduced at the design stage, for a given heat duty, in two ways; by increasing the heat transfer coefficient or by increasing the heat transfer area, see eq. (7) and (8).

$$\dot{Q} = U \cdot A \cdot \vartheta_m \tag{7}$$

which also may be written as

$$\dot{Q} = U \cdot A \cdot \vartheta_{LMTD} \cdot F \tag{8}$$

The mean temperature difference for a pure counter current single phase heat exchanger is equal to the logarithmic mean temperature difference, ϑ_{LMTD}, defined as

$$\vartheta_{LMTD} = \frac{\vartheta_1 - \vartheta_2}{\ln\left(\frac{\vartheta_1}{\vartheta_2}\right)} \tag{9}$$

where the temperature differences are defined in Figure 2.

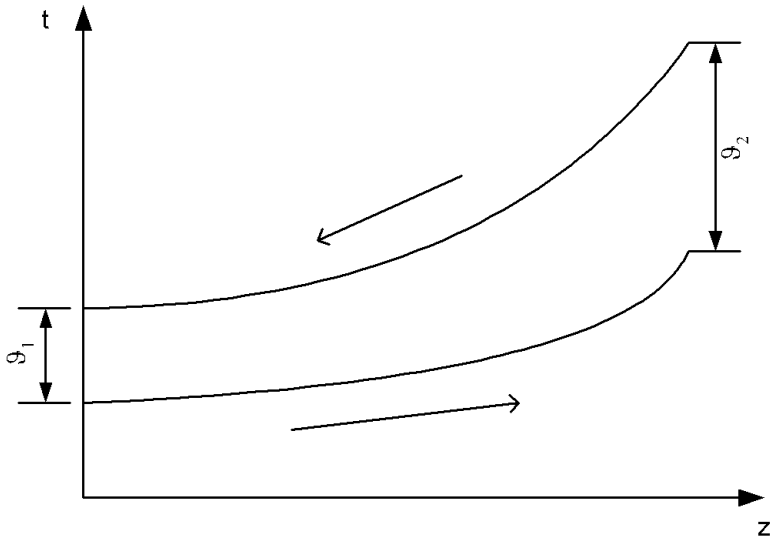

Figure 2: Schematic temperature profiles in a counter-current heat exchanger.

The derivation of the above equation may be found in most textbooks on basic heat transfer, e.g. Incropera and DeWitt (1996). The correction factor F equals unity for pure co- and counter current heat exchangers, and for evaporators and condensers if the overall heat transfer coefficient, U, is constant along the surface of the heat exchanger. For any other kind of heat exchanger, this factor is less than one.

The overall heat transfer coefficient, U, is calculated as

$$U = \frac{1}{\frac{1}{\alpha_h} + \frac{1}{\alpha_c} + \frac{\delta_{ss}}{\lambda_{ss}} + \sum R_{th}} \tag{10}$$

where α are the individual film heat transfer coefficients. R_{th} are additional heat transfer resistances that may exist, e.g. fouling. In eq. (10), the heat transfer area on each side is assumed equal. If this is not the case a simple correction is undertaken. Eq. (10) may easily be obtained by adding the temperature differences from one fluid side to the other fluid side, by setting the sum equal to the total temperature difference.

The correlation to calculate the individual heat transfer coefficients on each fluid side, sometimes referred to as film heat transfer coefficients, depends on the heat transfer geometry. For instance, a well known correlation, applicable for turbulent flow (Re > 10 000) in circular tubes, is

$$Nu = C \cdot Re^n \cdot Pr^m \tag{11}$$

and the film heat transfer coefficient is calculated as

$$\alpha = Nu \cdot \frac{\lambda}{d_h} \tag{12}$$

This type of correlation has been extended to several different geometries, though with different constants C, n and m. Other correlations are also available. One worth mentioning is the one by Sieder and Tate (1936), which incorporated a viscosity ratio between the bulk fluid and the fluid at the wall temperature, both for laminar and turbulent flows.

The use of the logarithmic mean temperature difference is convenient and straightforward when all four terminal temperatures are known, i.e. at the design stage of a heat exchanger. However, predicting the outlet temperatures of an existing heat exchanger at given flow rates and inlet temperatures yields an iterative solution when the LMTD approach is used. In such cases, the ε-NTU

method is more straightforward. The effectiveness of the heat exchanger is defined as

$$\varepsilon = \frac{\dot{Q}}{\dot{Q}_{max}} \tag{13}$$

This can sometimes be simplified into

$$\varepsilon = \frac{\Delta t_{(\dot{m}\cdot c_p)_{min}}}{\Delta t_{in}} \tag{14}$$

The Number of Transfer Units (NTU) is defined as

$$NTU = \frac{U \cdot A}{(\dot{m} \cdot c_p)_{min}} \tag{15}$$

Relations between ε and NTU have been established and are reported in the literature for several types of heat exchangers. For instance, a counter current single phase heat exchanger has the relation (Incropera & DeWitt, 1996)

$$\varepsilon = \frac{1 - e^{-NTU\cdot\left(1-\frac{(\dot{m}\cdot c_p)_{min}}{(\dot{m}\cdot c_p)_{max}}\right)}}{1 - \frac{(\dot{m}\cdot c_p)_{min}}{(\dot{m}\cdot c_p)_{max}} \cdot e^{-NTU\cdot\left(1-\frac{(\dot{m}\cdot c_p)_{min}}{(\dot{m}\cdot c_p)_{max}}\right)}} \tag{16}$$

The derivation of the logarithmic mean temperature difference, eq. (9) and eq. (16), does include some assumptions which limits its range of application. One important assumption will be discussed briefly.

It is assumed that the overall heat transfer coefficient is constant throughout the entire heat exchanger. This implies, in practice, that the individual film heat transfer coefficients are constant from the inlet to the outlet of the heat exchanger. For single phase heat exchangers, it is almost always assumed that this assumption is valid. However, for an evaporator, in which one fluid is boiling, this may not necessarily be true. As will be seen later, flow boiling heat transfer depends on several local parameters that vary along the flow path; hence, the heat transfer coefficient may not be regarded as constant.

For a single phase heat exchanger, the correction factor F for any heat exchanger deviating from pure co- or counter current flow is less than one, as already mentioned. However, the correction factor F is assumed to equal one for

any kind of heat exchanger type if one, or both, of the fluid streams change its phase at constant temperature, Incropera & DeWitt (1996). This is assumed to apply for condensers and evaporators, where heat transfer occurs without changing the temperature of one of the two fluid streams.

However, one should be careful and acknowledge the fact that the local overall heat transfer coefficients during flow boiling and flow condensation are generally not constant along the heat transfer surface. In addition, the local temperature in evaporators and condensers depends on the local pressure. As with all fluid flow, pressure decreases along the flow path. If the pressure drop is “small”, the corresponding saturation temperature change may be neglected. If, however, the pressure drop is “significant”, the temperature profile in the boiling fluid must be accounted for. A correction factor F should be selected accounting for the heat exchanger design, the temperature profile, and the fact that the overall heat transfer coefficient is not constant along the heat transfer surface.

7 FLOW BOILING

In the literature, two types of boiling of a saturated fluid are described, pool boiling and flow boiling. In pool boiling, heat is transferred to a stagnant fluid, a pool. During flow boiling, heat is transferred to a fluid having a velocity relative to the surface from where the heat is supplied. In a compact brazed plate heat exchanger operating as evaporator the fluid is in motion, hence flow boiling applies.

In saturated flow boiling heat is transferred by two different mechanisms, nucleate boiling and convective evaporation. Convective evaporation resembles ordinary convective heat transfer in single phase heat transfer, i.e. the main resistance to heat transfer is at the heated wall. This part of the heat transfer is often modeled using heat transfer correlations similar to single phase heat transfer correlations. In nucleate boiling, heat is mainly transferred into the bulk of the gas/liquid by means of bubbles nucleating on the surface, growing and finally detaching from the surface. This part of the heat transfer is similar to pool boiling and is often modeled as pool boiling. The total heat transfer coefficient is then calculated accounting (by weighting) for both mechanisms.

The weighting is carried out differently, as may be found in the literature. In most cases, a correction factor is introduced into the pure convective and nucleate parts. The convective part is often said to be enhanced due to the presence of bubbles. In a similar way, the nucleate part is often said to be suppressed due to the fact that the flow of the liquid may suppress bubble nucleation. The combined effect of these two mechanisms is not yet well understood and several different approaches may be found in the literature.

In addition, the size of the channel is expected to be important for flow boiling heat transfer. As the size of the channel decreases, the departure bubble size approaches that of the channel. It may therefore be expected that other forces, such as surface tension, are becoming important. In recent years, a large number of investigations have been conducted, reporting on heat transfer in mini- and micro-channels. No clear, widely accepted, definition is presented on the limits of large channels, mini channels or microchannels. Several different definitions exist. It should perhaps be noted that plate heat exchangers is in the midrange between large channels and small channels.

7.1 Flow patterns

As for single phase flow (laminar and turbulent), there exist different characteristics of the flow during two-phase flows (flow patterns). However, the number of different flow patterns is higher than for singe phase flow. In addition, the flow patterns of horizontal and vertical flow generally differ. Even

the vertical up flow may have different flow patterns compared to vertical down flow.

Taitel et al. (1980) identified four different flow patterns in vertical upwards two-phase flows; Bubble, Slug, Churn, and Annular flow.

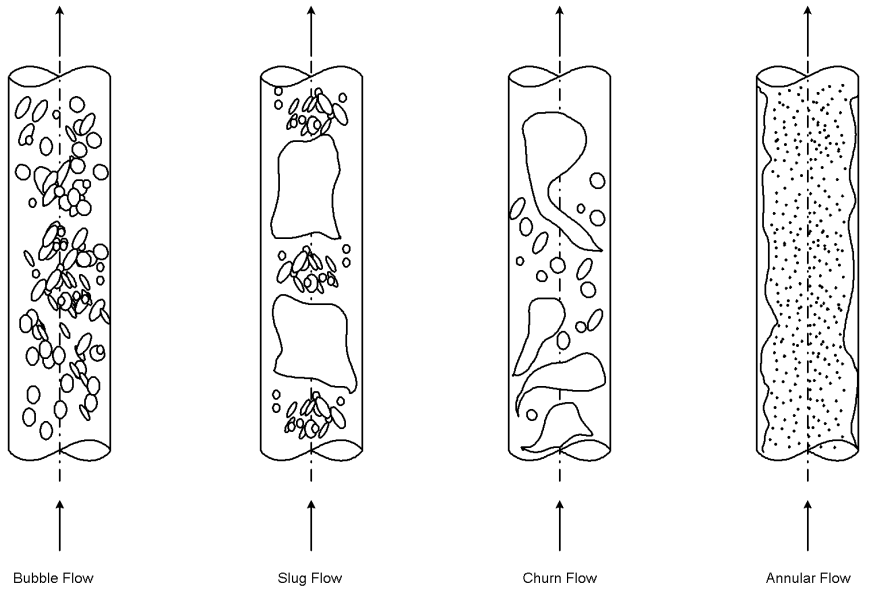

Figure 3: Flow patterns in vertical two-phase flow
(adopted from Taitel et al., 1980).

Many others have investigated flow patterns in two-phase flow, both vertical and horizontal. In recent years, focus has been on two-phase flow in small channels. Since surface tension forces may become more important, it may be expected that the flow patterns for large tube are not entirely applicable.

Most investigations studies two-phase flow in single channels, with some exceptions, either with circular tubes or in rectangular channels. However, the present thesis investigates evaporation in plate heat exchangers, a geometry quite different from a straight circular tube. Hence, it is the belief of the author of this thesis that the classical flow pattern maps found in the literature generally does not apply to plate heat exchangers. Very few investigations on flow patterns in plate heat exchangers have been conducted, as will be seen in chapter 8.

7.2 Flow boiling heat transfer correlations

Numerous flow boiling correlations exist in the literature. In this section, some of the better known correlations are listed.

7.2.1 Chen (1966) correlation

Chen (1966) published his classical paper on flow boiling, where the evaporating heat transfer coefficient was a sum of macro and micro mechanisms.

$$\alpha = \alpha_{mic} + \alpha_{mac} \tag{17}$$

The microscopic evaporation, nucleate boiling, was calculated as

$$\alpha_{mic} = 0.00122\left(\frac{\lambda_l^{0.79}\cdot c_{p_l}^{0.45}\cdot \rho_l^{0.49}\cdot g_c^{0.25}}{\sigma^{0.5}\cdot \mu_l^{0.29}\cdot \Delta h_{fg}^{0.24}\cdot \rho_g^{0.24}}\right)\cdot \Delta t^{0.24}\cdot \Delta p^{0.75}\cdot S \tag{18}$$

and the macroscopic evaporation, convective evaporation, was calculated as

$$\alpha_{mac} = 0.023\cdot Re_l^{0.8}\cdot Pr_l^{0.4}\cdot\frac{\lambda_l}{d}\cdot F \tag{19}$$

where the parameter S is the suppression factor for nucleate boiling and the parameter F is the enhancement factor of convective heat transfer. In the original paper, these two were presented graphically. Good agreement with experimental results was obtained.

7.2.2 Chato et al. (1995) correlation

Chato et al. (1995) presents a general heat transfer correlation valid for horizontal flow with a diameter larger than ~4mm. They claim that the correlation holds for pure, azeotropic and near azeoptropic refrigerants.

Nucleate boiling term was calculated using a correlation by Cooper (1984), with surface roughness set to 1μm.

$$Nu_{NB} = \frac{d}{\lambda_l}\cdot\frac{55\cdot q''^{0.67}\cdot p_r^{0.12}}{M^{0.5}\cdot\left(-\log_{10}(p_r)\right)^{0.55}} \tag{20}$$

The convective term was calculated with a Dittus-Boelter type of correlation, with enhancement for two-phase flow.

$$Nu_{CB} = 0.023 \cdot Re_l^{0.8} \cdot Pr_l^{0.4} \cdot \left[1 + \frac{1.925}{X_{tt}^{0.83}}\right] \cdot F \qquad (21)$$

where F was a function of the Froude number, Fr_l. The total heat transfer was calculated by an asymptotic model.

$$Nu_{TP} = \left(Nu_{CB}^n + Nu_{NB}^n\right)^{1/n} \qquad (22)$$

where n=2.5.

7.2.3 Kandlikar (1990, 2003) correlations

Kandlikar (1990) presented a general correlation for prediction of the heat transfer coefficient in flow boiling. The final correlation consists of two sets of constants, one for the convective evaporation dominated regime and one for the nucleate boiling dominated regime. The correlation is

$$\frac{\alpha_{TP}}{\alpha_l} = C_1 \cdot Co^{C_2} \cdot \left(25 \cdot Fr_{lo}\right)^{C_5} + C_3 \cdot Bo^{C_4} F_{fl} \qquad (23)$$

and the constants are give in the table below.

Table 1: Constants in Kandlikar (1990) correlation.

Constant	Convective evaporation	Nucleate boiling
C_1	1.1360	0.6683
C_2	-0.9	-0.2
C_3	667.2	1058.0
C_4	0.7	0.7
C_5	0.3	0.3

The correlation is calculated twice using each set of constants and the greater of the two values is used as the heat transfer coefficient. The Froude number is calculated with the entire flow as liquid.

$$Fr_{lo} = \frac{G^2}{\rho_l^2 \cdot g \cdot d} \qquad (24)$$

If the Froude number is larger than 0.04 or if the flow is vertical, C_5 is set to zero. F_{fl} is a fluid dependent parameter valid for copper surfaces. In Kandlikar and Steinke (2003), it is reported for R134a to be 1.63. For all other surface materials, however, it is recommended to be set to 1. It was also reported in the same reference that heat transfer coefficients in minichannels present roughly the same trends as large channels. They also conclude that the constant C_5 should be set to zero for mini- and microchannels. In addition, they extend the correlation by Kandlikar (1990) to be valid in the mini- and microchannel range by allowing the all-liquid heat transfer coefficient to be laminar whenever necessary.

7.2.4 Shah (1976, 1982) correlations

Shah (1976) constructed a graphical correlation for flow boiling in pipes. Four dimensionless numbers were used:

$$\psi = \frac{\alpha_{TP}}{\alpha_l} \tag{25}$$

$$Co = \left(\frac{1}{x} - 1\right)^{0.8} \cdot \left(\frac{\rho_g}{\rho_l}\right)^{0.5} \tag{26}$$

$$Bo = \frac{q''}{G \cdot \Delta h_{lg}} \tag{27}$$

$$Fr_{lo} = \frac{G^2}{\rho_l^2 \cdot g \cdot d} \tag{28}$$

The convective number, Co, was introduced for the first time in this publication. The single phase heat transfer was calculated using Dittus-Boelter equation and only the liquid fraction of the flow was considered. No account for laminar film flow was done.

$$\alpha_l = 0.023 \cdot \left(\frac{G \cdot (1-x) \cdot d}{\mu_l}\right)^{0.8} \cdot Pr_l^{0.4} \cdot \frac{\lambda_l}{d} \tag{29}$$

The final form of the graphical correlation may be found in Appendix C.

Later, Shah (1982) developed equations for use in computer calculations. The correlation starts with the determination of the parameter N as

$$N = \begin{cases} 0.38 \cdot Fr_{lo}^{-0.3} \cdot Co & \text{Horizontal tube, } Fr_{lo} \le 0.04 \\ Co & \text{Otherwise} \end{cases} \tag{30}$$

Now, a second parameter, F, is determined as

$$F = \begin{cases} 14.7 & Bo \ge 11 \cdot 10^{-4} \\ 15.43 & Bo < 11 \cdot 10^{-4} \end{cases} \tag{31}$$

Depending on the value of parameter N, three different sets of equations is chosen between.

For N > 1.0, the following equations apply

$$\psi_{nb} = \begin{cases} 230 \cdot Bo^{0.5} & Bo \ge 0.3 \cdot 10^{-4} \\ 1 + 46 \cdot Bo^{0.5} & Bo < 0.3 \cdot 10^{-4} \end{cases} \tag{32}$$

and

$$\psi_{cb} = \frac{1.8}{N^{0.8}} \tag{33}$$

The actual heat transfer enhancement is the greater of the two, i.e.

$$\psi = \max\left(\psi_{cb}, \psi_{nb}\right) \tag{34}$$

For 0.1 < N ≤ 1.0, the following equations apply

$$\psi_{bs} = F \cdot Bo^{0.5} \cdot e^{2.74 \cdot N^{-0.1}} \tag{35}$$

and

$$\psi_{cb} = \frac{1.8}{N^{0.8}} \tag{36}$$

The actual heat transfer enhancement is the greater of the two, i.e.

$$\psi = \max\left(\psi_{cb}, \psi_{bs}\right) \tag{37}$$

Finally, for N ≤ 0.1 the following equations apply

$$\psi_{bs} = F \cdot Bo^{0.5} \cdot e^{2.74 \cdot N^{-0.15}} \tag{38}$$

and

$$\psi_{cb} = \frac{1.8}{N^{0.8}} \tag{39}$$

The actual heat transfer enhancement is again the greater of the two, i.e.

$$\psi = \max\left(\psi_{cb}, \psi_{bs}\right) \tag{40}$$

Shah recommends these equations for vertical flow without any restriction on the Boiling number.

7.2.5 Steiner and Taborek (1992) model

Steiner and Taborek (1992) developed an open ended model, i.e. parts of the model may be exchanged to fit the problem at hand without invalidating the final results.

The model is an asymptotic model. The local flow boiling heat transfer coefficient is calculated from the two individual heat transfer coefficients, convective evaporation and nucleate boiling, as

$$\alpha_{TP} = \sqrt[n]{\alpha_{nbf}^{n} + \alpha_{cb}^{n}} \tag{41}$$

The individual parts of the heat transfer coefficients consist of the pure mechanism and a flow correction factor. Thus, the nucleate flow boiling part is calculated as

$$\alpha_{nbf} = \alpha_{nb,of} \cdot F_{nbf} \tag{42}$$

and the convective flow boiling part as

$$\alpha_{cb} = \alpha_{lo} \cdot F_{tp} \tag{43}$$

The single phase heat transfer α_{lo} is calculated assuming all flow as liquid. The pool boiling heat transfer coefficient, $\alpha_{nb,of}$ is calculated at normalized conditions. n is set to 3. Any preferred nucleate boiling correlation may be used. In the original reference, pre-calculated values for various common fluids is included, see Appendix D for an abridged table. This table can be reproduced using the suggested pool boiling correlation. If the reference nucleate heat transfer coefficient is to be calculated, whether by the suggested correlation or any other correlation, the normalized values of heat flux, surface roughness and so on, must be used.

The correction factor for the convective heat transfer, F_{tp}, is calculated as

$$F_{tp_{0.0\le x\le 0.6}} = \left[(1-x)^{1.5} + 1.9 \cdot x^{0.6} \left(\frac{\rho_g}{\rho_l} \right)^{0.36} \right]^{1.1} \tag{44}$$

for vapor qualities between zero and 0.6, and

$$F_{tp_{0.6<x\le 1.0}} = \left[\left(\left[(1-x)^{1.5} + 1.9 \cdot x^{0.6} \cdot (1-x)^{0.01} \cdot \left(\frac{\rho_g}{\rho_l} \right)^{0.35} \right]^{-2.2} + \left\{ \frac{\alpha_{go}}{\alpha_{lo}} \cdot x^{0.01} \cdot \left[1 + 8 \cdot (1-x)^{0.7} \left(\frac{\rho_g}{\rho_l} \right)^{0.67} \right] \right\}^{-2} \right)^{0.5} \right]^{-1} \tag{45}$$

for vapor qualities up to one. The correction factor for nucleate boiling is

$$F_{nbf} = F_{pf} \cdot \left[\frac{q''}{q''_{of}} \right]^{nf(p_r)} \cdot \left[\frac{d}{d_o} \right]^{-0.4} \cdot \left[\frac{R_a}{R_{a,o}} \right]^{0.133} \cdot F(M) \tag{46}$$

where

$$F_{pf} = 2.816 \cdot p_r^{0.45} + \left(3.4 + \frac{1.7}{1-p_r^7} \right) \cdot p_r^{3.7} \tag{47}$$

which is valid up to reduced pressures of 0.95. The exponent on the heat flux is calculated as

$$nf(p_r) = 0.8 - 0.1 \cdot e^{1.75 \cdot p_r} \tag{48}$$

for refrigerants. The normalized heat flux to use for refrigerants is 20 000 W/m². It has been found in various reports that the molar mass of the fluids influences the pool boiling heat transfer. Steiner and Taborek (1992) reports the dependency according to

$$F(M) = 0.377 + 0.199 \cdot \ln(M) + 2.8427 \cdot 10^{-5} \cdot M^2 \tag{49}$$

The function is not to be larger than 2.5. It should perhaps be commented that the author of the present thesis is not able to reproduce figure 14 in the original reference, which is said to be calculated using eq. (49). A better fit is suggested as

$$F(M) = 0.3246 + 0.1387 \cdot \ln(M) + 1.6093 \cdot 10^{-5} \cdot M^{2.1} \qquad (50)$$

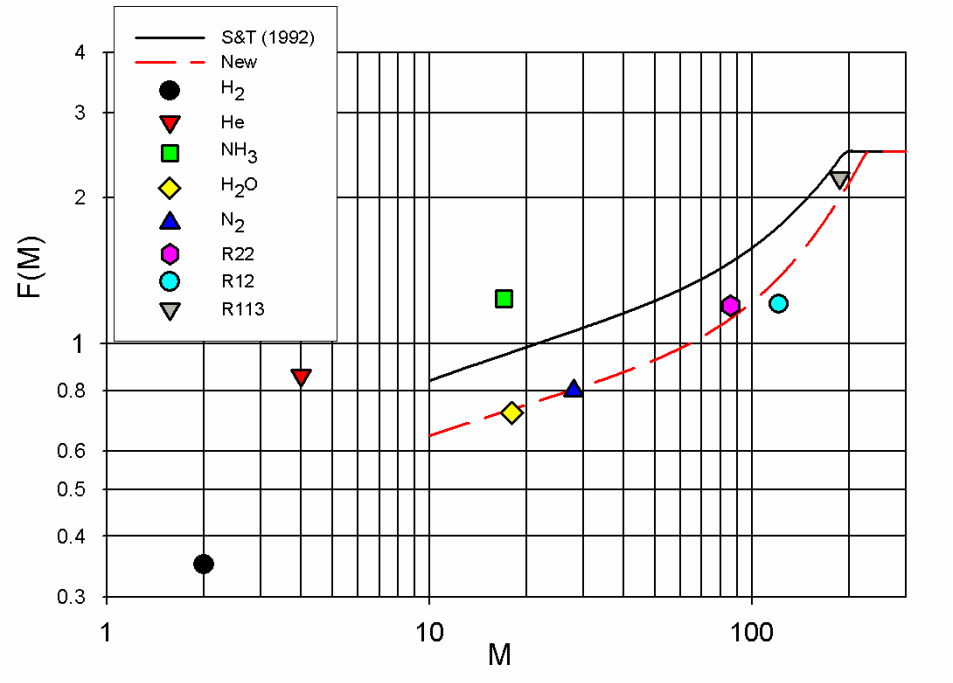

Figure 4: Correction factor as a function of molecular weight.

Finally, before the nucleate boiling term can be used, it has to be checked whether nucleation is possible. The onset of nucleate boiling is calculated according to

$$q''_{ONB} = \frac{2 \cdot \sigma \cdot T_{sat} \cdot \alpha_{lo}}{r_{cr} \cdot \rho_g \cdot \Delta h_{lg}} \qquad (51)$$

The critical radius is recommended to be $0.3 \cdot 10^{-6}$ m.

7.2.6 Gungor and Winterton (1986, 1987) correlations

Gungor and Winterton (1986) presented a flow boiling heat transfer correlation for both vertical and horizontal flows. Later, Gungor and Winterton (1987) modified this correlation, obtaining a simpler, more accurate correlation. The resulting correlation was

$$\alpha_{tp} = E \cdot \alpha_L \qquad (52)$$

where the enhancement factor E for saturated vertical flow was

$$E = 1 + 3000 \cdot Bo^{0.86} + 1.12 \cdot \left(\frac{x}{1-x} \right)^{0.75} \cdot \left(\frac{\rho_g}{\rho_l} \right) \tag{53}$$

The convective single phase heat transfer coefficient α_L was calculated with the Dittus-Boelter correlation using the liquid fraction of the flow. For annuli, the hydraulic diameter was based on the heated perimeter.

7.2.7 Jung and Radermacher (1991) correlation

Jung and Radermacher (1991) investigated the flow boiling of refrigerants in horizontal tubes. The applicable range of heat flux was 10 kW/m^2 to 45 kW/m^2 and mass fluxes between 250 kg/(m^2·s) and 720 kg/(m^2·s). The heat transfer correlation for pure fluids was based on the Chen correlation, however with several modifications. First, the enhancement factor F was slightly modified.

$$F = 2.37 \left(0.29 + \frac{1}{X_{tt}} \right)^{0.85} \tag{54}$$

The liquid heat transfer was calculated with the Dittus-Boelter correlation using the liquid fraction of the flow. The nucleate flow boiling part was calculated using Stephan and Abdelsalam´s pool boiling correlation and a boiling suppression factor, N. This differs from the original suppression factor by Chen. Jung and Radermacher´s suppression factor was allowed to be higher than one. In additional, this suppression factor was a function of heat flux.

The suppression factor was defined as

$$N = \begin{cases} 4048 \cdot X_{tt}^{1.22} \cdot Bo^{1.13} & X_{tt} \le 1 \\ 2.0 - 0.1 \cdot X_{tt}^{-0.28} \cdot Bo^{-0.33} & 1 \le X_{tt} \le 5 \end{cases} \tag{55}$$

The total flow boiling heat transfer was calculated as

$$\alpha_{tp} = \alpha_{nbc} + \alpha_{cec} = N \cdot \alpha_{SA} + F \cdot \alpha_l \tag{56}$$

7.2.8 Wadekar (1995) correlation

Wadekar (1995) presented a new flow boiling model. Contrary to most models, this was based on the suppression of convective heat transfer due to the presence of nucleate boiling. Comparison with experimental results showed good agreement. The total heat transfer from the surface was modeled as

$$q_T = (1 - A_{nb}) \cdot q''_c + q''_{nb} \tag{57}$$

where

$$A_{nb} = 1 - e^{-\frac{177 \cdot C \cdot \Delta T^{2.5} \cdot p_r}{Re_l \cdot F^{1.25}}} \tag{58}$$

$$q''_{nb} = \left\{ \frac{C \cdot \Delta T \cdot p_r^{0.12}}{\left[-\log_{10}(p_r) \right]^{0.55} \cdot \sqrt{M}} \right\}^3 \tag{59}$$

$$F = 1 + \frac{1.8}{X_{tt}^{0.87}} \tag{60}$$

and

$$q''_c = F \cdot \alpha_l \cdot \Delta T \tag{61}$$

7.2.9 Lazarek and Black (1982) correlation

Lazarek and Black (1982) investigated flow boiling in a small vertical channel. They tried several functional forms and the most successful was

$$Nu = 30 \cdot Re_{LO}^{0.857} \cdot Bo^{0.714} \tag{62}$$

where the Reynolds number was calculated using the entire flow as liquid. As seen in the above equation, no influence of the vapor quality is included. It was stated in the paper that the critical vapor quality was reached before the transition between nucleate dominated boiling and convective dominated boiling occurred. A reason for this might be the range of boiling number investigated.

7.2.10 Tran (1999) correlation

Tran (1999) investigated the flow boiling heat transfer in horizontal narrow channels. Both circular and rectangular channels were investigated. As for Lazarek and Black (1982), Tran did not find any influence of vapor quality on the flow boiling heat transfer coefficient. Tran used electrical heating (constant heat flux). Under these conditions, he concludes that the local heat transfer coefficient was equal to the average heat transfer coefficient. However, if the heat flux was varying, as for the case with water heating the tube, one need of course to calculate the heat transfer locally.

The model by Tran was based on the assumption that the heat transfer is governed by saturated nucleate boiling, which Tran conclude in his thesis is the main boiling mechanisms for smooth channels with wall superheat above 2.7 °C. He suggests a new correlation, including a confinement number N_{conf}, adopted from Kew and Cornwell (1994), accounting for the facts that the channel is rather small and that the growth of the bubble is restricted. The proposed correlation was

$$Nu = 770 \cdot \left(Bo \cdot Re_{lo} \cdot N_{conf} \right)^{0.62} \cdot \left(\frac{\rho_g}{\rho_l} \right)^{0.297} \tag{63}$$

where

$$N_{conf} = \frac{\sqrt{\frac{\sigma}{g \cdot (\rho_l - \rho_g)}}}{d_e} \tag{64}$$

Inserting the definitions of liquid Reynolds number with all flow as liquid and the Boiling number, Bo, into the correlation, will result in a Nusselt number being a function of fluid properties, pressure and heat flux.

7.3 Pressure drop correlations

There are numerous correlations on pressure drop in two-phase flows in the literature. The purpose of the present thesis is not to cover them all; merely the most important contributions will briefly be discussed. A good introduction of adiabatic two-phase flow pressure drop may be found in Chisholm (1983) and in Collier and Thome (1996).

Lockhart and Martinelli (1949) presented their classical paper where they introduced a new parameter, later denoted the Lockhart-Martinelli parameter, defined as

$$X^2 = \frac{\Delta p_l / \Delta L}{\Delta p_g / \Delta L} \tag{65}$$

They graphically correlated the two phase multiplier with the Lockhart-Martinelli parameter. The two phase multiplier was defined as

$$\phi_l^2 = \frac{\Delta p_{TP} / \Delta L}{\Delta p_l / \Delta L} \tag{66}$$

Baker (1954) presented a paper investigating pressure drop of simultaneous flow of oil and gas. The data does not correlate well with the Lockhart-Martinelli correlation. He observed a distinct change in slope when plotting the data in the Lockhart-Martinelli chart. He concludes that something radical changed the flow. He suggests different correlations for different flow regimes and stresses the importance of taking into account the actual flow pattern when correlating the pressure drop.

Chisholm and Laird (1958) revisited the work by Lockhart and Martinelli (1949) and suggested that the two-phase frictional data could be correlated with reasonable accuracy as

$$\frac{\Delta p_{TP}}{\Delta p_l} = 1 + C/\hat{X}^m \tag{67}$$

for rough tubes. The value of C and m depends on the tube surface and liquid flow rate. The variable $\hat{X}$ differs from the definition by Lockhart and Martinelli.

Later, Chisholm (1967) conducted a more refined analysis. However, at the end of the paper he states that the derived equations are too complicated for practical calculations and suggests

$$\phi_l^2 = 1 + C/X + 1/X^2 \tag{68}$$

where he now used the definition of X according to Lockhart-Martinelli. He also included the classical values for the Chisholm parameter, C, see Table 2.

These values may be found cited in numerous publications. Most of them, however, do not mention that the values are only valid for gas-liquid density ratios similar to air-water at atmospheric pressure.

Table 2: Classical values of the Chisholm parameter, valid for air/water mixtures at atmospheric pressure.

Flow Regime	C
turbulent – turbulent flow	20
viscous – turbulent flow	12
turbulent – viscous flow	10

viscous – viscous flow 5

One of the most recommended correlations for frictional two-phase pressure drop calculations was presented by Friedel (1979). It is actually two correlations, one for horizontal and vertical up flow and one for vertical down flow.

For horizontal and vertical upflow Friedel (1979) suggests

$$\frac{(\Delta p/\Delta l)_{tp}}{(\Delta p/\Delta l)_{l}} = A + \frac{3.21 x^{0.78}(1-x)^{0.224}\left(\frac{\rho_l}{\rho_g}\right)^{0.91}\left(\frac{\mu_g}{\mu_l}\right)^{0.19}\left(1-\frac{\mu_g}{\mu_l}\right)^{0.7}}{Fr_{tp}^{0.0454}\cdot We_{tp}^{0.035}} \tag{69}$$

and for vertical downflow

$$\frac{(\Delta p/\Delta l)_{tp}}{(\Delta p/\Delta l)_{l}} = A + \frac{48.6 x^{0.8}(1-x)^{0.29}\left(\frac{\rho_l}{\rho_g}\right)^{0.90}\left(\frac{\mu_g}{\mu_l}\right)^{0.73}\left(1-\frac{\mu_g}{\mu_l}\right)^{7.4}}{Fr_{tp}^{-0.03}\cdot We_{tp}^{0.12}} \tag{70}$$

where

$$A = (1-x)^2 + x^2\cdot\left(\frac{\rho_l\cdot\xi_g}{\rho_g\cdot\xi_l}\right) \tag{71}$$

He also includes a different set of equations, where the dimensionless numbers are based on liquid properties instead of two-phase properties as in the above equations.

A very simple correlation was suggested by Müller-Steinhagen and Heck (1986). They noted that the frictional pressure drop increases almost linearly with vapor quality up to approximately 80% vapor quality, then falling off to the gas-only frictional pressure drop. However, they also noted that the two-phase frictional pressure drop at 50% vapor quality was approximately equal to the pure gas frictional pressure drop. From this information, and assuming linear increase of pressure drop with vapor quality, they constructed a very simple pressure drop correlation. The correlation is

$$\left(\frac{dp}{dL}\right)_{tp} = \frac{G^2}{2\cdot d}\left\{\left[\frac{\xi_l}{\rho_l} + 2\cdot\left(\frac{\xi_g}{\rho_g}-\frac{\xi_l}{\rho_l}\right)\cdot x\right]\cdot(1-x)^{1/3} + \frac{\xi_g}{\rho_g}\cdot x^3\right\} \tag{72}$$

where the all-liquid Reynolds number should be higher than 100.

In recent years, the research community has focused on two-phase applications in narrow channels. Holt and Azzopardi (1995) studied two-phase flow in compact heat exchangers. They recommended not to use the Friedel (1979) pressure drop correlation. They found best agreement with the correlation by Lockhart-Martinelli. Lowry and Kawaji (1988) concluded from their experiment with air/water in narrow channel between flat plates that the basic flow patterns for large tubes were also observed in narrow channels, however the points of transitions changed. The two-phase frictional pressure drop multiplier was mainly dependent on superficial gas velocity and only to a small extent of the superficial liquid velocity. On the other hand, Damianides and Westwater (1988) concluded from their experiment with air/water that the liquid velocity was the important parameter, not the gas velocity.

Wambsganss et al. (1990a, 1990b, 1991 and 1992) investigated adiabatic air/water flow in small channels. Neither the Friedel (1979) nor the Chisholm (1967) correlations performed well. They adjusted the Chisholm correlation by correlating the Chisholm parameter, C, as

$$C = f\left(X, Re_{lo}\right) = a \cdot X^{b} \tag{73}$$

where

$$a = f\left(Re_{lo}\right) = -2.44 + 0.00939 \cdot Re_{lo} \tag{74}$$

and

$$b = f\left(Re_{lo}\right) = -0.938 + 0.00432 \cdot Re_{lo} \tag{75}$$

Many investigators, especially those studying narrow channels, conduct this kind of adjustment of the Chisholm correlation, adjusting the Chisholm parameter to fit their experimental data.

Wambsganss et al. (1990b) also investigated the normalized multiplier as suggested by Chisholm (1983). The normalized two-phase multiplier is defined as

$$\Psi = \frac{\phi_{lo}^{2} - 1}{\Gamma^{2} - 1} \tag{76}$$

where

$$\Gamma^2 = \frac{\Delta p_{go}}{\Delta p_{lo}} \tag{77}$$

is a fluid property parameter. Chisholm claimed that a simple relation between vapor quality and the normalized two-phase multiplier, even linear, might be used. However, Wambsganss et al. (1990b) did not find this approach successful. However, there might be a principal advantage with the normalized multiplier. The normalized multiplier has the correct limits when the vapor quality reaches its limits. On the contrary, a multiplier based on liquid fraction flow does go to infinity approaching a vapor quality of one. Similarly, a vapor fraction based multiplier goes to infinity approaching zero vapor quality.

7.4 Conclusion

The amount of available reports in the literature on two-phase flow, two phase flow pressure drop, and flow boiling heat transfer is extensive. In the above chapter, some selected references were given; however, this selection is by no means complete.

The research community seems to agree that heat transfer in flow boiling is governed by two mechanism, convective evaporation and nucleate boiling. They also seem to agree that these mechanisms may occur simultaneously. How to account for each mechanism (by the suppression and enhancement factors) is still a rather open question.

There seems to be an agreement that for small tubes, the surface tension may become important.

The approach by Lockhart-Martinelli, with the Chisholm equation, has almost become de facto standard in correlating two-phase frictional pressure drop. However, the original values of the Chisholm parameter do not always give accurate results. Many investigators conduct regression analysis and correlate the Chisholm parameter to fit their specific geometry and fluids.

8 COMPACT BRAZED PLATE HEAT EXCHANGERS[i]

Compact brazed plate heat exchangers are developed from the gasketed plate heat exchangers. Plate heat exchangers consist of several plates stacked to form multiple parallel channels. Most common is to use identical plates; however, to better meet heat transfer demand and available pressure drop, mixed plates may also be used. The plate heat exchanger was originally used in the dairy industry due to the ease at which the plates could be cleaned. In addition, due to high heat transfer coefficients, small temperature difference was obtained, yielding small wall temperature differences, which also was beneficial in the dairy industry. In refrigerating applications, the gasketed plate heat exchangers are not common; instead, compact brazed plate heat exchangers are used. The major reason for this is that brazed plate heat exchangers are tight to the surrounding and are able to withstand high operating pressures. This has become very important in light of the green house effect and the impact of chlorinated refrigerants on the ozone layer.

The most common plate, which also is subject to investigation in the present thesis, is the corrugated plated, also called chevron type or herringbone type. In principal, the plates are pressed with a sinusoid like pattern, where the corrugations are oriented at some angle (denoted chevron angle) with respect to the main flow direction. The corrugation pattern provides many contact points between two adjoining plates, at which the plates are brazed together, and offer therefore a strong unit. The brazed plate heat exchanger has typical maximum operating pressure above 30 bar(a).

A compact brazed plate heat exchanger is normally manufactured from stainless steel plates, pressed to the desired pattern. Every second plate is rotated and put on top on the previous one, see Figure 5 and Figure 6. In between the plates, a copper (normally) sheet is placed. The number of plates depends on the desired load the heat exchanger should have. Simply by adding more plates, larger heat loads may be transferred.

[i] This chapter is based on: Claesson J, Thermal and Hydraulic Characteristics of Brazed Plate Heat Exchangers – Part I: Review of Single- and Two-Phase Adiabatic and Flow Boiling Characteristics, Accepted for publication and presentation at the ASHRAE Wintermeeting 2005, Orlando, Florida, USA, SYMP-00112-2004.

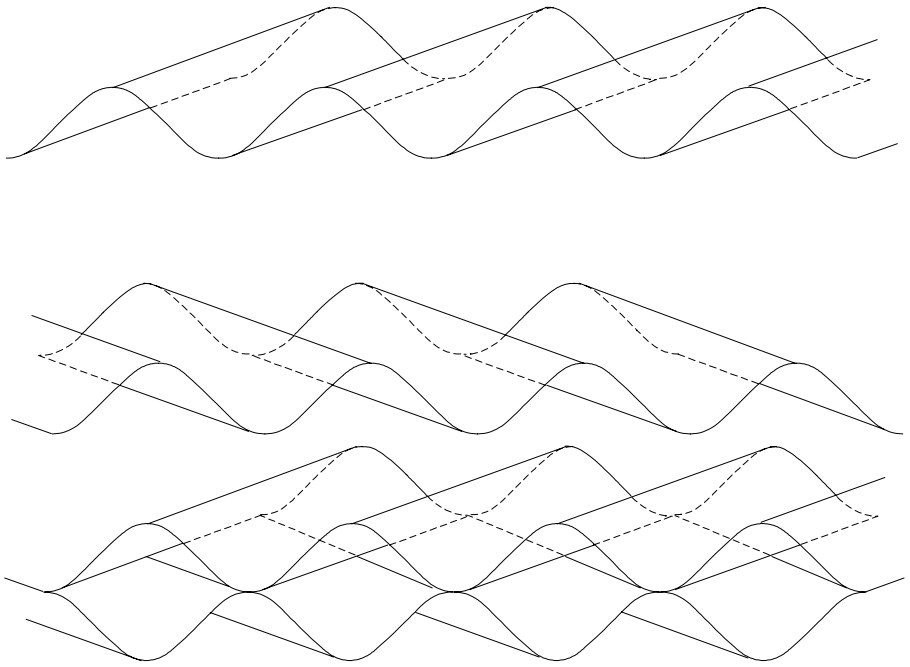

Figure 5: Plate assembly.

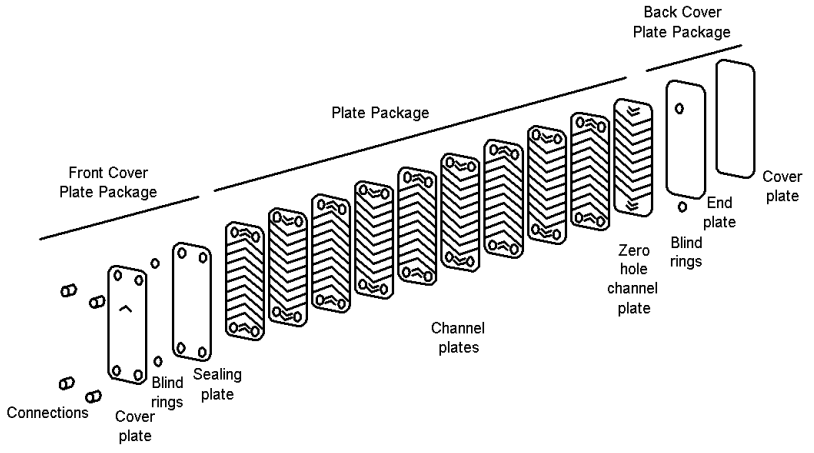

Figure 6: Assembly of a brazed plate heat exchanger
(Adopted from SWEP International AB).

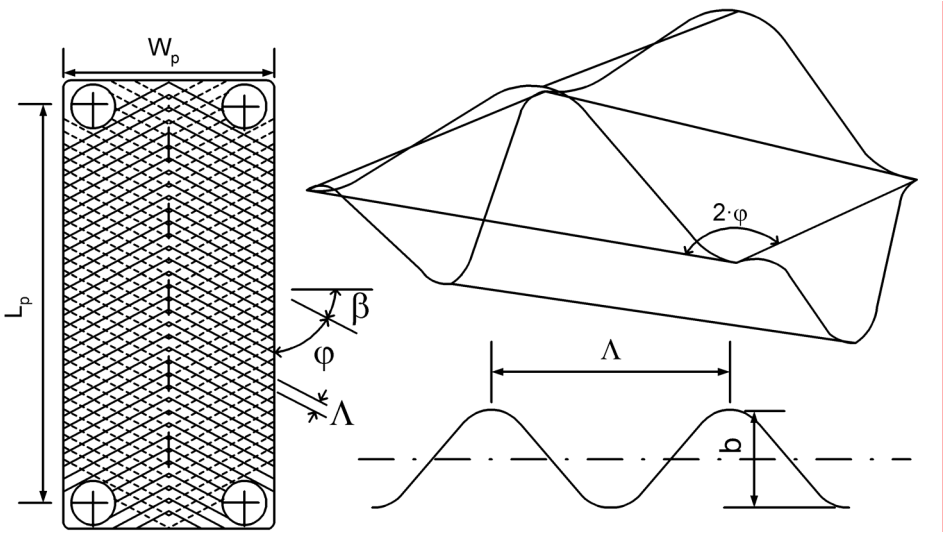

Figure 7: Plate heat exchanger geometry.

8.1 Plate geometry

In Figure 7 the important geometrical parameters for a plate heat exchanger are defined, the chevron angle (φ), corrugation (pressing) depth[i] (b), and the corrugation pitch (Λ). A closer view of the corrugation itself is show in Figure 8. As may be seen, the geometry consists of a circle segment with radius r, then a straight line connecting to the "upper" circle segment. This pattern is then repeated over and over. It has been convenient also to define the parameter "Surface enlargement factor" (ϕ). Using basic trigonometric, equations for the circle segments and the equation for a straight line, the equation for the corrugation pattern may be obtained as

[i] Sometimes also referred to as the average plate spacing.

$$y(\xi)=\begin{cases} r-\sqrt{r^2-\xi^2} & 0\le\xi\le\xi_T \\ r\cdot\dfrac{\left(1+\dfrac{1}{\cos\left(\sin^{-1}\left(\dfrac{\xi_T}{r}\right)\right)}\right)}{\left(1-\dfrac{4\cdot\xi}{\Lambda}\right)^{-1}}+\dfrac{4\cdot\xi}{\Lambda}\cdot\dfrac{b}{2} & \xi_T<\xi\le\dfrac{\Lambda}{2}-\xi_T \\ b-r-\sqrt{r^2-\left(\xi-\dfrac{\Lambda}{2}\right)^2} & \dfrac{\Lambda}{2}-\xi_T<\xi\le\dfrac{\Lambda}{2} \end{cases} \quad (78)^{i}$$

where ξ_T is the tangent point where the circle segments and the straight line connects. This position may be calculated by setting the derivatives of the circle segment and the straight line equal, see eq. (79).

$$\frac{\xi_T}{\sqrt{r^2-\xi_T^2}}=\frac{4}{\Lambda}\left(\frac{b}{2}-r+\frac{r}{\cos\left(\sin^{-1}\left(\dfrac{\xi_T}{r}\right)\right)}\right) \quad (79)$$

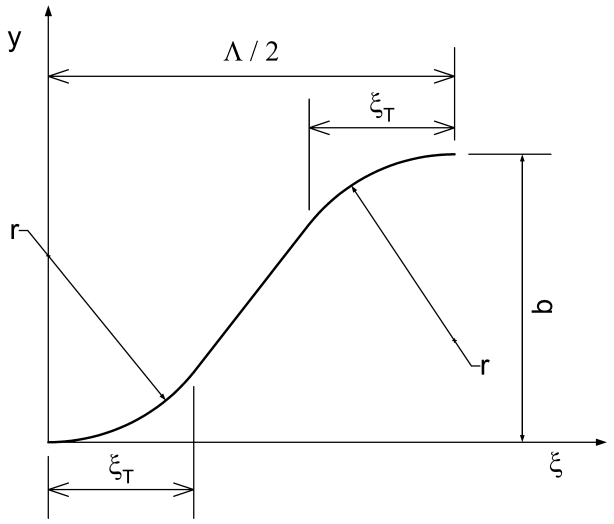

Figure 8: Close up view of corrugation geometry.

[i] A simpler function would be a simple sine, which may be found having being used in the literature. The final result change only marginal, i.e. eq. (80) would instead be $\phi = 1.183$.

Once the equation for the corrugation is known, the surface enlargement factor may be calculated as

$$\phi = \frac{1}{\Lambda/2} \int_0^{\Lambda/2} \sqrt{1 + \left(\frac{d}{d\xi} \left(y(\xi) \right) \right)^2} \, d\xi \tag{80}$$

For instance, using a radius of r = 1.6 mm, corrugation pitch of Λ = 6.9 mm and a corrugation depth of b = 2 mm yields a surface enlargement factor of ϕ = 1.189. The tangent point is located at ξ_T = 1.07 mm. Commercial plates have commonly surface enlargement factors of ϕ = 1.15 to ϕ = 1.25.

8.2 Complex flow geometry

Due to the angle of the corrugations, φ or β see Figure 7, the flow pattern of the fluid becomes complex. The plate pattern promotes early transition to turbulent flow, with a secondary swirl flow, see Figure 9. This complex flow results in high heat transfer coefficients and pressure drops. In fact, for a commercial plate heat exchanger in a typical heat pump installation, the heat transfer coefficients on the two fluid sides are at the same order of magnitude, or even with a higher heat transfer coefficient on the secondary refrigerant side.

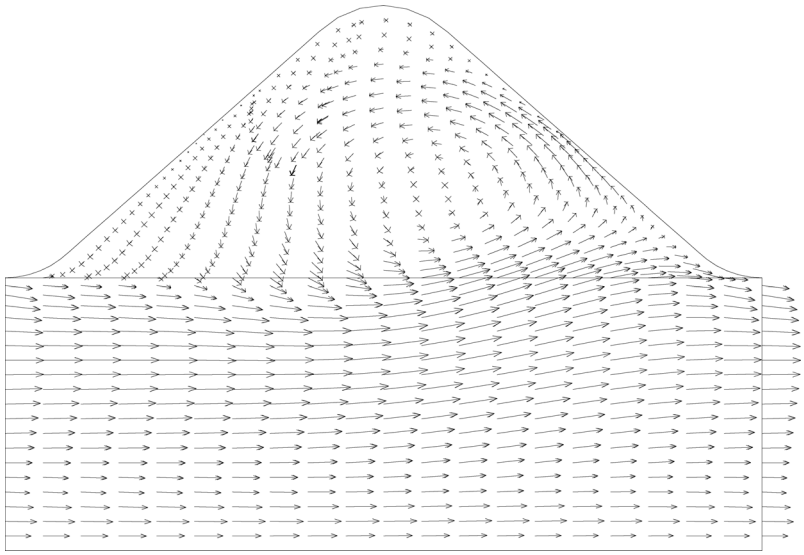

Figure 9: Example of flow pattern in CBE (from Claesson, 1996).

As the number of plates increase, the maldistribution between the flow channels may increase. Especially, in a dry expansion (DX) evaporator, the inlet fluid to the evaporator consists of part vapor and part liquid. It is therefore important to

obtain as even flow distribution as possible between the different channels of vapor and liquid. To facilitate an even flow distributions of the two-phase mixture in the inlet of the evaporator, special inlet devices are sometimes positioned in the inlet port, see Figure 10. The shape of these inlet devices differs among different manufacturers. Perfect distribution is of course desired; however, perhaps difficult to obtain.

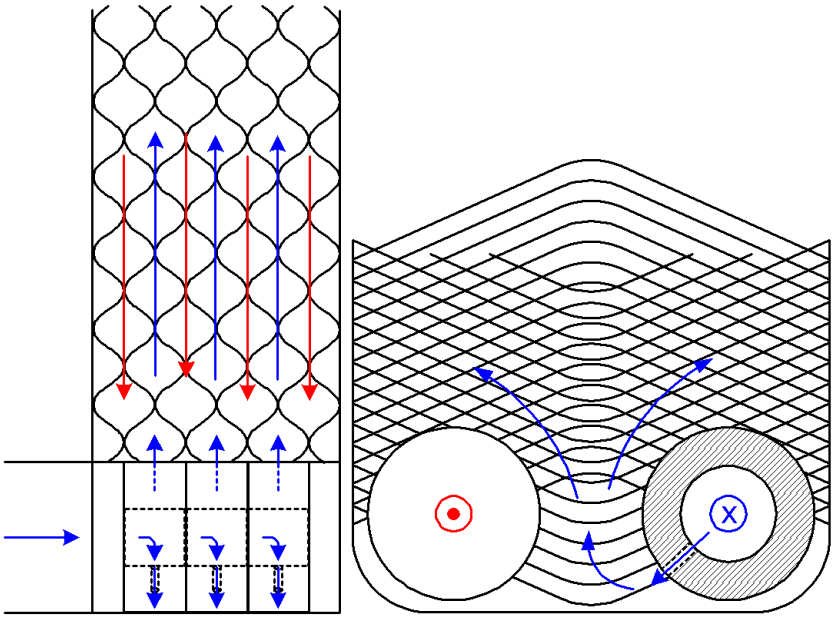

Figure 10: Plate heat exchanger equipped with an inlet flow distributor in the refrigerant inlet port.

8.3 Hydraulic diameter, Reynolds and Nusselt number, and friction factor

In the treatment of plate heat exchangers in the literature, at least two different definitions of the hydraulic diameter are used. The perhaps most common definition used is similar to the definition of two wide parallel plates, with a distance of b between the plates, hence

$$d_e = 2 \cdot b \tag{81}$$

The other definition, perhaps more "physically" correct as it is defined according to the non-circular tube definition of the hydraulic diameter, is

$$d_h = \frac{4 \cdot V}{A} = \frac{2 \cdot b}{\phi} \qquad (82)^{i}$$

In the following, we distinguish between these two by the use of different subscript, e for effective diameter and h for hydraulic diameter, as suggested by Shah and Focke (1988).

Now, the Reynolds and the Nusselt numbers may be defined as

$$Re = \frac{\rho \cdot u_m \cdot d_e}{\mu} = \frac{G \cdot d_e}{\mu} \qquad (83)$$

and

$$Nu = \frac{\alpha \cdot d_e}{\lambda} \qquad (84)$$

where the effective diameter is used. When using correlations from the literature it is very important to adhere to the definitions used in the original texts. Especially confusing is the definition of the friction factor, where an extra geometrical parameter, the flow length, is added. Two different definitions of flow length can be found in the literature, developed flow length and the length between the inlet and outlet ports. These have been mixed freely with different definitions of hydraulic diameter. The friction factor of a plate heat exchanger in this work is defined based on the effective diameter and the projected length between the inlet and outlet ports, as

$$f = \frac{\rho \cdot \Delta p \cdot d_e}{2 \cdot L_p \cdot G^2} \qquad (85)$$

However several different definitions may be found in the literature, see Table 3. In Table 3, index “core” indicates definitions where the pressure drop in the heat transfer section of the plate heat exchanger only are used. The other may include the pressure drop in the ports. The reader is referred to the original references for specific details.

---

[i] The last results may be obtained by integrating the corrugation line equation in order to obtain the area underneath the curve, then in the denominator calculate the perimeter as $\int_0^{\Lambda/2} \sqrt{1 + (y'(\xi))^2}\, d\xi$. The obtained hydraulic diameter is then compared to the effective diameter, which leads to the final results of eq. (82).

Table 3: Definitions of friction factor from the literature.

Reference	*Definition*	*Length scales*	
Martin (1996) Edwards et al. (1974)	$\xi = \frac{2 \cdot \rho \cdot \Delta p \cdot d_h}{G^2 \cdot L_p}$	L_p = Port center-to-center distance	(86)
Bogaert and Bölcs (1995)	$f = \frac{\rho \cdot \Delta p \cdot d_e}{2 \cdot L \cdot G^2}$ $F_p = \frac{\Delta p \cdot \rho}{G^2 \cdot b^2 \cdot W_p^2}$	L = A / W (flow length)	(87)
Wanniarachchi et al. (1995)	$f = \frac{\Delta p \cdot d_e \cdot \rho \cdot g_c}{2 \cdot L \cdot G^2} \cdot \left(\frac{\mu_b}{\mu_w} \right)^{0.17}$	L = A / W (flow length)	(88)
Focke (1983) Focke et al. (1985) Talik et al. (1995a,b)	$\xi = \frac{2 \cdot \rho \cdot \Delta p \cdot d_e}{G^2 \cdot L_p}$		(89)
Muley and Manglik (1999)	$f = \frac{\rho \cdot \Delta p_{core} \cdot d_e}{2 \cdot G^2 \cdot L_p}$		(90)
Muley et. al. (1999)	$f = \frac{\rho \cdot \Delta p_{core} \cdot d_e}{2 \cdot G^2 \cdot L}$	L = A / W (flow length)	(91)

In the references of Table 3, there seems to be no clear explanation for choosing the developed flow length instead of the distances between the ports. Wanniarachchi et al. (1995) mentioned that it is "…more reasonable…" but does not offer any explanation. Bogaert and Bölcs (1995) mention the difficulties of defining an appropriate flow length in a 3-D flow geometry, and develops a plate specific, dimensional, frictional function to avoid the difficulties. Muley (1997), Muley and Manglik (1999) used the distances between the ports, but Muley et al. (1999) instead chooses to use the developed flow length. No explanation or reason for the change was given.

One may also think of a physical benefit of using the actual fluid velocity rather than the mass flow velocity used in eq. (83). The actual fluid velocity, assuming a two-dimensional flow, would be the velocity the fluid has as it flows in the

corrugations. The flow would then resemble a fluid system with many parallel channels. The relation between the actual fluid velocity, u, and the mass flow velocity, u_m, would be

$$u = \frac{u_m}{\cos \varphi} \tag{92}$$

or equivalently

$$u = \frac{G}{\rho \cdot \cos \varphi} \tag{93}$$

The appropriate Reynolds number, based on the actual fluid velocity, would also become a function of the chevron angle. In this sense, use of an actual flow length, which would be a function of the plate length and the chevron angle, similar to eq. (92), would be rational rather than the developed flow length used in eqs. (87), (88) and (91). In addition, using this concept would facilitate the use of the analogy between heat transfer and pressure drop. One major drawback with this approach is that the flow may not be following the corrugations from side to side, but rather take a spiraling path along the main direction of the flow, as discussed by Shah and Focke (1988). The actual flow length and the actual number of changes in the flow direction are therefore not known.

Thus, it is simpler to consider the plate heat exchanger as a rough channel; using the mass flow velocity, the actual heat transfer area, the effective diameter, and finally the length between port centers as characteristic length to correlate friction pressure drop and heat transfer, see eqs. (81) and (83) thru (85).

Plotting the friction factor and the Nusselt number vs. the Reynolds number indicate one benefit of using plate heat exchangers in single phase flow: the thermal and hydraulic characteristics for different Reynolds numbers display no abrupt change in neither of the two, see Figure 11, in the transition from low to high Reynolds numbers. This feature is especially beneficial in applications in which the flow rate is changed for capacity control.

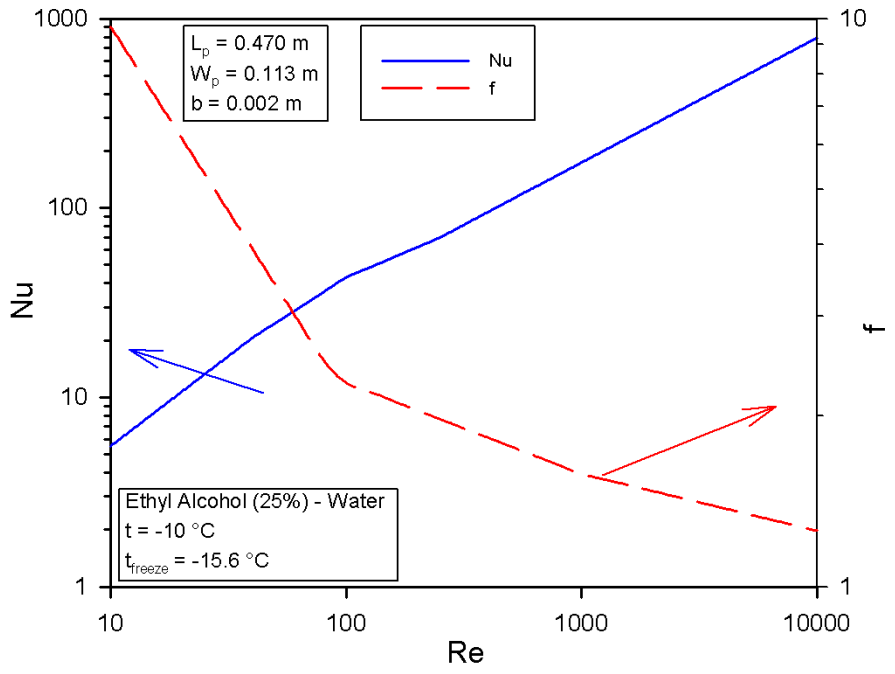

Figure 11: Single phase thermal and hydraulic characteristics as function of Reynolds number. The curves area calculated using correlations from one manufacturer.

8.4 Single phase flow

The heat transfer and pressure drop in plate heat exchangers have been investigated for several years, and the number of reports has become rather extensive. On the other hand, the possible combinations of geometric parameters are almost infinite. Hence, there does not exist any general theory or correlation covering all geometrical combinations. Each investigation should therefore rather be regarded as a special case and the results only applicable for the specific geometry tested. Unfortunately, all geometric parameters are seldom reported in detail.

8.4.1 Overall thermal performance

Bounopane et al. (1963) presented an overview of the thermal performance of plate heat exchangers and suggested values for the correction factor for the logarithmic mean temperature difference. For a two-channel heat exchanger (one thermal plate), pure counter-current flow may be assumed. For all other single pass heat exchangers, the correction factor was given as 0.967 and 0.942 for even and odd number of thermal plates, respectively. Kandlikar and

Shah (1989a,b) later conducted a more refined analysis, where correction factors for LMTD and effectiveness-NTU correlations were given for a number of different flow configurations.

Bond (1981) presented data for plate heat exchangers from the APV Company. He states that mixed angle plates may be used to extend the range of available chevron angles. The performance of the mixed plates may be estimated using the average chevron angle, according to the author. This was later confirmed by Walton (2001), who used mass transfer tests to determine local mass transfer coefficients in mixed angle plate heat exchangers. Walton states that even though the individual plates have very different mass transfer characteristics, the integral mass transfer performance is very similar to a plate pair having a single chevron angle equal to the arithmetic mean of the chevron angles of the two mixed plates.

One of the major contributors to the knowledge of single phase heat transfer and pressure drop of plate heat exchangers is Focke. Together with co-workers he has published several papers concerning e.g. effect of chevron angle (Focke 1983, Focke et al. 1985), asymmetrically corrugated plates (Focke, 1985), flow visualizations (Focke and Knibbe 1986), and a method of selecting optimum plate heat exchanger surface pattern using heat transfer pressure drop analogies (Focke 1986).

8.4.2 Film heat transfer coefficient

The film heat transfer coefficient for plate heat exchangers has been investigated by several researches. Most of them correlate the heat transfer coefficient using a modified Dittus-Boelter type of equation, where the constants and exponents are changed.

Focke (1995) investigated several heat transfer analogies. He concludes that all the transport analogies tested approximately holds for plate heat exchangers.

Bogaert and Bölcs (1995) investigated experimentally heat transfer and pressure drop of plate heat exchangers from SWEP. This paper is interesting since it is almost the only one where the exponents on the Prandtl number and on the viscosity ratio are not constants, and are explicitly given. A similar expression for the exponent on the viscosity ratio for calculation of the friction factor has also been reported by Shah and Focke (1988). The Nusselt number was given by Bogaert and Bölcs (1995) as

$$Nu = B_1 \cdot Re^{B_2} \cdot Pr^{\frac{1}{3}e^{\frac{6.4}{Pr+30}}} \cdot \left(\frac{\mu}{\mu_w}\right)^{\frac{0.3}{(Re+6)^{0.125}}} \qquad (94)$$

where B_1 and B_2 are empirical constants specific for a certain plate and a certain Reynolds number range. This kind of correlation is recognized as a modification of the well-known Dittus-Boelter correlation. It is the absolutely most common type of heat transfer correlation for plate heat exchangers found in the literature, even though the constants are different, and the exponents on the Prandtl number and the viscosity ratio are often constants.

A similar correlation was suggested by Muley (1997). He developed empirical correlations for the parameters B_1 and B_2 in eq. (94), both being functions of the chevron angle and the area enlargement factor. The same correlations are also reported in Muley and Manglik (1999). The correlations are based on data from the literature as well as on their own experimental data. The final correlation for the Nusselt number at low Reynolds numbers was stated as

$$\mathrm{Nu} = 0.44 \cdot \left(\frac{\varphi}{30} \right)^{0.38} \cdot \mathrm{Re}^{0.5} \cdot \mathrm{Pr}^{1/3} \left(\frac{\mu}{\mu_w} \right)^{0.14} \qquad \begin{bmatrix} 30° \le \varphi \le 60° \\ 30 \le \mathrm{Re} \le 400 \end{bmatrix} \quad (95)$$

and for higher Reynolds numbers

$$\mathrm{Nu} = \mathrm{A}(\varphi) \cdot \mathrm{B}(\phi) \cdot \mathrm{Re}^{\mathrm{C}(\varphi)} \cdot \mathrm{Pr}^{1/3} \cdot \left(\frac{\mu}{\mu_w} \right)^{0.14} \qquad \begin{bmatrix} 30° \le \varphi \le 60° \\ \mathrm{Re} \ge 1\,000 \end{bmatrix} \quad (96)$$

where

$$\mathrm{A}(\varphi) = 0.2668 - 0.006967 \cdot \varphi + 7.244 \cdot 10^{-5} \cdot \varphi^2 \quad (97)$$

$$\mathrm{B}(\phi) = 20.7803 - 50.9372 \cdot \phi + 41.1585 \cdot \phi^2 - 10.1507 \cdot \phi^3 \quad (98)$$

and

$$\mathrm{C}(\varphi) = 0.728 + 0.0543 \sin\left(2 \cdot \pi \cdot \varphi / 90 + 3.7\right) \quad (99)$$

No correlation was given for Reynolds numbers between 400 and 1 000.

Crozier et al. (1964) described the use of plate heat exchangers with non-Newtonian fluids. However, perhaps the most interesting fact with this paper is the statement that the heat transfer in plate heat exchangers may be calculated using the Lévêque approximation under certain conditions. This idea was exploited independently by Martin (1996) who developed a semi-theoretical correlation for heat transfer and pressure drop in plate heat exchanger. Martin used the hydraulic diameter in defining the Reynolds and Nusselt numbers, thus

$$Re = Re_h \cdot \phi \tag{100}$$

and

$$Nu = Nu_h \cdot \phi \tag{101}$$

Martin developed his correlation by extending the Lévêque theory into the turbulent region. The final expression for the Nusselt number was given as

$$Nu_h = 0.122 \cdot Pr^{1/3} \cdot \left(\frac{\mu}{\mu_w} \right)^{1/6} \cdot \left[\xi \cdot Re_h^2 \cdot \sin(2 \cdot \varphi) \right]^{0.374} \tag{102}$$[i]

The range of validity of the correlation is not explicitly given in the original reference, however it seems that the Reynolds number was varied between 400 to 10 000. The reader is referred to the sources of the original reference.

Gaiser and Kottke (1998) also investigated the chevron angle (φ) and the effect of corrugation pitch (Λ) on heat transfer and pressure drop. With a large chevron angle, small corrugation pitch gave lower heat transfer coefficients than a wider corrugation pitch. There was no significant difference obtained for small chevron angles.

A comparison of the three correlations explicitly given above is interesting:

Eq. (94) is used by a major Swedish plate heat exchanger manufacturer. The constant and exponents are fitted to experimental data for each heat exchanger. The two correlations by Muley, eq. (95) and eq. (96), is an attempt to generalize the Dittus-Boelter type of correlation as dependencies of chevron angle and enlargement factor are included. However, these correlations are still merely curve fits using the standard form of the correlation for the Nusselt number. The Martin (1996) correlation is another attempt to generalize the correlation for the Nusselt number by applying a heat transfer-pressure drop analogy. However, several of the parameters are fitted to experimental data, making this a semi-empirical correlation.

In addition to the correlations mentioned above, Wanniarachchi et. al. (1995) investigated heat transfer in chevron type plate heat exchangers for different chevron angles. They correlated the data with an asymptotic correlation, with two parts, laminar and turbulent. The correlation is

---

[i] N.B. Martin used the hydraulic diameter, d_h, in his correlation.

$$j_{Nu} = \sqrt[3]{j_{Nu_l}^3 + j_{Nu_t}^3} \tag{103}$$

where

$$j_{Nu,l} = \frac{3.65}{\beta^{0.455} Re_{d_h}^{0.339}} \tag{104}$$

$$j_{Nu,t} = \frac{12.6}{\beta^{1.142}} Re_{d_h}^{0.646+0.00111\cdot\beta} \tag{105}$$

and

$$j_{Nu} = \frac{Nu_{d_h}}{Pr^{1/3} (\mu/\mu_w)^{0.17}} \tag{106}$$

However, if the chevron angle β is smaller than 28°, then the heat transfer coefficient is evaluated using $\beta = 28°$. The relation between the different chevron angles is

$$\beta = 90 - \varphi \tag{107}$$

It may be interesting to investigate the performance of some of the available correlations from literature, compared to one manufacturers (SWEP) correlation for a specific plate. For this, the correlations by Martin (1996), Wanniarachchi et. al. (1995), and Muley (1997) were used. These correlations are somewhat general in the sense of including some of the effects of the plate geometry.

As may be seen in Figure 12, good agreement was obtained with Martin (1996) and Wanniarachchi et al. (1995). The correlation of Muley (1997) under-predicts the heat transfer at low Reynolds numbers, and over predicts the heat transfer at high Reynolds numbers.

Wanniarachchi et. al. (1995) suggested that their correlation would be used as a preliminary design tool. Good agreement with one tested plate heat exchanger was obtained. Regarding the correlation suggested by Martin (1996) the difference is somewhat larger at lower Reynolds numbers and a slightly better agreement is found at higher Reynolds numbers. In this correlation, there is also the possibility to adjust some of the parameters if experimental data is available.

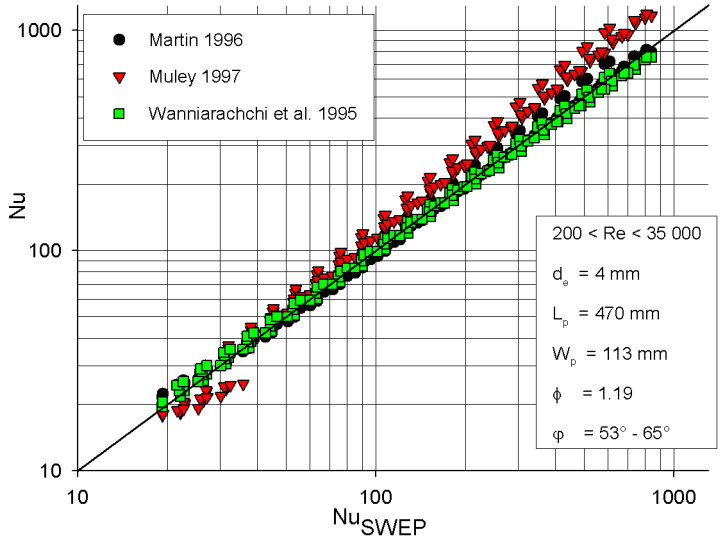

Figure 12: Comparison between Martin (1996), Wanniarachchi et al. (1995), Muley (1997), and the correlation by SWEP International AB.

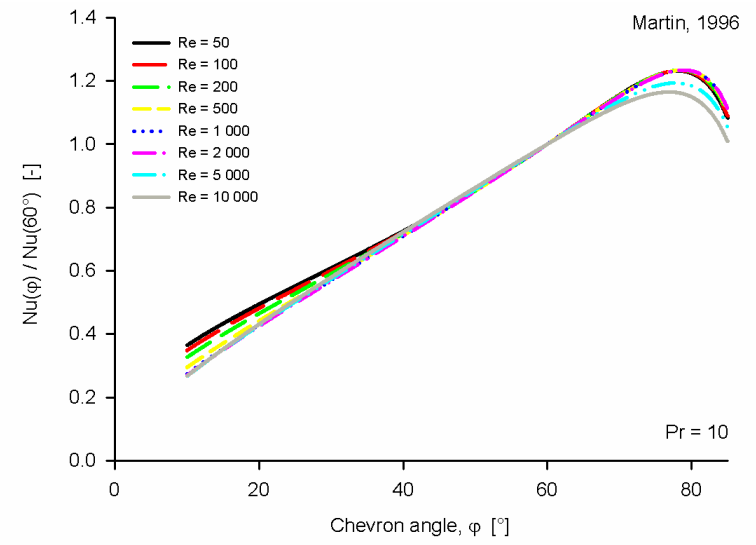

Figure 13: Influence of chevron angle on the heat transfer coefficient according to Martin (1996).

The chevron angle is perhaps the most important geometrical parameter on heat transfer and pressure drop. The effect of chevron angle on the heat transfer is shown in Figure 13, where the correlation by Martin (1996) has been used. As

may be seen, significant different heat transfer coefficient may be expected with different chevron angles.

8.4.3 Pressure drop performance

Martin (1996) developed his heat transfer correlation by extending the Lévêque theory into the turbulent region. The pressure drop was correlated, using the Moody friction factor, as

$$\frac{1}{\sqrt{\xi}} = \frac{\cos\varphi}{\sqrt{0.18\tan\varphi + 0.36\sin\varphi + \xi_0 / \cos\varphi}} + \frac{1-\cos\varphi}{\sqrt{3.8\cdot\xi_{1,0}}} \tag{108}$$

where

$$\mathrm{Re_h} < 2000 \Rightarrow \begin{cases} \xi_0 = \dfrac{64}{\mathrm{Re_h}} \\ \xi_{1,0} = \dfrac{597}{\mathrm{Re_h}} + 3.85 \end{cases}$$

$$\mathrm{Re_h} \geq 2000 \Rightarrow \begin{cases} \xi_0 = \left(1.8\log_{10}\mathrm{Re_h} - 1.5\right)^{-2} \\ \xi_{1,0} = \dfrac{39}{\mathrm{Re_h}^{0.289}} \end{cases} \tag{109}$$

Similar as for the heat transfer case, Muley (1997) developed an empirical pressure drop correlation with dependencies of the chevron angle and the surface enlargement factor. The frictional pressure drop factor was correlated as

$$\mathrm{f} = \left[\left(\frac{30.2}{\mathrm{Re}}\right)^5 + \left(\frac{6.28}{(\mathrm{Re})^{0.5}}\right)^5\right]^{1/5} \cdot \left(\frac{\varphi}{30}\right)^{0.83} \cdot \left(\frac{\mu}{\mu_w}\right)^{-0.22} \qquad \begin{bmatrix} 30° \leq \varphi \leq 60° \\ 2 \leq \mathrm{Re} \leq 400 \end{bmatrix} \tag{110}$$

for low Reynolds numbers and

$$\mathrm{f} = \mathrm{A}(\varphi)\cdot\mathrm{B}(\phi)\cdot\mathrm{Re}^{\mathrm{C}(\varphi)}\cdot\left(\frac{\mu}{\mu_w}\right)^{-0.22} \qquad \begin{bmatrix} 30° \leq \varphi \leq 60° \\ \mathrm{Re} \geq 1\,000 \end{bmatrix} \tag{111}$$

where

$$\mathrm{A}(\varphi) = \left(2.917 - 0.1277\cdot\varphi + 2.016\cdot10^{-3}\cdot\varphi^2\right) \tag{112}$$

$$B(\phi) = \left(5.4742 - 19.0197 \cdot \phi + 18.9338 \cdot \phi^2 - 5.3405 \cdot \phi^3\right) \quad (113)$$

and

$$C(\varphi) = -\left\{0.2 + 0.0577 \sin\left(2 \cdot \pi \cdot \varphi/90 + 2.1\right)\right\} \quad (114)$$

for higher Reynolds numbers. No correlations were given for the intermediate range of Reynolds numbers.

Lee et al. (2000) investigated the influence of plate length to plate width ratio (denoted as Aspect Ratio) on the overall heat transfer and pressure drop performance. They modified a correlation from the literature (Muley and Manglik, 1999) to account for different aspect ratios. Three different plates, with two different lengths and two different widths, were investigated. They found that for Aspect Ratio 4 and 2.4, the frictional pressure drop performances were the same. These Aspect Ratios correspond to the smaller plate width. It may be speculated that the width of the plate is the main parameter affecting the frictional pressure drop performance, since a larger part of the heat exchanger is used for distributing the flow across the width of the plate for a wider plate having the same plate length.

The pressure drop in the ports is also important. One widely cited reference giving a correlation for this pressure drop is Shah and Focke (1988). This review paper summarizes the current knowledge of single phase flow in plate heat exchangers at that time. In this paper, an estimation of the pressure drop in the ports was given, without any reference, as

$$\Delta p_{\text{manifolds and ports}} = 1.5 \cdot \left(\frac{G^2}{2 \cdot \rho}\right)_i \cdot N \quad (115)$$

where N is the number of fluid passes (usually one for heat pump applications).

8.4.4 Numerical simulations of heat transfer and fluid flow and the implications on experimental true local film heat transfer coefficients

A number of CFD simulations of the flow in plate heat exchanger have been reported, e.g. Mehrabian (1996), Claesson (1996), Manglik and Ding (1997), Sawyers et al. (1998), Sadasivam et al. (1999), Mehrabian and Poulter (2000), Ciofalo et al. (2000), Blomerius and Mitra (2000), Ciofalo and Di Piazza (2002), Croce and D'Agaro (2002), and Metwally and Manglik (2004). Most of them (all) concerns heat transfer and pressure drop in one or a few unitary cells, i.e. the repetitive pattern occurring in plate heat exchangers. The present author is not aware of any published reference of CFD-simulation of an entire plate.

Claesson (1996) found that the local heat transfer coefficient within a unitary cell varies significantly. Walton (2001) observed similar variation in his mass transfer tests. These local variations within each cell will make it difficult to obtain truly local flow boiling heat transfer coefficients, since the wall temperature may be expected to vary locally within each cell. In addition, it is already difficult to get an accurate temperature reading at one location without disturbing the flow field and hence alter the heat transfer coefficient. How difficult would it not be to measure the temperature field across an entire surface, within a rather narrow geometry, and at the same time measure two local fluid temperatures, again without significantly disturbing the flow field and thus the heat transfer? It is the belief of the present author that truly local flow boiling coefficients will not be obtainable within the near future, due to the above mentioned reasons. We will have to cope with "semi-local" heat transfer coefficients, i.e. measure, directly or indirectly, the average unitary cell heat flux and use single phase correlations on the heating (water) side to obtain a unitary cell average wall temperature. Thus, the unitary cell flow boiling heat transfer coefficient will be based on that wall temperature.

8.4.5 Flow distribution between channels and within a single channel

Few reports are published on the flow distribution between the different flow channels. Heggs et al. (1996) investigated the detrimental effect of flow maldistribution in plate heat exchangers by varying the number of plates and testing both U- and Z-flow configuration. They found that the effectiveness reached an asymptotic value less than one as the number of plates was increased. The effectiveness calculated with uniform flow distribution will never be reached. Kandlikar and Shah (1989b) found that the LMTD correction factor reached asymptotic values, close to one, as the number of plates become large, typically more than 40 plates. Kandlikar and Shah (1989a) continued and derived closed form effectiveness-NTU formulas for the 'many plates' case ($n_p = \infty$) for a number of pass arrangements. Rao et al. (2002) presented a mathematical model predicting the effectiveness of plate heat exchangers accounting for flow maldistribution between channels. Nuijens et al. (1991) presented a mathematical model for the U-flow (see Figure 14) arrangement, including header frictional pressure drop. Thonon and Mercier (1996), Amooie-Foumeny (1977), and Wilkinson (1974) also investigated the effect of maldistribution between channels in plate heat exchangers, see Figure 14.

In addition to the above, another flow maldistribution occurs in plate heat exchangers, i.e. the maldistribution of the flow within each channel. André (2001) conducted an appealing simple approach in his Master of Science thesis. He used friction factors being functions of flow direction relative to main flow direction to simulate the 2D flow field in the plate heat exchanger channel. Haseler et al. (1992) investigated experimentally the temperature profiles on the

port side and non-port side, thus observing if the flow distribution deviates from perfect, in the channel and observed a difference.

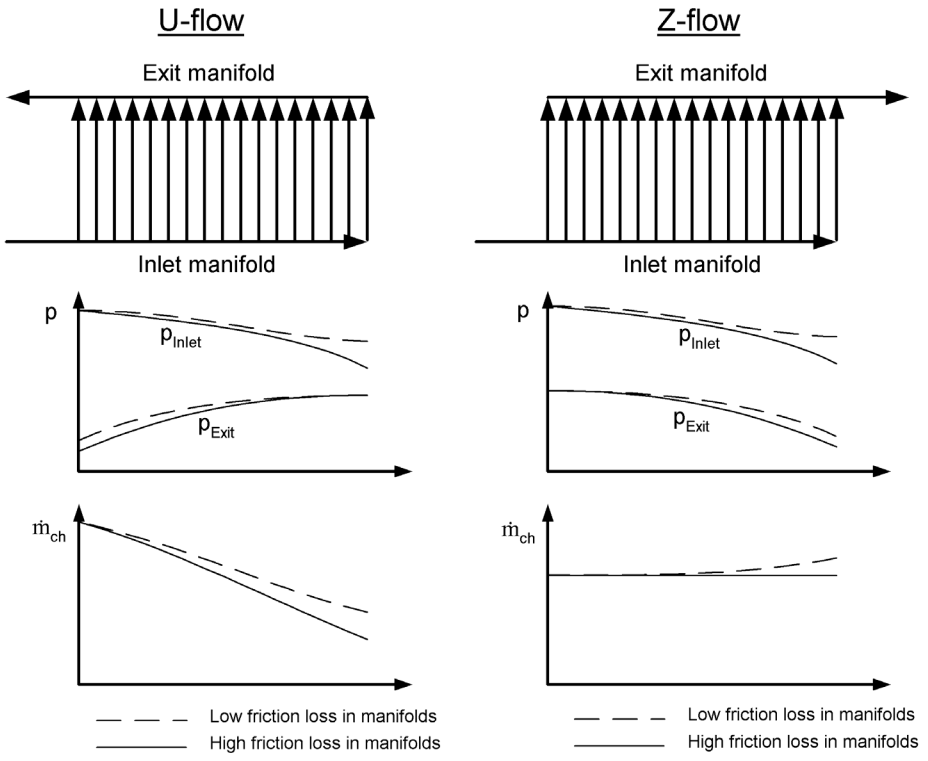

Figure 14: Manifold pressure and channel flow distribution of U and Z flow arrangement, adopted from Wilkinson, 1974.

8.5 Two phase flow

The literature on two-phase flow and flow boiling in plate heat exchangers is not as extensive as the corresponding literature for single phase flow. In this section, some of the literature for two-phase flow and heat transfer during boiling will be reviewed.

8.5.1 Adiabatic two-phase flow characteristics

Reports on a number of investigations on adiabatic two-phase flows in plate heat exchangers have been published in the literature. Most of the investigations of adiabatic flows concern pressure drops and flow visualizations.

Kreissig and Müller-Steinhagen (1992) experimentally determined the frictional pressure drop in two commercial plate heat exchangers for water and air mixtures. The pressure drops in the ports were estimated and subtracted from the measured values. Tribbe and Müller-Steinhagen (1997) studied air-water as fluid pair and observed an almost linear relationship between vapor quality and pressure drop at high vapor qualities. Only a small influence of the channel gap (pressing depth) was observed. Tribbe (1998) studied air combined with several fluids in plate heat exchangers. The pressure drop over the entire plate heat exchanger as well as over the heat transfer section was measured. Depending on the chevron angle, different relations between Lockhart-Martinelli parameter and the two-phase multiplier were obtained. The Chisholm parameter, C, was reported to range from 4 to 20.

Winkelman et al. (1999) studied air-water pressure drop in plate heat exchangers. Using the Lockhart-Martinelli approach the data was correlated with the Chisholm parameter set to 6. They also reported that no mist flow was observed during the experiments. Bai and Newell (2000) investigated air and alkylbenzene oils. They found the oil/air pressure drop curve having similar trend as the dry air pressure drop curve, indicating that the two phase flow pressure drop may be predicted using a similar correlation as used for single phase flow. Tribbe and Müller-Steinhagen (2001 a,b) studied mixtures of air and water or air and carboxymethylcellulose in a typical industrial plate heat exchanger. They found that, when modeling the two-phase flow using the Lockhart-Martinelli approach, the Chisholm parameter C seemed to be influenced by the Lockhart-Martinelli parameter, X, and liquid viscosity. They recommend not to use a single value of the Chisholm parameter, since large errors may be expected.

Vlasogiannis et al. (2002) investigated air-water flow in plate heat exchangers. The two-phase mixture was supplied via a traditional inlet port of the heat exchanger. A flow map was constructed. Five different flow regimes were identified. Shiomi et al. (2004) studied water and air in a geometry similar to plate heat exchangers with different chevron angles, however no ports were used. In vertical flow direction, only dispersed bubble flow pattern (see Figure 3: Bubble flow) was observed. Good agreement with data was obtained using a low value ($C = 5 – 10$) of the Chisholm parameter.

The above references concern two-component, two-phase flows, which differs from the evaporator application, with one-component, two-phase flows. However, as is known from circular tube tests, the Lockhart-Martinelli approach developed for air-water at atmospheric pressure seems to work for one-component, two-phase flows.

8.5.2 Flow boiling heat transfer characteristics

The number of publications concerning flow boiling heat transfer in plate heat exchangers is increasing, and in this section, a brief summary of some of the existing investigations are given.

Panchal et al. (1983) investigated ammonia and R22 in plate heat exchangers. They could not determine the individual film heat transfer coefficients since the refrigerant side heat transfer coefficient seemed to be affected by the water flow rate. They found indications that heat transfer was governed by nucleate boiling, and by applying "Linde High Flux" coating on the heat transfer wall they increased the boiling heat transfer coefficient with more than a factor two. They suggest that the ammonia boiling heat transfer coefficient would be rather insensitive to the chevron angle and ammonia flow rate at a given heat load.

Cohen and Carey (1989) investigated flow boiling in cross-ribbed channels, a geometry very similar to plate heat exchangers. A transparent plate facilitated visual inspection of the flow boiling. The rib spacing and rib angle had a significant effect on flow boiling. Very little bubble nucleation was visually observed. However, for two tested geometries, the heat transfer data suggested that the heat transfer coefficient varied with heat flux. For the other two tested geometries, no evidence of heat flux dependency was observed.

Engelhorn and Reinhart (1989) measured heat transfer coefficients during evaporation in a plate heat exchanger. The refrigerant mass flow rate had only a slight effect on boiling heat transfer, while the water flow rate and the heat flux had a larger influence. The same authors (Engelhorn and Reinhart, 1990) also tested a plate heat exchanger evaporator with and without inlet distributor, and with and without superheating the refrigerant at the exit of the evaporator. The overall heat transfer coefficient decreased by 25% when the gas was superheated[i] at the exit.

Osterberger and Slipcevic (1990) tested the boiling heat transfer in plate heat exchangers using R22 as refrigerant. The mass and heat flux were in a typical range for heat pump applications. They concluded that the governing mechanism was nucleate boiling.

Kumar (1992) investigated boiling heat transfer and concluded that dryout occurs at rather high vapor qualities, above 70%. He also found that the heat transfer coefficient is independent of mass flux.

---

[i] No information on the amount of superheat was given in the reference.

Heggs et al. (1993) presented effectiveness – NTU and LMTD-corrections for plate heat exchangers where one stream undergoes phase change. Three cases were considered; a) the phase change stream has one more flow channel than the single phase stream, b) phase change stream has one less flow channel than the single phase stream, and finally c) equal number of flow channels. They conclude from their investigation that the two outermost channels should contain the phase changing stream, quite opposite common practice for evaporators in domestic heat pumps.

Haseler and Butterworth (1995) discussed flow boiling heat transfer in compact heat exchangers (plate heat exchanger being one of the types discussed). They suggest that the Lockhart-Martinelli parameter should be calculated from the original definition, i.e. the ratio of the pressure drops of gas and liquid fractions. In addition, they suggest that plate heat exchangers with high single phase heat transfer coefficients do not necessarily have high boiling heat transfer coefficients.

Thonon et al. (1995, 1997) reported on recent research in plate heat exchangers. They used the product of the boiling number and the Lockhart-Martinelli parameter as a criterion for the transition between nucleate boiling and convective evaporation.

Margat et al. (1997) found that the heat transfer coefficient was not influenced by the electrically imposed heat flux, but rather by vapor quality and mass flux.

Pelletier (1998) investigated the use of propane and other hydrocarbons as a substitute for R-22 in domestic heat pumps. The performances of the different heat pump components were evaluated. For the evaporator it was found that the pool boiling correlation by Cooper (1984) correlated well the total area averaged refrigerant side film heat transfer coefficient, with five degrees of superheat of the refrigerant at the exit of the evaporator.

Yan and Lin (1999) investigated flow boiling of R134a in a single channel plate heat exchanger. This paper is one of few which reports local heat transfer coefficients. They observed a sharp increase in the heat transfer coefficient at a vapor quality of 45%. At this high vapor quality, they claimed that the liquid film breaks up into tiny droplets. The resulting mist flow is then supposed to drastically increase the local heat transfer coefficient due to impinging droplets on the wall. They could not find any significant effect of the local heat flux in the higher vapor quality range. They also conducted visualization tests and observed intense nucleation at the refrigerant inlet. At higher vapor qualities, they observed mist flow which was claimed to dominate in a larger portion of the channel.

Donowski and Kandlikar (2000) reused the experimental data from Yan and Lin (1999) and adjusted the Kandlikar (1990) correlation to fit the data.

Hsieh and Lin (2002) studied boiling of R410A in a plate heat exchanger. They reported that mass flux affects the boiling heat transfer only at high imposed heat flux. The heat transfer coefficient seemed to vary almost linearly with imposed heat flux.

In a later publication (Hsieh and Lin 2003) they reported that the heat transfer coefficient increases with increased vapor quality, except at low vapor qualities. In addition, raising the heat flux significantly increased the heat transfer coefficient.

Han et al. (2003) investigated heat transfer and pressure drop in plate heat exchangers with different chevron angles using R22 and R410A. The refrigerant heat transfer coefficient increased with increasing vapor quality and with decreasing evaporating temperature. They suggest that convective evaporation is the main boiling mechanism.

According to the cited references, it is still not clear whether the flow boiling heat transfer coefficient is governed by nucleate or convective boiling. Both mechanisms have been reported in the literature as the governing heat transfer mechanism. It may be reasonable to assume that, as reported by Thonon et al. (1995, 1997), the heat transfer coefficient may be governed by both mechanisms, as is the case for large smooth pipes.

8.5.3 Flow boiling pressure drop characteristics

As for flow boiling heat transfer, the number of publications concerning flow boiling pressure drop in plate heat exchangers is not extensive. In this section a brief summary of some of the existing investigations are given.

Le Pellec et al. (1996) conducted tests with ammonia in an evaporator configured as a DX-evaporator as well as a flooded evaporator. The results from the evaporator with direct expansion indicated the importance of having an appropriate inlet flow distribution device. The flooded configuration using gravity for circulating the ammonia displayed no such distribution problems. However, several problems with flow instabilities were encountered.

Sterner and Sundén (1997) used ammonia in four different commercial plate heat exchangers. The Chisholm parameter in the Lockhart-Martinelli approach were estimated for the different heat exchangers. They found the Chisholm parameter to be significantly higher than that reported by other investigators, and correlated the Chisholm parameter with the all-liquid Reynolds number.

Margat et al. (1997) found that the void fraction was over predicted using the homogeneous model. The pressure drop was correlated successfully using the approach by Lockhart-Martinelli with the Chisholm parameter, C, equal to 3.

In conclusion, the research community seems to agree on the use of the Lockhart-Martinelli approach to calculate two-phase pressure drop in plate heat exchangers. However, the value of the Chisholm parameter is not agreed on, even though most investigations indicate the value to lie within the classical range (5 – 20) as originally stated by Chisholm (1967) for gas-liquid density ratios similar to air-water at atmospheric pressure.

8.6 Conclusion

This brief literature survey presented above indicates that the single phase heat transfer is well explored and correlated. Three different one-phase correlations have been compared to an experimentally based one-phase heat transfer correlation. Two of the suggested correlations deviate less than 10 % within the tested range. The correlation suggested by Wanniarachchi et. al. (1995) is by far the simplest of the three; however it seems that the correlation by Martin (1996) has a wider applicability due to the wider possibility to adjust the correlation to experimental data, if available.

As may be noted, there is still some debate in the literature concerning the mechanisms behind heat transfer of flow boiling in plate heat exchangers. As for small tubes, some authors claim that the main heat transfer mechanism is convective evaporation; others claim that it is nucleate boiling, and some suggest both mechanisms.

Concerning two-phase flow pressure drop, most investigators employ the classical Lockhart-Martinelli approach. However, different investigators present different values on the Chisholm parameter.

PART II

THE EVAPORATOR CONSIDERED AS A ONE ZONE HEAT EXCHANGER

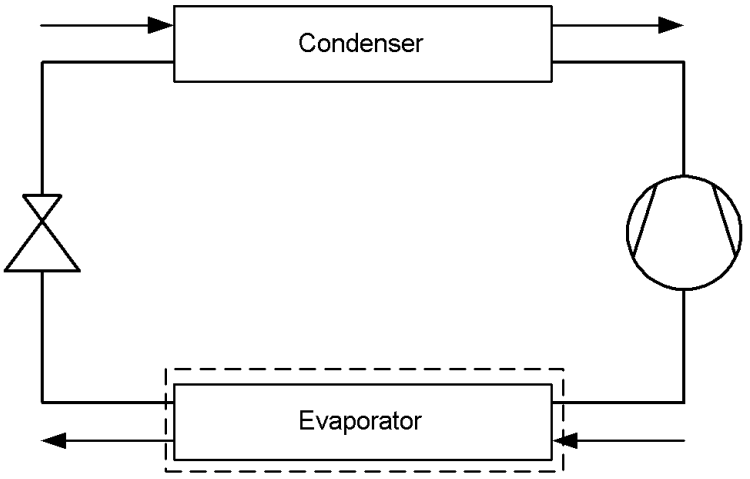

9 INTRODUCTION – PART II

This section of the thesis considers the evaporator as a one-zone heat exchanger, using the terminal temperatures and pressures to evaluate the performance. No information of the processes occurring inside the evaporator is measured. Even so, the temperature of the brine at the location where the refrigerant becomes saturated vapor is calculated from an energy balance. However, the actual position in evaporator where this occurs is not known and is not considered. The evaporator may be though of just as one of the components in the heat pump system considered. The impact of different heat pump running conditions is of interest in this chapter.

The section starts with an investigation where the overall heat flux is kept low. The reason for this is the demand for more efficient heat pumps. One way of increasing the efficiency of the heat pump is to decrease the temperature differences in the heat exchangers. This may be done by increasing the heat transfer area, thus decreasing the total area averaged heat flux. At these conditions, local temperature differences at the inlet or outlet may become small and limit the performance of the evaporator.

Next the influence of brine mass flow is investigated. The purpose is to investigate any change in performance of the evaporator as different brine mass flow rates are used. Then the section continues by investigating the possible benefit of using co- instead of counter-current flow configuration. The purpose is to explore whether increased wall superheat at the refrigerant inlet and decreased wall temperature at the high vapor quality range is beneficial from a performance point of view.

Then, the above experimentally tested running conditions are investigated numerically using two different boiling models. The purpose is to investigate different boiling models and compare the numerical trends with experimentally obtained trends. Even though the analysis is detailed and by no means treats the evaporator as a black box, the results are closely connected to the other chapters in this section, and are therefore placed here.

Finally, the section ends with a short chapter illustrating the impact of the design of the inlet refrigerant flow distributor and the resulting overall performance.

10 EXPERIMENTAL SETUP – PART II

The experimental equipment used during the tests consists of a well-instrumented lab rig; see Figure 15, simulating a domestic heat pump. R134a is used as refrigerant and a mixture of Ethanol (~24% by mass) and water is used as secondary refrigerant (brine). Water is used as heat carrier. An electric expansion valve from Siemens and a PID-controller from Eurotherm are used to control the superheat.

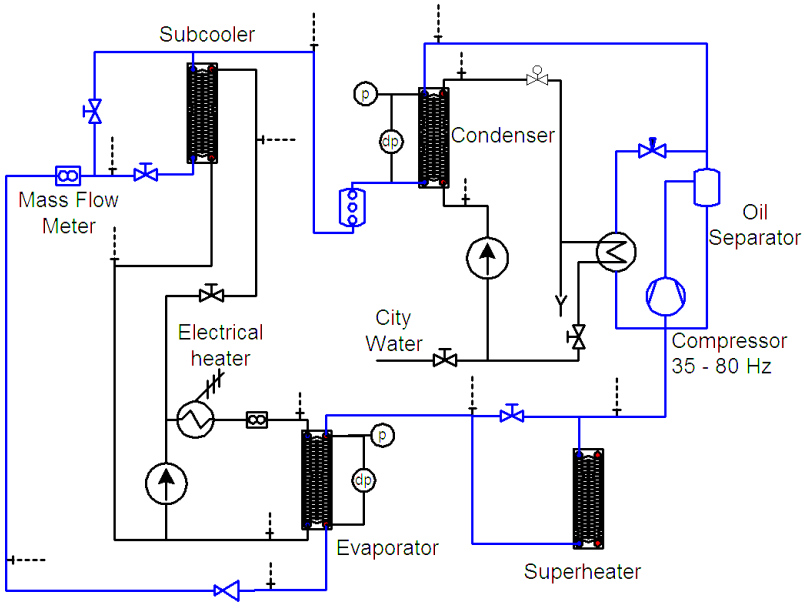

Figure 15: Experimental test rig.

A hermetic scroll compressor from Copeland is used, and a frequency inverter, allowing for testing different heat loads, adjusts its speed. Brazed plate heat exchangers from SWEP are used as evaporator and condenser.

The mass flow rate of the refrigerant is measured using a Micromotion Coriolis Mass Flow Meter and the brine volumetric flow rate is measured using a MagnetoFlow Primo from BadgerMeter. All temperatures are measured with T-type thermocouples. The cold junctions of each and every one of the thermocouples are connected to an isothermal block. The temperature of the isothermal block is measured by the logger and used as reference temperature. Pressure transducers from Druck limited are used for measuring absolute pressures (PDCR 960 & 961) and differential pressures (PDCR 2110 & 2160). Campbell Scientific Instrument type CSI 21X is used as data logger.

A computer program written in HP VEE communicates with the logger and retrieves the data. A reading is taken every 10th second and every measured point consists of 120 sequential readings from the logger. A stability criterion is used where 8 pre-chosen temperatures have to be within certain limits.

For all these 8 temperatures, HP VEE calculates the standard deviation. If the standard deviation is too large, the measured point is rejected and then a new trial is initiated. If the standard deviation is within the limit[i] then eight straight lines, one for each temperature, are produced using regression analysis. The difference between the first point (corresponding to the oldest reading) and the last point (corresponding to the newest reading) should not be greater than a preset value. If it is, the measurement point is rejected and a new trial is initiated. Having a too large difference between the most recent reading and the oldest reading indicates that the system has not reached steady state.

If all criteria are within the given range, HP VEE transfers all measured data for the last 120 readings into MS Excel. Then the set point for the next point (e.g. a new brine flow rate) is set to the auxiliary equipment and the computer waits for the next steady state.

[i] This was usually set to 0.1 K except for the temperature of the refrigerant leaving the evaporator.

11 DATA REDUCTION – PART II

In this section the evaporator is considered as a "classical" heat exchanger, i.e. the performance of the evaporator is determined from the terminal (inlet and outlet) temperatures. No information is retained of the actual evaporating process inside the evaporator.

Even so, we still wish to obtain some measure on the performance of the refrigerant side of the evaporator, i.e. a measure of the refrigerant side heat transfer coefficient. The problem, however, is that the evaporator consists of one boiling and one superheating section. Different approaches in calculating the temperature difference in the evaporator may be used:

1. Direct use of the terminal temperatures and calculating the LMTD as if it was a traditional single phase heat exchanger.

2. Disregarding the superheated section of the evaporator and using the terminal temperatures of the brine side and the saturation temperature of the refrigerant at both the refrigerant inlet and outlet of the evaporator.

3. Acknowledge the fact that the evaporator consists of two parts, make an assumption regarding the distribution and then calculate the temperature as an average of the two sections.

In this thesis, the third approach is chosen. The procedure followed seems to be first suggested by Dutto et al. (1991). The typical temperature profiles are shown in Figure 16. In this approach, the logarithmic mean temperature differences (LMTD) in the boiling and superheated sections are required. The LMTD in the boiling section is defined as

$$\vartheta_{evap} = \frac{\vartheta_1 - \vartheta''}{\ln\left(\frac{\vartheta_1}{\vartheta''}\right)} \tag{116}$$

and in the superheated section as

$$\vartheta_{sup} = \frac{\vartheta'' - \vartheta_2}{\ln\left(\frac{\vartheta''}{\vartheta_2}\right)} \tag{117}$$

The brine temperature at the location where the refrigerant becomes saturated vapor is calculated from an energy balance, i.e.

$$t''_{brine} = t_{brine_{in}} - \frac{\dot{m}_R \cdot c_{p_R} \cdot \Delta t_{sup}}{\dot{m}_{brine} \cdot c_{p_{brine}}} \tag{118}$$

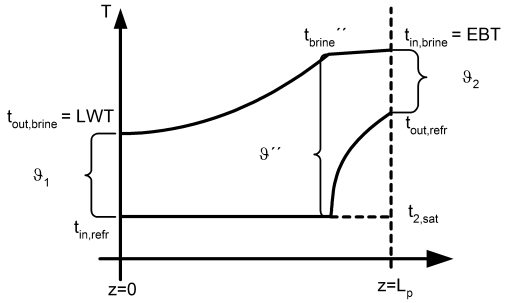

Figure 16: Typical temperature profiles in an evaporator.

The overall heat transfer coefficient is defined according to the approach by Dutto et al. (1991). They defined the overall heat transfer coefficient as the area averaged value of the boiling and superheated sections.

$$U_{CBE} \cdot A_{tot} = U_{evap} \cdot A_{evap} + U_{sup} \cdot A_{sup} \tag{119}$$

For each term of eq. (119), the following applies

$$UA = \frac{\dot{Q}}{\vartheta} \tag{120}$$

Hence, eq. (119) transforms into

$$\frac{\dot{Q}_{tot}}{\vartheta_{CBE}} = \frac{\dot{Q}_{evap}}{\vartheta_{evap}} + \frac{\dot{Q}_{sup}}{\vartheta_{sup}} \tag{121}$$

or equivalently

$$\vartheta_{CBE} = \frac{t_{brine_{in}} - t_{brine_{out}}}{\frac{t''_{brine} - t_{brine_{out}}}{\vartheta_{evap}} + \frac{t_{brine_{in}} - t''_{brine}}{\vartheta_{sup}}} \tag{122}$$

where we have assumed constant specific heat on the brine side throughout the entire heat exchanger. Using this expression as the appropriate temperature mean difference in the heat exchanger, the overall heat transfer coefficient may be calculated as

$$U_{CBE} = \frac{\dot{Q}_{tot}}{A_{tot} \cdot \vartheta_{CBE}} \tag{123}$$

Now, using this total area averaged overall heat transfer coefficient, a corresponding total area averaged film heat transfer coefficient on the refrigerant side may be calculated as

$$\alpha_{R,Dutto} = \frac{1}{\frac{1}{U_{CBE}} - \frac{1}{\alpha_{brine}} - \frac{\delta_{SS}}{\lambda_{SS}}} \tag{124}$$

To obtain the heat transfer coefficient on the refrigerant side, the film heat transfer coefficient on the brine side is apparently required, see eq. (124).

The measured mass flow rate of the brine fluid is used to calculate the brine side Reynolds number as

$$Re_{brine} = \frac{G_{brine} \cdot d_e}{\mu_{brine}} \tag{125}$$

where

$$G_{brine} = \frac{2 \cdot \dot{m}_{brine}}{W \cdot b \cdot n_p} \tag{126}$$

The Nusselt number on the brine side is calculated as (Pelletier, 1999)

$$Nu_{brine} = C_{Nu}\left(Re_{brine}\right) \cdot Re_{brine}^{C_{Re}(Re_{brine})} \cdot Pr_{brine}^{\frac{e^{6.4/(Pr_{brine}+30)}}{3}} \cdot \left(\frac{\mu_{brine}}{\mu_{brine_W}}\right)^{\frac{0.3}{(Re_{brine}+6)^{0.125}}} \tag{127}$$

In the present thesis, the last term (viscosity ratio) is neglected, due to the limited impact in heat pump applications, where the wall temperature and the bulk temperature of the brine only differ a few degrees. However, for single phase applications, where significant temperature difference between the bulk and the wall may be present, the viscosity ratio may not be neglected.

Using the Nusselt number, the film heat transfer coefficient on the brine side may be calculated as

$$\alpha_{brine} = \frac{Nu_{brine} \cdot \lambda_{brine}}{d_e} \tag{128}$$

The above analysis also holds for the case where the refrigerant leaves the evaporator without any superheat. In that case, eq. (122) is reduced to the logarithmic mean temperature difference of the boiling section, which in that case is the entire heat exchanger. The derivation of the uncertainty of the measurement and eq. (124) is found in Appendix E.

12 EVAPORATOR HEAT TRANSFER PERFORMANCE AT LOW HEAT FLUX AND LOW BRINE FLOW RATE[i]

The primarily goal of this investigation is to study how the evaporator performs under low overall heat flux, and in particular, low temperature difference in the upstream part (refrigerant inlet) of the evaporator. To this end, low brine flow rates are used, giving a high brine temperature change in the evaporator. Three different brine temperature drops are investigated; 5 K, 10 K, and 15 K. The overall heat flux is varied from 1 500 W/m² to 4 500 W/m².

12.1 Test procedure

The tests are conducted in a test facility very similar to Figure 15, using the same kind of measuring equipment. The major difference is the compressor and how the refrigerating power is controlled. Further information on the specific test facility may be found in Claesson et al. (2003).

The refrigerating power in the evaporator (a V16x70 from SWEP International AB) is controlled using a valve situated in the suction line. The set point to the condenser is adjusted to give an inlet vapor quality to the evaporator of 20%. Then, the water flow is adjusted to give the desired water temperature drop in the evaporator. The superheat in the evaporator is kept to 7 K for all tests. Evaporating temperatures of 0.5 °C, 2.5 °C and 5 °C are tested (corresponding to evaporation pressure of R134a of 2.98 bar(a), 3.2 bar(a) and 3.50 bar(a) respectively). As already mentioned, the heat flux is varied between 1 500 W/m² and 4 500 W/m² and three different water temperature drops, 5 K, 10 K and 15 K, are tested.

12.2 Data reduction

The heat loads in the evaporator are calculated on the refrigerant side, $Q_{2,refr}$, and on the water side, $Q_{2,brine}$. The mean value of these two is used as the heat load in the evaporator and the respective mass flows are adjusted accordingly. The thermodynamic properties of R134a are estimated using Refprop 6.01 from NIST (1998) and Wagner & Kruse (1998) is used for estimating the properties of water.

---

[i] This chapter is based on: Claesson J., Afghani M., Palm B., 2003, Influence of large temperature difference in a compact brazed plate evaporator with low overall heat flux, in Proc. Eurotherm no. 72: Thermodynamics, Heat and Mass Transfer of Refrigeration machines and heat pumps, eds. J.M. Corberán, R. Royo, Valencia, Spain, March 31 – April 2, pp. 33-37.

The data reduction procedure has already been presented in chapter 11. The uncertainty analysis of the experimental data is found in Appendix E.

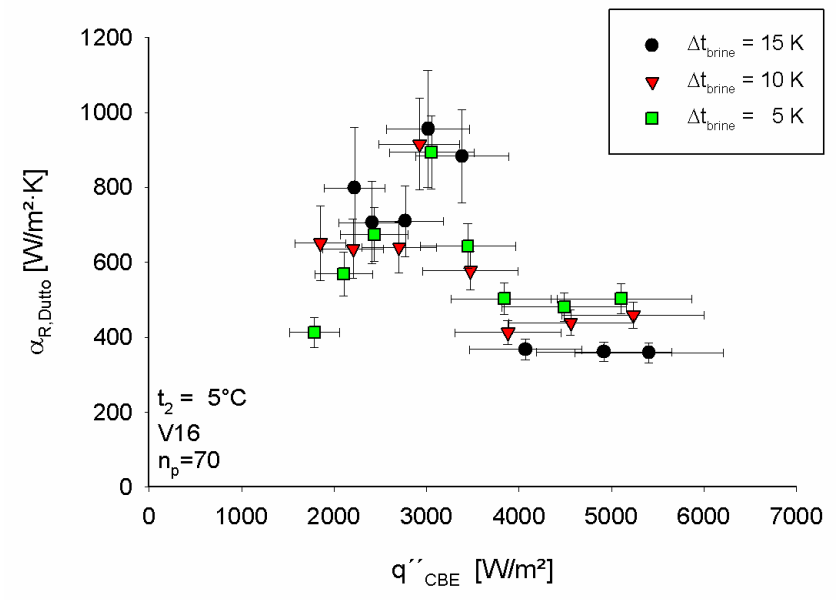

Figure 17: Heat transfer coefficients as a function of heat flux, $t_{2,sat}$ = 5°C.

12.3 Experimental results and discussion

The total area averaged refrigerant film heat transfer coefficients are plotted in Figure 17. It seems to exist a maximum of the heat transfer coefficient at approximately 3 000 W/m². At low heat flux the heat transfer coefficient seems to increase to some extend with increasing heat flux and suddenly reaching the maximum value, then rapidly decrease to a value even lower than at low heat flux.

Figure 17 also shows the estimated uncertainty of the measurements. The highest uncertainty is observed at the peak of the heat transfer coefficient. The uncertainty becomes rather low in the higher heat flux range. It should perhaps also be noted that the major contributor to the uncertainty of the heat flux is the determination of the specific enthalpy of the refrigerant. It is assumed that this uncertainty is 5 % of its value.

It may also be seen in Figure 17 that the temperature drop on the brine side of the evaporator does influence the heat transfer coefficient, not only in the lower heat flux region but also in the higher heat flux region.

In the kind of system considered, domestic heat pumps, it is important to not only focus on the heat transfer coefficient on the refrigerant side. The

Coefficient Of Performance, COP_1, is the means to estimate the efficiency of the heat pump. For an ideal (Carnot) heat pump, this is entirely determined from the evaporating and condensing temperatures (Moran and Shapiro, 1998). One should therefore minimize the temperature difference between the available heat source and the evaporating refrigerant, as discussed in chapter 5. A heat pump is often sized to have a certain temperature drop, both on the secondary refrigerant side and on the heat carrier side, at dimensioning heat duty (Forsén, 2002). To illustrate this, Figure 17 is re-plotted in Figure 18 as the difference between Entering Brine Temperature (EBT) and the evaporating temperature vs. heat flux.

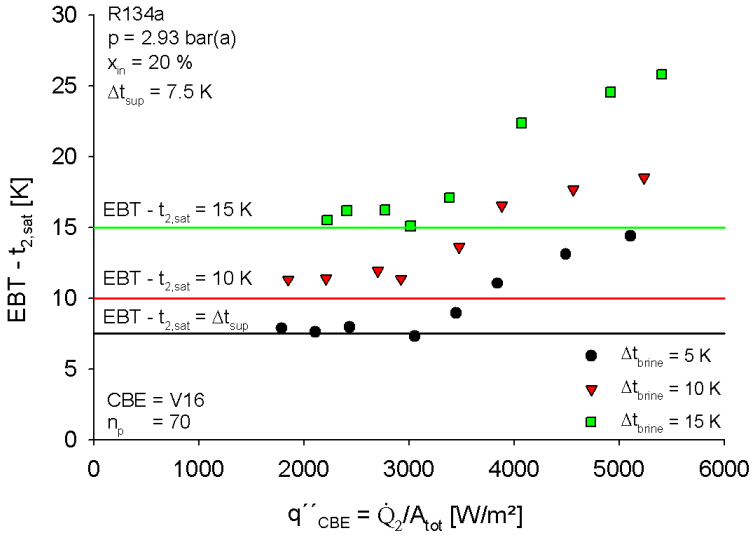

Figure 18: Maximal temperature difference in evaporator.

As shown in Figure 18, the highest COP_1 (smallest EBT-$t_{2,sat}$) is achieved by using a small temperature drop on the brine side. One may also see that the EBT-$t_{2,sat}$ does not decrease continuously with decreasing heat flux, but levels out at about 3 000 W/m² which also was the position of the local maximum (and maximum uncertainty) of the total area average refrigerant film heat transfer coefficient. It is, thus, no reason to decrease the heat flux (i.e. increase the heat transfer area at design stage) below this point since no additional increase in the performance of the heat pump would be expected. It may also be seen in Figure 18 that the EBT ─ $t_{2,sat}$ for Δt_{brine} = 5 K temperature drop at low heat flux almost corresponds to the amount of superheat used in the experiments. It is, of course, not possible to have a lower EBT-$t_{2,sat}$ than what the expansion valve is set on. Regarding the other two, Δt_{brine} = 10 °C & Δt_{brine} = 15 °C, the leveling out at low heat flux occur near the minimal temperature difference available, i.e. (EBT-$t_{2,sat}$) ≈ Δt_{brine}. Note that no account for pressure drop has been taken. The small

temperatures differences in the low heat flux range explains the high uncertainty observed in Figure 17.

One conclusion would be that the temperature drop on the brine side should not be higher than the amount of superheat used, see Figure 19. If a higher temperature drop is used, the heat pump is not working at the highest possible efficiency. However, too low temperature drop on the brine side is not preferable, since excessive pumping power is required, without increasing the efficiency of the heat pump (rather the opposite). Essentially, the brine flow rate should be selected to give equal terminal temperature differences, i.e. $\vartheta_1 = \vartheta_2$ (cf. Figure 16). Next step is to select the size of the evaporator. The area should be selected large enough in such a way that no further decrease of the terminal temperature differences is expected, reaching the point indicated in Figure 19.

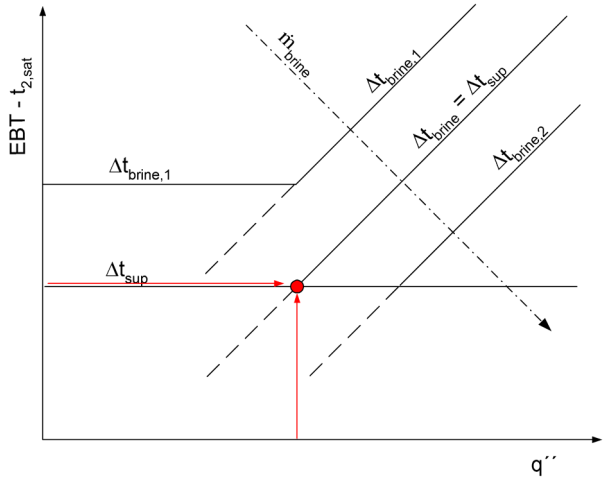

Figure 19: Schematic temperature lines as measured.

It should always be kept in mind, however, that the heat transfer in the "other" heat exchanger in the brine circuit (e.g. a bore hole) is also dependent of the brine flow. Too low brine flow rate may cause the flow to become laminar, resulting in a much too low heat transfer coefficient. Of course, the amount of superheat should be kept as low as possible.

The discussion above is, of course, only applicable in applications where small temperature differences are used, e.g. domestic heat pumps. At higher heat fluxes, approaching temperatures are not obtained.

12.4 Conclusions

A compact brazed plate heat exchanger used as evaporator in a lab-rig simulating a domestic heat pump has been experimentally investigated. The temperature drop on the brine side was kept rather high, $\Delta t_{brine} = 5$ K, $\Delta t_{brine} = 10$ K & $\Delta t_{brine} = 15$ K, in comparison to commercial heat pumps. In addition to that, the average heat flux was kept quite small, so that the temperature difference between the brine and refrigerant side to be extremely low upstream in the evaporator.

The relation between suitable brine mass flow rate and the size (heat flux) of the heat exchanger was discussed. In order to have an efficient heat pump (with low heat flux), the temperature drop of the brine fluid should equal the setting on the expansion device (amount of superheat). The size of the evaporator should be selected in such a away that that the temperature difference between the leaving brine and the entering refrigerant barely reaches each other. Of course, the amount of superheat should always be kept as low as the stability of the system allows.

13 EFFECT OF BRINE FLOW RATE ON REFRIGERANT SIDE TOTAL AREA AVERAGED FILM HEAT TRANSFER COEFFICIENT[i]

The brine mass flow rate in commercial heat pumps is often designed to give 3 K temperature difference on the brine as it passes the evaporator. As shown in chapter 12, this may not be the most energy efficient choice. It was also noted in chapter 12 that for high heat flux, the brine mass flow rate seemed to influence the total area averaged refrigerant film heat transfer coefficient. In this chapter we will explore this in more detail.

13.1 Test procedure and data reduction

Two different heat loads is tested; 5 kW/m² and 2.5 kW/m² (corresponding to total heat loads of 10 kW and 5 kW, respectively). The refrigerant side is kept constant during each of these series, i.e. the same heat flux (± 1 % for 5 kW/m² and –9 % to 6 % for 2.5 kW/m²), the same evaporating temperature (0 ± 0.2 °C for 5 kW/m² and 0 ± 0.4 for 2.5 kW/m²) and the superheat are kept low (0.5 K to 4 K). The brine mass flow rate is the parameter that is varied systematically, and the brine inlet temperature is allowed to change in order to keep the saturation temperature constant. The heat is supplied by an electrical heater to the secondary refrigerant (Ethanol mixed with water by ~24 % by mass). The deviation on the heat balance between the refrigerant side and the brine side is never greater than 2.4 %. The inlet mass quality of the refrigerant into the evaporator is kept within 18 %-22 % throughout the test series.

The experimental setup is described in detail in chapter 10 and the data reduction is described in chapter 11. The uncertainty analysis is outlined in Appendix E.

13.2 Experimental results

As shown in Figure 20, the total area averaged refrigerant film heat transfer coefficient increases with decreasing temperature drop on the brine side, i.e. increases with increasing brine flow. How does the heat pump system gain from this increase in heat transfer coefficient? Inspecting Figure 21 it may be seen that, for a given evaporating temperature, the inlet temperature of the brine to the evaporator decreases as the brine temperature drop decreases (increasing the

---

[i] This chapter is based on: Claesson J., 2004a, The influence of brine flow on the flow boiling refrigerant heat transfer coefficient in a compact brazed plate heat exchanger, Accepted for publication in International Journal of Heat Exchangers.

brine mass flow rate). From the heat pump system point of view, decreasing the temperature difference in the evaporator, while keeping condensing pressure constant, increases the COP_1 of the heat pump.

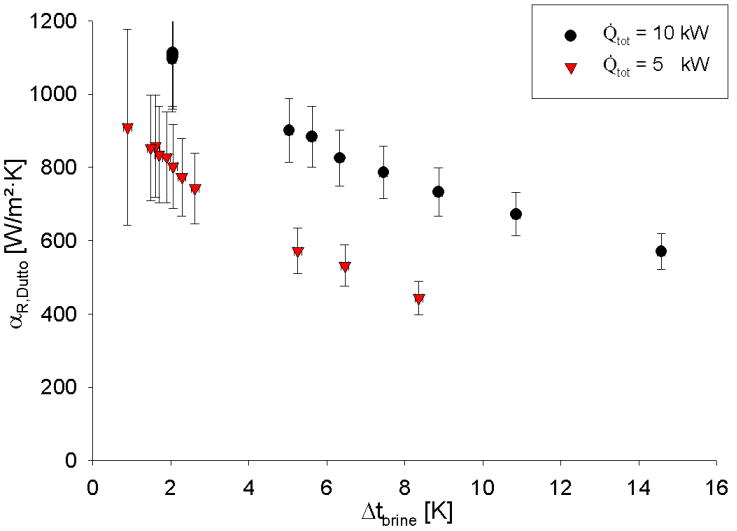

Figure 20: Area averaged refrigerant heat transfer coefficient as a function of temperature drop of the brine fluid.

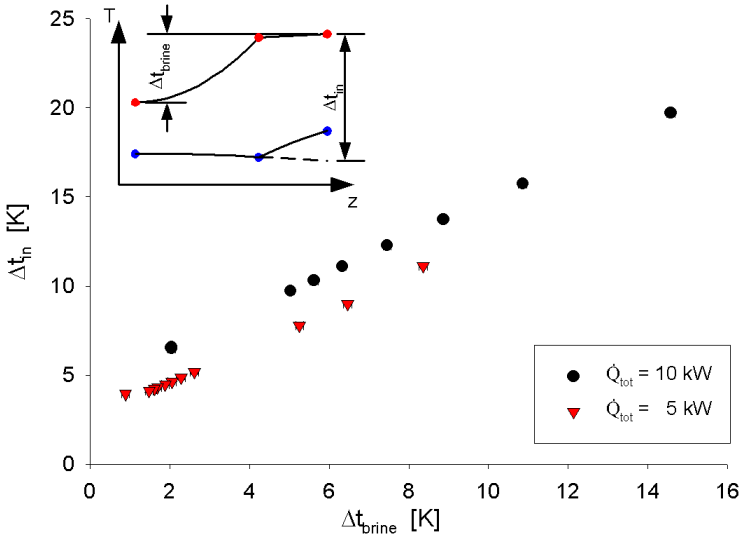

Figure 21: Temperature difference between inlet brine temperature and refrigerant saturation temperature at refrigerant outlet.

It should be noted, that in Figure 21 the increase of the heat transfer on the brine side is also included, i.e. the improvement is not only due to increase in

refrigerant heat transfer. In addition, it may also be interesting to note that the difference between leaving brine temperature and the evaporating temperature (Δt_{LWT}), calculated from exit pressure, is almost constant within each test series, see Figure 22. Thus, in a real system with a given inlet brine temperature, the COP_1 will increase due to increased evaporation temperature when the brine mass flow rate is increased.

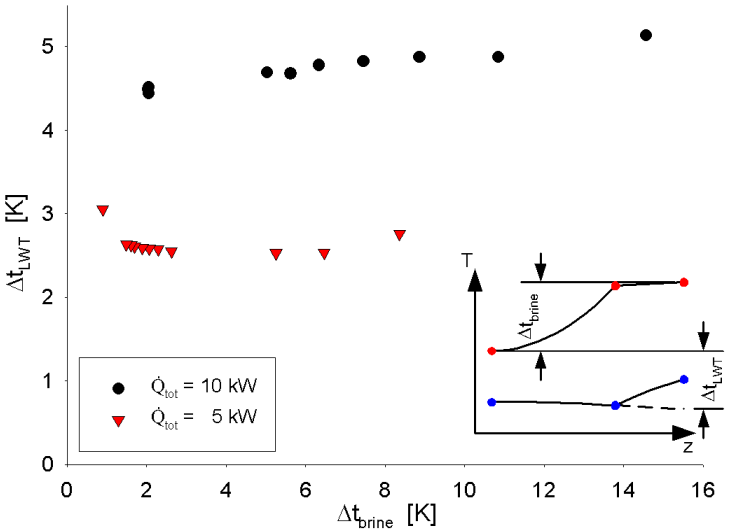

Figure 22: Difference between leaving brine temperature and evaporating temperature.

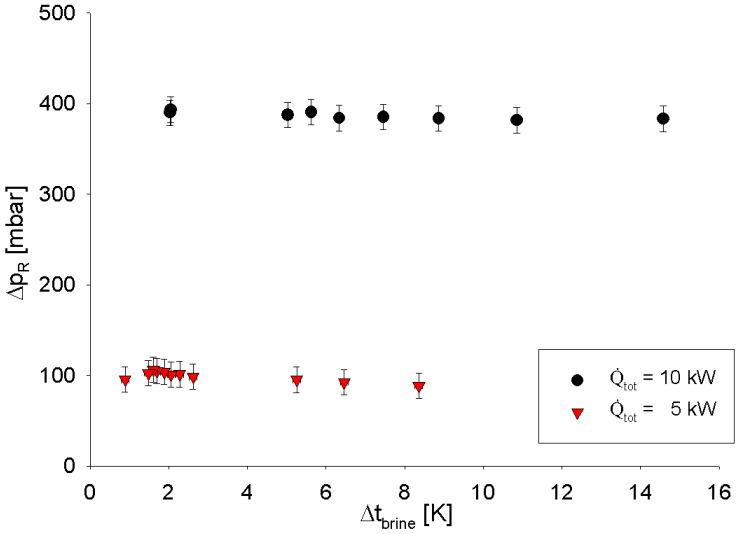

Figure 23: Refrigerant pressure drop.

It may also be interesting to see how the refrigerant pressure drop during the tests changed, see Figure 23. As seen, the pressure drop does not change to any large extent. This indicates that the decrease in inlet temperature difference seen in Figure 21 in conjunction with the nearly constant leaving brine temperature difference, as indicated in Figure 22, is not wasted due to an increase of the pressure drop in the refrigerant side.

13.3 Discussion

It seems clear that the heat transfer coefficient on the refrigerant side increases as the brine flow rate increases. There are several possible explanations for this behavior. Although efforts were made to keep the superheat constant, it varied a few degrees. High superheat occurred during the highest brine flows. If the superheat has any influence at these low superheats, it would be expected that the heat transfer coefficient would decrease with increasing superheat. So, if anything, even larger changes in heat transfer coefficients would have been obtained if it had been possible to keep the superheat truly constant.

The definition of the mean temperature difference used should also be commented. First, the applicability of the Dutto et al. (1991) approach for calculating the average temperature difference, which includes both the superheated section and the evaporating section of the evaporator, may be argued. However, as the superheat is small, disregarding the superheated section when defining the mean temperature difference would make no significant difference. Secondly, when defining the temperature difference in the boiling part of the evaporator, the standard textbook definition of logarithmic mean temperature difference is employed. This approach does assume constant heat transfer coefficients along the flow path of the heat exchanger. During flow boiling it is well established in the literature that the heat transfer coefficient may be dependent on mass flux, vapor quality and heat flux. Thus, the temperature profile on the brine side influences the heat transfer coefficient on the refrigerant side.

It is commonly accepted that if the heat transfer coefficient mainly depends on the mass flux and vapor quality, convective evaporation occurs. However, if the heat transfer coefficient mainly depends on heat flux, nucleate boiling occurs. These two different mechanisms may also occur at the same time during flow boiling. Depending on which heat transfer mechanism is assumed to govern the heat transfer, different explanations for the behavior observed would apply. In both cases, we will have Figure 24 in mind.

Increasing the brine flow rate decreases the temperature drop on the brine side, as already discussed. It also results in a higher heat transfer coefficient on the brine side. Now, first note that the temperature difference between leaving brine and entering refrigerant was almost constant, see Figure 22. Secondly, by

realizing that an increased heat transfer coefficient on the brine side decreases the temperature difference between brine fluid and heat transfer wall, the temperature difference between heat transfer wall and refrigerant increases at the location of entrance of the refrigerant, resulting in an increase of the heat transfer in that location. Higher heat flux upstream on the refrigerant side, would imply lower heat flux downstream, or rather that less evaporating heat transfer area would be needed. At the same time, at the exit of the evaporator, the expansion device controls the superheat. As the driving temperature difference in the superheated section of the evaporator decreases with increased brine flow, more heat transfer area is required in the superheated section. It seems that increasing the brine flow will result in a redistribution of heat transfer area and heat flux in the evaporator. This is true for both nucleate boiling and convective evaporation.

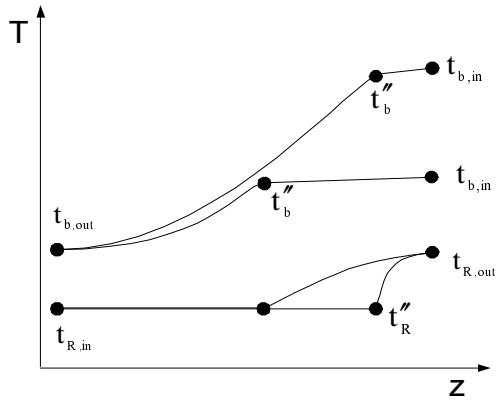

Figure 24: Schematic temperature profiles.

Now, if the heat transfer is governed mainly by forced convective evaporation one could assume, at a given vapor quality and with constant mass flux, that the local refrigerant heat transfer coefficient does not change, as the heat transfer coefficient is independent of wall superheat. Hence, the average convective boiling refrigerant heat transfer coefficient over a certain vapor quality range is constant for a given mass flux.

$$\bar{\alpha} = \frac{1}{x_{out} - x_{in}} \int_{x_{in}}^{x_{out}} \alpha(G,x)dx = \text{Constant} \qquad (129)$$

However, a certain vapor quality may be reached at different locations in the evaporator, and a constant heat transfer coefficient according to eq. (129) does not necessarily imply constant area averaged heat transfer coefficient. Thus, the increase of heat transfer coefficient during convective evaporation dominated heat transfer would therefore correspond to a redistribution of the local heat flux

and vapor quality. If heat flux is increased at the refrigerant inlet end of the evaporator, a larger portion of the boiling area will be in the higher vapor quality range, where the heat transfer coefficient is expected to be higher. The area averaged heat transfer coefficient would then be expected to increase.

Now, assume the heat transfer being mainly nucleate boiling dominated. For nucleate boiling during flow boiling, the heat transfer coefficient is expected to vary as

$$\alpha = C \cdot q''^{n} \tag{130}$$

However, the local heat flux is calculated as

$$q'' = \alpha \cdot \Delta t_w \tag{131}$$

Combining eqs. (130) and (131) yields

$$\alpha = C^{\frac{1}{1-n}} \cdot \Delta t_w^{\frac{n}{1-n}} \tag{132}$$

or

$$q'' = C^{\frac{1}{1-n}} \cdot \Delta t_w^{\frac{1}{1-n}} \tag{133}$$

Hence, if the main mechanism of heat transfer is nucleate boiling, the increase in wall superheat clearly increases the heat transfer coefficient. It seems that the heat flux, and heat transfer area, is redistributed.

In reality, it is difficult to know the actual without knowledge of the actual local heat transfer. Both mechanisms seem to increase the area averaged refrigerant side heat transfer coefficient in the boiling region. The difference between them seems to be the magnitude of increase. The local heat flux increases linearly with the increase in wall superheat for convective evaporation. However, for nucleate boiling the local heat flux increases with wall superheat raised to the power of $1/(1-n) \approx 3$, eq. (133). Thus, it may be expected that nucleate boiling dominated heat transfer would cause a larger redistribution of heat flux and heat transfer area.

The fact that the temperature difference between the refrigerant and the brine at the refrigerant inlet is close to constant throughout the tests indicates that the wall superheat increases at that location as the brine mass flow rate increases. Hence, as the wall superheat increase, the heat flux also increases at the refrigerant inlet. At the same time, the temperature difference between the brine and the refrigerant at the exit of the refrigerant decreases with increased brine

flow rate, indicating a decrease of heat flux downstream in the refrigerant channel and an increase of superheated area. As the heat flux most probably increases upstream in the refrigerant channel as the brine flow rates increases, it might be expected that the heat transfer coefficient is more and more nucleate boiling dominated: It is well established in the literature; the likelihood of having nucleate boiling dominated heat transfer increases at lower vapor quality and higher heat fluxes.

Furthermore, decreasing the heat flux at high vapor qualities may be beneficial in the view of dry-out, i.e. at constant mass flux it may be expected that the critical vapor quality at which dry-out occur would increase.

Finally, as the refrigerant side total area averaged film heat transfer was found to be affected by the temperature profile on the brine side, the widespread Wilson-plot method should be used with care.

13.4 Conclusions

The refrigerant area average heat transfer coefficient in a compact brazed plate heat exchanger has been investigated experimentally during constant heat load but with different brine flows. It was found from the experiments that the average refrigerant heat transfer coefficient increased with increasing brine flow. In addition, possible physical reasons for the behavior were discussed. It was suggested that the increase of the brine flow redistribute the local heat transfer towards the upstream part of the evaporator, i.e. towards lower vapor quality.

14 COMPARISON OF CO- AND COUNTER-CURRENT FLOW IN A COMPACT BRAZED PLATE HEAT EXCHANGER EVAPORATOR[i]

As is well known for single-phase applications, a heat exchanger with the two streams running in counter-current with each other yields the highest effectiveness. In co-current mode, the lowest effectiveness is obtained. However, some benefits with co-current do exist, such as small thermal stresses in the wall due to a more uniform wall temperature. For evaporators, a higher inlet wall superheat is achieved, promoting nucleate boiling at the entrance of the evaporator (Taborek, 1998).

The common way to install a CBE evaporator in a domestic heat pump is in counter-current mode. The reason for this is that the superheat required, protecting the compressor from liquid droplets, is difficult to achieve with a single co-current heat exchanger. It is however common to run flooded CBE-evaporators in co-current mode (Pelletier, 2002).

Even though the CBE is a rather inexpensive heat exchanger, even simpler geometries may be used for superheating the refrigerant. If the superheat was dealt with in a dedicated "superheater", the evaporator would resemble a flooded evaporator. It is the purpose of the present chapter to explore possible benefits of running the evaporator in co-current mode.

14.1 Experimental procedure and data reduction

Two different evaporators are tested, having identical heat transfer areas but equipped with different refrigerant inlet flow distributors. The heat load is approximately the same for all tests.

The brine mass flow rate is the parameter varied systematically, and the brine inlet temperature is allowed to change in order to keep the saturation temperature constant. The heat is supplied by an electrical heater to the secondary refrigerant (Ethanol mixed with water by ~24% by mass). The deviation on the heat balance between the refrigerant side and the brine side is never greater than 3 %. The inlet mass quality of the refrigerant into the evaporator is kept within 18 %-22 % throughout the entire test series.

---

[i] This chapter is based on: Claesson J., Palm B., 2003, Performance of a compact brazed plate heat exchanger evaporator run in co-current and counter-current, in Proceeding 5th International Conference on Boiling Heat Transfer, Montego Bay, Jamaica, May 5 – May 8, Session VIII: Heat Transfer and Heater Characteristics, third paper.

The experimental setup is described in detail in chapter 9 and the data reduction is described in chapter 11. The uncertainty analysis is outlined in Appendix E.

14.2 Experimental results

In order to investigate the influence of the temperature profile on the average refrigerant heat transfer coefficient, several different brine flow rates are tested. The brine fluid is run both co-current and counter-current with the refrigerant. To avoid that the superheat influence the results, a very low superheat is used, however the superheat varies somewhat during the experiments, see Figure 25. The experiments are run with half of the points decreasing the brine flow rate and half of the points increasing the brine flow rate.

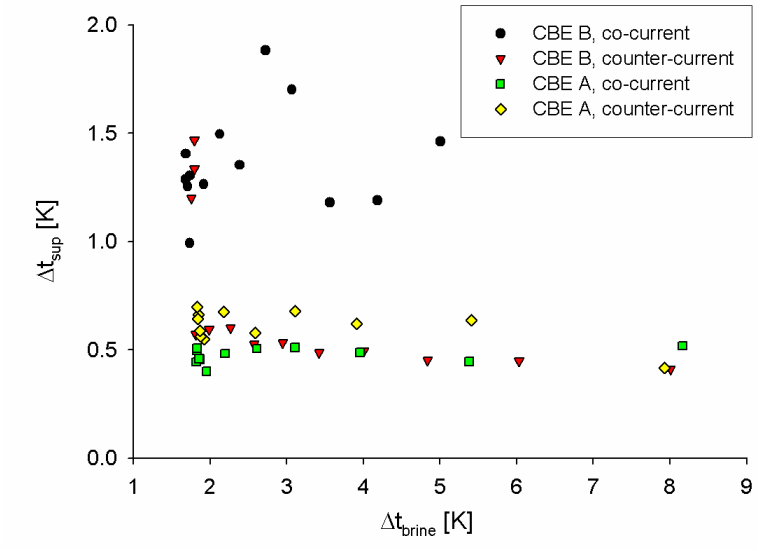

Figure 25: Variation of superheat during experiments.

It may be seen in Figure 26 that the heat transfer coefficient for co- and counter-current is very close to each other, within the experimental uncertainty of the measurements. So, even if the co-current heat transfer coefficient seems slightly higher than for counter-current case, at high brine flow rates, the uncertainty of the measurements does not allow any conclusions whether any difference actually did occur.

In additional, it may be seen that the heat transfer coefficient is clearly influenced by the brine flow for both flow arrangements, as discussed in the previous chapter.

In Figure 26, the average heat flux tested and its corresponding standard deviations are noted. It may be observed that the heat flux tested for the counter-current configuration is slightly higher than the corresponding co-current configuration. Higher heat flux indicates, for a given heat transfer area, higher refrigerant mass flow rate. Therefore, for an experiment with slightly higher heat flux and mass flow rate, slightly higher flow boiling film heat transfer coefficient may be expected. In addition, for CBE B, the superheat is higher in the co-current flow configuration. It may therefore be expected that the small difference between counter-current and co-current observed at low brine temperature drop in Figure 26 is perhaps slightly underestimated.

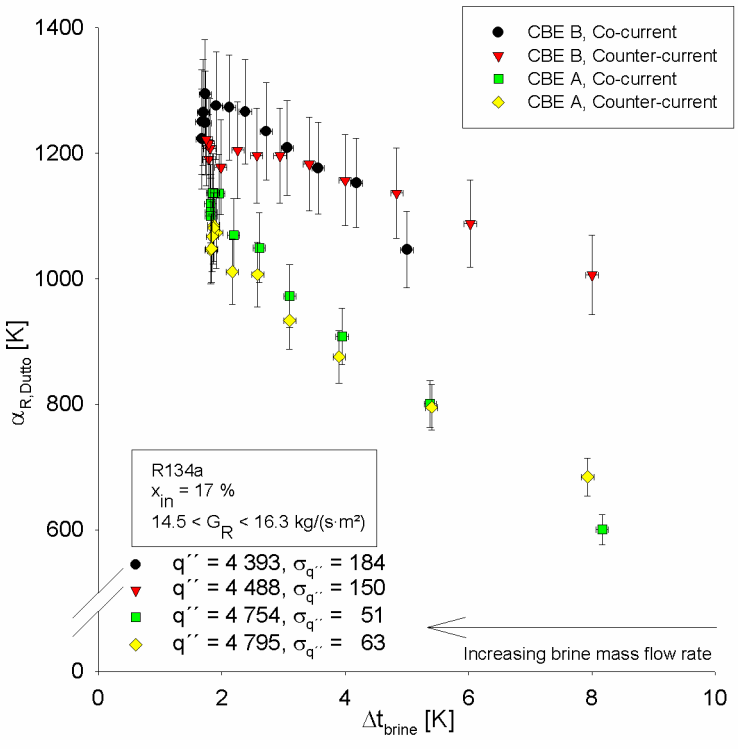

Figure 26: Refrigerant average heat transfer coefficient for different brine flows and configurations.

14.3 Discussion

During flow boiling it is well established in the literature that the heat transfer coefficient may be dependent on mass flux, vapor quality and heat flux. It is commonly accepted that if the heat transfer coefficient is mainly dependent on the mass flux and vapor quality, convective evaporation occurs. If, however, the heat transfer coefficient is mainly dependent on heat flux, nucleate boiling

occurs. These two different mechanisms may also occur at the same time during flow boiling.

In co-current configuration, the upstream temperature difference between the evaporating refrigerant and the brine is large. It is believed that nucleation is promoted in that section compared to counter-current configuration, where the temperature difference is quite low. For counter-current flow configuration, as the temperature difference becomes low at the refrigerant inlet, the nucleate boiling part may be entirely suppressed, as the wall superheat is not high enough to initiate nucleation (c.f. pool boiling).

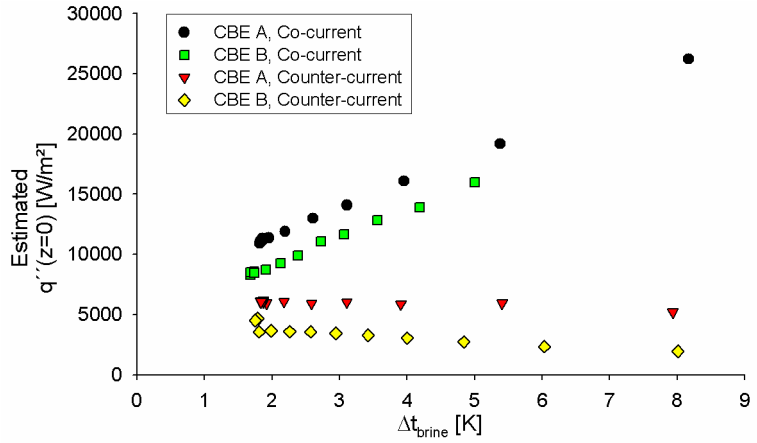

Figure 27: Estimated local heat flux at refrigerant entrance.

To be able to estimate the wall temperature, it is assumed that the heat transfer coefficient on the refrigerant side, at the refrigerant entrance, may be calculated with a pool boiling correlation. The correlation by Cooper (1984) was used, adjusted according to Claesson and Palm (1999) (see chapter 20). The measured temperatures of the brine and saturated refrigerant (from pressure) have been used in the calculations. The resulting estimated local heat flux at the refrigerant entrance is plotted in Figure 27. It may be seen that the heat flux decreases for the counter-current case when the brine flow rate decreases, and the opposite occur in the co-current case. The individual factors of the heat flux in Figure 27, i.e. the estimated refrigerant wall superheat and the estimated local refrigerant heat transfer coefficient, are plotted in Figure 28 and Figure 29. It should be noted that no account for the pressure drop has been taken. It may be seen from Figure 28 and Figure 29 that the steep increase in local heat flux, for the co-current case, is attributed to a combined increase of both the local heat transfer coefficient and an increase of the wall superheat.

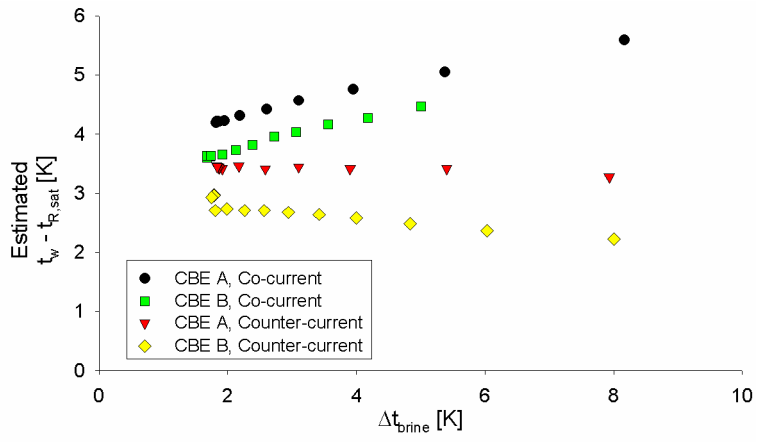

Figure 28: Estimated wall superheat at refrigerant inlet.

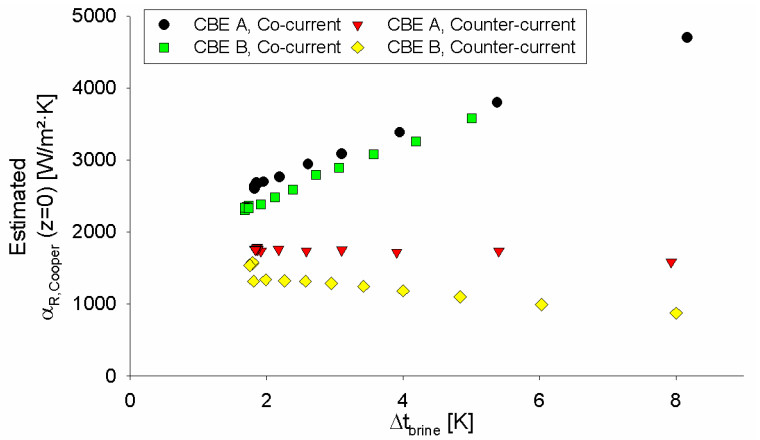

Figure 29: Estimated local refrigerant heat transfer coefficient at the refrigerant inlet.

In Figure 28, it may be seen that the estimated wall superheat at the refrigerant entrance decreases slightly as the brine flow rate decreases for the counter-current case. The local refrigerant heat transfer, plotted in Figure 29, also decreases with decreasing brine flow rate. The reason for this is, of course, that we assumed nucleate boiling; hence the local refrigerant heat transfer coefficient is proportional to the wall superheat to the power of ~2. When the film heat transfer coefficient on the brine side decreases, in the counter-current case, due to lower brine flow rate, the temperature difference between the brine fluid and the wall increases (with constant heat flux). Hence, the temperature difference between the wall and the refrigerant decreases and, thus, the local refrigerant heat transfer coefficient decreases. For the co-current case, a decrease in the brine flow rate increases the total inlet temperature difference to

an extent that the refrigerant wall temperature superheat increases, thus increasing the local refrigerant heat transfer coefficient.

As previously mentioned, pressure drop in the evaporator has not been included in the calculations. The reason is that the actual pressure at the inlet to the refrigerant heat transfer channel is not measurable, due to the presence of flow distributors. However, the pressure drop has been measured for an identical heat transfer surface, a CBE without the flow distributors, and is plotted in Figure 30. If we neglect the pressure drop in the ports, the pressure in the inlet of the refrigerant channel may be estimated. In Figure 30, using heat flux of 4 500 W/m², and an inlet vapor quality of 20 %, it may be expected that the pressure drop inside the heat transfer channels, in this kind of corrugated channel, is about 150 mbar.

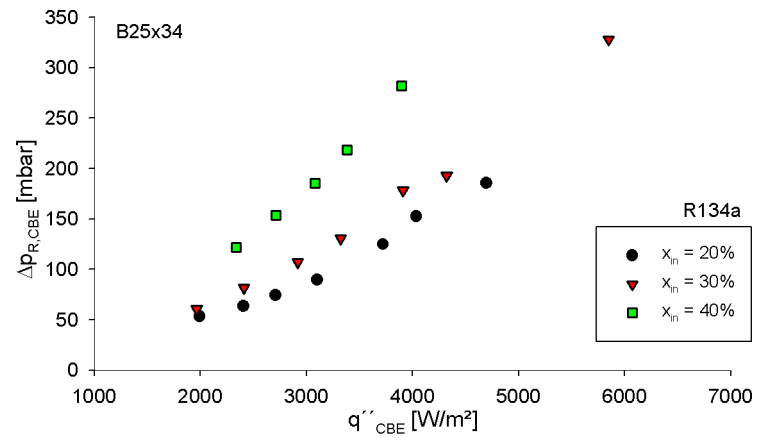

Figure 30: Pressure drop for evaporator B25 at different inlet qualities.

This corresponds to a temperature drop due to pressure drop in the channel of approximately 1.6 °C. Hence, the estimated temperature differences at the inlet of the evaporator in Figure 28 should be decreased by 1.6 °C. Accounting for the pressure drop in Figure 27 to Figure 29 does change the levels but not the trends. It may be seen that the temperature drop due to pressure drop in the channel, almost equals the temperature drop of the brine at the highest brine flow rates.

The total pressure drop (including the pressure drop in the inlet port distributor) in CBE B is plotted in Figure 31.

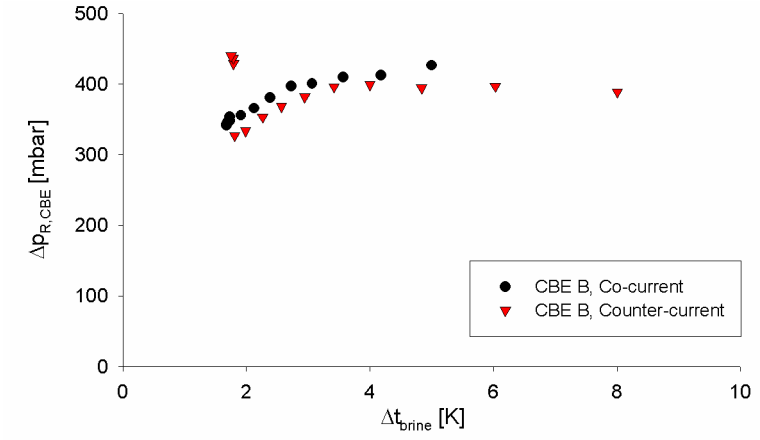

Figure 31: Total pressure drop of the refrigerant in CBE B.

In Figure 31, it may be seen that the pressure drop in the evaporator on the refrigerant side is depended on the brine flow. At some point, when Δt_{brine} is approximately 3 °C, the pressure drop levels out to a certain value. Higher brine flow rate yields lower pressure drop of the boiling refrigerant. It was observed during the experiment that the superheat for co-current was higher than for counter-current, which may be the explanation for the difference in pressure drop between co-current and counter-current. However, the difference in superheat between the series does not explain the trend of the pressure drop observed in Figure 31. One could speculate that the distribution of gas/liquid along the refrigerant path in the evaporator is different for different temperature drops on the brine side, i.e. the locus of significant boiling in the evaporator differ and that this may be the cause of the difference in pressure drop.

It may be concluded from the above discussion that the co-current configuration should be expected to facilitate nucleation in the upstream part of the evaporator and lowers the wall superheat downstream in the evaporator, preventing premature dry-out of the walls. The opposite may be stated for the counter-current configuration, less nucleation is occurring upstream, whilst a high wall temperature superheat is obtained downstream in the evaporator. However, the difference of the overall performance between the two flow arrangements is small, within the experimental uncertainty, and it may be concluded that there are no specific benefit in operating the evaporator in co-current flow arrangement[i].

[i] There is a Swedish saying:"…det man förlorar på karusellen tas igen på gungorna..."

14.4 Conclusions

In this investigation the total area average refrigerant film heat transfer coefficients were experimentally determined, operating the evaporator both in co- and counter-current configuration with different brine mass flow rates.

The refrigerant total area average film heat transfer coefficient for the co-current configuration was only slightly higher than for the counter-current configuration, within the experimental uncertainty. It was concluded that there were no specific benefit in operating the evaporator in co-current flow arrangement. On the contrary, for a DX evaporator requiring a certain amount of superheat, counter-current would perform far better than co-current.

15 WHAT HAPPENS WITH THE EVAPORATOR WHEN SUPERHEAT, BRINE MASS FLOW RATE, NUMBER OF PLATES OR FLOW CONFIGURATION CHANGES?[i]

The present chapter theoretically investigates what happens in an evaporator under various running conditions. The purpose of the chapter is to compare observations from numerical simulations with experimental observations made in the previous chapters. Thus, the different running condition investigated resembles the one experimentally tested. Two different cases are studied, convective evaporation refrigerant dominated heat transfer coefficient and heat flux dominated boiling refrigerant heat transfer coefficient.

15.1 Method

The plate heat exchanger, operating as evaporator in a domestic heat pump is under consideration in the present investigation. Several parameters may be investigated, however in the present investigation, the amount of superheat, brine side mass flow rate, the number of plates, and the flow configuration are the main parameters that are altered. All other parameters are then a result of the calculations.

Some simplifications and assumptions are introduced in order to calculate the heat transfer in the evaporator. These are given below:

1. Constant heat load, $\dot{Q}_2$ = 10 000 W.
2. R134a is used as refrigerant
3. Ethyl Alcohol (20 % by mass) mixed with water is used as secondary fluid (brine).
4. Evaporation is assumed to occur at -10 °C.
5. The pressure drop of the refrigerant is neglected.
6. The thermophysical properties of the refrigerant are evaluated using Refprop 6.01 (1988), and the properties of the brine are evaluated according to Melinder (1997).

---

[i] This section is based on: Claesson J., 2004c, Theoretical study of a compact brazed plate heat exchanger operating as evaporator, Submitted for publication in the International Journal of Refrigeration.

7. The brine side heat transfer coefficient is evaluated using the single phase correlation developed by the manufacturer for the specific heat exchanger.

8. For convective evaporation, the correlation developed by Donowski and Kandlikar (2000) is employed, however, slightly modified. For nucleate boiling heat transfer, the pool boiling correlation by Cooper (1984) is employed.

9. The refrigerant film heat transfer coefficient in the superheating section of the evaporator is calculated using the single phase correlation developed by the manufacturer for the specific heat exchanger.

10. It is assumed that ε-NTU method may be used in the superheated section.

11. A pure counter-current heat exchanger is assumed.

12. Boiling is assumed to occur up to vapor qualities of 1.00. Mist flow is not considered

13. The inlet vapor quality of the refrigerant entering the evaporator is $x_{in} = 20\%$.

The overall heat transfer coefficient in the superheated section of the evaporator is calculated as

$$U_S = \frac{1}{\frac{1}{\alpha_S} + \frac{1}{\alpha_{brine}}} \tag{134}$$

The single phase heat transfer correlation used in the above equation is

$$Nu = B_1 \cdot Re^{B_2} \cdot Pr^{\frac{1}{3}e^{\frac{6.4}{Pr+30}}} \cdot \left(\frac{\mu}{\mu_w}\right)^{\frac{0.3}{(Re+6)^{0.125}}} \tag{135}$$

The specific values of the constants are proprietary information of the manufacturer and may not be published. The convective evaporation heat transfer coefficient is calculated using the flow boiling heat transfer correlation by Donowski and Kandlikar (2000). However, as the original correlation does display large heat transfer coefficients at vapor qualities above 90%, it is modified in order to approach the single phase gas heat transfer coefficient as vapor quality approaches unity. A similar approach as suggested by Müller-Steinhagen and Heck (1986) for their two phase pressure drop model is

employed. The final correlation used in the convective evaporation case is thence

$$\alpha_{CB}\left(G,x,q''\right)=\left\{\left[\alpha_{DK}\left(G,x,q''\right)\cdot\left(1-x\right)^{1/3}\right]^{0.8}+\left[\alpha_{GO}\left(G\right)\cdot x^{3}\right]^{0.8}\right\}^{1/0.8} \qquad (136)$$

where $\alpha_{GO}(G)$ is the all-flow-as-gas single phase heat transfer coefficient calculated using eq. (135). $\alpha_{DK}(G,x,q'')$ is the correlation of Donowski and Kandlikar (2000) calculated as

$$\alpha_{DK}\left(G,x,q''\right)=\begin{bmatrix}2.312\cdot Co^{-0.3}\cdot E_{CB}+\\+667.3\cdot Bo^{2.8}\cdot F_{fl}\cdot E_{NB}\end{bmatrix}\cdot\left(1-x\right)^{0.003}\cdot\alpha_{LO}\left(G\right) \qquad (137)^{i}$$

where $\alpha_{LO}(G)$ is the all-flow-as-liquid single phase heat transfer coefficient calculated using eq. (135). Two dimensionless numbers are used in this correlation, the boiling number (Bo) and the Convective number (Co). They are defined, respectively

$$Bo=\frac{q''}{G\cdot\Delta h_{fg}} \qquad (138)$$

and

$$Co=\left(\frac{1-x}{x}\right)^{0.8}\cdot\left(\frac{\rho_g}{\rho_l}\right)^{0.5} \qquad (139)$$

The difference between Donowski and Kandlikar (2000), and eq. (136) are shown in Figure 32. It may be seen that the difference is not insignificant, however for the purpose of this investigation, where the difference between convective evaporation and nucleate boiling is investigated, the modified correlation serves its purpose. It should perhaps also be noted that the heat flux is also included in the Donowski & Kandlikar (2000) correlation, however its effect is negligible at the heat flux encountered in the application of interest in this investigation.

[i] In this work, with a stainless steel plate, F_{fl} is set to unity. The $E_{CB} = 0.512$ and $E_{NB} = 0.338$ is used as recommended in the original reference.

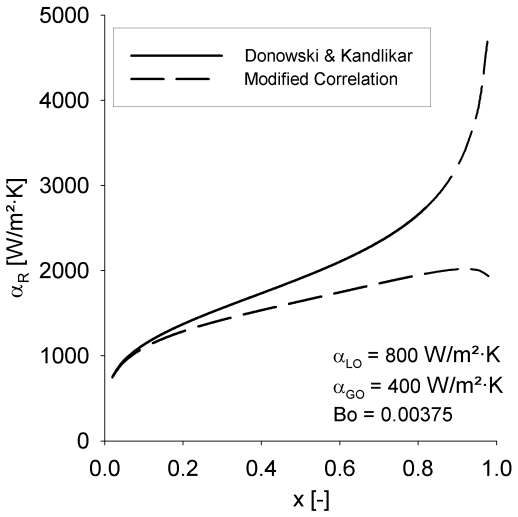

Figure 32: Comparison between the original correlation as suggested by Donowski and Kandlikar (2000) and the modified correlation used in the present work.

As an alternative, the heat transfer coefficient is calculated using the saturated nucleate pool boiling correlation by Cooper (1984). It was found in Claesson and Palm (1999) that this correlation estimated the boiling section averaged refrigerant heat transfer coefficient rather well at varying conditions, if the correlation is multiplied by 1.5. The correlation by Cooper (1984) is

$$\alpha_{NB} = C \cdot \frac{55 \cdot p_r^{\,0.12-0.2\cdot\log_{10} R_p}}{\left(-\log_{10} p_r\right)^{0.55} \cdot \tilde{M}^{0.5}} \cdot q''^{0.67} \tag{140}$$

where C = 1.5 in the present study. The surface roughness R_p is set to 1 μm.

The mass flow rate for the brine side is calculated as

$$\dot{m}_{brine} = \frac{\dot{Q}_2}{c_{p_{brine}} \cdot \Delta t_{brine}} \tag{141}$$

and the mass flow rate of the refrigerant as

$$\dot{m}_R = \frac{\dot{Q}_2}{\Delta h_{fg} \cdot \left(1 - x_{IN}\right) + c_{p_{R,sup}} \cdot \Delta t_{sup}} \tag{142}$$

The temperature differences used are defined in Figure 33.

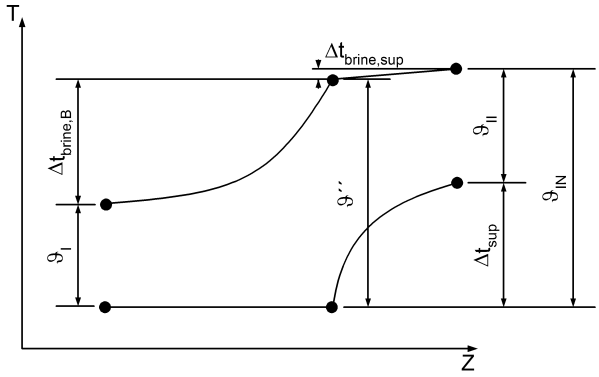

Figure 33: Schematic temperature profile.

The corresponding heat capacity rates are calculated as

$$C_{sup} = \dot{m}_R \cdot c_{p_{R,sup}} \tag{143}$$

and

$$C_{brine} = \dot{m}_{brine} \cdot c_{p_{brine}} \tag{144}$$

The individual temperature drops of the water side in each section is calculated as

$$\Delta t_{brine,sup} = \Delta t_{sup} \frac{C_{sup}}{C_{brine}} \tag{145}$$

and

$$\Delta t_{brine,B} = \Delta t_{brine} - \Delta t_{sup} \frac{C_{sup}}{C_{brine}} \tag{146}$$

The effectiveness of the superheating section is calculated as

$$\varepsilon_{sup} = \frac{\Delta t_{sup}}{\vartheta_{IN}} \tag{147}$$

The Number of Transfer Units (NTU), assuming pure counter-current heat exchanger configuration, is calculated as (Incropera and DeWitt 1996)

$$NTU_{sup} = \frac{1}{\frac{\min\left(C_{sup}, C_{brine}\right)}{\max\left(C_{sup}, C_{brine}\right)} - 1} \cdot \ln\left(\frac{\varepsilon_{sup} - 1}{\varepsilon_{sup} \cdot \frac{\min\left(C_{sup}, C_{brine}\right)}{\max\left(C_{sup}, C_{brine}\right)} - 1} \right) \tag{148}$$

The area required for superheating is calculated as

$$A_{sup} = \frac{NTU_{sup} \cdot C_{sup}}{U_{sup}} \tag{149}$$

The boiling heat transfer area is calculated by solving the governing differential equations (using the 4th order Runge-Kutta method) for the brine side temperature and refrigerant side vapor quality. The differential equation for the brine side temperature is

$$\frac{dt_{brine}}{dz} = \frac{\alpha_{brine} \cdot W_p \cdot \phi \cdot \left(n_p - 2\right)}{\dot{m}_{brine} \cdot c_{p_{brine}}} \cdot \left(t_{brine} - t_w\right) \tag{150}$$

and the corresponding differential equation for the vapor quality of the refrigerant is

$$\frac{dx}{dz} = -\frac{\alpha_R \cdot W_p \cdot \phi \cdot \left(n_p - 2\right)}{\dot{m}_R \cdot \Delta h_{fg}} \cdot \left(t_R - t_w\right) \tag{151}$$

Of course, the wall temperature is not known, and an iterative process is undertaken. A guess value of the refrigerant heat transfer coefficient and for the local wall temperatures initiates the calculation sequence. Then eq. (150) and eq. (151) are solved up to the point were x = 100 %. For each position, the corresponding wall temperature is solved. The new local wall temperatures are used in the next sweep along the boiling path in the evaporator for calculating local heat transfer coefficients. This procedure is repeated until the boiling length, and the amount of transferred heat, does not change from the previous sweep. The outlined procedure is very similar to the SEWTLE method as suggested by Corberán et al. (2001).

The calculation procedure is initiated by setting the four main parameters, i.e. desired brine temperature change over the evaporator (brine mass flow rate), the amount of superheat, flow configuration, and the number of plates in the evaporator. Next, the temperature of the exiting brine fluid is guessed. The resulting heat transfer area for the boiling section and superheated section are then calculated, as outlined above. If the sum of these two areas does not equal the total available heat transfer area, a new temperature of the exiting brine is

guessed. This iterative procedure continues until the sum of the areas equals the total available heat transfer area.

Once the boiling heat transfer area and the leaving brine temperature are solved, the performance of the heat exchanger may be calculated. The logarithmic mean temperature difference for the superheating section is calculated as

$$\vartheta_{m,sup} = \frac{\vartheta_{II} - \vartheta''}{\ln\left(\frac{\vartheta_{II}}{\vartheta''}\right)} \tag{152}$$

and for the boiling section as

$$\vartheta_{m,B} = \frac{\vartheta_{I} - \vartheta''}{\ln\left(\frac{\vartheta_{I}}{\vartheta''}\right)} \tag{153}$$

To find an area averaged refrigerant side heat transfer coefficient, two different methods are used. First, the appropriate temperature difference of the entire evaporator is calculated according to Dutto et al. (1991) as

$$\vartheta_{m,HEX_{Dutto}} = \frac{\Delta t_{brine}}{\frac{\Delta t_{brine,B}}{\vartheta_{m,B}} + \frac{\Delta t_{brine,sup}}{\vartheta_{m,sup}}} \tag{154}$$

To obtain this expression for the temperature difference it is assumed that the UA value of the entire evaporator is the sum of the UA – values of the boiling section and the superheating section,

$$U_{HEX_{Dutto}} \cdot A_{tot} = U_B \cdot A_B + U_{sup} \cdot A_{sup} \tag{155}$$

The total area averaged refrigerant heat transfer coefficient may be calculated as

$$\alpha_{HEX_{Dutto}} = \frac{1}{\frac{1}{U_{HEX_{Dutto}}} - \frac{1}{\alpha_{brine}}} \tag{156}$$

where

$$U_{HEX_{Dutto}} = \frac{\dot{Q}_2}{A_{tot} \cdot \vartheta_{m,HEX_{Dutto}}} \tag{157}$$

Second, the area averaged refrigerant heat transfer coefficient is calculated as

$$\alpha_{HEX,true} = \frac{1}{L_p} \cdot \left(\int_0^{z_{boiling}} \alpha_R \cdot dz + \int_{z_{boiling}}^{L_p} \alpha_S \cdot dz \right) \tag{158}$$

Eq. (156) and eq. (158) should (if the averaging is correct) give the same results. However, as will be seen, they do not. There is a small difference between the two approaches. However, from measurements when the individual heat transfer areas are not known, the approach by Dutto et al. (1991) may still, with fairly good accuracy, be used to estimate the total area averaged refrigerant film heat transfer coefficient.

15.2 Results and discussion

From the above analysis, the boiling heat transfer area is solved for different cases of superheats. The resulting heat transfer coefficients calculated from eq. (156) and (158) are plotted in Figure 34 vs. the effectiveness of the superheating section of the evaporator. The effectiveness is calculated according to eq. (14). As may be seen, the two different ways of calculating the total area averaged refrigerant heat transfer coefficients do not give the same value. In each diagram, it is noted which refrigerant heat transfer coefficient that has been used in the boiling section. The approach by Dutto et al. (1991) underestimates slightly the average heat transfer coefficient at high effectiveness in the superheated section and slightly overestimates the average heat transfer coefficient at lower effectiveness.

It may be interesting to compare the total area averaged refrigerant heat transfer coefficient for the evaporator using the two different boiling correlations, see Figure 34. For convective evaporation, a small heat exchanger seems to yield larger change in total area averaged refrigerant heat transfer coefficient as the superheat changes. The reason for the change in slope with effectiveness is the redistribution of heat transfer area between the boiling and superheating sections. For nucleate boiling, the three trends look similar, but with a smaller difference in their respective values. It seems that a nucleate governed flow boiling heat transfer coefficient does not suffer as much as convective evaporation governed heat transfer as the superheat increases. The reason for this would be the increase in wall superheat, which boosts the heat transfer coefficient for nucleate dominated flow boiling compared with convective dominated evaporation where the heat transfer coefficient is mainly a function of mass flux and vapor quality.

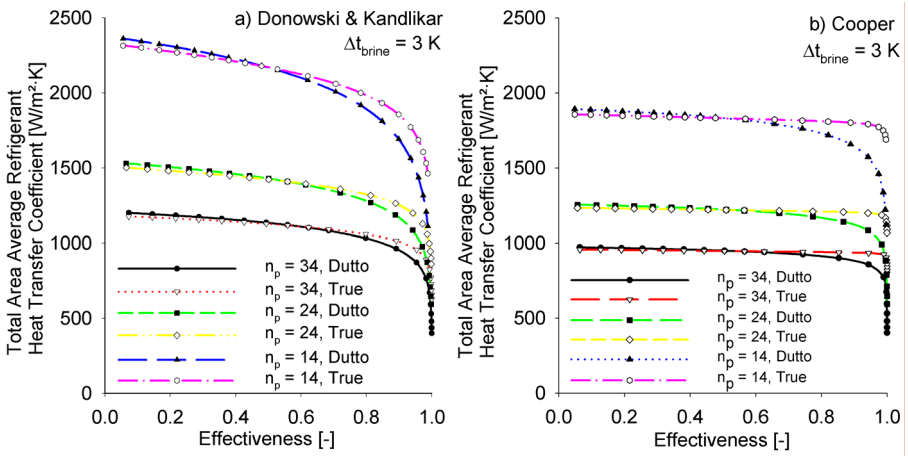

Figure 34: Difference between the two ways of calculating area averaged refrigerant heat transfer coefficient. Δt_{brine} = 3 K. The effectiveness is defined as $\Delta t_{sup}/\vartheta_{IN}$.

For both cases, large superheating heat transfer area yields smaller average heat transfer coefficients.

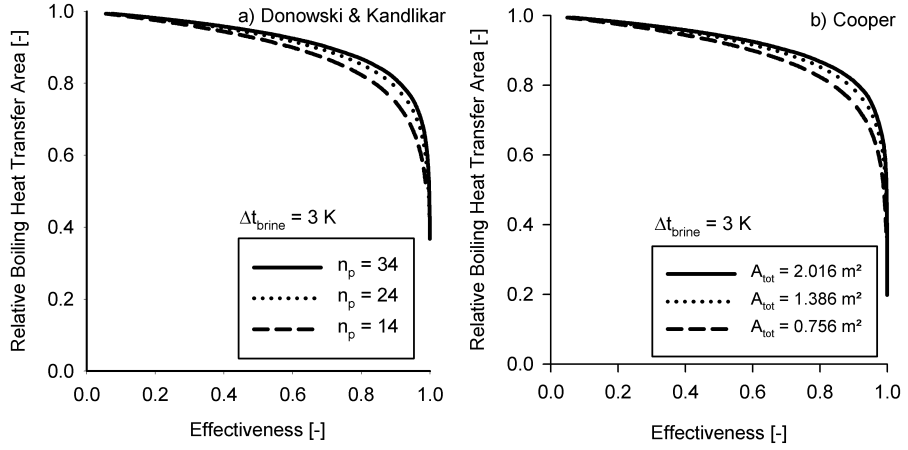

Figure 35: Dimensionless boiling heat transfer area for different superheats, Δt_{brine} = 3 K. The effectiveness is defined as $\Delta t_{sup}/\vartheta_{IN}$.

In Figure 35, the calculated relative boiling heat transfer area (A_B/A_{tot}) is calculated for different superheats and different number of plates. It may be seen that a large heat exchanger has relatively larger area used for boiling. The predicted difference between convective evaporation and nucleate boiling dominated heat transfer may also be observed in Figure 35. The difference is

surprisingly small, even though the Cooper (1984) correlation predicts slightly larger boiling heat transfer areas.

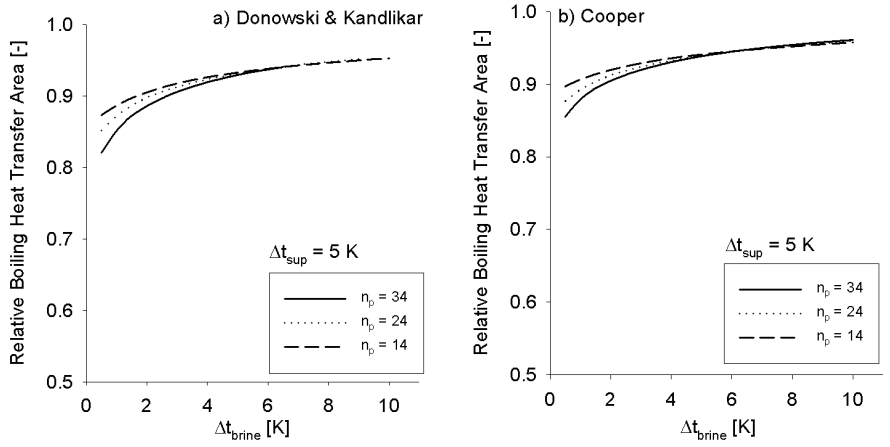

Figure 36: Boiling Heat Transfer Area for different brine mass flow rates, Δt_{sup} = 5 K.

The distribution of the heat transfer area between the superheating section and boiling section of the evaporator is also expected to change when the brine temperature drop changes. The single phase heat transfer coefficient on the brine side as the mass flow rate changes is calculated with eq. (135). In Figure 36, the relative boiling heat transfer area is shown. The relative boiling heat transfer area increases as the brine flow decreases (or equivalently, as the brine temperature drop increases). The reason is of course that the driving temperature difference in the superheated section increases as the brine flow decreases. Again, only a very small difference between the two models is observed.

It may be seen in Figure 37 that the refrigerant heat transfer coefficient decreases only slightly as the brine flow rate decreases. This is in agreement with what has been found experimentally and discussed previously in chapter 13 (Claesson 2004a) and chapter 14 (Claesson and Palm 2003). It was found that the total area averaged refrigerant film heat transfer coefficient decreases as the temperature drop on the brine side increases for a brazed plate heat exchanger, however with a greater magnitude than simulated in the present investigation. A rather low superheat (0.5 K to 3 K) was used in those experiments.

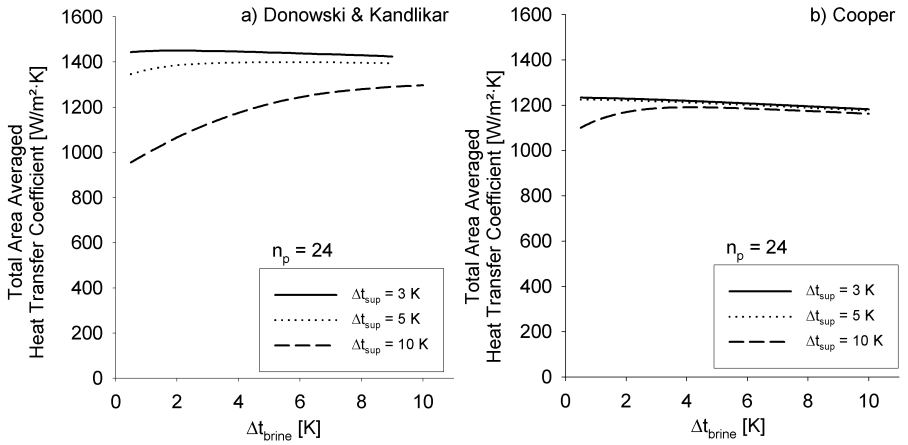

Figure 37: Area average refrigerant heat transfer coefficient for different brine temperature drops. Number of plates is 24.

It may also be interesting to compare the two different models operating in co- and counter- current, as experimentally investigated in chapter 14. The superheat was thus set to 0.5 K. As may be seen in Figure 38, the convective evaporation model gives a different trend of the heat transfer coefficient as the brine flow rate changes for the two flow configurations. The nucleated boiling model gives almost identical results, however a small difference at high temperature drop on the brine side is obtained, see Figure 39. Inspecting Figure 26, it may be seen that the experimentally observed trends for co- and counter-current are similar. Hence, the nucleate boiling model seems to catch the trends better than the convective evaporation model.

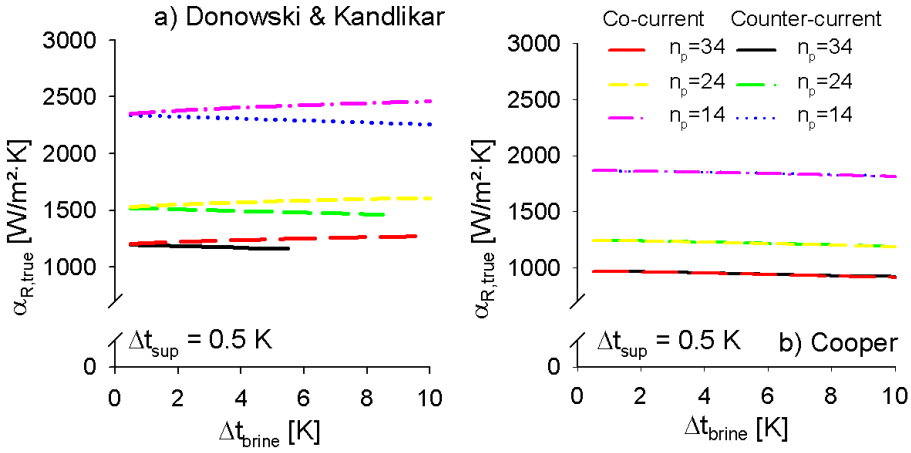

Figure 38: Comparison between co- and counter-current flow arrangement.

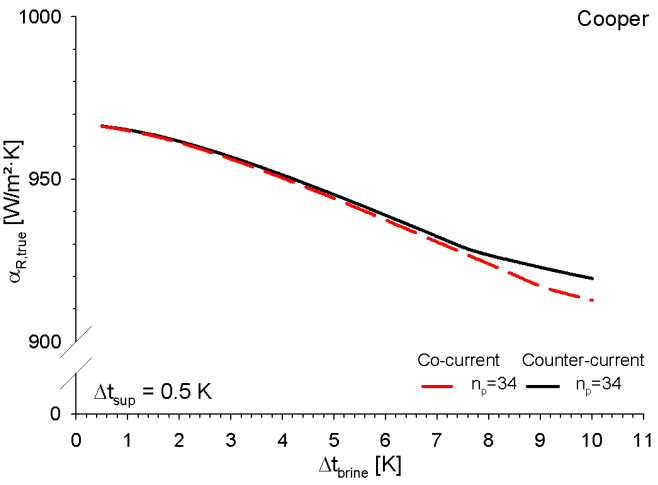

Figure 39: Difference between co- and counter-current flow arrangement obtained using nucleate boiling model.

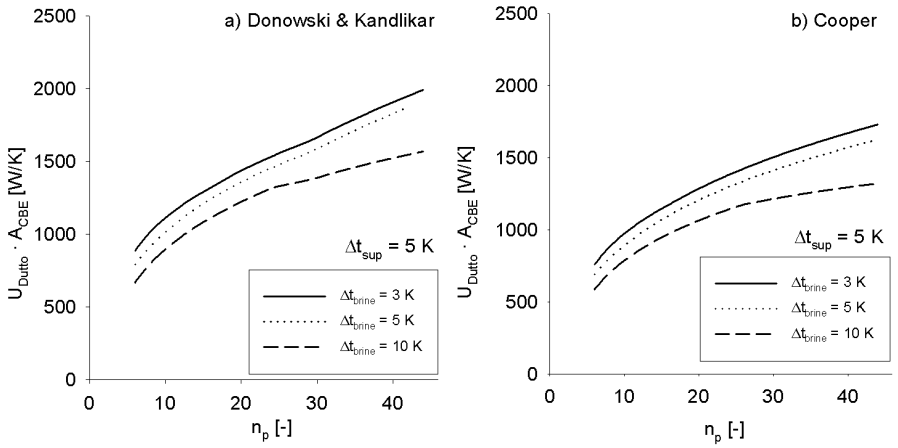

Figure 40: Overall performance of the evaporator using different number of plates in the evaporator. Only even numbers have been considered, i.e. 6, 8, 10…Δt_{sup} = 5 K is used.

Finally, the overall performance of the plate heat exchanger using different number of plates is investigated. The overall performance increases as the number of plates increases (Figure 40), as expected. The highest performance is obtained using highest brine flow rate (lowest Δt_{brine}). The superheat was 5 K in this simulation. One would perhaps also expect a leveling out of the performance as the effectiveness of the evaporator approaches unity, i.e. as the brine and refrigerant temperature difference at $z = 0$ or $z = L_P$ approaches zero.

However, up to 44 plates, no such trend is observed. Claesson et al. (2003) observed this trend experimentally to occur as the total area heat flux was less than 3 500 W/m^2 using 70 plates. The total heat load in this investigation is 10 000 W and 44 plates corresponds to a total area heat flux of 3 800 W/m^2.

15.3 Conclusion

The area distribution between the boiling section and the superheating section in an evaporator has been investigated theoretically. It was shown that the heat transfer area used for boiling decreases with increasing superheat, as expected. The total heat transfer area and the brine temperature difference determine the magnitude of the decrease. Further, the area averaged refrigerant heat transfer coefficient decreases in the same manner. In addition, it was found that the area averaged refrigerant heat transfer coefficient, in most cases, decreases slightly as the brine flow rate decreases, as previously experimentally observed. A comparison between the two boiling correlations displayed surprisingly small differences. However, regarding co- and counter-current flow arrangement, different trends were obtained with the convection evaporation model but not with the nucleate boiling model. The nucleate boiling model seems to predict the trends better than the convective evaporation model. Finally, the overall performance (UA-value) of the evaporator was investigated using different total heat transfer areas. The performance was found to improve monotonously as the number of plates was increased.

16 INFLUENCE OF DIFFERENT INLET REFRIGERANT FLOW DISTRIBUTION DEVICES[i]

To accurately predict the performance of a plate heat exchanger operating as evaporator in a heat pump or refrigeration system, it is important to have knowledge of the local flow boiling heat transfer coefficient along the refrigerant channels. However, flow maldistribution between the parallel refrigerant channels may also impact the overall performance. The refrigerant leaving the expansion valve, entering the evaporator, consists of a mixture of vapor and liquid. Thus, depending on the flow pattern in the inlet port of the evaporator, the liquid and vapor may divide differently into the boiling channels. To decrease the amount of maldistribution, a distributor, consisting of some type of constriction of the flow, is usually installed at the inlet of each channel in plate heat exchanger evaporators, see Figure 41.

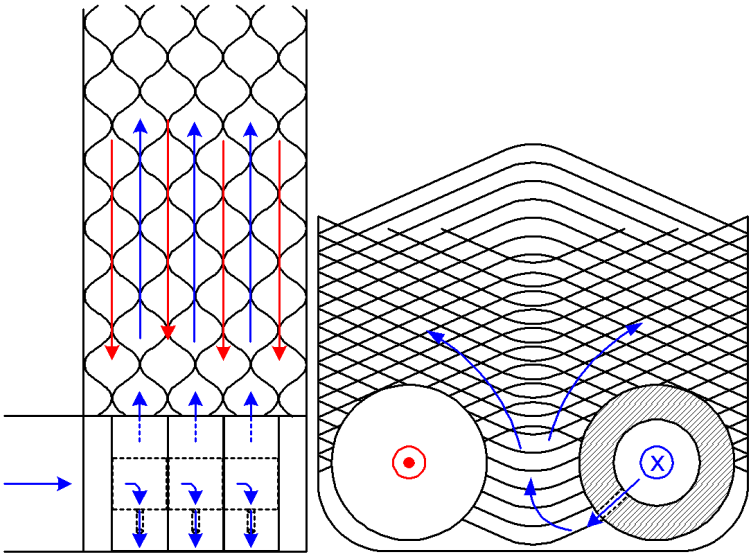

Figure 41: Principal sketch of the inlet refrigerant flow distributor in a plate heat exchanger having 8 plates.

[i] This chapter is based on a section from: Claesson J., 2005, Thermal and Hydraulic Characteristics of Brazed Plate Heat Exchangers – Part II: Current research on evaporators at KTH, Accepted for presentation and publication at the ASHRAE Winter meeting, 2005, Orlando, Fl., USA.

16.1 Experimental results

In order to investigate the impact of distributor design on flow distribution between refrigerant channels, five evaporators with identical heat transfer surface, but with different refrigerant inlet distributors are investigated. A sixth heat exchanger with slightly different design is also tested. Two of the five similar evaporators, and the odd sixth evaporator, are commercially available from SWEP International, labeled B25, V25 and V80, respectively. The other three are prototypes with modified distributors. B25 has no distributor, while the three prototypes, 1, 2, 3 and V25 all have distributors with successively larger orifices. All five evaporators have sixteen refrigerant channels.

The resulting heat transfer coefficients, as may be seen in Figure 42, are rather different. In Figure 42, the refrigerant mass flux is also indicated. In all tests, the inlet vapor quality, evaporating pressure, and the amount of superheat are kept constant, and therefore, the mass flux is directly proportional to the heat flux. It may be concluded from the results that the flow distributor has an significant effect on the performance. This emphasizes the importance of having a correct sized flow distributor for the application at hand.

Figure 43 illustrates visually the flow distribution in an evaporator. The two IR-photos show the temperature distribution in the same heat exchanger at different heat fluxes. The heat exchanger is shown from the side with the refrigerant entering from the bottom right, passing through a number of parallel vertical channels and leaving at the top right corner. As may be seen, at the lower cooling capacity, liquid refrigerant is distributed towards the refrigerant channel furthest away from the inlet pipe of the evaporator, resulting in less superheat in those channels. However, increasing the cooling capacity by means of increasing the speed of the compressor, and keeping the amount of superheat constant, a redistribution of the liquid refrigerant occurs towards the channels close to the refrigerant inlet side.

16.2 Discussion

It would of course be desirable to have completely uniform flow distribution. This would require a more homogeneous mixture between the two phases present in the inlet port, as is the case in flooded evaporators (with only liquid). It is expected that increasing the pressure drop in the inlet flow distributor would improve the flow distribution between the refrigerant channels in the evaporator. However, this limits the upper capacity range in which the evaporator may be operated, i.e. as the capacity increases, more and more pressure drop occurs over the flow distributor, until the expansion valve is fully open and the expansion device can no longer control the amount of superheat.

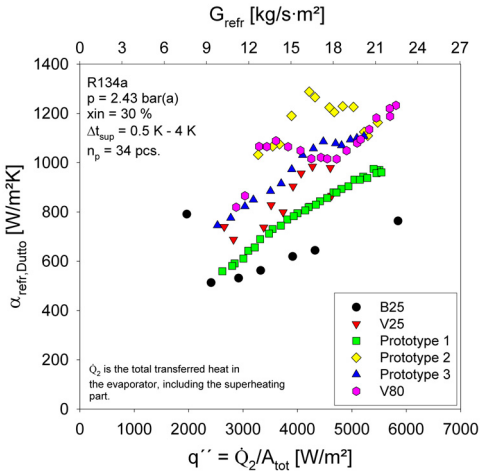

Figure 42: Total area averaged heat transfer coefficient at –5°C evaporation and 30 % inlet vapor quality for five identical heat exchangers (B25 to Prototype 3) with different distributor designs. V80 has a slightly different plate pattern. The wavy patterns of some of the heat exchangers have been verified in several tests.

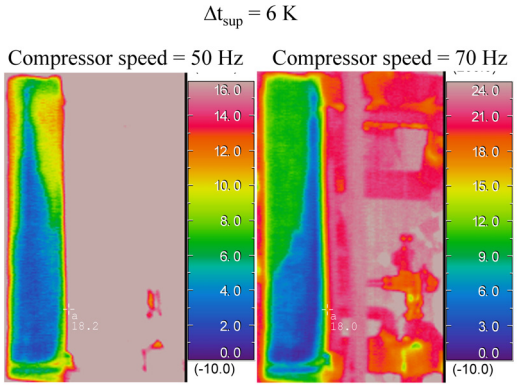

Figure 43: Temperature distributions, indicating mass flow distributions, in a plate heat exchanger, at two different cooling capacities. The evaporator is viewed from the side with the refrigerant inlet at the lower right end, and the refrigerant exit at the upper right end.

16.3 Conclusions

As may be seen from the experimental results, the impact of the inlet flow distributor is significant. Thus, proper design of the distributor is essential. The main difficulty in doing so is to account for different operating conditions.

17 CONCLUSIONS – PART II

The performance of a plate heat exchangers operating in a domestic heat pump have been investigated under various running conditions. For very low heat flux and low brine mass flow rates, limiting performance improvement was observed due to approaching temperatures of the two fluid streams. The appropriate sizing and selection of brine mass flow rate in order to obtain a heat pump as efficient as possible is essential.

The influence of brine mass flow rate on the total area average refrigerant film heat transfer coefficient was investigated. The refrigerant side heat transfer coefficient increased as the brine mass flow rate increased. It was suggested that the redistribution of local heat flux was responsible. Further, the impact of running the evaporator in co- and counter-current flow configuration was investigated. No significant difference in their performance was observed and there seems to be no specific benefit in running the evaporator in co-current mode.

The experimentally tested running conditions were also tested in a numerical model, using two different boiling models. Only small difference between the models was observed. However, running the evaporator in co-current resulted in trends opposite to experimentally observed for the convective evaporation model. It was concluded that the nucleate boiling model agrees better with experiments.

Finally, the importance of having correct refrigerant inlet flow distributor was illustrated by measurements of the overall performance of several evaporators having identical heat transfer area but different refrigerant inlet flow distributors. The resulting flow distribution between the refrigerant channels was also illustrated with two IR-pictures of the same heat exchanger but at different heat loads.

PART III

THE EVAPORATOR CONSIDERED AS A TWO ZONE HEAT EXCHANGER

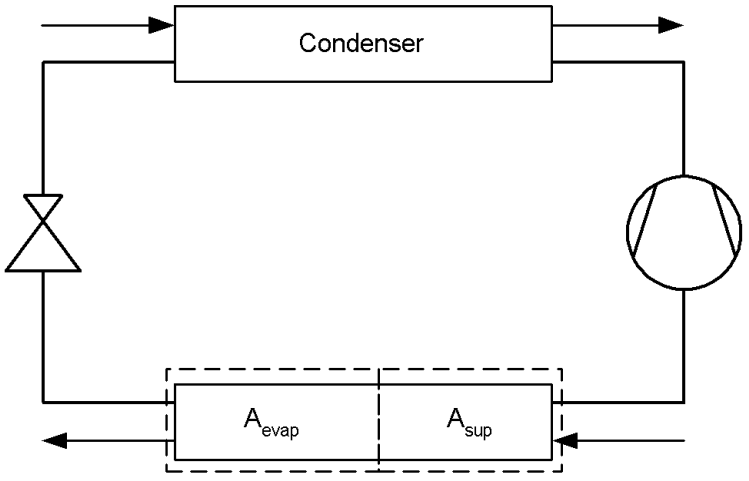

18 INTRODUCTION – PART III

This section of the thesis considers the evaporator as a two zone heat exchanger, i.e. the evaporator is divided into an evaporating zone and a superheating zone. However, the terminal temperatures and pressures are still used to evaluate the heat transfer coefficient in the evaporating section. The main difference between this section and the previous section is that the distribution of heat transfer area between boiling and superheating is required. Two different ways of determining these areas will be employed in the analysis.

First, the boiling heat transfer area is measured using thermochromic liquid crystals (TLC). As the heat transfer is known, the boiling section area averaged film heat transfer coefficient may be determined.

The LMTD approach is used in the evaluation of the boiling area averaged heat transfer coefficient in the above investigation, and the applicability of that method is investigated. One could expect that this method may fail as the flow boiling heat transfer coefficient is not constant. In the general case it depends on the mass flux, heat flux and vapor quality.

Second, the boiling heat transfer area is determined "backwards", by first calculating the area required for the superheated section, using single phase correlations on both fluid sides. As it will be found that the boiling heat transfer area estimated with this method does not give the same results as the first method, where the boiling heat transfer area was measured, possible reasons for the difference is discussed. In addition, the impact of chevron angle on the overall performance of the evaporator is also investigated.

19 DATA REDUCTION – PART III

In this part of the thesis, the evaporator is considered as two "classical" heat exchangers, the superheater and the boiler. In order to calculate the two heat exchangers, the area of the respective section of the heat exchanger is required. At least two different ways are possible to use in order to determine the areas; direct measurement of the areas, or indirect determination using single phase correlation in the superheated section. In this part of the thesis, both methods will be employed.

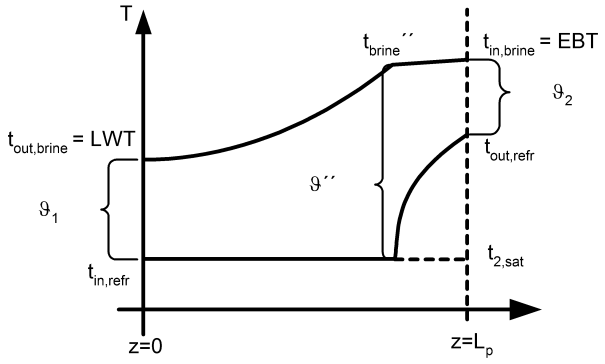

Figure 44: Typical temperature profiles in an evaporator.

Regardless of the method used, the logarithmic mean temperatures are required of the two sections. Typical temperature profiles are shown in Figure 16. The LMTD in the boiling section is defined as

$$\vartheta_{evap} = \frac{\vartheta_1 - \vartheta''}{\ln\left(\frac{\vartheta_1}{\vartheta''}\right)} \tag{159}$$

and in the superheated section as

$$\vartheta_{sup} = \frac{\vartheta'' - \vartheta_2}{\ln\left(\frac{\vartheta''}{\vartheta_2}\right)} \tag{160}$$

The brine temperature at the location where the refrigerant becomes saturated vapor is calculated from an energy balance, i.e.

$$t''_{brine} = t_{brine_{in}} - \frac{\dot{m}_R \cdot c_{p_R} \cdot \Delta t_{sup}}{\dot{m}_{brine} \cdot c_{p_{brine}}} \tag{161}$$

19.1 Known (or measured) boiling and superheated areas

The overall heat transfer coefficient of the boiling section is

$$U_{evap} = \frac{\dot{Q}_{evap}}{\vartheta_{m_{evap}} \cdot A_{evap}} \tag{162}$$

The boiling area averaged refrigerant side heat transfer coefficient may be calculated as

$$\alpha_R = \frac{1}{\frac{1}{U_{evap}} - \frac{1}{\alpha_{brine}}} \tag{163}$$

19.2 Estimating superheated and boiling heat transfer areas

The overall heat transfer coefficient in the superheated section is

$$U_{sup} = \frac{1}{\frac{1}{\alpha_{brine_{sup}}} + \frac{1}{\alpha_{R_{sup}}}} \tag{164}$$

The area required to superheat the refrigerant a given amount is calculated as

$$A_{sup} = \frac{\dot{Q}_{sup}}{\vartheta_{m_{sup}} \cdot U_{sup}} \tag{165}$$

As the heat transfer area required for the superheated section of the evaporator is estimated, the accompanying heat transfer area used for the boiling section is calculated as

$$A_{evap} = A_{tot} - A_{sup} \tag{166}$$

Thus, the overall heat transfer coefficient of the boiling section is

$$U_{evap} = \frac{\dot{Q}_{evap}}{\vartheta_{m_{evap}} \cdot A_{evap}} \tag{167}$$

and finally the flow boiling heat transfer coefficient on the refrigerant side is calculated as

$$\alpha_R = \frac{1}{\frac{1}{U_{evap}} - \frac{1}{\alpha_{brine}}} \tag{168}$$

19.3 Single phase heat transfer coefficient on the brine side and the superheated section on the refrigerant side

To obtain the heat transfer coefficient on the refrigerant side, the film heat transfer coefficient on the brine side and the single phase heat transfer coefficient of the superheated refrigerant are required. Both these heat transfer coefficients are calculated in similar ways, using the same heat transfer correlation (Pelletier 1999)

$$Nu_{brine} = C_{Nu}\left(Re_{brine}\right)\cdot Re_{brine}^{C_{Re}\left(Re_{brine}\right)}\cdot Pr_{brine}^{\frac{e^{6.4/(Pr_{brine}+30)}}{3}}\cdot\left(\frac{\mu_{brine}}{\mu_{brine_W}}\right)^{\frac{0.3}{\left(Re_{brine}+6\right)^{0.125}}} \tag{169}$$

and

$$Nu_{R_{sup}} = C_{Nu}\left(Re_{R_{sup}}\right)\cdot Re_{R_{sup}}^{C_{Re}\left(Re_{R_{sup}}\right)}\cdot Pr_{R_{sup}}^{\frac{e^{6.4/\left(Pr_{R_{sup}}+30\right)}}{3}}\cdot\left(\frac{\mu_{R_{sup}}}{\mu_{R_{sup}W}}\right)^{\frac{0.3}{\left(Re_{R_{sup}}+6\right)^{0.125}}} \tag{170}$$

The measured mass flow rates are used to calculate the Reynolds numbers as

$$Re = \frac{G\cdot d_e}{\mu} \tag{171}$$

where

$$G_{brine} = \frac{2\cdot\dot{m}_{brine}}{W_p\cdot b\cdot n_p} \tag{172}$$

and

$$G_R = \frac{\dot{m}_R}{W_p\cdot b\cdot\left(\frac{n_p}{2}-1\right)} \tag{173}$$

for n_p being an even number, 2, 4…70. For the special case of a three plate heat exchanger, eq. (172) and (173) changes into

$$G_{brine} = \frac{\dot{m}_{brine}}{W_p \cdot b} \tag{174}$$

and

$$G_R = \frac{\dot{m}_R}{W_p \cdot b} \tag{175}$$

respectively.

The film heat transfer coefficient of the superheated refrigerant and of the brine are calculated as

$$\alpha = \frac{Nu \cdot \lambda}{d_e} \tag{176}$$

20 DETERMINATION OF BOILING HEAT TRANSFER AREA AND FLOW BOILING HEAT TRANSFER COEFFICIENT[i]

The purpose of this chapter is to determine the percentage of the plate heat exchanger used for boiling and the percentage used for superheating the refrigerant and to evaluate the resulting boiling area averaged film heat transfer coefficient. The operating conditions are those of a typical liquid chiller, i.e. the heat load is 5 – 15 kW/m². R-22 is used as refrigerant.

To be able to distinguish between the boiling and the superheated sections in the evaporator, the surface temperature of the refrigerant channel wall is measured. To allow this measurement a plate heat exchanger is manufactured, having one refrigerant channel, one brine channel and no end plate or cover plate outside of the refrigerant channel (cf. Figure 4). To determine the surface temperatures, thermochromic liquid crystal (TLC) is painted on the outer surface of the corrugated channel. Since the color of the TLC correspond to a certain temperature, the boiling area of the evaporator could be measured visually as the area where the temperature was equal to the saturation temperature of the refrigerant.

20.1 Thermochromic liquid crystals

As mentioned, TLC reacts on temperature change by changing color. TLC starts to show red color at a temperature called “Red Start” and as the temperature increases, TLCs show color with decreasing wavelength in the visible spectra. Eventually, a temperature is reached where the color no longer is visible to the naked eye. The “Bandwidth” is defined as the difference between “Red Start” and “Blue Start”, Hallcrest (1991). Figure 45 shows a typical response of wavelength to temperature. The borderline between the boiling and superheating regions is very clearly identified from the difference in color, as may be seen in Figure 49.

[i] This chapter is based on: Claesson J., Palm B., 1999, Boiling mechanism in a small compact brazed plate heat exchanger (CBE) determined by using thermochromic liquid crystals (TLC), 20th Int. Congr. of Refrigeration, IIR/IIF, Sydney, 1999, paper 117.

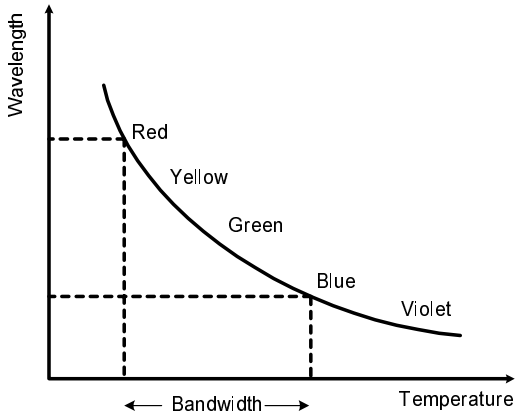

Figure 45: Reflected wavelength as a function of temperature, adopted from Hallcrest (1991).

20.2 Experimental setup

A simple refrigerating system was built, with both manual expansion device and thermostatic expansion device. R-22 is used as working fluid. Ordinary tap water is used as secondary refrigerant as well as coolant for the condenser. A constant pressure valve, positioned in the suction line of the compressor, controls the evaporating pressure. The mass flow rate of the refrigerant is measured after the high pressure receiver. To be certain that no vapor is present in the flow meter a sight glass is positioned downstream for visual inspection. The pressure and temperature at the inlet to the evaporator, differential pressure over the evaporator and the temperature of the refrigerant leaving the evaporator are also measured.

The evaporator is supplied with heat from an electrical heater, via the secondary refrigerant (water). The heater is adjusted manually via a transformer. The amount of water flowing through the evaporator and the temperature entering and leaving the evaporator are also measured.

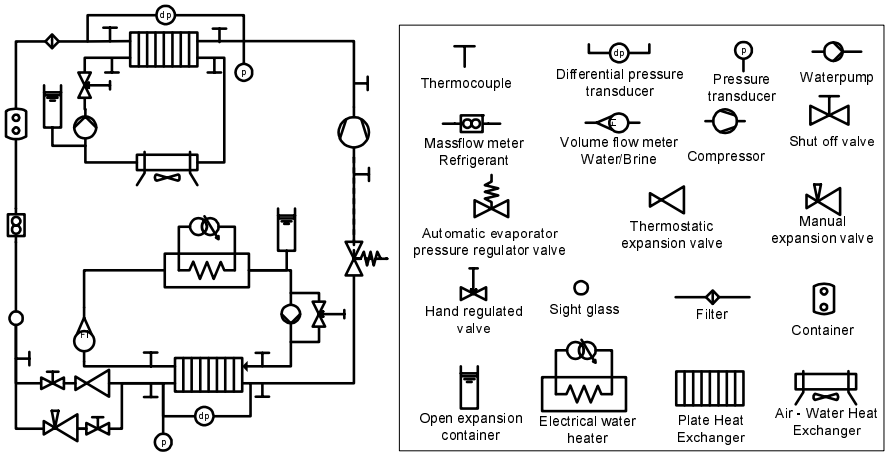

Figure 46: Experimental setup and measuring equipment.

Just upstream of the expansion valve there is a measuring point for the temperature, making it possible to take into account any subcooling of the refrigerant. The condenser is water-cooled and the water flow on both the low and high pressure sides are adjustable via manually controlled valves.

At the same time as all pressures, mass flow rates and temperatures are measured, a CCD camera take pictures of the colorplay of the TLC. Each measured point in Figure 48 represents an average of 100 pictures. For each of these pictures, the number of pixels containing a color corresponding to the saturation temperature in the evaporator is counted. Then the average value of the one hundred pictures is calculated, corresponding to the averaged measured boiling heat transfer area of that measured point. Figure 47 shows the principal setup of the CCD-camera.

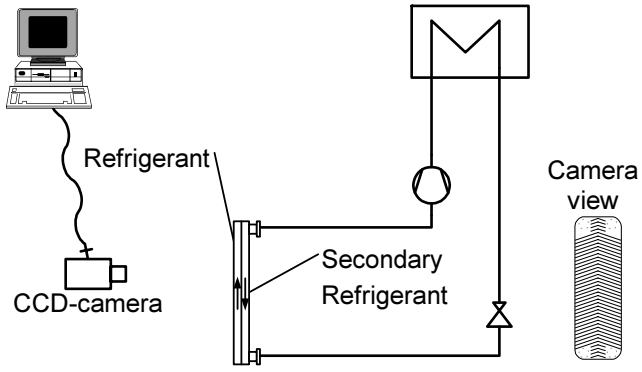

Figure 47: Principal setup for CCD-camera.

20.3 Experimental results and discussion

Approximately 64 measurements have been conducted, at four different heat loads, different superheating and different water flow rates. Figure 48 shows the percentage of the area used for boiling, determined from the photos of the TLC. Typical examples of pictures on which Figure 48 is based may be seen in Figure 49.

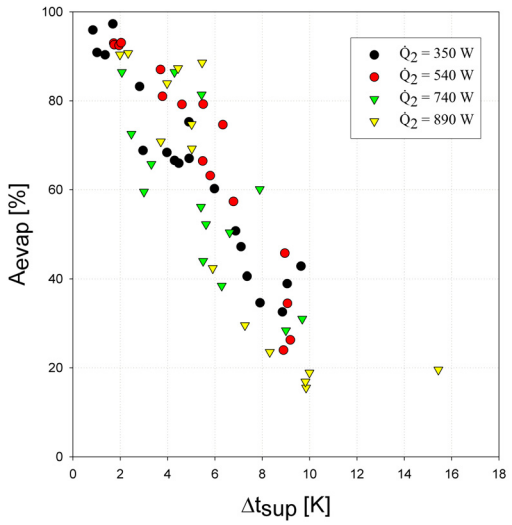

Figure 48: Percentage of area used for evaporation versus superheat.

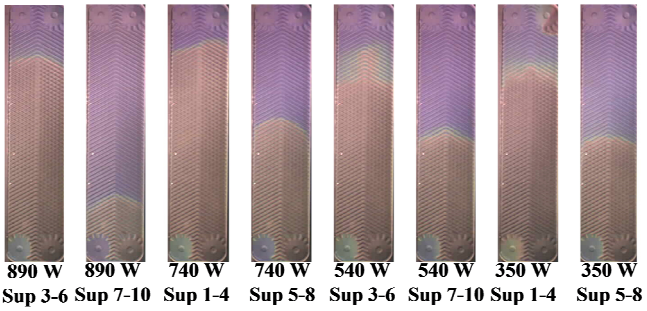

Figure 49: Typical colorplay of TLC during measurements.

In Figure 48, there is a slight trend towards steeper negative slope for higher heat loads. This could indicate that, for a given superheat, more area is required

for superheating the refrigerant at higher heat loads, compared to lower heat loads. It could also indicate that mist flow occurs at lower vapor fractions[i].

In general, if the boiling heat transfer coefficient ($\alpha_{R,evap}$) increases with the mass flux, the heat transfer can be assumed to be governed by forced convective evaporation. However, if $\alpha_{R,evap}$ is a function of the heat flux only, nucleate boiling is the dominating heat transfer mechanism, Collier and Thome (1996).

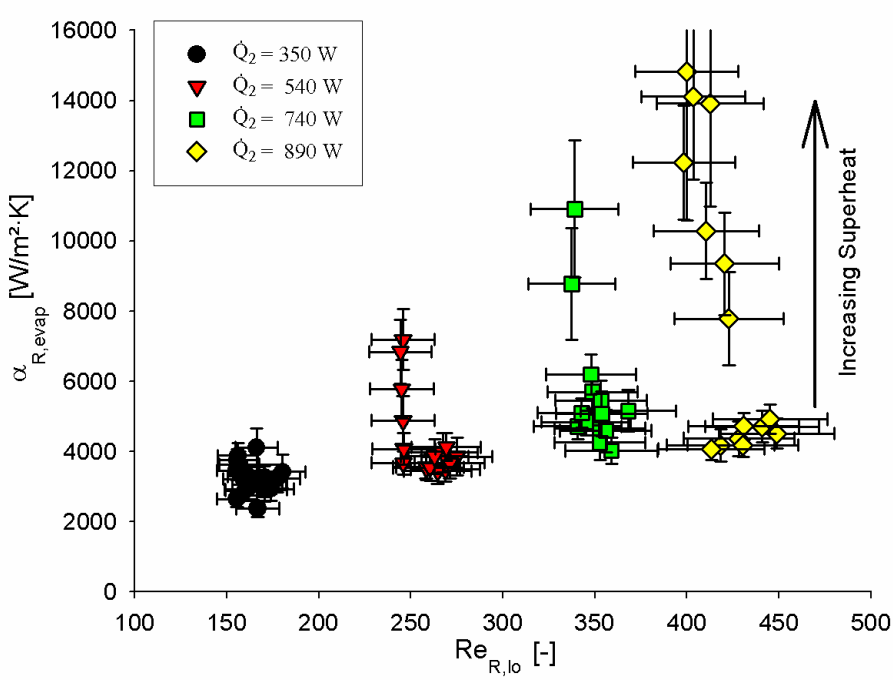

Figure 50: $\alpha_{refr,evap}$ versus the refrigerant Reynolds number.

Since the area for both the boiling and the superheated region is known the heat flux in each of these regions can be calculated. From Figure 50 it may be seen that the boiling heat transfer coefficient, at any total heat load, seems to be independent of the Reynolds number. The scatter among the data points within each heat load is mainly due to different superheats, which results in different heat flux in the boiling region. Figure 51 shows the boiling heat transfer coefficient versus the boiling heat flux. It may be seen that the boiling heat transfer coefficients approximately falls onto a single line. Thus, it seems clear that the boiling area averaged refrigerant film heat transfer coefficient, $\alpha_{R,evap}$, is mainly a function of the boiling heat flux and not of the mass flux.

[i] See chapter 22 and 23.

It may be concluded that the measured boiling area averaged flow boiling film heat transfer coefficient seems to be mainly in the heat flux dependent region. The convective evaporation part of the heat transfer process may still be present, but is negligible compared to the nucleate boiling part during these experiments done under "typical" refrigeration running conditions.

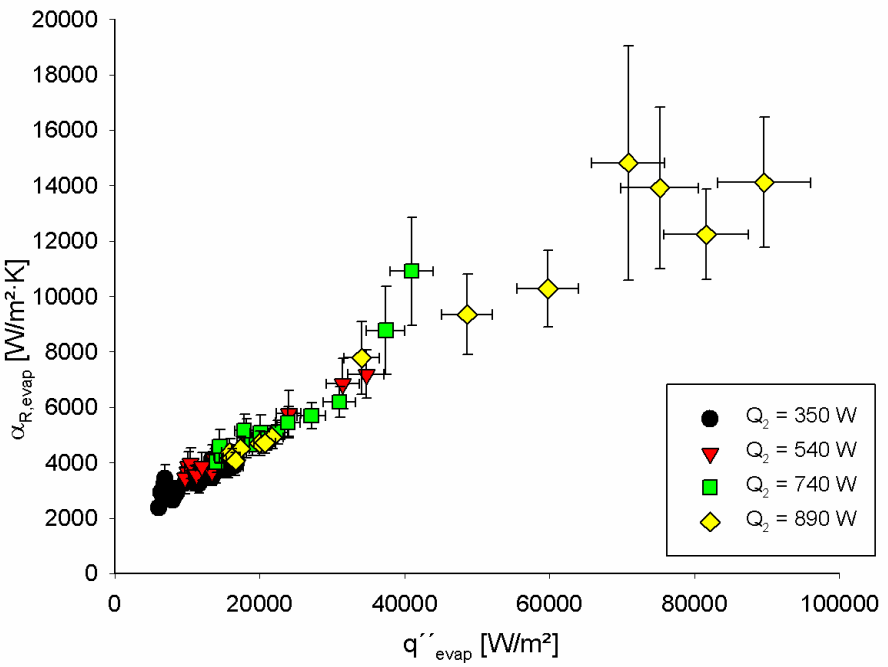

Figure 51: $\alpha_{R,evap}$ versus the boiling heat flux.

According to Collier and Thome (1996), the preferred correlation for refrigerants in nucleate boiling is proposed by Cooper (1984) as

$$\alpha_{Cooper} = C \cdot \frac{55 \cdot p_r^{\,0.12-0.2\cdot\log_{10} R_p}}{\left(-\log_{10} p_r\right)^{0.55} \cdot \tilde{M}^{0.5}} \cdot q''^{0.67} \qquad (177)$$

Plotting the experimental data versus eq. (177), assuming a surface roughness R_p of 1 µm and the correction constant C to be 1.0, yields a systematic deviation from the correlation, see Figure 52.

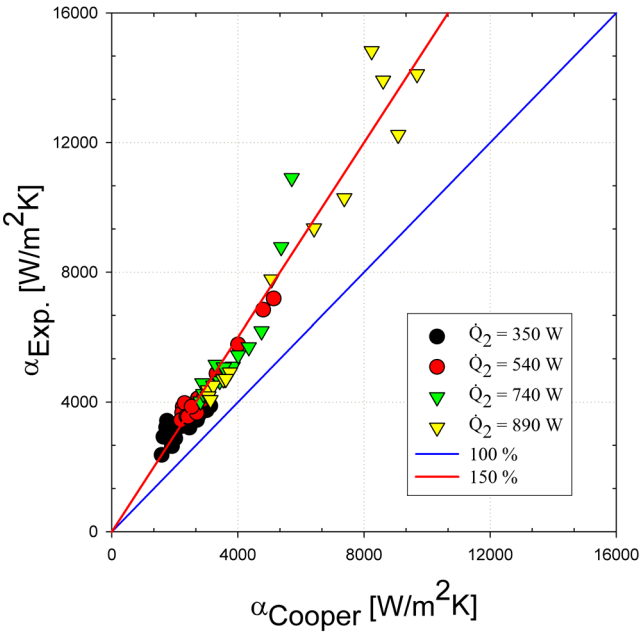

Figure 52: Comparison between experiment and correlation by Cooper.

From Figure 52 it may be seen that the correlation by Cooper yields too low values. Cooper recommend however that for boiling from a horizontal copper cylinder, the constant C is set to 1.7. C can thus be considered as a geometry-dependent constant. It seems that a value of 1.5 is a good value for this constant for plate heat exchangers, based on the experimental data obtained in this investigation.

The use of Cooper's correlation for plate heat exchangers is not new, Pelletier (1998) used the total heat flux based on the entire heat exchanger area and for superheats between 4-6 K. He found excellent agreement between experimental data and the original Cooper correlation without the need to correct the correlation. Inspecting Figure 48, five degrees of superheat correspond approximately to 70 % of the total heat transfer area used for boiling. Using this value to estimate the total area refrigerant heat transfer coefficient one obtains roughly the values as predicted by the Cooper correlation, with C = 1.0. This findings in this chapter is thus in agreement with the findings by Pelletier (1998).

20.4 Conclusion

As the refrigerant side film heat transfer coefficient, $\alpha_{R,evap}$, was found to be practically independent of the mass flux but dependent on the heat flux it may

be concluded that the boiling mechanism in an compact brazed plate heat exchanger (CBE) is mainly nucleate boiling dominated. The correlation by Cooper with an adjusted constant, $C = 1.5$, was found to correlate the experimental data quite well.

21 LMTD CORRECTION IN AN CBE EVAPORATOR[i]

The logarithmic mean temperature difference concept assumes that the film heat transfer coefficients, on both sides, do not change along the heat exchanger. However, the flow boiling heat transfer coefficient depends in general on local parameters such as vapor quality, mass flux and heat flux. In an evaporator for refrigerating applications, the heat flux changes along the flow path, as does the vapor quality. In the previous chapter, we found that the boiling area average refrigerant film heat transfer coefficient may be estimated using the boiling area average heat flux and the pool boiling correlation by Cooper (1984). If we apply this concept, and assume, in addition, that the Cooper correlation applies locally, we could estimate the LMTD correction factor. This chapter will conduct this analysis and estimate the LMTD correction factor.

21.1 The LMTD approach

Using terminal temperatures to estimate the heat transfer coefficient requires a suitable temperature difference, ϑ_m. The heat transferred from the water/brine side to the refrigerant may be expressed as

$$\dot{Q} = U \cdot A \cdot \vartheta_m \tag{178}$$

In addition, the logarithmic mean temperature difference approach, found in any textbook on heat transfer, e.g. Incropera and DeWitt (1996), may be used. For any heat exchanger the heat transfer may be expressed as

$$\dot{Q} = U \cdot A \cdot \vartheta_{LMTD} \cdot F \tag{179}$$

where F is the correction factor used for heat exchangers other than pure co-current or counter-current. ϑ_{LMTD} is the logarithmic mean temperature difference.

Several assumptions are involved in deriving the logarithmic mean temperature difference (Incropera and DeWitt 1996):

1. Steady state operation.

---

[i] This chapter is based on: Claesson J., 2004b, Correction of Logarithmic Mean Temperature Difference in Compact Brazed Plate Heat Evaporator with Heat Flux Governed Flow Boiling Heat Transfer Coefficient, Accepted for publication in International Journal of Refrigeration, doi:10.1016/j.ijrefrig.2004.09.011.

2. Overall heat transfer, U, is constant.

3. Temperature and flow are uniformly distributed across the heat transfer surface.

4. No heat conduction in axial direction in the wall or in the fluids.

5. No heat losses.

6. Fluid properties are constant.

In a CBE evaporator, restriction 2 does not hold. Even though the governing heat transfer mechanism is not established in the literature and a widely accepted heat transfer correlation for flow boiling is not available for a CBE, it is commonly assumed that boiling heat transfer in general is either nucleate boiling dominated, convective evaporation dominated or possibly a combination of both. Hence, in the general case,

$$\alpha_R = f(\dot{m}_R, x, q'') \tag{180}$$

Both vapor quality and the heat flux varies along the evaporator, influencing the local boiling heat transfer and the overall heat transfer coefficient. Hence, assumption 2 is not correct.

21.2 General analysis

In this section, the general equations will be established. Later, simplifications are introduced and the correction factor is calculated. In the analysis, only the boiling section of the evaporator is investigated, leaving the superheated section out of the analysis. The schematic temperature profiles are shown in Figure 53.

Thus, the local heat transfer is, see Figure 53,

$$d\dot{Q} = U \cdot \vartheta \cdot dA \tag{181}$$

where U is the local overall heat transfer coefficient.

$$U = \frac{1}{1/\alpha(\dot{m}_R, x, q'') + 1/\alpha_{brine}} \tag{182}$$

The resistance in the wall is neglected, but may easily be incorporated. The heat transfer may also be calculated for each flow stream as

$$d\dot{Q} = \dot{m}_{brine} \cdot c_{p,brine} \cdot dt_{brine} \tag{183}$$

and

$$d\dot{Q} = \dot{m}_R \cdot dh_R \tag{184}$$

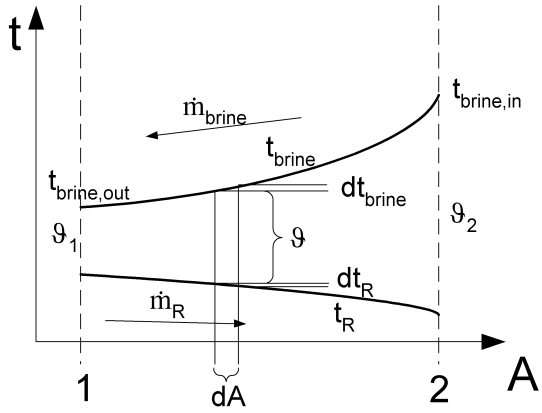

Figure 53: General temperature profiles.

The change in enthalpy of the refrigerant in the saturated region may be rewritten, accounting for pressure drops, as

$$dh_R = \frac{\partial h'}{\partial p} \cdot dp + \frac{\partial \Delta h_{fg}}{\partial p} \cdot x \cdot dp + \Delta h_{fg} \cdot dx \tag{185}$$

where the two first terms may be calculated using thermophysical properties and a suitable two-phase pressure drop correlation for the geometry at hand.

With this set of equations, along with a suitable pressure drop correlation, heat transfer correlations and void fraction correlations (necessary for calculating pressure drop) the heat transfer is difficult (impossible) to solve analytically. However, a numerical procedure with small incremental steps may be used. The starting point is then to calculate for each step the pressure drop and heat transfer (eq. 181). Then the increase in vapor quality of the refrigerant and the temperature change of the water/brine may be determined from eqs. (184-185). New temperatures are obtained at the new position (z+dz) in the evaporator.

21.3 Simplified analysis

A simplification of the above analysis is desired, making it somewhat easier. Below, the following simplifications will be introduced:

1. No pressure drop.

2. Brine side heat transfer coefficient is constant.

3. Boiling mechanism is governed by nucleate boiling only.

The previous assumptions 1, 3-6 are retained. Simplification 1 simplifies eq. (185) to

$$dh_R = \Delta h_{fg} \cdot dx \tag{186}$$

These additional simplifications yields a slightly different physical model compared to Figure 53. The actual simplified physical model is depicted in Figure 54.

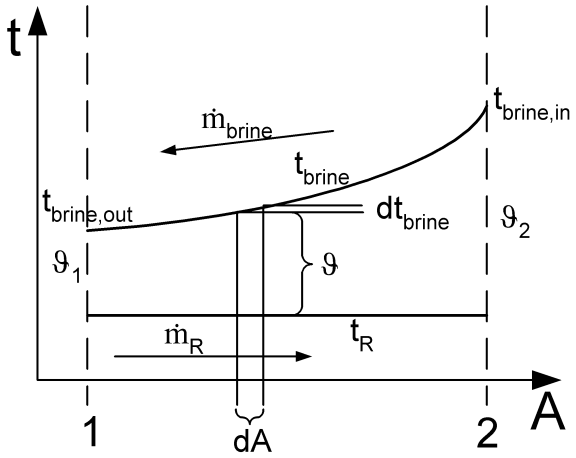

Figure 54: Simplified model.

As was shown in the previous chapter, the flow boiling heat transfer coefficient in plate heat exchangers is mainly heat flux dominated. It was also shown that the correlation by Cooper (1984), eq. (187), with the constant C = 1.5 gave fairly accurate boiling area averaged refrigerant film heat transfer coefficients.

$$\alpha_R = C \cdot 55 \cdot p_r^{0.12-0.2\cdot\log_{10} R_p} \cdot \left(-\log_{10} p_r\right)^{-0.55} \cdot \tilde{M}^{-0.5} \cdot q''^{0.67} = C_c \cdot q''^{0.67} \tag{187}$$

It should be noted that the heat flux used in the previous chapter is the boiling area averaged heat flux, excluding the superheated region.

Combining eqs. (181 - 183) yields

$$\frac{1}{\vartheta}\frac{1}{\left(\frac{1}{\alpha_R}+\frac{1}{\alpha_{brine}}\right)^{-1}}dt_{brine}=\frac{1}{\dot{m}_{brine}\cdot c_{p,brine}}dA \tag{188}$$

The driving force for heat transfer, the temperature difference between the two streams, is

$$\vartheta = t_{brine} - t_R \tag{189}$$

Hence, since we do not account for pressure drop

$$d\vartheta = dt_{brine} \tag{190}$$

Substituting eq. (190) into eq. (188) yields

$$\frac{1}{\vartheta}\frac{1}{\left(\frac{1}{\alpha_R}+\frac{1}{\alpha_{brine}}\right)^{-1}}d\vartheta=\frac{1}{\dot{m}_{brine}\cdot c_{p,brine}}dA \tag{191}$$

The local refrigerant heat transfer may be expressed as

$$q'' = \alpha_R \cdot \Delta t_w \tag{192}$$

where Δt_w is the local wall superheat, i.e. the temperature difference between the wall and the refrigerant. Collecting, for simplicity, all terms but the heat flux in eq. (187) into a constant C_C and substituting eq. (192) into eq. (187) we obtain

$$\alpha_R = C_C{}^3 \cdot \Delta t_w^2 \tag{193}$$

where C_c is

$$C_C = C \cdot 55 \cdot p_r^{0.12-0.2\cdot\log_{10} R_p} \cdot \left(-\log_{10} p_r\right)^{-0.55} \cdot \tilde{M}^{-0.5} \tag{194}$$

To be able to integrate eq. (188) with eq. (193) inserted we have to find an expression for the local wall superheat, Δt_w. On the brine side, the heat transfer may be expressed in an analogous way as eq. (192), i.e.

$$q'' = \alpha_{brine} \cdot \left(t_{brine} - t_w\right) \tag{195}$$

Combining eqs. (189, 192, 193 and 195) gives

$$\Delta t_w^3 + \frac{\alpha_{brine}}{C_C^3} \cdot \Delta t_w - \frac{\alpha_{brine}}{C_C^3} \cdot \vartheta = 0 \tag{196}$$

which has one real root (Råde and Westergren 1990). The solution is

$$\Delta t_w(\vartheta) = \sqrt[3]{\frac{\alpha_{brine} \cdot \vartheta}{2 \cdot C_C^3} + \sqrt{\left(\frac{\alpha_{brine}}{3 \cdot C_C^3}\right)^3 + \left(-\frac{\alpha_{brine} \cdot \vartheta}{2 \cdot C_C^3}\right)^2}} + \sqrt[3]{\frac{\alpha_{brine} \cdot \vartheta}{2 \cdot C_C^3} - \sqrt{\left(\frac{\alpha_{brine}}{3 \cdot C_C^3}\right)^3 + \left(-\frac{\alpha_{brine} \cdot \vartheta}{2 \cdot C_C^3}\right)^2}} \tag{197}$$

Substituting eq. (196) into eq. (188) and integrating, which may be done numerically, yields the heat transfer area required for evaporation.

$$\frac{A}{\dot{m}_{brine} \cdot c_{p,brine}} = \int_{\vartheta_1}^{\vartheta_2} \frac{1}{\vartheta} \cdot \frac{1}{\left(\frac{1}{C_C^3 \cdot \Delta t_w(\vartheta)^2} + \frac{1}{\alpha_{brine}}\right)^{-1}} d\vartheta \tag{198}$$

MathCad 2001 Professional is used for the numerical integration. The total heat transfer in the evaporator may be calculated according to

$$\dot{Q} = \overline{U} \cdot \vartheta_m \cdot A \tag{199}$$

and

$$\dot{Q} = \dot{m}_{brine} \cdot c_{p,brine} \cdot \left(t_{brine,in} - t_{brine,out}\right) \tag{200}$$

Combining eqs. (198 - 200), an expression for the average heat flux is obtained

$$\frac{\dot{Q}}{A} = \overline{q}'' = \overline{U} \cdot \vartheta_m = \frac{\vartheta_2 - \vartheta_1}{\int_{\vartheta_1}^{\vartheta_2} \frac{1}{\vartheta} \cdot \frac{1}{\left(\frac{1}{C_C^3 \cdot \Delta t_w(\vartheta)^2} + \frac{1}{\alpha_{brine}}\right)^{-1}} d\vartheta} \tag{201}$$

where

$$\vartheta_2 - \vartheta_1 = t_{brine,in} - t_{brine,out} \tag{202}$$

since the refrigerant temperature is assumed constant.

Substituting average heat flux (eq. 201) into the boiling heat transfer correlation (eq. 187) and then into eq. (182), the area averaged overall heat transfer coefficient is obtained.

$$\bar{U} = \frac{1}{\frac{1}{C_C \cdot \bar{q}''^{2/3}} + \frac{1}{\alpha_{brine}}} \tag{203}$$

The appropriate temperature difference is apparently

$$\vartheta_m = \frac{\bar{q}''}{\bar{U}} \tag{204}$$

The logarithmic mean temperature difference (LMTD) is convenient to use when calculating heat transfer in heat exchangers. The correction factor, F, necessary to use when LMTD is used is obtained by combining eq. (178) and eq. (179).

$$F = \frac{\vartheta_m}{\vartheta_{LMTD}} \tag{205}$$

where the logarithmic mean temperature difference is calculated as

$$\vartheta_{LMTD} = \frac{\vartheta_2 - \vartheta_1}{\ln \frac{\vartheta_2}{\vartheta_1}} \tag{206}$$

21.4 Theoretical results

Using the above analysis, the correction factor, F, may be calculated. As already mentioned, the integral in eq. (201) is evaluated numerically in MathCad 2001 Professional. Different temperature drop of the brine is simulated, along with different values of the brine heat transfer coefficient, see Figure 55 and Figure 56. Refrigerant R-22 at a saturation temperature of +5 °C is assumed for evaluating the heat transfer coefficient in eq. (194).

The influence of brine temperature drop and brine heat transfer coefficient may be seen in Figure 55 and Figure 56, respectively. The values in the charts should be interpreted as a rough estimate of the magnitude of correction needed. As may be seen, the correction is not very significant, for moderate to large logarithmic mean temperature differences, and it may be concluded that the LMTD approach is sufficient accurate for these applications.

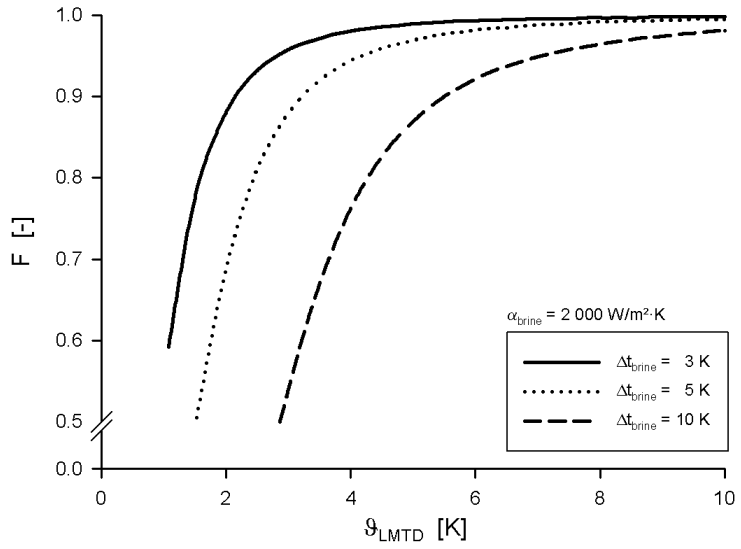

Figure 55: Correction factor when using LMTD for α_{brine} = 2 000W/m²K for different brine temperature drops.

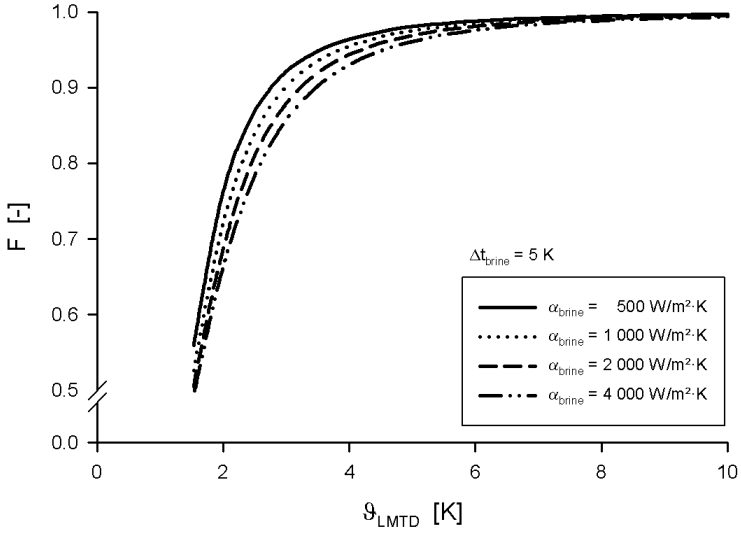

Figure 56: Correction factor when using LMTD for different α_{brine} at 5 K brine temperature drop.

At very low temperature difference at the brine outlet end of the evaporator, ϑ_1, the validity of using a correlation for nucleate boiling is questionable, as it

might be expected the wall superheat at some point may be too low to initiate nucleation. However, no such consideration has been done in the present analysis.

21.5 Conclusions

The applicability of the logarithmic mean temperature difference (LMTD) has been investigated in a compact brazed plate heat exchanger (CBE), assuming the boiling heat transfer governed by nucleate boiling only and the correlation by Cooper (1984) is applicable. A general set of equations was first identified, and then a few simplifications were introduced. From the analysis, the appropriate mean temperature difference could be calculated and compared to the LMTD. The relation between them, F, was plotted for a limited number of selected cases.

It was shown that the correction factor F is close to one and may be neglected for moderate to high logarithmic mean temperature differences and that the LMTD approach is sufficiently accurate for predicting boiling heat transfer in plate heat exchangers. It may be concluded that the LMTD approach may be used determining the heat flux governed flow boiling heat transfer coefficient calculated backwards without introducing any significant error.

22 INFLUENCE OF CHEVRON ANGLE[i]

It is a well known fact that the chevron angle is one of the most important geometrical factor affecting the single phase heat transfer coefficient. However, as stated by Haseler and Butterworth (1995), a plate heat exchanger with high single phase heat transfer coefficient does not necessarily have high flow boiling heat transfer coefficient. It is the purpose of this chapter to investigate the performance of several evaporators, having geometrically similar plates but with different chevron angles.

The actual experiments on which this chapter is based were conducted at SWEP International AB in Landskrona, Sweden. They have been kind enough to supply the author of this thesis with the experimental data of their experiments. Unfortunately, only the average values of temperatures, flow rates, and pressures were available, i.e. the raw data of the measurements had not survived time.

The effect of the chevron angle on the overall heat transfer coefficient, based on the entire heat transfer area in the heat exchanger, is investigated and the results are reported in this chapter. In addition, the boiling area in the heat exchanger is estimated, by subtracting the predicted heat transfer area required for superheating the refrigerant according to

$$A_{evap} = A_{tot} - A_{sup} \tag{207}$$

where A_{sup} is predicted using single phase correlations. The single phase correlation, eq. (127), is supplied to the author by the manufacturer of the heat exchangers. The calculation procedure is outlined in chapter 19.

22.1 Experimental results

The tests are carried out with different heat loads and superheats. All tests are carried out at 5 bar(a) evaporating pressure, inlet vapor quality within 11% to 19% and with R-22 as the working fluid. The different cooling capacities are set by adjusting the rotational speed of the compressor, and at the same time maintaining the brine temperature drop of approximately 5 K.

---

[i] This chapter is based on: Claesson J., Palm B., Pelletier O., 2001, "On the influence of geometry on evaporation in compact brazed plate heat exchangers", ICMF-2001 4th International Conference on Multiphase Flow, E.E. Michaelides ed., May 27 to June 1, 2001, New Orleans, Louisiana, USA, paper 156.

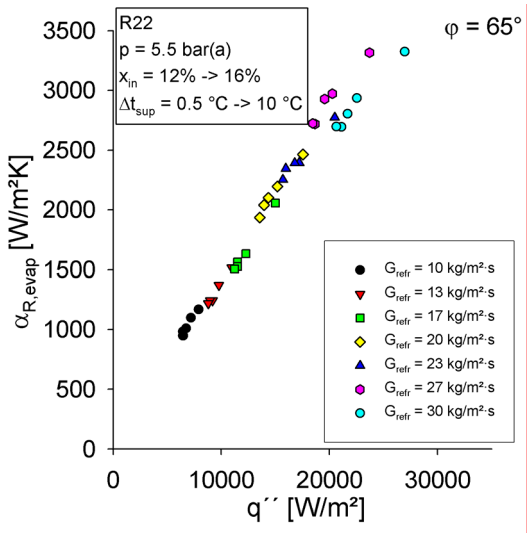

Figure 57: Estimated boiling area averaged refrigerant film heat transfer coefficient as a function of predicted boiling heat flux for chevron angle φ = 65°.

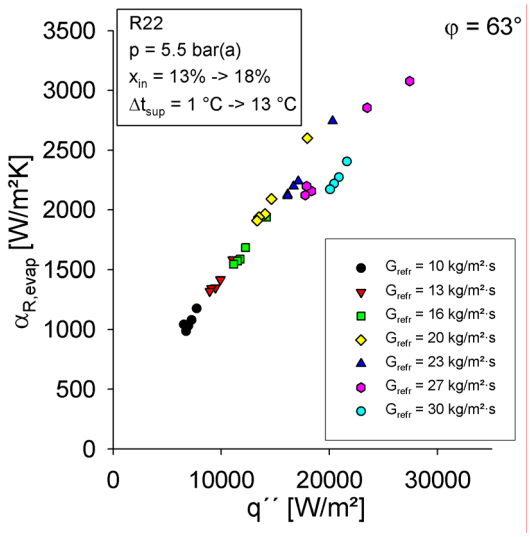

Figure 58: Estimated boiling area averaged refrigerant film heat transfer coefficient as a function of predicted boiling heat flux for chevron angle φ = 63°.

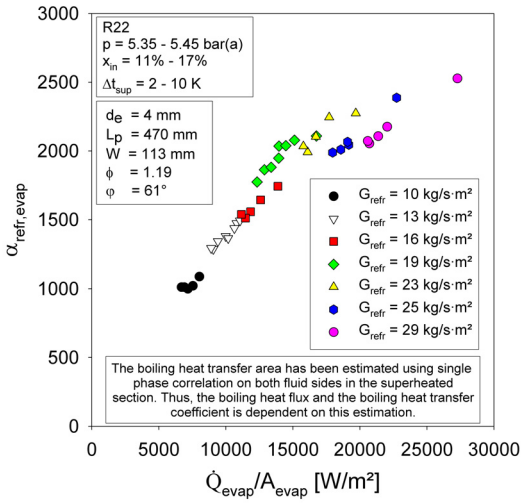

Figure 59: Estimated boiling area averaged refrigerant film heat transfer coefficient as a function of predicted boiling heat flux for chevron angle φ = 61°.

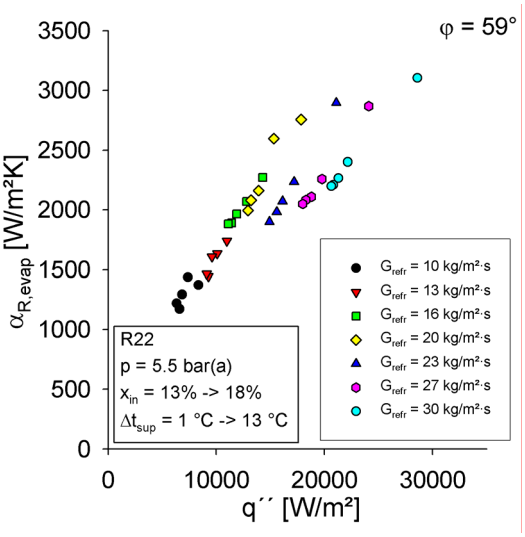

Figure 60: Estimated boiling area averaged refrigerant film heat transfer coefficient as a function of predicted boiling heat flux for chevron angle φ = 59°.

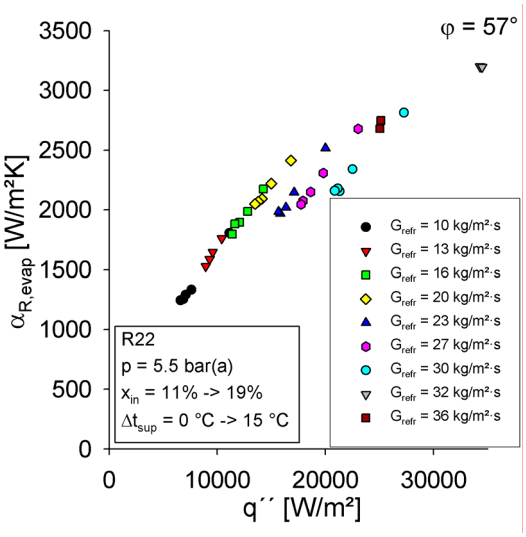

Figure 61: Estimated boiling area averaged refrigerant film heat transfer coefficient as a function of predicted boiling heat flux for chevron angle φ = 57°.

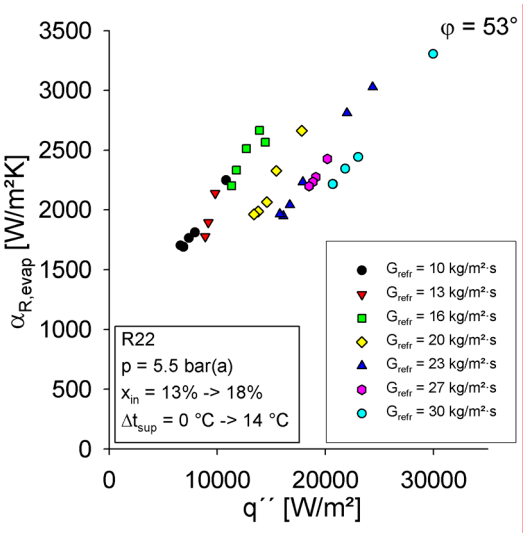

Figure 62: Estimated boiling area averaged refrigerant film heat transfer coefficient as a function of predicted boiling heat flux for chevron angle φ = 53°.

The estimated boiling area averaged refrigerant film heat transfer coefficients are seen in Figure 57 to Figure 62 for the tested chevron angles. It may be observed from the figures that the heat transfer coefficient seems to be a strong function of the boiling area averaged heat flux, q". The heat transfer coefficient for chevron angles 65° and 63° are very similar. The values for the chevron

angle 61° are somewhat higher and very similar results is displayed with 59° and 57°. At low heat flux, chevron angle of 53° displays the highest heat transfer coefficients.

The scatter in the calculated two-phase heat transfer is larger at higher heat flux. The different mass fluxes used during the experiments are indicated in the figures. It seems that the scatter occurs at higher mass fluxes, typically for G_R > 19 kg·m^{-2}·s^{-1}. It is not clear what this behavior originate from. Several reasons may be thought of, e.g.:

1. The one-phase correlations are less accurate at higher Reynolds numbers.
2. Another boiling phenomenon becomes dominant.
3. Refrigerant flow maldistribution between refrigerant channels.
4. Mist flow does occur, with tiny droplets of liquid traveling in the gas core.

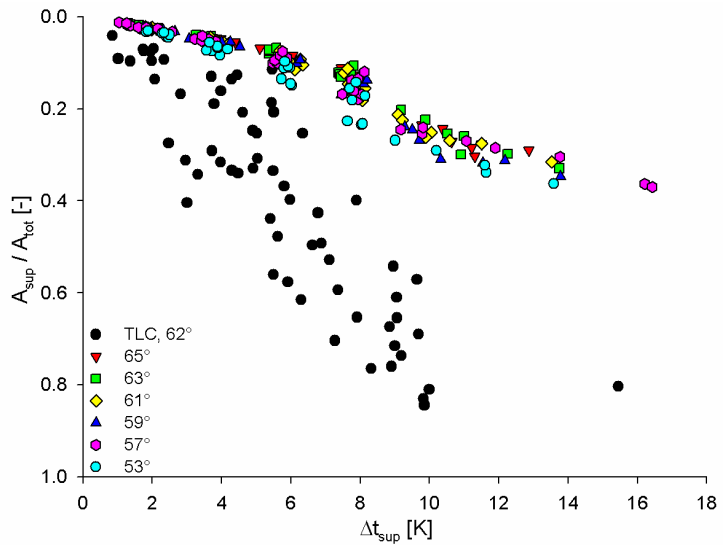

Figure 63: Used superheated area as a function of the superheat.

A sensitivity analysis of the boiling heat transfer coefficient has been conducted. If the one-phase correlation has an accuracy of ± 5%, the calculated boiling heat transfer coefficients are changed by about the same percentage. Thus, any difference in two-phase heat transfer due to some simple imposed error in the one-phase heat transfer coefficient is not sufficient to explain the scatter observed at high heat flux.

In Figure 63, the area used for superheating the refrigerant calculated backwards, according to eq. (165), is plotted. Comparison with data from chapter 20 (Claesson and Palm, 1999) indicates that the used area for superheat is less than experimentally observed. The boiling area in chapter 20 was determined using thermochromic liquid crystals painted on the outer surface, indicating the position where the outer wall temperature increased rapidly.

An in-depth discussion regarding these observations and the obvious discrepancy will be carried out in chapter 23.

In Figure 64, the total overall heat transfer coefficients are shown for all the tested chevron angles. As seen, no chevron angle displays the largest overall heat transfer over the entire range of heat loads tested. At low heat load, chevron angle of 53° display the best performance. At higher heat loads the highest angle tested, φ = 65°, has the best performance. Over the entire range of heat loads, it seems that a chevron angle of 61° may be preferable.

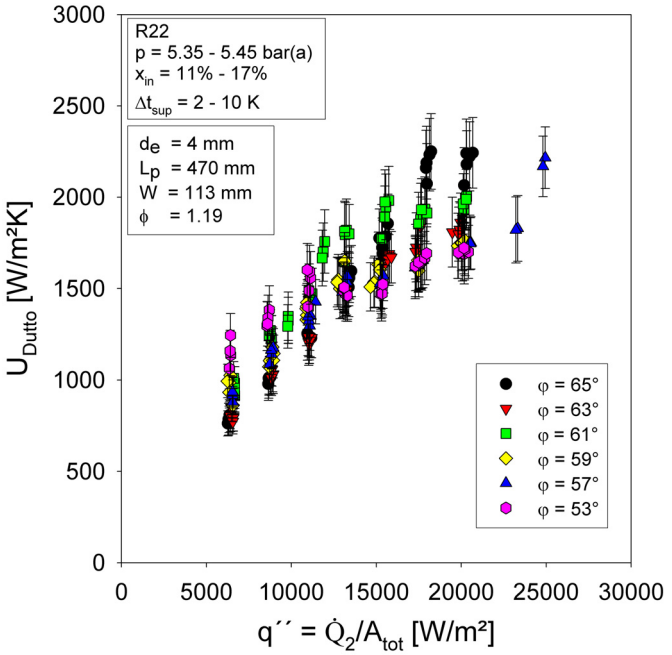

Figure 64: Overall heat transfer coefficient as a function of heat flux.

22.2 Conclusion

This chapter reported on boiling two-phase flow heat transfer coefficients for compact brazed plate heat exchangers with several chevron angles, ranging from 53° to 65°. A wide range of heat loads was tested.

Experiments were conducted with R-22. From the experiment the boiling heat transfer was determined from the inlet and outlet temperatures and the brine mass flow rate, using the one-phase heat transfer coefficients for the brine side and the superheated section. The different chevron angles display very similar values of the boiling heat transfer coefficient. Considering the overall heat transfer, it seems that the chevron angle 61° displays the best performance over the tested range.

A significant scatter of the boiling area averaged refrigerant side film heat transfer was observed at mass flux above 19 kg/m²·s.

23 POSSIBLE REASONS FOR THE DIFFERENCE BETWEEN MEASURED AND CALCULATED SUPERHEATED HEAT TRANSFER AREA[i]

In the evaporator, two main regions are present – the boiling and superheating regions. When predicting the performance of the evaporator, these two regions have to be treated individually. First, the area of each region must be determined. With a given superheat and mass flows of both fluids known, the superheating area is readily calculated since both fluids are in single phase, i.e. single phase correlations can be used. The remaining heat transfer area would then be used to evaporate the refrigerant. However, in chapter 22 (Claesson et al., 2001) we found that this approach did not provide consistent results. The boiling heat transfer coefficients were expected to be a function of the boiling heat flux, as found in chapter 20 (Claesson and Palm, 1999). However, the resulting heat transfer coefficient displayed a considerable scatter. The reason for this scatter was not clear and a comparison between the measured area for superheat in chapter 20 (Claesson and Palm 1999), and the predicted area for superheat in chapter 22 (Claesson et al. 2001), showed a considerable deviation.

The present chapter investigates this described discrepancy between the "backwards" calculated superheating area and the observed superheating area. From simultaneous measurements of superheating area and temperature, mass flows and so forth, the discrepancy is readily calculated. The superheating area is measured with Thermochromic Liquid Crystals (TLC), a temperature sensitive paint, and an ordinary CCD-camera. The measurements are described in detail in chapter 20 and in Claesson and Palm (1999).

23.1 Calculation of superheated heat transfer area

The simplest way to find the heat transfer area for the superheating region as well as the evaporating region is to assume that the single-phase correlations for the heat transfer coefficient holds in the superheating region. For a performance evaluation process the backwards-calculating procedure is outlined as follows:

---

[i] This chapter is based on: Claesson J., Palm B., 2002, Discrepancy between calculated and measured superheated area in an evaporator plate heat exchanger, HEFAT 2002, 1st Int. Conf. on Heat Transfer, Fluid Mechanics and Thermodynamics, 8-12 April, Kruger Park, South Africa, vol. 1, pt. 2, pp. 1079-1086.

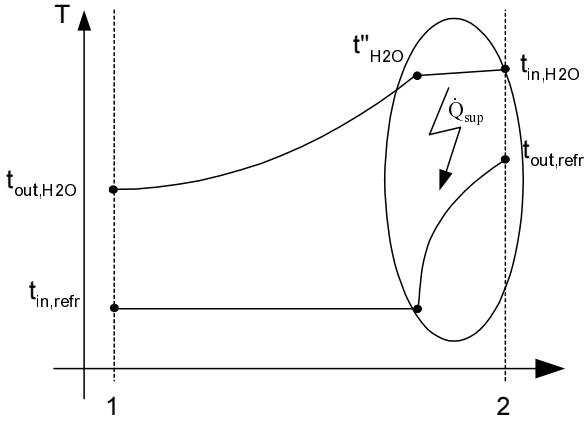

Figure 65: Temperature profile in the evaporator, superheating region highlighted.

In the superheating region, highlighted in Figure 65, from measured mass flow, temperatures and pressures on both sides, eq. (169) and eq. (170) are used for calculation of the heat transfer coefficients. The overall heat transfer coefficient is calculated according to

$$\left(\frac{1}{U_{sup}}\right)_{pred} = \left(\frac{1}{\alpha_{sup_{refr}}}\right)_{pred} + \left(\frac{1}{\alpha_{sup_{H_2O}}}\right)_{calc} \tag{208}$$

In the experiment carried out the secondary refrigerant was water and thus denoted in eq. (208) as H_2O.

From the measured heat load in the superheating region, the area required to transfer that heat is readily calculated as

$$A_{sup_{pred}} = \frac{\dot{m}_R \cdot c_{p_{R,sup}} \cdot \Delta t_{sup}}{U_{sup_{pred}} \cdot \vartheta_{m_{sup}}} \tag{209}$$

where

$$\vartheta_{m_{sup}} = \frac{\left(t''_{H_2O} - t_{R,sat}\left(p_{R_{out}}\right)\right) - \left(t_{in_{H_2O}} - t_{out_{refr}}\right)}{\ln\left(\frac{t''_{H_2O} - t_{R,sat}\left(p_{R_{out}}\right)}{t_{in_{H_2O}} - t_{out_{refr}}}\right)} \tag{210}$$

is the logarithmic mean temperature difference over the superheating region. It is assumed that no pressure drop occurs in the evaporator. Accounting for the

pressure drop in the superheated section of the evaporator does not affect the results presented in this chapter.

The evaporating heat transfer area is the total heat transfer area minus the required superheating area calculated.

The total heat load, $\dot{Q}_{tot}$, is calculated by taking the enthalpy difference times the mass flow on each fluid side. Comparison between the two values indicate a total energy balance better than 10%. The total heat load used in the calculations is taken as the arithmetic mean. The losses to the surrounding from the un-insulated surface are estimated to less than one watt. Such a low value was obtained since the surrounding was kept at the same temperature as the evaporating temperature. The mass flow rate of each fluid side is then adjusted to match the averaged heat load.

23.2 Measured superheated heat transfer area

The refrigerant film heat transfer coefficients in the superheated section predicted by eq. (170) were compared to values based on the measured area determined by TLC measurements. The calculations are quite straightforward and are briefly shown here. As for the calculation of the superheating areas described in the previous section the heat transfer coefficient on the water side is calculated by eq. (169). From measured heat load, heat transfer area (from TLC measurements) and logarithmic mean temperature in the superheating region, the overall heat transfer coefficient is determined by

$$U_{sup_{meas}} = \frac{\dot{m}_R \cdot c_{p_{R,sup}} \cdot \Delta t_{sup}}{A_{sup_{meas}} \cdot \vartheta_{m_{sup}}} \tag{211}$$

The measured heat transfer coefficient on the refrigerant side is then calculated as

$$\left(\alpha_{sup_{refr}}\right)_{meas} = \frac{1}{\frac{1}{U_{sup_{meas}}} - \left(\frac{1}{\alpha_{sup_{H_2O}}}\right)_{calc}} \tag{212}$$

The uncertainty in the heat transfer coefficient calculated in eq. (212) is estimated by propagation of error to be ± 11 % for low superheat and ± 6 % for high superheat.

23.3 Results

The outlined procedure in section 23.1 is used to calculate the superheating area in all tests with the three-plate heat exchanger. The result is presented in Figure 66 together with the experimentally determined superheating areas. It can be seen that at low superheats, the absolute discrepancy is not large, however at large superheats the discrepancy becomes significant. A few of the calculated areas agree well with measured areas, corresponding to the lowest total heat load (mass fluxes between 8 and 9). In addition, the same discrepancy as observed in the previous chapter is observed here. Thus, it may be concluded that the number of refrigerant channels is not important[i] in this respect.

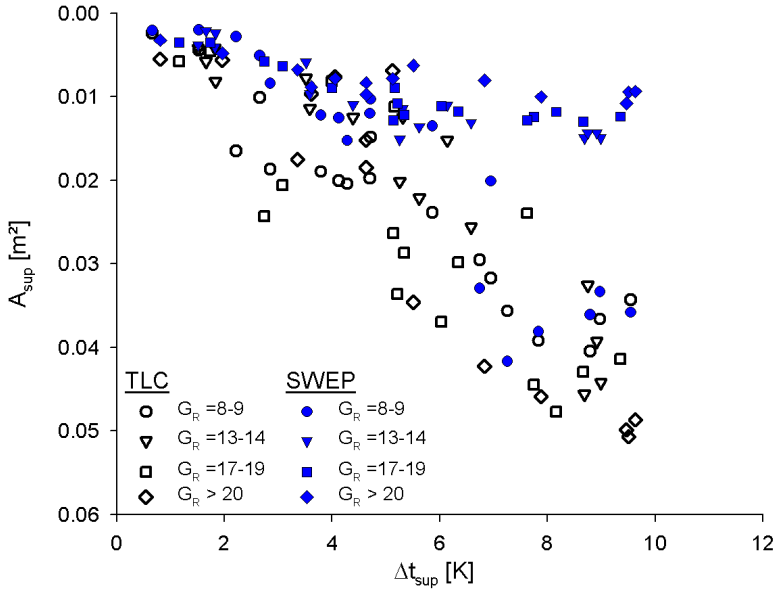

Figure 66: Area required for superheating.

A comparison between the predicted and the measured, based on the apparent non-boiling heat transfer area, heat transfer coefficients as a function of the superheat is shown in Figure 67. The mass fluxes of the series are also indicated. It is clear that the mass flux (Reynolds number) is not by itself responsible for the deviation. The predicted heat transfer coefficient, eq. (170), seems to be an upper limit of the measured heat transfer coefficient in the superheating area. Neither can the uncertainty of the transferred heat in the superheated section since all points with superheat higher than 2 K have the

[i] One could have argued that the maldistribution of refrigerant between the refrigerant channels was responsible for the discrepancy.

same relative uncertainty (7%) (assuming that vapor quality equals one at the position where TLC indicated start of the superheated section).

It may be assumed that the deviation is dependent on the refrigerant side only and that the waterside is appropriately modeled, since the heat transfer coefficient on the waterside is more than an order of magnitude larger than the refrigerant heat transfer coefficient in the superheating region. Thus, no significant error is introduced by this assumption. In addition, as indicated in chapter 22, a reasonable simple error in superheated refrigerant film heat transfer coefficient, eq. (170), is not sufficient to explain the apparent difference.

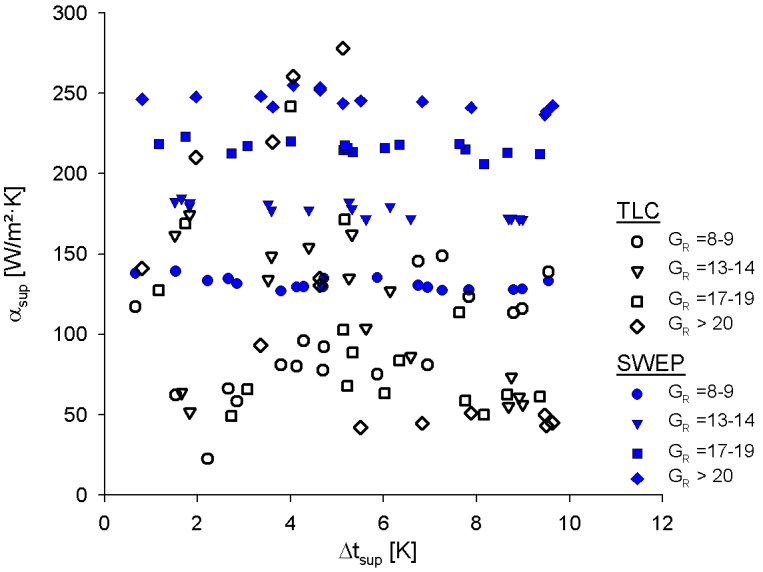

Figure 67: Measured and predicted heat transfer coefficient as a function on Reynolds number.

23.4 Discussion

In this section several possible and perhaps less possible reasons for the difference observed will be discussed.

23.4.1 Longitudinal heat transfer in the wall

One possible reason for the discrepancy might be that the longitudinal heat transfer in the wall is important and that heat is transferred from the superheated section to the boiling section through the wall. The reason for this would be that the wall temperature just upstream of the boundary between the boiling and superheating region is lower than predicted by traditional logarithmic mean

temperature difference procedure, due to the high upstream boiling heat transfer coefficient. To explore this possibility, a simple finite difference scheme was employed.

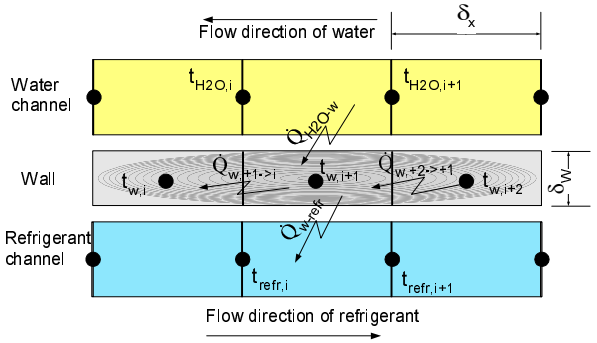

Figure 68: Finite difference scheme.

The calculation scheme starts at the position were the superheat begins. The corresponding water temperature is calculated through a heat balance in the superheating region. The wall temperature is set to the arithmetic mean of the refrigerant and the water temperatures, i.e. assuming equal heat transfer coefficients on the water and the refrigerant sides in the boiling region. The heat transfer area of each cell is set to a fixed value, ΔA_w, and the total heat transfer area required to heat the refrigerant to the known leaving temperature of the heat exchanger is the total sum of the ΔA_w. At the exit of the heat exchanger, the longitudinal heat transfer in the wall is set to zero, i.e. $\left.{}^{dt_w}/_{dx}\right|_{x=L} = 0$.

Now, consider a small section of the heat exchanger, see Figure 68. The energy balance on the water side is constructed of three equations. The first is delivered heat from the water to the wall.

$$\dot{Q}_{H_2O\to w} = \alpha_{H_2O} \cdot \Delta A_w \cdot \left(\frac{t_{H_2O_{i+1}} + t_{H_2O_i}}{2} - t_{w_{i+1}} \right) \tag{213}$$

We thus have a decrease of water temperature over the section

$$\dot{Q}_{H_2O} = \dot{m}_{H_2O} \cdot c_{p_{H_2O}} \cdot \left(t_{H_2O_{i+1}} - t_{H_2O_i} \right) \tag{214}$$

The amount of these two should equal, hence

$$\dot{Q}_{H_2O\to w} = \dot{Q}_{H_2O} \tag{215}$$

On the refrigerant side, the same principle is used, thus

$$\dot{Q}_{w\to refr} = \alpha_{refr} \cdot \Delta A_w \cdot \left(t_{w_{i+1}} - \frac{t_{refr_{i+1}} + t_{refr_i}}{2} \right) \tag{216}$$

$$\dot{Q}_{refr} = \dot{m}_{refr} \cdot c_{p_{refr}} \cdot \left(t_{refr_{i+1}} - t_{refr_i} \right) \tag{217}$$

$$\dot{Q}_{w\to refr} = \dot{Q}_{refr} \tag{218}$$

The equations over the wall are

$$\dot{Q}_{w_{+1\to i}} = \lambda_w \cdot W \cdot \delta_w \frac{t_{w_{i+1}} - t_{w_i}}{\delta_x} \tag{219}$$

$$\dot{Q}_{w_{+2\to +1}} = \lambda_w \cdot W \cdot \delta_w \frac{t_{w_{i+2}} - t_{w_{i+1}}}{\delta_x} \tag{220}$$

and finally the energy balance over a small segment of the wall

$$0 = \dot{Q}_{H_2O\to w} + \dot{Q}_{w_{+2\to +1}} - \dot{Q}_{w\to refr} - \dot{Q}_{w_{+1\to i}} \tag{221}$$

The complete set of equations along with the boundary conditions was set up and calculated in MS-Excel. Eq. (169) and eq. (170) were used for calculating the heat transfer coefficients on respective fluid sides. The calculations indicated, even though up to more than 10% of the heat leaving the water is not retained on the refrigerant side but transported along the wall into the boiling region, that the effect of longitudinal heat transfer in the wall is not responsible for the deviation between eq. (170) and the measured refrigerant film heat transfer coefficient in the superheated section. The main influence the longitudinal heat transfer will have on the superheating region is that the water entering into the superheating region will have somewhat lower temperature than calculated by an energy balance between water and refrigerant only. However, the changes in the water temperature due to the increase of heat leaving the water side is quite small since the heat capacity rate of water is comparatively large.

23.4.2 The effect of gas maldistribution in the superheated section

Another phenomenon that may play a role for the discrepancies is the maldistribution of the superheated gas. As seen in Figure 49, the boiling region seems to have no, or very little, maldistribution, thus the gas leaving the boiling region is thought to be evenly distributed. If the superheat is low, i.e. the onset of superheat is near the outlet port, the gas is in good contact over a large part of the superheating region. However, if the superheat increases, the gas is flowing

towards the outlet port, creating a relatively larger portion of the heat transfer area in which the mass flow is low, hence decreasing the average heat transfer coefficient.

One observation does however indicate the insignificance of this phenomenon; the fact that the difference between measured and predicted heat transfer area increases as the superheat increases, see Figure 66. If this phenomenon was important, it would be expected that the observed difference would decrease as a larger part, with increasing superheat, of the heat exchanger operate as a gas heater.

Even if the maldistribution of the gas don't have any significant practical effect, it is still interesting from an academic point of view to investigate in the future how the plate heat exchanger performs locally in this "cross-flow" part.

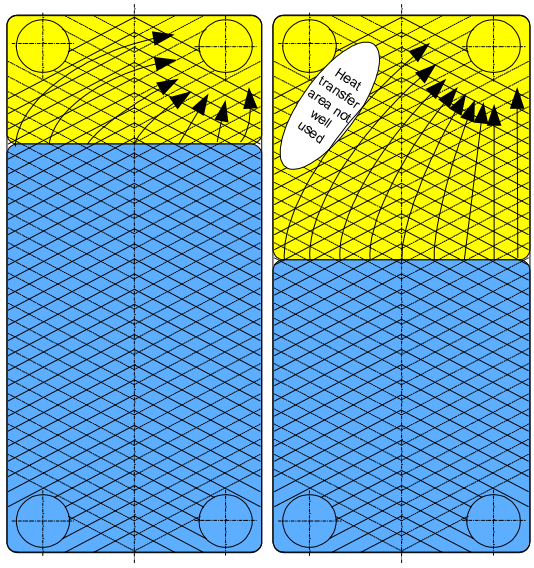

Figure 69: Moderate and low superheat, heat transfer area not well used market in the right figure.

23.4.3 Additional note

It should also be remembered that the investigation carried out heated the refrigerant from one side only. Thus, the mass flow rate in the refrigerant channel is half of what would be encountered in commercial plate heat exchangers. In this chapter, this effect was adjusted according to standard correlations for annulus (Gnielinski 1993) with one side heated and one unheated. The correction made may not be applicable for the plate heat exchangers. Even so, this effect is not expected to be large enough to explain the discrepancy observed. In addition, similar discrepancy was observed in the

last chapter, having the refrigerant heated from both sides. Further tests determining the superheating area in channels with double sided heating is however needed. This is an experimentally challenging task.

23.5 Is mist flow responsible?

The above discussion indicates that none of the discussed possible reasons seems to be responsible for the discrepancy. Remains does the possibility of mist flow, or dry-out of the wall at a vapor quality less than unity.

This would indicate that the area determined with Thermochromic Liquid Crystals (TLC) is not the correct one. The error may be one of two possible:

1. No mist flow but the heat transfer area measured with TLC is not correct.

2. Mist flow is present, hence the measured area with TLC is not the superheated area, but rather the sum of the superheated and mist-flow areas.

Regarding the first point, the superheated area was measured by TLC. 100 pictures of the colorplay were taken during the experiments for each measured point. In each of these 100 pictures, the number of pixels with a certain color (temperature) were counted in a software and compared to the total number of pixels (approximately 68 000) of the plate heat exchanger. Hence, the error in the measurements regarding the area is expected to be small.

The second point is not as easy to discard as the first point. Mist flow is known to occur in evaporators having refrigerant boiling in straight tubes. However, as a swirl flow exists in CBE (Claesson (1996), Mehrabian (1996)), it may be argued that any droplets existing in the gas-core would be thrown onto the wall, hence re-wetting the wall. A distinct transition from wetted wall to pure gas flow with no entrained droplets in the gas core has indeed been visually observed (Pelletier 2002) using the naked eye.

In addition, no correlation between the discrepancy and the predicted dry-out quality calculated according to Sthapak et al. (1975) could be found. Sthapak et al. developed their correlation for 6.55 mm diameter horizontal tube. Further, the nonequilibrium factor, as defined by Katsaounis (1993), is very close to one, indicating that thermodynamic equilibrium prevails near the dry-out point.

However, Yan and Lin (1999) found that mist flow do occur at higher vapor qualities. This contradicts the finding of Pelletier (2002). However, the mass fluxes were higher in Yan & Lin compared to the present investigation and the

saturation pressures were substantially higher. It is also stated that the "…mist flow results in a substantial rise in the heat transfer coefficient. The high-speed turbulent mist flow continuously wets the heat transfer wall…". Thus, if entrained droplets exist in the vapor core, the heat transfer is not reduced and the wall temperature is maintained at the saturated temperature of the refrigerant.

In the above paragraphs, the possibility of mist flow was discussed. Lets, however, assume that mist flow do occur, could this explain the discrepancy observed?

In order for mist flow being the responsible mechanism, the droplets need to be small enough to follow the gas flow, i.e. the droplet travels roughly at the same speed as the gas. By definition, the slip ratio is one and homogeneous two phase flow occurs. The void fraction and an estimated droplet size of the two phase flow is plotted in Figure 70, assuming homogeneous flow, as a function of the vapor quality. The initial droplet size estimation is calculated according to Whalley (1987).

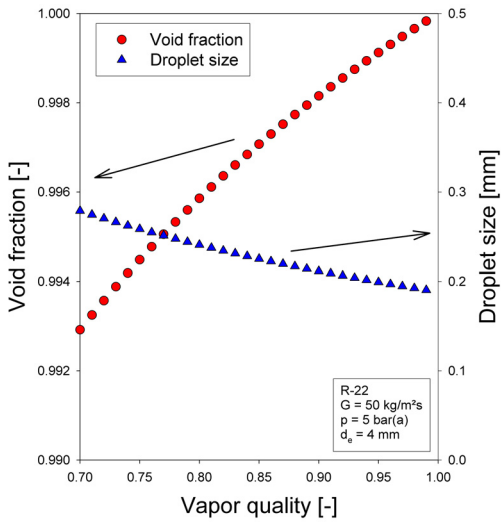

Figure 70: Homogeneous void fraction as a function of vapor quality.

Assuming wall dry-out with a subsequent mist flow, what vapor quality would be necessary to explain the observed deviations? Using a simple energy balance, assuming eq. (170) to be valid for the single phase heat transfer coefficient also in the mist flow regime, quite reasonable values for the dryout quality are found, as may be seen in Figure 71.

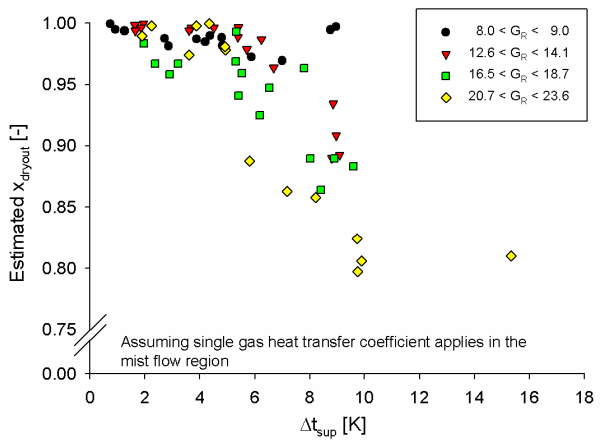

Figure 71: Estimated dryout vapor quality.

In chapter 20, the heat transfer was based on the assumption that boiling occurs up to saturated vapor. Re-examinating the data in chapter 20, accounting for the estimated vapor quality where dryout would occur, change the result slightly. The experimental results are best correlated if the leading constant in the Cooper correlation, C, is changed from 1.5 to 1.385, see Figure 72.

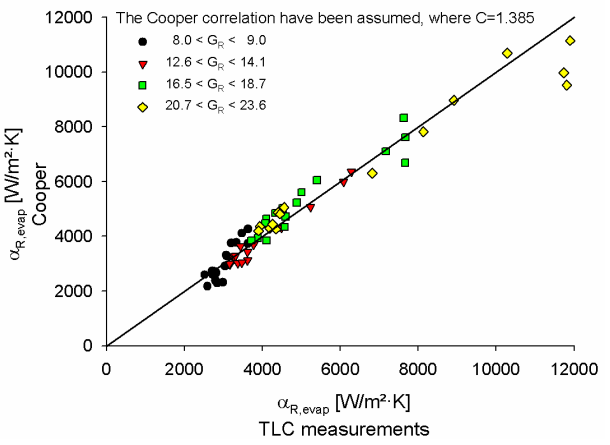

Figure 72: Comparison between TLC experiment in chapter 20, accounting for mist flow, and the Cooper correlation with a new fitting constant, C = 1.385.

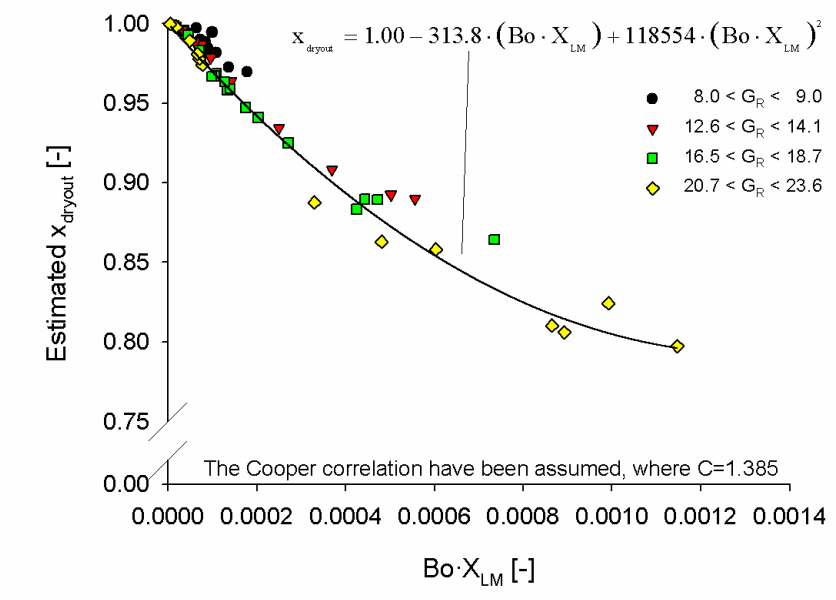

Figure 73: Estimated dry-out quality as a function of the local boiling number, estimated using the Cooper correlation with the new fitting constant, and the Lockhart-Martinelli parameter.

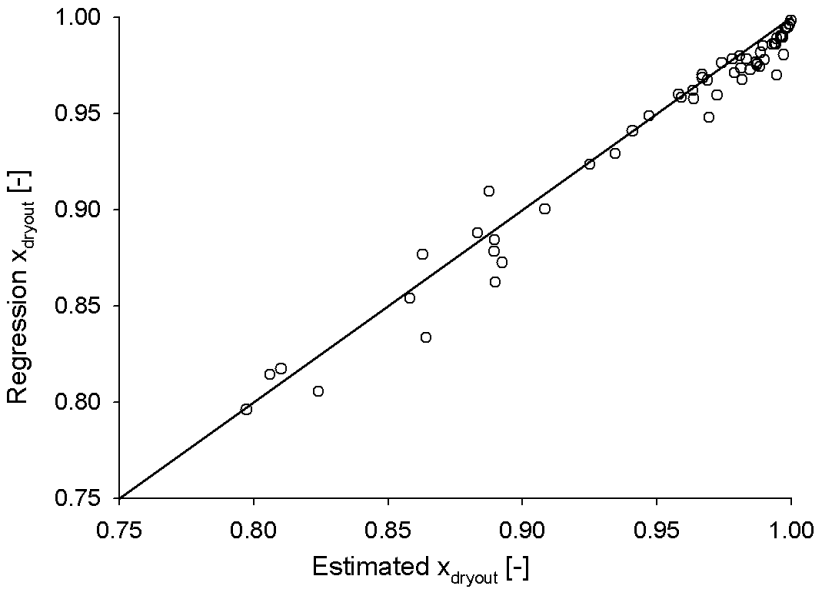

Figure 74: Correlated and estimated dryout quality.

Different approaches may be found in the literature concerning dry-out. In this thesis we assume that the dry-out mechanism is a local mechanism, i.e. the onset of dryout depends only on local values such as local vapor quality, local heat flux etc. Using the estimated values of the dry-out quality, applying the Cooper correlation locally with the new fitted constant, it was found that the dryout quality correlated with, see Figure 73 and Figure 74,

$$x_{dryout} = 1.00 - 313.8 \cdot \left(Bo \cdot X_{LM}\right) + 118554 \cdot \left(Bo \cdot X_{LM}\right)^2 \qquad (222)$$

where Bo is the boiling number and X_{LM} is the Lockhart-Martinelli parameter.

The validity range of the purely empirical eq. (222) is given in Table 4. In Figure 74, a comparison between the correlated and the estimated dryout quality, based on an energy balance and single phase correlations, is shown. As may be seen, good agreement was obtained. This could perhaps indicate mist flow as on of the major contributors for the discrepancy earlier discussed.

Table 4: Range of validity for eq. (222).

Parameter	**Lower Range**	**Upper Range**
Heat flux, $q''_{tot} = \frac{\dot{Q}_{tot}}{A_{tot}}$ [W/m²]	5 500	15 000
Superheat, Δt_{sup} [K]	0.5	10
Brine flow rate, Re_{brine} [-]	210	1000
Refrigerant mass flux G_R [kg/(s·m²)]	8.0	23.6
Local Boiling number[i] Bo [-]	0.005	0.025
Lockhart-Martinelli parameter X_{LM} [-]	$6.7 \cdot 10^{-4}$	0.047

[i] One side heated channel!

23.6 Conclusion

The present section investigated possible explanations to the observed difference between the measured and the predicted heat transfer area required for superheating the refrigerant in a Compact Brazed Plate Heat Exchanger used as evaporator in a small refrigerating unit. A finite difference scheme was employed, which indicated that the longitudinal wall heat transfer is not sufficient to explain the discrepancies. Also the possibility that maldistribution of the superheated gas affect the discrepancy has been shown unlikely. In addition, it was noted that only one wall in the refrigerant channel was heated. However, as similar discrepancy was observed in a double sided heat exchanger, this was not believed to be responsible for the observed discrepancy.

Finally, the possibility of dry-out and a sub sequential mist flow was discussed as being the most probable reason for the observed discrepancy. The dry-out quality were estimated using an simple energy balance, based on the "mist-flow" heat transfer area and assuming single gas heat transfer coefficient to applies. Reasonable values were obtained. The estimated dry-out quality was correlated with the local boiling number and the Lockhart-Martinelli parameter. Good agreement was obtained. It may be suggested that mist-flow is responsible for the discrepancy observed.

24 CONCLUSION – PART III

The boiling heat transfer area was determined in two different ways as the evaporator was considered as a two-zone heat exchanger. The first method, in which the boiling heat transfer area was measured using Thermochromic Liquid Crystals, indicated that the boiling area averaged refrigerant flow boiling film heat transfer coefficient is mainly depended on the boiling area averaged heat flux. The data correlated much better with the heat flux than the refrigerant Reynolds number. The pool boiling correlation by Cooper (1984) was successful in correlating the data, if the leading constant was set to 1.5.

As the LMTD method was used for evaluating the boiling heat transfer coefficient in the above investigation, the applicability of that method was investigated numerically. The Cooper correlation was assumed to be valid locally as well as globally. The results indicated that the correction factor needed in order to use the LMTD method in these applications, where the boiling heat transfer coefficient depends on the heat flux, is negligible for medium to large temperature differences. However, for small temperature differences the correction needed may be significant.

The second method to determine the boiling heat transfer coefficient employs single phase correlations on both fluid sides in the superheated zone of the evaporator. The area required in the superheated zone was calculated and the boiling heat transfer area was then the remaining area of the heat exchanger. This method did not give the same results as the first method. Possible reasons for this discrepancy were discussed and it was concluded that mist flow is the most probable explanation for the observed discrepancy. In addition, assuming mist flow and single phase gas heat transfer coefficient applies in the mist flow regime enabled an estimation of the dry-out quality. The estimated dryout quality agree qualitatively with what would be expected, dry-out occurs earlier if mass flux increases and/or if heat flux increases. The estimated dry out quality was correlated using the local boiling number and the Lockhart-Martinelli parameter. It was suggested that mist-flow was responsible for the observed discrepancy.

PART IV

LOCAL PERFORMANCE DURING FLOW BOILING CONDITIONS

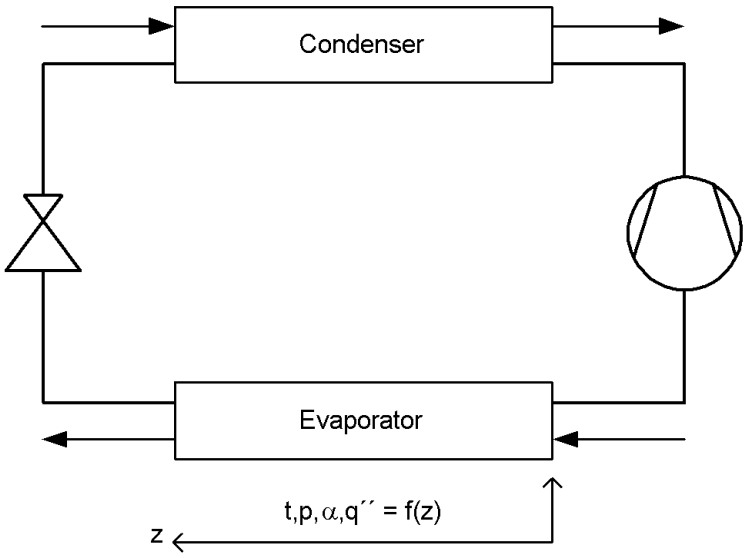

25 INTRODUCTION – PART IV

This section of the thesis considers the evaporator as a "many" zone heat exchanger, i.e. local values of flow boiling heat transfer coefficient and pressure drops are investigated. For the purpose of this part of the thesis, a completely different experimental approach has been undertaken. Instead of using a complete heat pump system with compressor, a refrigerant pump has been utilized; hence, no oil is present during the experiments. This section consists of two main parts; adiabatic hydraulic performance in a CBE, and flow boiling heat transfer coefficient in a CBE.

In the first part, adiabatic pressure drops are experimentally measured using a wide range of mass fluxes and vapor quality. The measured terminal pressure drop will be used in order to extract the frictional pressure drop in the heat transfer section of the evaporator. Additional pressure drops are also present: in the inlet and outlet pipes, acceleration of the fluid, and difference in elevation between the inlet and outlet. The frictional pressure drop will be correlated using classical two-phase friction models, slightly modified.

In the second part, local flow boiling heat transfer is experimentally measured using a novel technique for flow boiling in plate heat exchanger. The temperature of the water along the heat exchanger is measured in detail. The measured temperatures are used to perform a non-linear regression analysis. The curve-fitted equation will then be used to estimate the local heat flux, wall temperatures and local flow boiling heat transfer coefficients.

26 EXPERIMENTAL SETUP – PART IV

The experimental test equipment, see Figure 75, consists of a refrigerant pump from ISMATEC, plate heat exchangers as condenser and preheater, and a suction-gas-liquid heat exchanger as sub-cooler. The preheater is heated with water and the condenser and sub-cooler are cooled by an auxiliary cooling unit. The absolute pressures are measured before the preheater and the test object with absolute pressure transducers from Druck. In addition, the pressure drops over the preheater and the test object are measured with differential pressure transducers from Druck. The refrigerant mass flow is measured with a Coriolis mass flow meter from Micromotion. Flow meters from Siemens, SITRANS FM Intermag 2, measures the water flow rate in the preheater and test object. All temperatures are measured with T-type thermocouples connected to a HP logger, via an isothermal box. A Pt-100 element measures the reference temperature in the isothermal box. The uncertainty in absolute temperature readings is expected to be less than 0.1 K. R-134a is used as refrigerant.

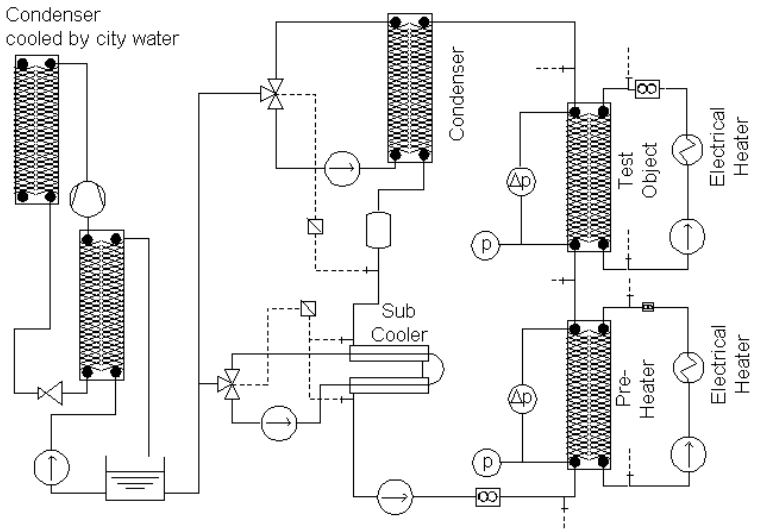

Figure 75: Schematic experimental setup.

27 ADIABATIC TWO-PHASE FLOW HYDRAULIC PERFORMANCE[i]

In this section, the adiabatic two-phase flow hydraulic performance of a plate heat exchanger is investigated. Refrigerant R-134a is used as refrigerants. The test object is a modified, three plates, commercial brazed plate heat exchanger, mounted in vertical position. The heat exchanger tested has three plates, i.e. one channel for the refrigerant and one channel for water. As the tests are conducted under adiabatic conditions, no water is flowing through the heat exchanger.

27.1 Data reduction

The pressure drop from the inlet to the exit of the test object is measured. This pressure drop consists of several parts, i.e. pressure drop in the ports, pressure drop due to acceleration, pressure drop due to change in elevation and finally pressure drop due to friction in the corrugated channel, see eq. (223).

$$\Delta p_{meas} = \Delta p_{inport} + \Delta p_{acc} + \Delta p_{elev} + \Delta p_{outport} + \Delta p_f \tag{223}$$

The focus here is on the friction pressure drop; hence, the other terms in eq. (223) must be subtracted from the measured pressure drop. Following the outline by Yan and Lin (1999) and Shah and Focke (1988), the pressure drop in the inlet port and the outlet port may be calculated according to eq. (224).

$$\Delta p_{port} = 1.5 \cdot \left(\frac{v_{tp} \cdot \dot{m}^2}{2 \cdot A_{channel}^2} \right) \cdot \frac{1}{2} \tag{224}$$

where

$$v_{tp} = v_l + x \cdot \left(v_g - v_l \right) \tag{225}$$

The last factor in eq. (224) is due to the assumption that half of the total port pressure drop, as calculated by Shah and Focke (1988), is occurring in the inlet port and half at the exit port. Since different qualities are present (due to the pressure drop) at the inlet and the outlet ports, these have to be separated. The

---

[i] Parts of this chapter have previously been published in: Claesson J., Simanic B., 2003, Pressure drop and visualization of adiabatic R134a two-phase flow inside a chevron type plate heat exchanger, 21st Int. Congr. of Refrigeration, IIR/IIF, Washington D.C., USA, paper 314.

pressure drop due to acceleration is calculated according to (Collier and Thome 1996)

$$\Delta p_{acc} = \dot{m}^2 \cdot \left\{ \frac{v_{tp,outport}}{A^2_{outport}} - \frac{v_{tp,inport}}{A^2_{inport}} \right\} \tag{226}$$

The elevation pressure drop is calculated as (Yan and Lin, 1999)

$$\Delta p_{elev} = \frac{g \cdot L_p}{v_{tp}} \tag{227}$$

Once the measured two-phase adiabatic pressure drop has been extracted, the two-phase multiplier (Lockhart and Martinelli 1949) could be calculated, eq. (228)

$$\phi_l^2 = \frac{(\Delta p/\Delta L)_{tp}}{(\Delta p/\Delta L)_l} \tag{228}$$

and the Lockhart – Martinelli parameter, X_{LM}, as

$$X^2_{LM} = \frac{(\Delta p/\Delta L)_l}{(\Delta p/\Delta L)_g} \tag{229}$$

For the single-phase pressure drops, several correlations exist, e.g. Shah and Focke (1988), Muley (1997), Martin (1996) and Bogaert and Bölcs (1995). In the present work, the correlation developed by the manufacturer for the heat exchanger model tested has been used.

27.2 Experimental results and discussion

The plate heat exchanger tested in this investigation is identical to the CBE used in chapter 20. Several refrigerant mass flow rates (18 kg/s·m² to 80 kg/s·m²) and vapor qualities (0.1 to 0.8) are tested. The measured frictional pressure drops are shown in Figure 76. The pressure drop varies almost linearly with the vapor quality, and increases with mass flux, as expected.

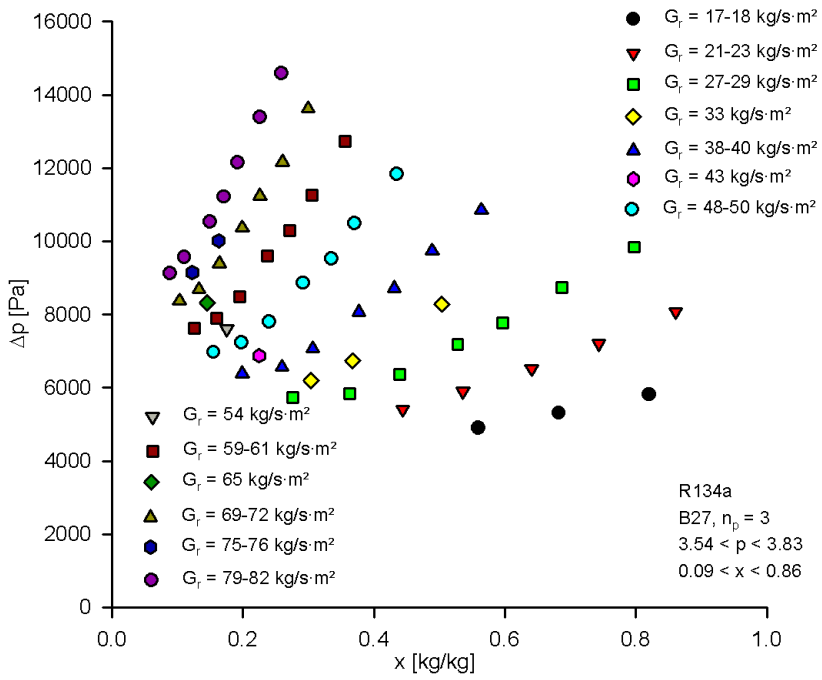

Figure 76: Measured frictional pressure drop vs. vapor quality and mass flux.

The two-phase flow frictional pressure drop is often represented via any of the several available two-phase multipliers. In Figure 77, the two-phase multiplier based on the liquid fraction of flow flowing alone as liquid in the channel is plotted against the Lockhart-Martinelli parameter (Lockhart and Martinelli 1949). The shape is very similar to what has been expected, and the data correlates rather well with the classical correlation by Chisholm (1967), eq. (68). A good fit was obtained using 4.67 as single value for the Chisholm parameter, C. However, even better fit was obtained as

$$\phi_l = 1.215 + \frac{1.247}{X_{LM}} - \frac{0.0041}{X_{LM}^2} \tag{230}$$

There is, however, a drawback of using the liquid based two-phase multiplier in dry-expansion evaporators. As the vapor quality approaches unity, i.e. as the refrigerant becomes saturated vapor, the liquid based multiplier approaches infinity. The classical correlation by Chisholm (1967) may be transformed into a gas based multiplier, which does not display this problem. The correlation is

$$\phi_g^2 = 1 + C \cdot X_{LM} + X_{LM}^2 \tag{231}$$

However, this correlation has similar problems near the saturated liquid line.

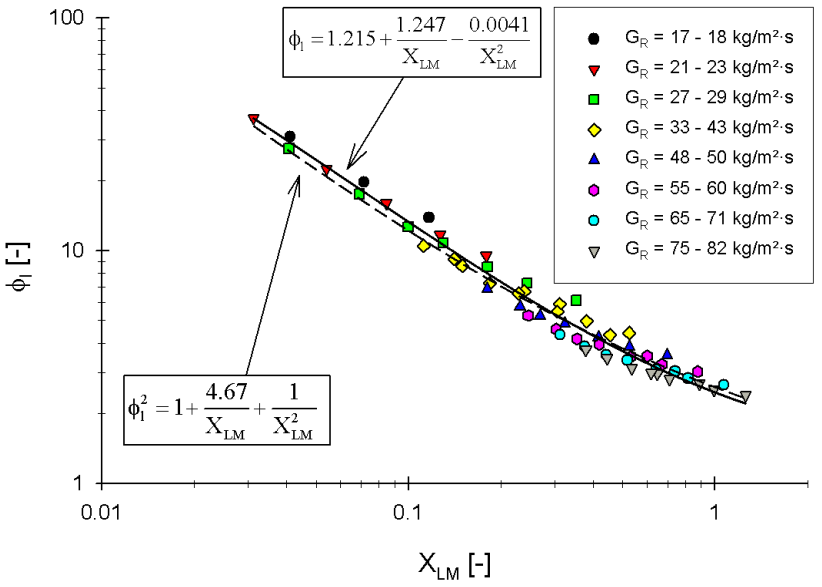

Figure 77: Two-phase multiplier based on pressure drop of the liquid fraction of the flow flowing alone in the channel vs. the Lockhart-Martinelli parameter.

Inspecting Figure 77, a dependency of the mass flux may be observed. Indeed, allowing the Chisholm parameter to be a function of the two-phase kinetic energy per volume an excellent fit between predicted pressure drop and experimental pressure drop is obtained. Jassim et al. (2001) suggested correlating the two-phase frictional pressure drop using the kinetic energy per volume in a plate heat exchanger. However in this thesis it is suggested that the classical Chisholm correlation, eq. (231), is used in conjunction with the correlated Chisholm parameter using the kinetic energy per volume, as

$$C = 0.6 + \frac{76.66}{\frac{G_{refr}^2}{2 \cdot \rho_{homo}}} - \frac{25.52}{\left(\frac{G_{refr}^2}{2 \cdot \rho_{homo}}\right)^2} \tag{232}$$

The kinetic energy per volume, as defined by Jassim et al. (2001), is

$$\frac{K.E.}{V} = \frac{G_{refr}^2}{2 \cdot \rho_{homo}} \tag{233}$$

where the homogeneous density (Jassim et al. 2001) is

$$\rho_{homo} = \left(1 - \alpha_{homo}\right) \cdot \rho_l + \alpha_{homo} \cdot \rho_g \tag{234}$$

and the homogeneous void fraction is (Jassim et al. 2001)

$$\alpha_{homo} = \frac{x \cdot \rho_g}{x \cdot \left(\rho_l - \rho_g\right) + \rho_l} \tag{235}$$

The predicted two-phase frictional pressure drop, using eq. (232), compared to the experimentally obtained two-phase frictional pressure drop is shown in Figure 78. As may be seen, the data is correlated within ± 10 %.

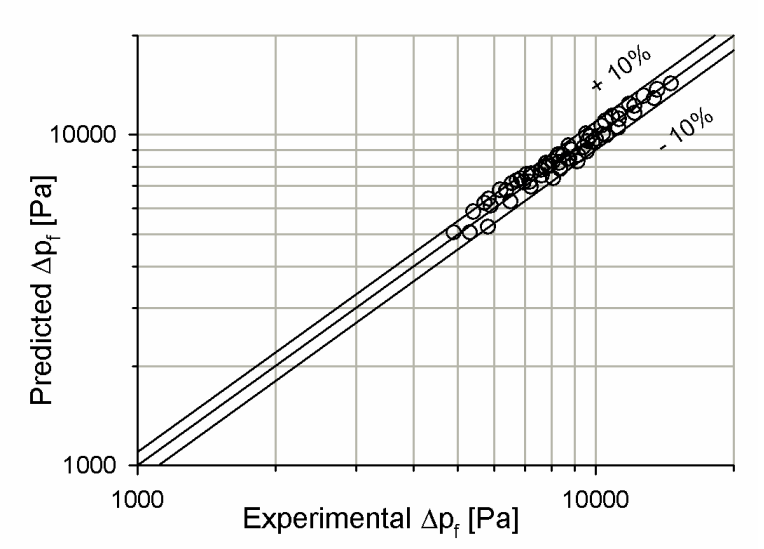

Figure 78: Predicted vs. experimental adiabatic two phase frictional pressure drop in a compact brazed plate heat exchanger.

27.3 Flow visualization

In a separate adiabatic pressure drop investigation, the flow structure of the two-phase flow inside the heat exchanger is visually investigated. The test object is a modified, three plates, commercial brazed plate heat exchanger, mounted in vertical position. The outer plate is constructed of transparent material, facilitating visual observation of the upward two-phase flow. The test object has an inlet flow distributor, to simulate normal running conditions.

It is very difficult to get the whole picture of the flow pattern, due to the complex flow geometry. However, the flow has been recorded using a standard digital video camera, Sony DCR-TRV-890E. No gas-continuous patches could be observed. This is in agreement with Vlasogiannis et al. (2002) as all the present experiments lie in flow regime A, as denoted by Vlasogiannis et al.

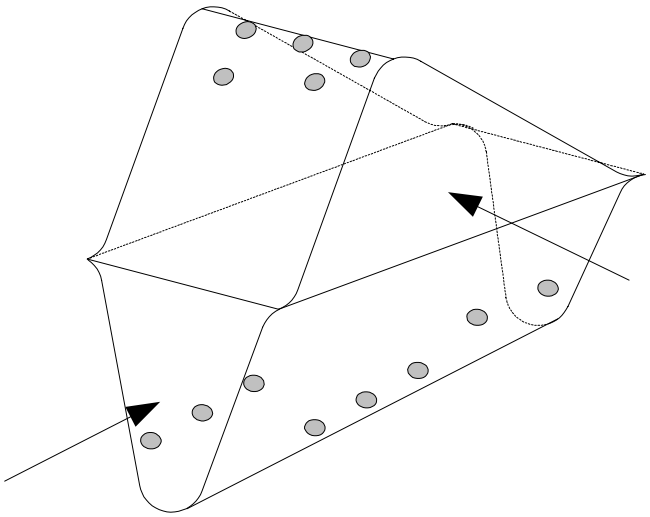

Figure 79: Droplet on the unheated wall at high mass flux.

An interesting observation made during the experiments was the presence of liquid droplets in the furrow, see Figure 79, at high mass flux and higher vapor qualities. These droplets did not seem to move, but were "stuck" onto the surface, indicating no or little interaction with the flowing refrigerant. This might indicate that there is at some point a dry-out of part of the heat transfer wall, as stated by Yan and Lin (1999). On a heated wall, these observed droplets would eventually evaporate and the wall would be dry.

In addition, small samples of liquid were observed to be collected at each contact point between the two adjoining plates. These pools of liquid refrigerant seemed to interact with the flow core, since small portions of liquid was observed leaving the pool and flowing with the flow core. The presence of liquid pools at the contact points is beneficial. Walton (2001) showed that the maximum single phase heat transfer coefficient occurs close to these contact points.

27.4 Conclusion

The adiabatic two phase flow frictional pressure drop was experimentally determined in this investigation. The pressure drop in plate heat exchangers does not seem to differ significantly from other reported geometries, in respect of dimensionless parameters as the two phase multiplier. Thus, the Chisholm

correlation with the Chisholm parameter, C, set to 4.67 correlated the data well. However, the Chisholm parameter seemed to vary with mass flux, and correlating the Chisholm parameter with the kinetic energy per volume provides an excellent fit of the two phase adiabatic flow frictional pressure drop, within ± 10 %.

28 LOCAL FLOW BOILING HEAT TRANSFER COEFFICIENTS

This section introduces, to the best knowledge of the present author, a novel technique to determine the local flow boiling film heat transfer coefficient in a compact brazed plate heat exchanger.

28.1 Experimental setup and test procedure

The experimental setup consists of the test object (compact brazed plate heat exchanger), a preheater, a refrigerant pump, a condenser, liquid receiver, a subcooler and piping to connect the different parts, see Figure 75. The test facility is described in detail in chapter 26.

The mass flow rate of the refrigerant is set by adjusting the speed of the refrigerant pump. In the same manner, the flow rates of the water sides are set by adjusting the speed of the water pumps. The operating pressure of the system is controlled by the water loop cooling the refrigerant in the condenser. The amount of heat rejected is controlled by a PID-controller, by changing the supply of fresh, cold water from the auxiliary refrigeration system. The amount of subcooling of the refrigerant is controlled in the same manner, having a separate loop, but using the same source of fresh cold water.

The test object consists of a special constructed plate heat exchanger, in which three stainless steel plates are brazed together. The fourth, and outermost, plate is a specially manufactured plastic plate, onto which the corrugation pattern is machined. In this plate, small holes are drilled, in which 32 thermocouple of T-type are inserted. The positions of the measuring points of the thermocouples are located at the midplane, in the water flow stream, between the plastic plate and the adjoining stainless steel plate. Two of the thermocouples are positioned at the inlet and outlet ports of the water. 15 thermocouples are positioned equally spaced between inlet and the outlet ports on the non-refrigerant port side of the heat exchanger, and the remaining 15 thermocouples are positioned in the same manner but on the refrigerant port side. This facilitates the possibility to observe any maldistribution of the water between the two sides of the centerline in the plate heat exchanger channel. The actual positions of the thermocouples are shown in Figure 80.

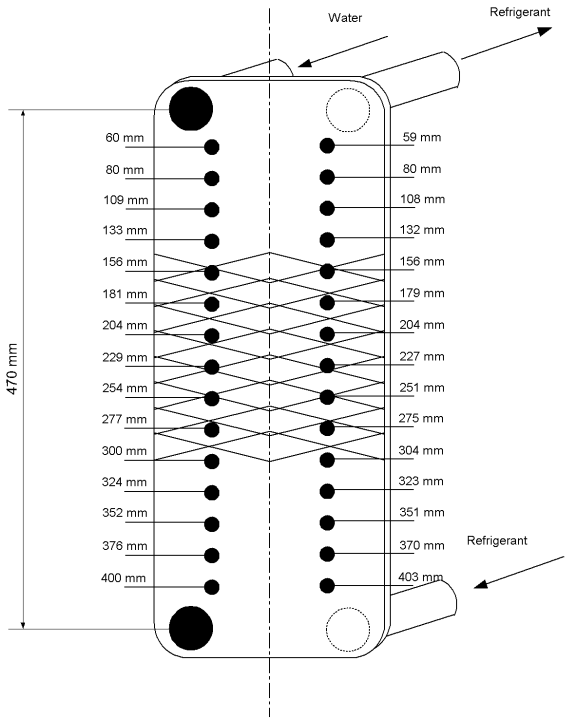

Figure 80: Positions of the thermocouples in the water side of the plate heat exchanger.

As already mentioned, the system is not a traditional refrigerating system, since the pressure is roughly the same throughout the system. A refrigerant liquid pump is used to control the refrigerant mass flow rate. Once the desired refrigerant mass flow rate has been set, the imposed electrical heat supply is set manually and individually on the preheater and test object water loops. Then, the desired water flow rate is set in these two loops in order to obtain reasonable temperature differences over the heat exchangers. A number of different water flow rates are used in the test object loop in order to obtain different heat flux distribution in the test object.

Once the temperatures, flow rates and pressures stabilize, which may take several hours, the actual measurement is conducted. Normally the duration of the measurement is between 30 to 60 minutes, giving between 500 – 1 000 readings.

28.2 Data reduction

Once the measurement is conducted, readings of pressures, temperatures and flow rates are converted into useful parameters, such as Reynolds numbers, heat

transfer coefficients and heat flux. In this section, this data reduction procedure is outlined.

Initially the energy balance between the water loops and the refrigerant loop is investigated. Thus, the rejected heat in the preheater and the test object are added together to a combined value, eq. (238). Hence

$$\dot{Q}_{H_2O,pre} = \rho_{H_2O,pre} \cdot \dot{V}_{H_2O,pre} \cdot c_{p_{H_2O,pre}} \cdot \left(t_{in_{H_2O,pre}} - t_{out_{H_2O,pre}} \right) \tag{236}$$

and

$$\dot{Q}_{H_2O,obj} = \rho_{H_2O,obj} \cdot \dot{V}_{H_2O,obj} \cdot c_{p_{H_2O,obj}} \cdot \left(t_{in_{H_2O,obj}} - t_{out_{H_2O,obj}} \right) \tag{237}$$

which yields

$$\dot{Q}_{H_2O,tot} = \dot{Q}_{H_2O,pre} + \dot{Q}_{H_2O,obj} \tag{238}$$

The properties of water are evaluated using the correlations in IAPWS-97 (Wagner and Kruse 1998). The obtained heat of the refrigerant is

$$\dot{Q}_{refr} = \dot{m}_{refr} \cdot \left(h_{out_{refr,obj}} - h_{in_{refr,pre}} \right) \tag{239}$$

where the refrigerant entering the preheater is slightly subcooled and the refrigerant leaving the test object is slightly superheated. Thus, the enthalpy in these two positions are calculated as

$$h_{refr} = f(p,t) \tag{240}$$

where the NIST database "Refprop" is employed. In most of the measurements, eq. (238) and eq. (239) differ slightly, and the transferred heat used in the analysis is calculated as the arithmetic mean,

$$\dot{Q} = \frac{\dot{Q}_{refr} + \dot{Q}_{H_2O}}{2} \tag{241}$$

The mass flow rates are then adjusted in order to meet this heat transfer rate. The difference between eq. (241) and eq. (239) is small[i].

[i] The difference is less than ± 1% for the higher refrigerant mass flow rate, and less than ±5.2% for the smallest refrigerant mass flow rate.

The next step is to determine the water temperature profile of the water as it flows through the test object. All readings of the thermocouples are used in a regression analysis to obtain a continuous temperature profile. A sigmoidal function is found successful. Before the regression analysis is carried out, the temperatures on the water side in the evaporator are normalized according to

$$y(z) = \frac{t_{H_2O}(z=0) - t_{H_2O}(z)}{t_{H_2O}(z=0) - t_{H_2O}(z=L_p)} \tag{242}$$

The sigmoidal function used to curve fit the data is

$$y(z) = y_0 + \frac{a}{\left(1 + e^{-\left(\frac{z-z_0}{b}\right)}\right)^c} \tag{243}$$

where different constants are determined for each measured point, consisting of more than 500 readings.

Now, once the temperature profile is known, the local heat flux may be determined. The heat transfer over a small area element may be written as

$$d\dot{Q} = \dot{m}_{H_2O,obj} \cdot c_{p_{H_2O,obj}} \cdot dt_{H_2O}(z) \tag{244}$$

and if we divide this with the small heat transfer area for which it occurs, we obtain

$$\frac{d\dot{Q}}{dA} = \dot{m}_{H_2O,obj} \cdot c_{p_{H_2O,obj}} \cdot \frac{dt_{H_2O}(z)}{dA} \tag{245}$$

Now, since

$$dA = \phi \cdot W_p \cdot (n_p - 2) \cdot dz \tag{246}$$

and

$$q'' = \frac{d\dot{Q}}{dA} \tag{247}$$

we obtain

$$q''(z) = \frac{\dot{m}_{H_2O,obj} \cdot c_{p_{H_2O,obj}}}{\phi \cdot W_p \cdot (n_p - 2)} \cdot \frac{dt_{H_2O}(z)}{dz} \tag{248}$$

Thus, using eq. (243) in eq. (248) yields

$$q''(z) = \frac{\dot{m}_{H_2O,obj} \cdot c_{p_{H_2O,obj}}}{\phi \cdot W_p \cdot (n_p - 2)} \cdot \left(- \frac{a \cdot c \cdot e^{-\left(\frac{z-z_0}{b}\right)}}{b \cdot \left(1 + e^{-\left(\frac{z-z_0}{b}\right)}\right)^{c+1}} \cdot \left(t_{H_2O_{in}} - t_{H_2O_{out}}\right) \right) \tag{249}$$

The purpose of this exercise is to obtain the refrigerant flow boiling heat transfer coefficient. For that we need to calculate the wall temperature at any given position. The wall temperature may be calculated as

$$t_W(z) = t_{H_2O}(z) - \frac{q''(z)}{\alpha_{H_2O}} \tag{250}$$

where α_{H2O} is the water side heat transfer coefficient. Different choices of calculation procedure may be undertaken for the water side heat transfer coefficient. For instance, one could account for the flow distribution of water flow in the channel. However, in this thesis, the heat transfer correlation determined by the manufacturer using terminal temperatures will be used. This implies constant heat transfer coefficient in the entire water side. The water side heat transfer is thus

$$Nu = B_1 \cdot Re^{B_2} \cdot Pr^{\frac{1}{3}} e^{\frac{6.4}{Pr+30}} \cdot \left(\frac{\mu}{\mu_w}\right)^{\frac{0.3}{(Re+6)^{0.125}}} \tag{251}$$

where

$$Nu = \frac{\alpha_{H_2O} \cdot d_e}{\lambda} \tag{252}$$

and

$$Re = \frac{\rho \cdot u \cdot d_e}{\mu} = \frac{G \cdot d_e}{\mu} = \frac{2 \cdot \dot{m}_{ch}}{W \cdot \mu} \tag{253}$$

The specific value of the constants used in eq. (251) depends on the Reynolds number and plate geometry.

It is now possible to determine the wall temperature at any given position in the plate heat exchanger. The next step is to determine the corresponding refrigerant temperature. In the superheated section, the temperature of the refrigerant is a direct function of the integration of the heat flux and the local wall temperature. However, in the two-phase section the temperature follows the pressure of the

refrigerant, and the pressure drop on the refrigerant side need to be accounted for.

The pressure drop on the refrigerant side in the superheated section is estimated using correlations supplied by the manufacturer. The appropriate correlation is

$$\frac{dp_{f_{refr,1\Phi}}}{dz} = -f_{1\Phi} \cdot \frac{G^2}{2 \cdot \rho_g \cdot d_e} \tag{254}$$

where the friction factor is correlated as

$$f_{1\Phi} = A + \frac{B}{Re^n} \tag{255}$$

Again, the specific value of the constants in eq. (255) depend on the specific plate and Reynolds number, and is proprietary information of the manufacturer.

The two-phase flow pressure drops were measured and correlated in chapter 27, at different mass flux and vapor qualities, in an identical plate geometry as here investigated and the reader is referred to that chapter.

The amount of heat transferred from the water side to the refrigerant side may easily be calculated. It is merely to sum up the local heat flux from the water inlet to any position in the heat exchanger.

$$\dot{Q}(z) = \int_0^z q''(z) \cdot \phi \cdot W_p \cdot (n_p - 2) \cdot dz \tag{256}$$

This heat gives the specific enthalpy of the refrigerant as

$$h_{refr}(z) = h_{out_{refr}}(p,t) - \frac{\dot{Q}(z)}{\dot{m}_{refr}} \tag{257}$$

This information, together with the pressure drop correlations, eq. (254) and eq. (231), enables us to determine the local refrigerant temperature , $t_{refr}(z)$, along the heat exchanger. Once the refrigerant temperature profile, the wall temperature profile and the local heat flux is known, the local refrigerant heat transfer coefficient may be determined as

$$\alpha_{refr}(z) = \frac{q''(z)}{(t_W(z) - t_{refr}(z))} \tag{258}$$

28.3 Experimental results

The above analysis is used to determine the flow boiling refrigerant heat transfer coefficient in the tested plate heat exchanger. The refrigerant mass fluxes tested ranges from 6.9 kg/m²·s to 32 kg/m²·s. For each refrigerant mass flux, several different water flow rates are used in order to obtain different water temperature profiles (heat flux profile) in the boiling part of the evaporator. The refrigerant leaves the evaporator superheated, however the amount of superheat varied between the measured points.

A typical measured normalized temperature profile is shown in Figure 81.

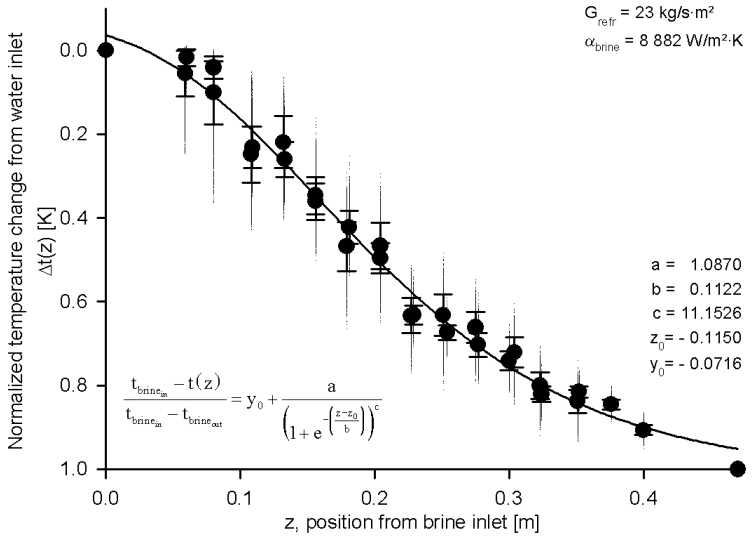

Figure 81: Typical normalized temperature profile obtained from experiments. One standard deviation is included together with the average values. In addition, the resulting regression curve with its constants is also included. Further, all readings for this measured point of the normalized temperature is included as small dots.

As may be seen in Figure 81, even though a rather wide range of the readings around the measured point is obtained, the standard deviation is rather low. The reason for the scatter is the fact that the boiling inside the plate heat exchanger seemed to pulsate, i.e. the temperature curve moved back and forth. Thus, it is suggested that the scatter is not a result of random individual fluctuations of each position, z, in the heat exchanger but rather a result of a pulsating boiling phenomenon. One may also note the small difference between two average points at the same position, z, along the heat exchanger. This small difference indicates that only a small maldistribution of the water is present in this specific measurement.

Using the obtained curve fit and the outlined data reduction procedure, the temperature profile of the water, refrigerant and wall may be obtained, see Figure 82.

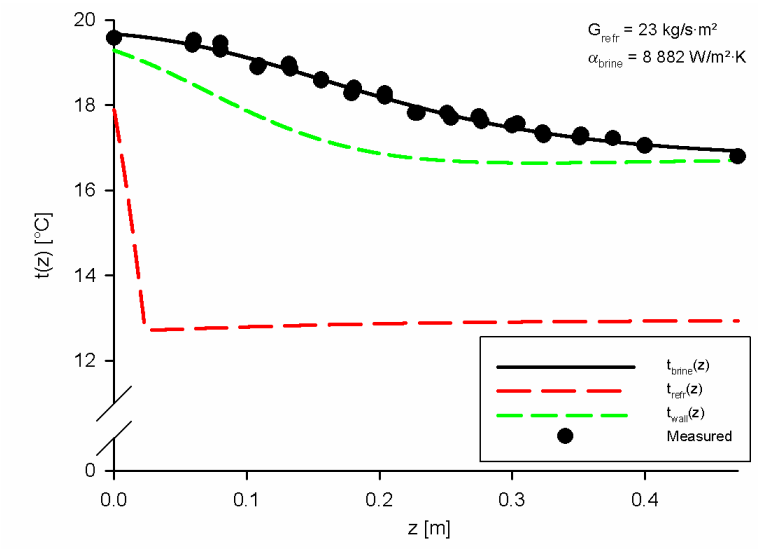

Figure 82: Calculated temperature profiles in the evaporator. The refrigerant enters the diagram on the right hand side, and the water enters on the left and side.

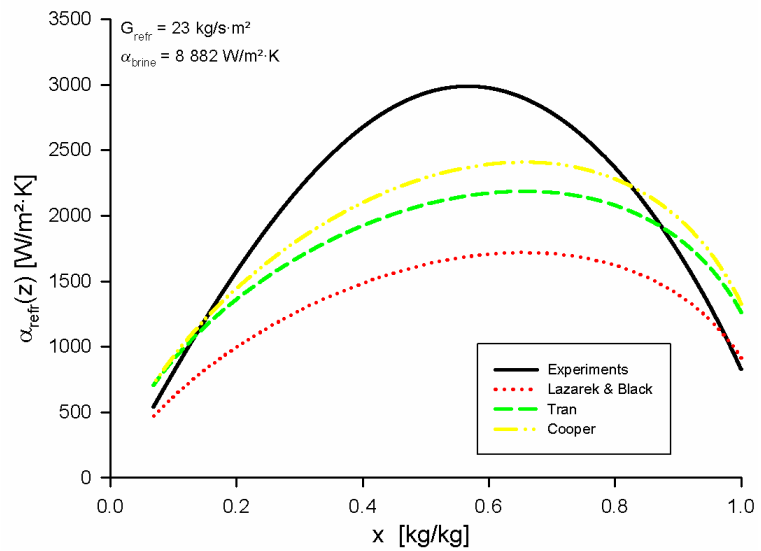

Figure 83: Refrigerant flow boiling film heat transfer coefficient, compared with selected flow boiling correlations.

It may also be interesting to plot the refrigerant flow boiling film heat transfer coefficient obtained from the outlined calculation procedure, see Figure 83. In addition to the experimental data, a few selected flow boiling correlations which fairly well agrees with the experimental data is included. Further discussion will follow in the next session.

28.4 Discussion

The experimentally obtained flow boiling film heat transfer coefficients are compared to several correlations published in the literature, discussed briefly in section 7.2. The performance of the different correlations and the experimental data are shown in Figure 84 thru Figure 89.

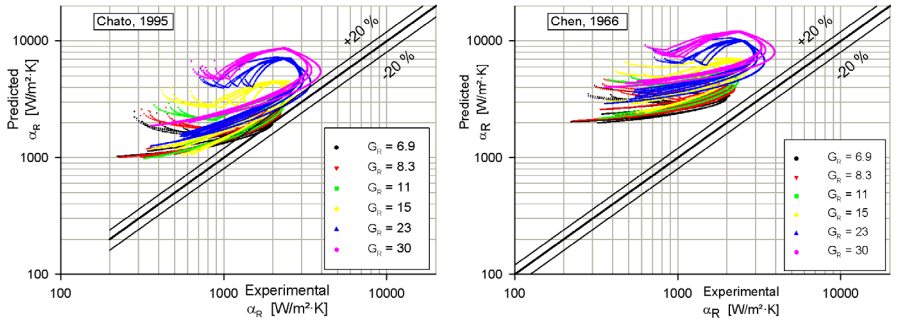

Figure 84: Comparison between experimental data and the correlations by Chato 1995 and Chen 1966.

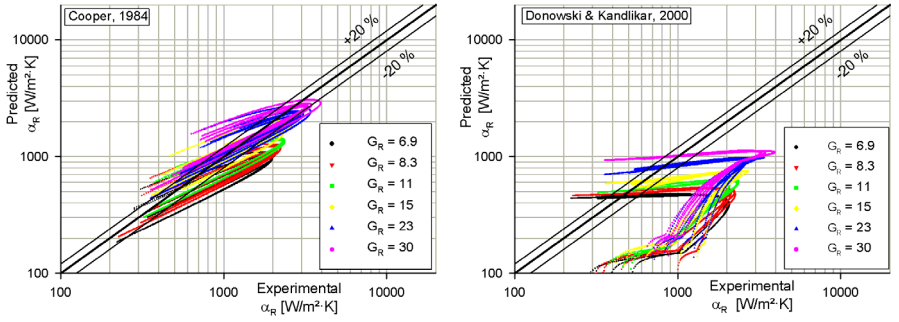

Figure 85: Comparison between experimental data and the correlations by Cooper 1984 and Donowski and Kandlikar 2000.

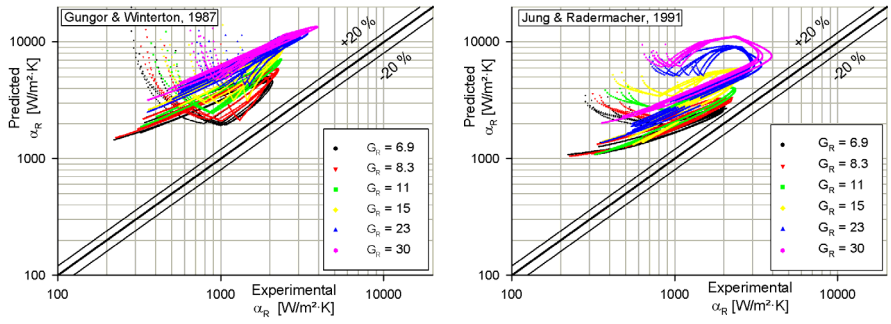

Figure 86: Comparison between experimental data and the correlations by Gungor and Winterton 1987 and Jung and Radermacher 1991.

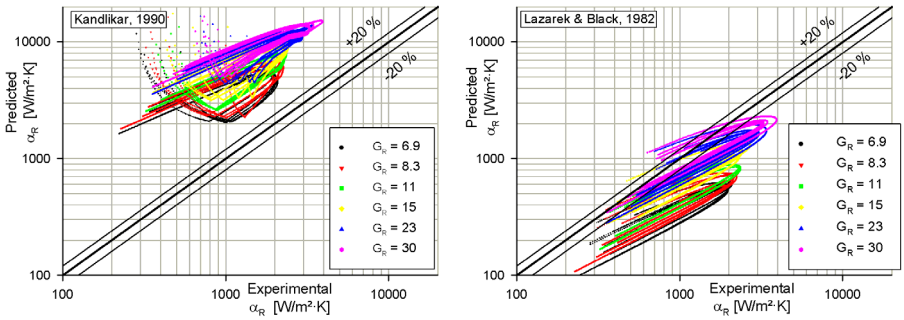

Figure 87: Comparison between experimental data and the correlations by Kandlikar 1990 and Lazarek and Black 1982.

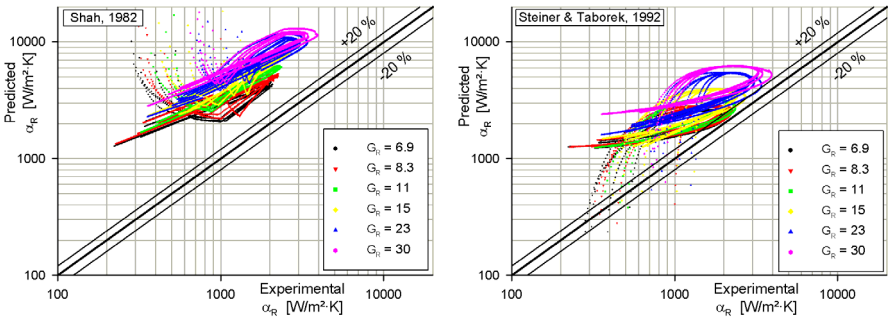

Figure 88: Comparison between experimental data and the correlations by Shah 1982 and Steiner and Taborek 1992.

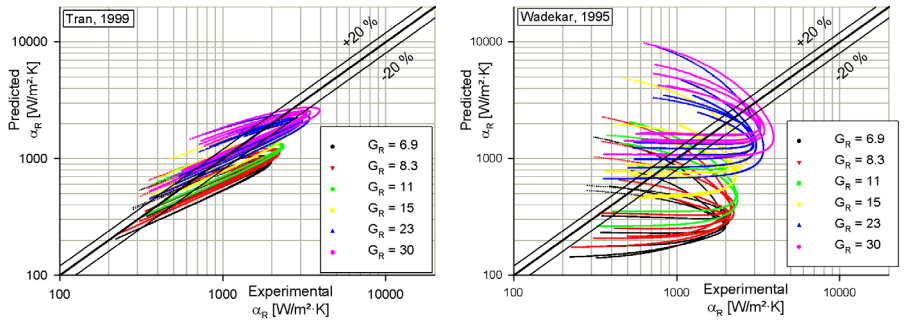

Figure 89: Comparison between experimental data and the correlations by Tran 1999 and Wadekar 1995.

It may be seen that no correlation fits the data very well, however the correlations by Cooper 1984, Tran 1999, and Lazarek and Black 1982 seems to predict experimental data slightly better than the other tested correlations. It should, however, be noted that the Cooper correlation and the correlation by Tran only depend on fluid parameters, geometry and heat flux. Thus, even though the correlated heat transfer data correlates fairly well, they will not be able to catch the decreasing trend of the heat transfer coefficient as the vapor fraction increases. Since the Lazarek and Black correlation also depends, in addition to heat flux, on the Reynolds number based on the entire flow flowing as liquid, this correlation will also not be able to catch the trend at high vapor fraction.

In this experiment, the heat flux may be regarded as "given", since it was measured using the temperature readings. However, in a stepwise calculation scheme, the temperature profile is not known but rather a result of the calculations. This indicates that when using purely heat flux governed heat transfer correlations, separate means of predicting the decrease in heat transfer coefficient at high vapor fraction is required.

28.5 Conclusions

The local flow boiling film heat transfer coefficient was determined using a novel experimental and data reduction technique for plate heat exchangers. The water side temperature profile was measured in detail, with a subsequent regression analysis. The obtained curve was used to obtain the local heat flux. From the heat flux and the water side film heat transfer coefficient, the refrigerant side flow boiling heat transfer coefficient could be estimated.

The experimentally obtained heat transfer coefficient was compared with several correlations from the literature. The experimental flow boiling heat transfer coefficient agreed best with correlations having nucleate boiling as their

main boiling mechanism, e.g. the pool boiling correlation by Cooper (1984), the narrow channel flow boiling correlation by Tran (1999) and the narrow channel flow boiling correlation by Lazarek and Black (1982). However, care should be taken at higher vapor fractions if the actual heat flux is not know beforehand.

29 CONCLUSION – PART IV

Local performances of a plate heat exchanger have been investigated in this part of the thesis. First the adiabatic two-phase flow frictional pressure drop was experimentally determined. The pressure drop varied almost linearly with vapor fraction, for a given mass flow rate. The pressure drop was then plotted in a traditional two-phase frictional pressure drop chart, i.e. with the two phase multiplier vs. the Lockhart-Martinelli parameter. The result agrees with what traditionally would have been expected. The two-phase multiplier was found to fairly well be correlated using the classical Chisholm equation, with the Chisholm parameter C set to 4.67. It was noted that the Chisholm parameter varied with the mass flux. However, using only the mass flux as correlating parameter for the Chisholm parameter did not give good results. Instead, using the kinetic energy per volume did correlate the Chisholm parameter. The resulting prediction of the two phase flow frictional pressure drop agreed excellently with the experimental pressure drop, within ± 10 %.

Second, local flow boiling heat transfer coefficients were experimentally determined using a novel measuring technique for flow boiling in plate heat exchangers. The water temperature was measured in detail. Employing a regression analysis on the measured water temperature was found to provide a good estimation of the measured temperatures. Having an analytical equation for the water temperatures enabled a subsequent analysis obtaining local heat flux in the evaporator. Knowing local heat flux in conjunction with known single phase heat transfer coefficient on the water side, the temperature profiles on both the water side (regression curve) and on the refrigerant side (from two phase pressure drop correlation) the refrigerant flow boiling film heat transfer coefficient could be determined. The resulting heat transfer coefficient was found to be best correlated using a nucleate boiling heat transfer correlation, such as the pool boiling correlation by Cooper (1984) and the narrow channel flow boiling correlation by Tran (1999).

PART V

CONCLUSIONS AND SUGGESTIONS FOR FURTHER WORK

30 CONCLUSIONS

Plate heat exchangers operating in domestic heat pumps have been investigated in several aspects. A summary of the conclusions from the different parts will first be presented. Then a general conclusion of the entire thesis will be presented.

30.1 Part II – One zone heat exchanger

For very low heat flux and low brine mass flow rates, limiting performance improvement was observed due to approaching temperatures of the two fluid streams. The appropriate sizing and selection of brine mass flow rate is essential in order to obtain an efficient heat pump.

The influence of brine mass flow rate on the total area average refrigerant film heat transfer coefficient was investigated. The refrigerant side heat transfer coefficient increased as the brine mass flow rate increased. It was suggested that the redistribution of local heat flux was responsible. Further, the impact of running the evaporator in co- and counter-current flow configuration was investigated. No significant difference in their performance was observed and it seems to be no specific benefit in running the evaporator in co-current mode.

The running conditions tested experimentally was also tested in a numerical model, using two different boiling models. Only very small differences between the models was observed, however running the evaporator in co-current resulted in trends opposite to experimentally observed for the convective evaporation model. It was concluded that the nucleate boiling model agrees better with experiments.

Finally, the importance of having correct refrigerant inlet flow distributor was illustrated by measurements of the overall performance of several evaporators having identical heat transfer area but different refrigerant inlet flow distributor. The resulting flow distribution between the refrigerant channels was illustrated with IR-pictures of the same heat exchanger but at different heat loads.

30.2 Part III – Two zone heat exchanger

The boiling heat transfer area was determined in two different ways as the evaporator was considered as two-zone heat exchanger. The first method, in which the boiling heat transfer area was measured using Thermochromic Liquid Crystals, indicated that the boiling area averaged refrigerant flow boiling film heat transfer coefficient is mainly depended on the boiling area averaged heat flux. The data correlated much better with the heat flux than the refrigerant

Reynolds number. The pool boiling correlation by Cooper (1984) was successful in correlating the data, if the leading constant was set to 1.5.

As the LMTD method is used for evaluating the boiling heat transfer coefficient in the above investigation, the applicability of that method is investigated numerically. The Cooper correlation was assumed to be valid locally as well as globally. The results indicated that the correction factor needed in order to use the LMTD method in these applications, where the boiling heat transfer coefficient depends on the heat flux, is negligible for medium to large temperature differences. However, for small temperature differences a significant correction may be needed.

The second method to determine the boiling heat transfer coefficient used single phase correlations on both fluid sides in the superheated zone of the evaporator. The area required in the superheated zone was calculated and the boiling heat transfer area was then the remaining area of the heat exchanger. This method did not give the same results as the first method. Possible reasons for this discrepancy were discussed and it was concluded that mist flow is the most probable explanation for the observed discrepancy. In addition, assuming mist flow and that single phase gas heat transfer coefficient apply in the mist flow regime enabled the estimation of the dry-out quality. The resulting dryout quality agree with what would be expected, dry-out occur earlier if mass flux increases and/or if heat flux increases. The estimated dry out quality was correlated using the local boiling number and the Lockhart-Martinelli parameter.

30.3 Part IV – Local thermal and hydraulic performance

Local performances of a plate heat exchanger have been investigated in this part of the thesis. First, the adiabatic two-phase flow frictional pressure drop was experimentally determined. The pressure drop varied almost linearly with vapor fraction, for a given mass flow rate. The pressure drop was then plotted in a traditional two-phase frictional pressure drop chart, i.e. the two phase multiplier vs. the Lockhart-Martinelli parameter. The result agrees with what traditionally would have been expected. The two-phase multiplier was found to be fairly well correlated using the classical Chisholm equation, with the Chisholm parameter C set to 4.67. It was noted that the Chisholm parameter varied with the mass flux. However, using only the mass flux as correlating parameter for the Chisholm parameter did not give good results. Instead, using the kinetic energy per volume did correlate the Chisholm parameter. With the suggested new correlation the resulting prediction of the two phase flow frictional pressure drop agreed excellently with the experimental pressure drop, within ± 10 %.

Second, local flow boiling heat transfer coefficients were experimentally determined using a novel measuring technique for flow boiling in plate heat

exchangers. The water temperature profile was measured in detail along the heat exchanger. Employing a regression analysis on the measured water temperatures was found to provide a correlation giving a good estimation of the measured temperatures. Having an analytical equation for the water temperatures enabled a subsequent analysis obtaining local heat flux in the evaporator. Knowing local heat flux in conjunction with known single phase heat transfer coefficients on the water side, the temperature profiles on both the water side (regression curve) and on the refrigerant side (from two phase pressure drop correlation) the refrigerant flow boiling film heat transfer coefficient could be determined. The resulting local heat transfer coefficient was found to be best correlated using a nucleate boiling heat transfer correlation, such as the pool boiling correlation by Cooper (1984) and the narrow channel flow boiling correlation by Tran (1999).

30.4 General conclusions

Plate heat exchangers under various operating conditions have been investigated in this thesis. It seems that all indications point towards nucleate boiling being the main boiling mechanism, e.g. the numerical simulations, the TLC measurements and not least the local flow boiling measurements. The two phase flow frictional pressure drop is well correlated using the classical correlation by Chisholm (1967) with the Chisholm parameter set to 4.67. Even better agreement is obtained if the Chisholm parameter is correlated using the kinetic energy per volume. Mist flow seems to be present at high vapor qualities and mass flux.

There is no difference between co-current and counter-current flow configuration when using low (no) superheats. The brine flow rate influence the refrigerant side heat transfer via a redistribution of the local heat flux. The error introduced by employing the LMTD method in evaluating the boiling area averaged heat transfer coefficient using the Cooper (1984) correlation is not significant for large temperature differences.

Finally, it may be concluded that there is still room for improvement of the effectiveness of the plate heat exchanger operating as evaporator in domestic heat pumps. For instance; the superheating section is taken out of the evaporator, the flow distribution between parallel refrigerant channels is improved, or by enhancement of the heat transfer surface since nucleate boiling seems to be the dominating heat transfer mechanism.

31 SUGGESTIONS FOR CONTINUED WORK

Even though several different approaches of determine the performance of plate heat exchangers operating as evaporators in domestic heat pumps were employed in the present thesis, the thesis is by no means complete regarding all aspects of flow boiling in plate heat exchangers. In this section the author of the present thesis whishes to suggest some areas which may be fruitful in order to obtain an increasing knowledge base concerning flow boiling in plate heat exchangers.

As was indicated in the thesis, the flow distribution of the two-phase mixture of refrigerant between the parallel flow channels affects the performance to a large extent. Thus, the problem of flow distribution needs to be resolved, or understood. Hence, it is suggested that further research is conducted in this area.

The local flow boiling thermal and hydraulic performances were also investigated in the present thesis, however only one fluid (R134a) was used in these experiment. In addition, the pressure range tested was rather limited. It is suggested to expand the database of local flow boiling heat transfer with a wider scope concerning different fluids and at different operating pressure levels.

In addition, the tested geometries in the local flow boiling tests are limited to only one. Hence, it would be desirable to increase the database using a wider range of plate heat exchanger geometries, i.e. pressing depth, corrugation pitch, and not least the chevron angle. However, this requires prototype manufacturing of specific plate heat exchangers, which may be expensive, or a close co-operation with a plate heat manufacturer.

Void fraction and flow patterns occurring during two-phase flow in plate heat exchangers are not extensively investigated in the literature and are also not included in the present thesis. This would be desirable to investigate.

Finally, as the efficiency of the heat pumps is becoming even more important, it would be desirable to investigate different solutions to reduce the temperature difference in the plate heat exchanger. This may be done in different ways, e.g. excluding the superheat from the evaporator and/or increasing the flow boiling heat transfer coefficient (since the brine/water side heat transfer coefficient is at the same order of magnitude, or even higher) by special surface treatments.

NOMENCLATURE

SI units have been used throughout the entire thesis, if not otherwise stated. For clarity all units will be displayed in the nomenclature.

A	Heat transfer area	m²
A	Area	m²
A	Constant	-
a	Regression analysis constants	
b	Regression analysis constants	
b	Pressing depth	m
B	Constant	
$Bo = \frac{q''}{G \cdot \Delta h_{lg}}$	Boiling number	-
C	Constant	-
c	Regression analysis constants	
C_C	Collective term of the Cooper correlation	
$Co = \left(\frac{1-x}{x}\right)^{0.8} \left(\frac{\rho_g}{\rho_l}\right)^{0.5}$	Convective number	-
COP	Coefficient Of Performance	-
c_p	Specific heat capacity	J/kg·K
D	Constant	
d_e	Effective diameter	m
d_h	Hydraulic diameter	m
E	Flow boiling heat transfer enhancement factor	-
EBT	Entering Brine Temperature	°C

F	LMTD correction factor	-
F	Enhancement factor	-
F	Variable in Shah correlation	-
f	Fanning friction factor	-
F_{fl}	Fluid/wall constant	-
$Fr_l = \frac{G^2}{\rho_l^2 \cdot g \cdot d}$	Froude number	-
G	Mass flux	kg/m²·s
g	Gravitational acceleration	m/s²
g_c	Gravitational constant, equals 1 in SI units	-
j_{Nu}	Heat transfer group	-
LMTD	Logarithmic Mean Temperature Difference	K
L_p	Plate length	m
LWT	Leaving Water Temperature	°C
m	Constant	-
$\dot{m}$	Mass flow rate	kg/s
n	Constant	-
N	Variable in Shah correlation	-
N	Number of fluid passes	-
$N_{conf} = \frac{\sqrt{\frac{\sigma}{g \cdot (\rho_l - \rho_g)}}}{d}$	Confinement number	-
n_p	Number of plates	-
$NTU = \frac{UA}{(\dot{m} \cdot c_p)_{min}}$	Number of Transfer Units	-

$Nu = \frac{\alpha \cdot d}{\lambda}$	Nusselt number	-
p	Pressure	Pa
$Pr = \frac{\mu \cdot c_p}{\lambda}$	Prandtl number	-
$p_r = \frac{p}{p_{crit}}$	Reduced pressure	-
q	Transferred heat	W/kg
Q	Transferred heat	W
r	Radius	m
R_a	Surface roughness	m
$Re = \frac{G \cdot d}{\mu}$	Reynolds number	-
R_{th}	Thermal resistance	K·m²/W
s	Entropy	J/kg·K
S	Suppression factor	-
$s_{q''}$	Standard deviation during experiments	W/m²
T	Temperature	K
t	Temperature	°C
U	Overall heat transfer coefficient	W/m²·K
u	Velocity	m/s
V	Volume	m³
v	Specific volume	m³/kg
$\dot{V}$	Volumetric flow rate	m³/s
$We = \frac{G^2 \cdot d}{\rho \cdot \sigma}$	Weber number	-

W_p	Plate width	m
$X = \sqrt{\frac{(dp/dl)_l}{(dp/dl)_g}}$	Lockhart-Martinelli parameter	-
x	Vapor quality	-
x	Length coordinate	m
y_0	Regression analysis constants	
z_0	Regression analysis constants	
z	Position in CBE from water inlet	m
α	Film heat transfer coefficient	$W/m^2 \cdot K$
α_{hom}	Void fraction	-
β	Chevron angle	°
δ_{SS}	Plate thickness	m
Δ	Difference	-
Δh_{fg}	Latent heat of vaporization	J/kg
ε	Work	W/kg
ε	Effectiveness	-
ϕ	Two phase pressure drop multiplier	-
ϕ	Surface enlargement factor	-
$\Gamma = \sqrt{\frac{(dp/dl)_{go}}{(dp/dl)_{lo}}}$	Fluid property parameter	-
ϑ	Temperature difference	K
Λ	Corrugation pitch	m
φ	Chevron angle	°
η	Efficiency	-

λ	Thermal conductivity	W/m·K
μ	Dynamic Viscosity	Pa·s
ρ	Density	kg/m³
σ	Surface tension	N/m
$\Psi = \frac{\phi_{lo}^2 - 1}{\Gamma^2 - 1}$	Two phase pressure drop normalized multiplier	-
$\psi = \frac{\alpha_{TP}}{\alpha_l}$	Flow boiling heat transfer multiplier	-
ξ	Moody friction factor	-
ξ	Local coordinate	

Index

1	High temperature side
1	Position 1 in heat exchanger
1Φ	Single phase value
2	Low temperature side
2	Position 2 in heat exchanger
acc	Acceleration term
b	Bulk
B	Boiling side of heat exchanger
brine	Brine side of heat exchanger
C	Carnot machine
c	Cold fluid
c	Convective evaporation

calc	Calculated value
CB	Convective Boiling
CBE	Entire heat exchanger
cec	Convective evaporation at flowing conditions
ch	Channel
conf	confinement
contr	Contraction
core	Heat transfer section of CBE
cr	Critical value
d	Diagram, Chart
distr	Distribution device at refrigerant inlet port
e	Effective
EBT	Entering Brine Temperature
elev	Elevation term
enl	Enlargement
evap	Boiling section of the heat exchanger
f	Frictional
fg	Liquid – Vapor
g	Vapor
GO	All flow as vapor
go	All flow as vapor
h	Hot fluid
h	Hydraulic
H_2O	Water side of heat exchanger
HEX	Heat Exchanger

hom	Homogenous model
i	Position in heat exchanger
i	i^{th} constant
in	Entering
inport	Inlet refrigerant port
l	Liquid
L	Liquid
l	Laminar
lg	Liquid – Vapor
LM	Lockhart-Martinelli
LMTD	Logarithmic mean temperature difference
LO	All flow as liquid
lo	All flow as liquid
LWT	Leaving Water Temperature
m	Mean
m	Mass flow
mac	Macroscopic
max	Maximum
$(\dot{m}\cdot cp)_{min}$	Fluid with minimum Heat Capacity Rate
$(\dot{m}\cdot cp)_{max}$	Fluid with maximum Heat Capacity Rate
mic	Microscopic
min	Minimum
NB	Nucleate Boiling
nb,of	Nucleate boiling without flowing conditions
nbc	Nucleate boiling at flowing conditions

nbf	Nucleate boiling at flowing conditions
Nu	Applies for Nusselt correlation
obj	Test object
of	Standard conditions
out	Exiting
outport	Refrigerant outlet port
p	Plate
pool	Pool boiling
pre	Preheater
pred	Predicted value
r	Reduced
R	Refrigerant side of heat exchanger
R,Dutto	Calculated according to approach by Dutto et al.
refr	Refrigerant side of heat exchanger
S	Superheated section of heat exchanger
SA	Stephan-Abdelsalam
sat	Saturated conditions
SS	Stainless Steel plate
sup	Superheated section of the heat exchanger
T	Total
T	Tangent
t	Turbulent
th	Thermal
tot	Entire heat exchanger
TP	Two-Phase

tt	Turbulent – Turbulent
tube	Tube
v	Vapor
W	Wall

APPENDIX A LMTD CORRECTION FACTOR

In the following section additional data not given in the text are given.

APPENDIX A - I F-FACTORS, Δt_{brine} = 3 K

	Δt_{brine} = 3K			
	α_{brine}=500 W/m²K	α_{brine}=1 000 W/m²K	α_{brine}=2 000 W/m²K	α_{brine}=4 000 W/m²K
ϑ_1	**F**	**F**	**F**	**F**
0.2	0.627	0.604	0.590	0.583
0.4	0.787	0.758	0.736	0.723
0.6	0.863	0.838	0.817	0.801
0.8	0.905	0.885	0.866	0.850
1.0	0.931	0.915	0.899	0.884
1.2	0.947	0.935	0.921	0.908
1.4	0.959	0.948	0.937	0.926
1.6	0.967	0.958	0.949	0.939
1.8	0.973	0.966	0.958	0.949
2.0	0.977	0.972	0.965	0.957
2.2	0.981	0.976	0.970	0.963
2.4	0.984	0.980	0.974	0.969
2.6	0.986	0.982	0.978	0.973
2.8	0.988	0.985	0.981	0.976
3.0	0.989	0.987	0.983	0.979
3.2	0.991	0.988	0.985	0.981
3.4	0.992	0.990	0.987	0.984
3.6	0.993	0.991	0.988	0.985
3.8	0.993	0.992	0.989	0.987
4.0	0.994	0.992	0.990	0.988
4.2	0.995	0.993	0.991	0.989
4.4	0.995	0.994	0.992	0.990
4.6	0.996	0.994	0.993	0.991
4.8	0.996	0.995	0.993	0.992
5.0	0.996	0.995	0.994	0.992
5.2	0.997	0.996	0.995	0.993
5.4	0.997	0.996	0.995	0.994
5.6	0.997	0.996	0.995	0.994
5.8	0.997	0.997	0.996	0.995
6.0	0.998	0.997	0.996	0.995
6.2	0.998	0.997	0.996	0.995
6.4	0.998	0.997	0.997	0.996
6.6	0.998	0.997	0.997	0.996

	Δt_{brine} = 3K			
	α_{brine}=500 W/m²K	α_{brine}=1 000 W/m²K	α_{brine}=2 000 W/m²K	α_{brine}=4 000 W/m²K
ϑ_1	**F**	**F**	**F**	**F**
6.8	0.998	0.998	0.997	0.996
7.0	0.998	0.998	0.997	0.996
7.2	0.998	0.998	0.997	0.997
7.4	0.998	0.998	0.997	0.997
7.6	0.999	0.998	0.998	0.997
7.8	0.999	0.998	0.998	0.997
8.0	0.999	0.998	0.998	0.997
8.2	0.999	0.998	0.998	0.997
8.4	0.999	0.999	0.998	0.998
8.6	0.999	0.999	0.998	0.998
8.8	0.999	0.999	0.998	0.998
9.0	0.999	0.999	0.998	0.998
9.2	0.999	0.999	0.998	0.998
9.4	0.999	0.999	0.999	0.998
9.6	0.999	0.999	0.999	0.998
9.8	0.999	0.999	0.999	0.998
10.0	0.999	0.999	0.999	0.998
10.2	0.999	0.999	0.999	0.998
10.4	0.999	0.999	0.999	0.999

APPENDIX A - II F-FACTORS, Δt_{brine} = 5 K

	Δt_{brine} = 5K			
	α_{brine}=500 W/m²K	α_{brine}=1 000 W/m²K	α_{brine}=2 000 W/m²K	α_{brine}=4 000 W/m²K
ϑ_1	**F**	**F**	**F**	**F**
0.2	0.551	0.520	0.501	0.491
0.4	0.727	0.686	0.655	0.635
0.6	0.816	0.780	0.748	0.723
0.8	0.867	0.838	0.808	0.783
1.0	0.899	0.875	0.850	0.826
1.2	0.921	0.901	0.880	0.858
1.4	0.936	0.920	0.901	0.882
1.6	0.947	0.934	0.918	0.901
1.8	0.956	0.944	0.931	0.916
2.0	0.963	0.953	0.941	0.928
2.2	0.968	0.959	0.949	0.937
2.4	0.972	0.965	0.956	0.945
2.6	0.976	0.969	0.961	0.952
2.8	0.978	0.973	0.966	0.957
3.0	0.981	0.976	0.969	0.962
3.2	0.983	0.978	0.973	0.966
3.4	0.985	0.981	0.975	0.969
3.6	0.986	0.982	0.978	0.972
3.8	0.987	0.984	0.980	0.975
4.0	0.989	0.986	0.982	0.977
4.2	0.990	0.987	0.983	0.979
4.4	0.990	0.988	0.985	0.981
4.6	0.991	0.989	0.986	0.982
4.8	0.992	0.990	0.987	0.984
5.0	0.993	0.991	0.988	0.985
5.2	0.993	0.991	0.989	0.986
5.4	0.994	0.992	0.990	0.987
5.6	0.994	0.992	0.990	0.988
5.8	0.994	0.993	0.991	0.989
6.0	0.995	0.993	0.992	0.989
6.2	0.995	0.994	0.992	0.990
6.4	0.995	0.994	0.993	0.991
6.6	0.996	0.995	0.993	0.991
6.8	0.996	0.995	0.994	0.992
7.0	0.996	0.995	0.994	0.992
7.2	0.996	0.995	0.994	0.993
7.4	0.997	0.996	0.995	0.993

	Δt_{brine} = 5K			
	α_{brine}=500 W/m²K	α_{brine}=1 000 W/m²K	α_{brine}=2 000 W/m²K	α_{brine}=4 000 W/m²K
ϑ_1	**F**	**F**	**F**	**F**
7.6	0.997	0.996	0.995	0.994
7.8	0.997	0.996	0.995	0.994
8.0	0.997	0.996	0.995	0.994
8.2	0.997	0.997	0.996	0.994
8.4	0.997	0.997	0.996	0.995
8.6	0.998	0.997	0.996	0.995
8.8	0.998	0.997	0.996	0.995
9.0	0.998	0.997	0.996	0.995
9.2	0.998	0.997	0.997	0.996
9.4	0.998	0.997	0.997	0.996
9.6	0.998	0.998	0.997	0.996
9.8	0.998	0.998	0.997	0.996
10.0	0.998	0.998	0.997	0.996
10.2	0.998	0.998	0.997	0.997
10.4	0.998	0.998	0.997	0.997
10.6	0.998	0.998	0.998	0.997
10.8	0.999	0.998	0.998	0.997
11.0	0.999	0.998	0.998	0.997
11.2	0.999	0.998	0.998	0.997
11.4	0.999	0.998	0.998	0.997
11.6	0.999	0.998	0.998	0.997
11.8	0.999	0.998	0.998	0.998
12.0	0.999	0.999	0.998	0.998
12.2	0.999	0.999	0.998	0.998
12.4	0.999	0.999	0.998	0.998
12.6	0.999	0.999	0.998	0.998
12.8	0.999	0.999	0.998	0.998
13.0	0.999	0.999	0.998	0.998
13.2	0.999	0.999	0.998	0.998
13.4	0.999	0.999	0.999	0.998
13.6	0.999	0.999	0.999	0.998
13.8	0.999	0.999	0.999	0.998
14.0	0.999	0.999	0.999	0.998
14.2	0.999	0.999	0.999	0.998
14.4	0.999	0.999	0.999	0.998
14.6	0.999	0.999	0.999	0.998

APPENDIX A - III F-FACTORS, Δt_{brine} = 10 K

	Δt_{brine} = 10 K			
	α_{brine}=500 W/m²K	α_{brine}=1 000 W/m²K	α_{brine}=2 000 W/m²K	α_{brine}=4 000 W/m²K
ϑ_1	**F**	**F**	**F**	**F**
0.2	0.463	0.421	0.395	0.381
0.4	0.653	0.596	0.551	0.520
0.6	0.755	0.703	0.655	0.616
0.8	0.815	0.772	0.727	0.686
1.0	0.854	0.818	0.778	0.739
1.2	0.881	0.851	0.816	0.780
1.4	0.901	0.875	0.845	0.812
1.6	0.916	0.894	0.867	0.838
1.8	0.928	0.908	0.885	0.858
2.0	0.937	0.920	0.899	0.875
2.2	0.944	0.929	0.911	0.889
2.4	0.951	0.937	0.921	0.901
2.6	0.956	0.944	0.929	0.911
2.8	0.960	0.950	0.936	0.920
3.0	0.964	0.954	0.942	0.927
3.2	0.967	0.958	0.947	0.934
3.4	0.970	0.962	0.952	0.939
3.6	0.973	0.965	0.956	0.944
3.8	0.975	0.968	0.959	0.949
4.0	0.977	0.970	0.963	0.953
4.2	0.979	0.973	0.965	0.956
4.4	0.980	0.975	0.968	0.959
4.6	0.981	0.976	0.970	0.962
4.8	0.983	0.978	0.972	0.965
5.0	0.984	0.979	0.974	0.967
5.2	0.985	0.981	0.976	0.969
5.4	0.986	0.982	0.977	0.971
5.6	0.987	0.983	0.978	0.973
5.8	0.987	0.984	0.980	0.974
6.0	0.988	0.985	0.981	0.976
6.2	0.989	0.986	0.982	0.977
6.4	0.989	0.987	0.983	0.978
6.6	0.990	0.987	0.984	0.979
6.8	0.990	0.988	0.985	0.981
7.0	0.991	0.989	0.985	0.982
7.2	0.991	0.989	0.986	0.982
7.4	0.992	0.990	0.987	0.983

	Δt_{brine} = 10 K			
	α_{brine}=500 W/m²K	α_{brine}=1 000 W/m²K	α_{brine}=2 000 W/m²K	α_{brine}=4 000 W/m²K
ϑ_1	**F**	**F**	**F**	**F**
7.6	0.992	0.990	0.987	0.984
7.8	0.993	0.991	0.988	0.985
8.0	0.993	0.991	0.989	0.986
8.2	0.993	0.991	0.989	0.986
8.4	0.994	0.992	0.990	0.987
8.6	0.994	0.992	0.990	0.987
8.8	0.994	0.993	0.990	0.988
9.0	0.994	0.993	0.991	0.988
9.2	0.995	0.993	0.991	0.989
9.4	0.995	0.993	0.992	0.989
9.6	0.995	0.994	0.992	0.990
9.8	0.995	0.994	0.992	0.990
10.0	0.995	0.994	0.993	0.991
10.2	0.996	0.994	0.993	0.991
10.4	0.996	0.995	0.993	0.991
10.6	0.996	0.995	0.993	0.992
10.8	0.996	0.995	0.994	0.992
11.0	0.996	0.995	0.994	0.992
11.2	0.996	0.995	0.994	0.992
11.4	0.996	0.995	0.994	0.993
11.6	0.997	0.996	0.994	0.993
11.8	0.997	0.996	0.995	0.993
12.0	0.997	0.996	0.995	0.993
12.2	0.997	0.996	0.995	0.994
12.4	0.997	0.996	0.995	0.994
12.6	0.997	0.996	0.995	0.994
12.8	0.997	0.996	0.995	0.994
13.0	0.997	0.997	0.996	0.994
13.2	0.997	0.997	0.996	0.995
13.4	0.997	0.997	0.996	0.995
13.6	0.998	0.997	0.996	0.995
13.8	0.998	0.997	0.996	0.995
14.0	0.998	0.997	0.996	0.995
14.2	0.998	0.997	0.996	0.995
14.4	0.998	0.997	0.996	0.995
14.6	0.998	0.997	0.997	0.996
14.8	0.998	0.997	0.997	0.996
15.0	0.998	0.997	0.997	0.996
15.2	0.998	0.998	0.997	0.996
15.4	0.998	0.998	0.997	0.996

	Δt_{brine} = 10 K			
	α_{brine}=500 W/m²K	α_{brine}=1 000 W/m²K	α_{brine}=2 000 W/m²K	α_{brine}=4 000 W/m²K
ϑ_1	**F**	**F**	**F**	**F**
15.6	0.998	0.998	0.997	0.996
15.8	0.998	0.998	0.997	0.996
16.0	0.998	0.998	0.997	0.996
16.2	0.998	0.998	0.997	0.996
16.4	0.998	0.998	0.997	0.997
16.6	0.998	0.998	0.997	0.997
16.8	0.998	0.998	0.997	0.997
17.0	0.998	0.998	0.998	0.997
17.2	0.998	0.998	0.998	0.997
17.4	0.999	0.998	0.998	0.997
17.6	0.999	0.998	0.998	0.997
17.8	0.999	0.998	0.998	0.997
18.0	0.999	0.998	0.998	0.997
18.2	0.999	0.998	0.998	0.997
18.4	0.999	0.998	0.998	0.997
18.6	0.999	0.998	0.998	0.997
18.8	0.999	0.998	0.998	0.997
19.0	0.999	0.998	0.998	0.998
19.2	0.999	0.998	0.998	0.998
19.4	0.999	0.999	0.998	0.998
19.6	0.999	0.999	0.998	0.998
19.8	0.999	0.999	0.998	0.998
20.0	0.999	0.999	0.998	0.998

APPENDIX B FLUID SURFACE PARAMETERS FROM KANDLIKAR AND STEINKE (2003)

Fluid	F_{fl}
Water	1.00
R-11	1.30
R-12	1.50
R-13B1	1.31
R-22	2.20
R-113	1.30
R-114	1.24
R-134a	1.63
R-152a	1.10
R-32/R-132	3.30
R-141b	1.80
R-124	1.00
Kerosene	0.488


(Kandlikar & Steinke 2003)
3.6
3.2
2.8
2.4
2.0
1.6
1.2
0.8
0.4
0.0
F_{fl}
R32
R22
R141b
R134a
R12
R11
R113
R114
R152a
Water
0
20
40
60
80
100
120
140
160
180
200
Molmass

APPENDIX C GRAPHICAL CORRELATION BY M.M. SHAH (1976)

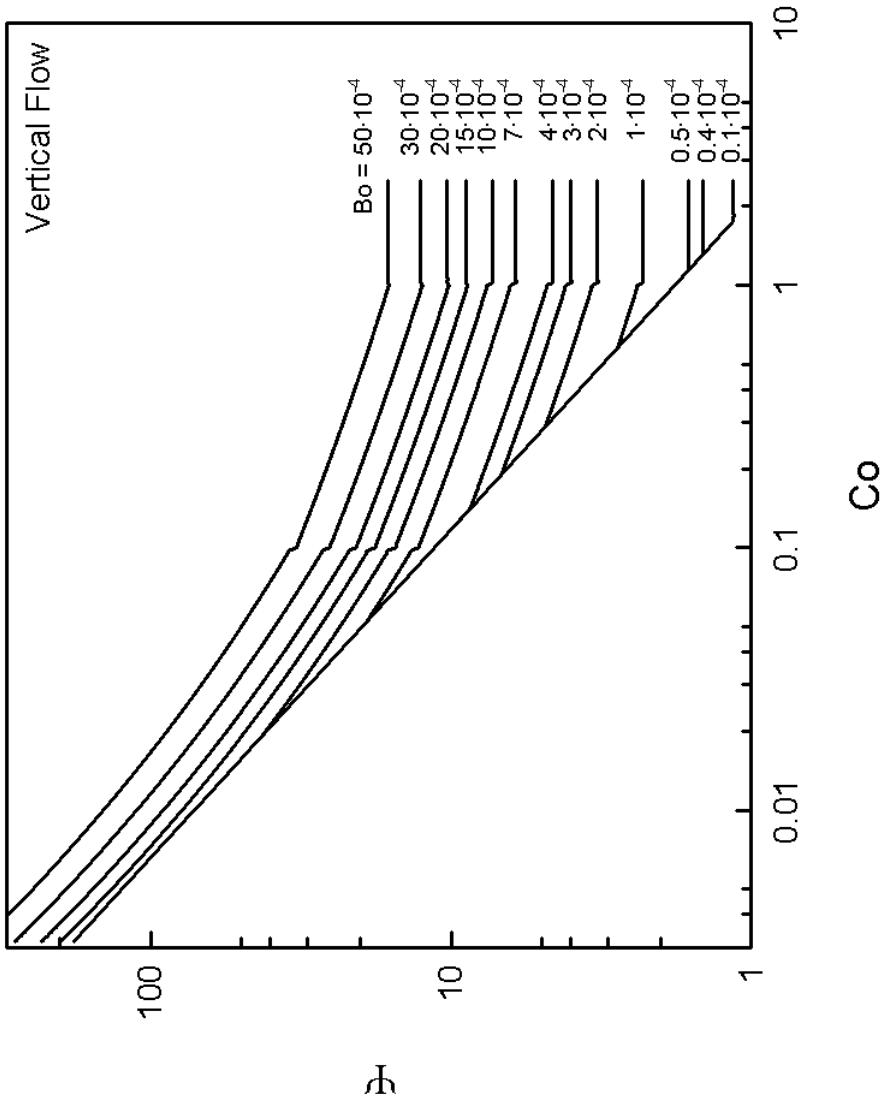

APPENDIX D POOL BOILING REFERENCE VALUES FOR STEINER AND TABOREK (1992) CORRELATION

The method on how to calculate the pool boiling heat transfer coefficient for different fluids for the Steiner and Taborek (1992) is outlined in this section. Included is also the table with the pre-calculated values originally given in Steiner and Taborek (1992).

The calculation procedure starts with the calculation of

$$\alpha_{nb,o|0.03} = 0.1\frac{\lambda_l}{d_b}\left(\frac{\rho_l}{\rho_g}\right)^{-0.156}\left(\frac{q''\cdot d_b}{\lambda_l\cdot T_{sat}}\right)^{0.674}\left(\frac{\Delta h_{lg}\cdot d_b^2}{a^2}\right)^{0.371}\left(\frac{a^2\cdot\rho_l}{\sigma\cdot d_b}\right)^{0.35}\left(\frac{\mu_l\cdot c_{p,l}}{\lambda_l}\right)^{-0.16} \tag{259}$$

The thermal diffusivity, a, is defined as

$$a = \frac{\lambda_l}{\rho_l\cdot c_{p,l}} \tag{260}$$

and d_b is the characteristic bubble departure diameter, calculated as

$$d_b = 0.0146\cdot\beta\cdot\sqrt{\frac{2\cdot\sigma}{g\cdot(\rho_l-\rho_g)}} \tag{261}$$

β is set to 45° for water, 1° for cryogenics and 35° for all other fluids. The value from eq. (259) is now recalculated using

$$\alpha_{nb,o} = \alpha_{nb,o|0.03}\frac{1}{1.2\cdot p_r^{0.27}+\left(2.5+\frac{1}{1-p_r}\right)\cdot p_r}\left(\frac{20\,000}{q''}\right)^{0.9-0.3\cdot p_r^{0.3}} \tag{262}$$

Now, this value is recalculated using

$$\alpha_{nb,of} = \alpha_{nb,o}\cdot\left(1.2\cdot p_r^{0.27}+\left(2.5+\frac{1}{1-p_r}\right)\cdot p_r\right)\cdot\left(\frac{q''_{of}}{20\,000}\right)^{0.9-0.3\cdot p_r^{0.3}} \tag{263}$$

Conducting these steps, results in the following table for different fluids.

The table shows values of some selected fluids.

Fluid	q''_{of}	$\alpha_{nb,of}$
R134a	20 000	3 500
R22	20 000	3 930
R290 (Propane)	20 000	4 000
Ammonia	150 000	36 640
CO_2	150 000	18 890
Water	150 000	25 580

A more comprehensive table may be found in the original reference.

APPENDIX E UNCERTAINTY ANALYSIS

The calculated heat transfer coefficient on the refrigerant side does have an uncertainty to its actual value. The reason is of course the uncertainty of the measured values from which the heat transfer coefficient is calculated. The magnitude of the uncertainty in the calculated heat transfer coefficient may be either estimated or calculated. Estimation of the uncertainty does require some sound feeling of the process under consideration and is, of course, subject to personal preferences.

A more objective method is to calculate the uncertainty and methods are available in the literature. In this work, the method by Kline and McClintock (1953) was used. The calculated result is denominated R, and the individual parameters of the function R are denoted v. The uncertainty of each of the individual parameters v is δv. Kline and McClintock suggested the uncertainty of the calculated value, δR, to be calculated as

$$\delta R = \sqrt{\left(\frac{\partial R}{\partial v_1}\cdot\delta v_1\right)^2 + \left(\frac{\partial R}{\partial v_2}\cdot\delta v_2\right)^2 + \ldots + \left(\frac{\partial R}{\partial v_n}\cdot\delta v_n\right)^2} \tag{264}$$

where

$$R = f\left(v_1, v_2, \ldots, v_n\right) \tag{265}$$

The uncertainty of each of the individual parameters has to be estimated to a given odds. This uncertainty may be found e.g. on the instrument used. If one or more of the individual parameters is not a measured value but a derived value, the uncertainty of that variable has to be calculated by eq. (264). This step is repeated until all individual variables are measured entities.

For a plate heat exchanger, the refrigerant heat transfer coefficient is calculated as

$$\alpha_R = \frac{1}{\frac{1}{U} - \frac{1}{\alpha_{brine}}} \tag{266}$$

where the heat transfer resistance in the heat transfer wall has been neglected. The corresponding partial derivatives are

$$\frac{\partial \alpha_R}{\partial U} = \frac{1}{\left(\frac{1}{U} - \frac{1}{\alpha_{brine}}\right)^2 \cdot U^2} \tag{267}$$

and

$$\frac{\partial \alpha_R}{\partial \alpha_{brine}} = \frac{-1}{\left(\frac{1}{U} - \frac{1}{\alpha_{brine}}\right)^2 \cdot \alpha_{brine}^2} \tag{268}$$

Now, the uncertainty of the refrigerant heat transfer coefficient may be written

$$\delta\alpha_R = \frac{1}{\left(\frac{1}{U} - \frac{1}{\alpha_{brine}}\right)^2} \sqrt{\left(\frac{\delta U}{U^2}\right)^2 + \left(-\frac{\delta\alpha_{brine}}{\alpha_{brine}^2}\right)^2} \tag{269}$$

However, the brine heat transfer coefficient is a function of Nusselt number, thermal conductivity of the brine and the effective diameter,

$$\alpha_{brine} = \frac{Nu_{brine} \cdot \lambda_{brine}}{d_e} \tag{270}$$

The partial derivatives are

$$\begin{aligned} \frac{\partial \alpha_{brine}}{\partial Nu_{brine}} &= \frac{\lambda_{brine}}{d_e} \\ \frac{\partial \alpha_{brine}}{\partial \lambda_{brine}} &= \frac{Nu_{brine}}{d_e} \\ \frac{\partial \alpha_{brine}}{\partial d_e} &= -\frac{Nu_{brine} \cdot \lambda_{brine}}{d_e^2} \end{aligned} \tag{271}$$

and the corresponding uncertainty

$$\delta\alpha_{brine} = \frac{Nu_{brine} \cdot \lambda_{brine}}{d_e} \cdot \sqrt{\left(\frac{\delta Nu_{brine}}{Nu_{brine}}\right)^2 + \left(\frac{\delta\lambda_{brine}}{\lambda_{brine}}\right)^2 + \left(-\frac{\delta d_e}{d_e}\right)^2} \tag{272}$$

The Nusselt number is calculated from the Reynolds and Prandtl numbers, as

$$Nu_{brine} = C \cdot Re_{brine}^{m} \cdot Pr_{brine}^{n} \tag{273}$$

The uncertainty of the Nusselt number is

$$\delta Nu_{brine} = Nu_{brine} \sqrt{\left(m \cdot \frac{\delta Re_{brine}}{Re_{brine}} \right)^2 + \left(n \cdot \frac{\delta Pr_{brine}}{Pr_{brine}} \right)^2 + \left(\frac{\delta f_{Nu}}{Nu_{brine}} \right)^2} \tag{274}$$

where δf_{Nu} is the uncertainty of the empirical function of Nusselt number. The Prandtl number is

$$Pr_{brine} = \frac{\mu_{brine} \cdot c_{p_{brine}}}{\lambda_{brine}} \tag{275}$$

Thus, the uncertainty is

$$\delta Pr_{brine} = Pr_{brine} \sqrt{\left(\frac{\delta \mu_{brine}}{\mu_{brine}} \right)^2 + \left(\frac{\delta c_{p_{brine}}}{c_{p_{brine}}} \right)^2 + \left(-\frac{\delta \lambda_{brine}}{\lambda_{brine}} \right)^2} \tag{276}$$

Now, the uncertainty of the thermophysical properties are a combined function of measured temperature and the uncertainty of its empirical function. In this work, the combined uncertainty of the thermophysical properties have been estimated to be 5% of predicted value.

The Reynolds number is calculated as

$$Re_{brine} = \frac{2 \cdot \dot{m}_{brine,ch}}{W_p \cdot \mu_{brine}} \tag{277}$$

Hence, the corresponding uncertainty is

$$\delta Re_{brine} = Re_{brine} \sqrt{\left(\frac{\delta \dot{m}_{brine,ch}}{\dot{m}_{brine,ch}} \right)^2 + \left(-\frac{\delta W_p}{W_p} \right)^2 + \left(-\frac{\delta \mu_{brine}}{\mu_{brine}} \right)^2} \tag{278}$$

The uncertainty in geometrical parameters, a uncertainty of 2% of the given value is assumed. Before the uncertainty of eq. (274) can be calculated, we need the uncertainty of mass flow on the brine side. The mass flow of brine is calculated as

$$\dot{m}_{brine} = \frac{\dot{V}_{brine} \cdot \rho_{brine}}{N_{ch_{brine}}} \tag{279}$$

where $N_{ch,brine}$ is the number of channel in the plate heat exchanger on the brine side. No uncertainty of $N_{ch,brine}$ is assumed, and hence

$$\delta\dot{m}_{brine,Ch} = \dot{m}_{brine,Ch}\sqrt{\left(\frac{\delta\dot{V}_{brine}}{\dot{V}_{brine}}\right)^2 + \left(\frac{\delta\rho_{brine}}{\rho_{brine}}\right)^2} \tag{280}$$

Once the uncertainty of Nusselt number, eq. (274), is calculated, the uncertainty in heat transfer coefficient on the brine side , eq. (272), may be calculated.

So, now we're done with one of the uncertainties in eq. (269). Now we will have to follow the path of the overall heat transfer coefficient, U, down to the actual measured values.

The overall heat transfer coefficient, U, is calculated as

$$U = \frac{\dot{Q}_2}{\vartheta_m \cdot A} \tag{281}$$

Hence, the uncertainty is

$$\delta U = U\sqrt{\left(\frac{\delta\dot{Q}_2}{\dot{Q}_2}\right)^2 + \left(-\frac{\delta\vartheta_m}{\vartheta_m}\right)^2 + \left(-\frac{\delta A}{A}\right)^2} \tag{282}$$

The uncertainty of the heat transfer area of the plate heat exchanger is assumed to be 2% of the heat transfer area reported. The heat load is calculated as

$$\dot{Q}_2 = \frac{\dot{Q}_{2,brine} + \dot{Q}_{2,R}}{2} \tag{283}$$

and thus

$$\delta\dot{Q}_2 = \frac{1}{2}\sqrt{\delta\dot{Q}_{2,brine}^2 + \delta\dot{Q}_{2,R}^2} \tag{284}$$

The heat load on the brine side is calculated as

$$\dot{Q}_{2,brine} = \dot{m}_{brine} \cdot c_{p_{brine}} \cdot \Delta t_{brine} \tag{285}$$

where Δt_{brine} is the temperature change on the brine side over the plate heat exchanger. The corresponding uncertainty of the heat load on the brine side is

$$\delta\dot{Q}_{2,brine} = \dot{Q}_{2,brine}\sqrt{\left(\frac{\delta\dot{m}_{brine}}{\dot{m}_{brine}}\right)^2 + \left(\frac{\delta c_{p_{brine}}}{c_{p_{brine}}}\right)^2 + \left(\frac{\delta\Delta t_{brine}}{\Delta t_{brine}}\right)} \tag{286}$$

The uncertainty of brine mass flow has already been estimated, eq. (279). As already mentioned, the assumed uncertainty of thermophysical properties is 5% of the value. In addition, temperature difference measured with two thermocouples have been estimated to be 0.1 K.

The heat load on the refrigerant side is calculated as

$$\dot{Q}_{2,R} = \dot{m}_R \cdot \left(h_{R_{out}} - h_{R_{exp}}\right) \tag{287}$$

where $h_{r,exp}$ is the specific enthalpy at the inlet to the expansion valve, determined by measuring the refrigerant temperature at that location. The estimated uncertainty is 5% of the calculated value. The specific enthalpy at the inlet of the compressor, $h_{R,out}$ is determined by measuring the pressure and temperature of the superheated refrigerant at that position. Again, the estimated uncertainty is 5%. The mass flow of the refrigerant is measured using a Coriolis mass flow meter from Micromotion, and the uncertainty is estimated to 1% of the reading. The uncertainty of the heat load on the refrigerant side is calculated as

$$\delta\dot{Q}_{2,R} = \sqrt{\left(\left(h_{R_{out}} - h_{R_{exp}}\right)\cdot\delta\dot{m}_R\right)^2 + \left(\dot{m}_R \cdot \delta h_{R_{out}}\right)^2 + \left(-\dot{m}_R \cdot \delta h_{R_{exp}}\right)} \tag{288}$$

Now the uncertainty of the heat load in the evaporator may be calculated, eq. (284). The mean temperature difference in the evaporator is calculated as

$$\vartheta_m = \frac{\Delta t_{brine}}{\frac{\Delta t_{brine,evap}}{\vartheta_{m,evap}} + \frac{\Delta t_{brine,sup}}{\vartheta_{m,sup}}} \tag{289}$$

according to Dutto et al. (1991). The corresponding uncertainty is

$$\delta\vartheta_m = \vartheta_m \cdot \left(\sqrt{ \left(\frac{\delta\Delta t_{brine}}{\Delta t_{brine}} \right)^2 + \left(\frac{-\vartheta_m}{\Delta t_{brine} \cdot \vartheta_{m,evap}} \delta\Delta t_{brine,evap} \right)^2 + \left(\frac{-\vartheta_m}{\Delta t_{brine} \cdot \vartheta_{m,sup}} \delta\Delta t_{brine,sup} \right)^2 + \left(\frac{\vartheta_m \cdot \Delta t_{brine,evap}}{\Delta t_{brine} \cdot \vartheta_{m,evap}^2} \right)^2 + \left(\frac{\vartheta_m \cdot \Delta t_{brine,sup}}{\Delta t_{brine} \cdot \vartheta_{m,sup}^2} \right)^2 } \right) \tag{290}$$

Starting with the superheated section, the brine temperature difference is calculated as

$$\Delta t_{brine,sup} = \frac{\dot{m}_R \cdot c_{p_R} \cdot \Delta t_{sup}}{\dot{m}_{brine} \cdot c_{p_{brine}}} \tag{291}$$

The superheat is “measured” using pressure transducer and thermocouples. The uncertainty is estimated to 0.2 K. All the other parameters have already been calculated or estimated. Thus, the uncertainty of the temperature change of the brine in the superheated section is

$$\delta\Delta t_{brine,sup} = \Delta t_{brine,sup} \cdot \left(\sqrt{ \left(\frac{\delta\dot{m}_R}{\dot{m}_R} \right)^2 + \left(\frac{\delta c_{p_R}}{c_{p_R}} \right)^2 + \left(\frac{\delta\Delta t_{sup}}{\Delta t_{sup}} \right)^2 + \left(-\frac{\delta\dot{m}_{brine}}{\dot{m}_{brine}} \right)^2 + \left(-\frac{\delta c_{p_{brine}}}{c_{p_{brine}}} \right)^2 } \right) \tag{292}$$

The temperature change in the boiling section of the evaporator is calculated as

$$\Delta t_{brine,evap} = \Delta t_{brine} - \Delta t_{brine,sup} \tag{293}$$

Hence, the uncertainty is

$$\delta\Delta t_{brine,evap} = \sqrt{\delta\Delta t_{brine}^2 + \left(-\delta\Delta t_{brine,sup}\right)^2} \tag{294}$$

The logarithmic mean temperature difference (LMTD) on the superheated section of the evaporator may be rewritten as

$$\vartheta_{m,sup} = \frac{-\Delta t_{sup} - \Delta t_{brine,sup}}{\ln\left(\frac{\Delta t_{z=L}}{\Delta t_{z=L} + \Delta t_{sup}}\right)} \tag{295}$$

where $\Delta t_{z=L}$ is the temperature difference between brine fluid and refrigerant at the exit of the heat exchanger. This is measured using two thermocouples and the estimated uncertainty is 0.1 K.

The derivatives of this function may be obtained by using the approach as listed by Råde and Westergren (1990). If the derivatives of function E(x) is sought, defined as

$$E(x) = \frac{f(x)^n}{g(x)^m} \tag{296}$$

then the derivatives may be calculated as

$$\frac{d}{dx}E(x) = \frac{f(x)^{n-1}}{g(x)^{m+1}} \cdot \left(n \cdot g(x) \cdot \frac{d}{dx} f(x) - m \cdot f(x) \cdot \frac{d}{dx} g(x) \right) \tag{297}$$

For the LMTD on the superheated section, the function f and g is apparently

$$f_{sup} = -\Delta t_{sup} - \Delta t_{brine,sup} \tag{298}$$

and

$$g_{sup} = \ln\left(\frac{\Delta t_{z=L}}{\Delta t_{z=L} + \Delta t_{sup}}\right) \tag{299}$$

Now, the partial derivatives may be determined for the LMTD of the superheated section, noting that n= 1 and m=1. First, with respect to Δt_{sup},

$$\frac{\partial \vartheta_{m,sup}}{\partial \Delta t_{sup}} = \frac{1}{\left(\ln\left(\frac{\Delta t_{z=L}}{\Delta t_{z=L} + \Delta t_{sup}}\right)\right)^2} \cdot \left\{ -\ln\left(\frac{\Delta t_{z=L}}{\Delta t_{z=L} + \Delta t_{sup}}\right) - 2 \cdot \frac{\Delta t_{sup} + \Delta t_{brine,sup}}{\Delta t_{z=L} + \Delta t_{sup}} \right\} \tag{300}$$

Second, with respect to $\Delta t_{z=L}$,

$$\frac{\partial \vartheta_{m,sup}}{\partial \Delta t_{z=L}} = \frac{1}{\left(\ln\left(\frac{\Delta t_{z=L}}{\Delta t_{z=L} + \Delta t_{sup}} \right) \right)^2} \cdot \cdot \left\{ \left(\Delta t_{sup} + \Delta t_{brine,sup} \right) \cdot \left(\frac{1}{\Delta t_{z=L}} - \frac{1}{\Delta t_{z=L} + \Delta t_{sup}} \right) \right\} \tag{301}$$

Thirdly, with respect to $t_{B,sup}$,

$$\frac{\partial \vartheta_{m,sup}}{\partial \Delta t_{brine,sup}} = \frac{-1}{\ln\left(\frac{\Delta t_{z=L}}{\Delta t_{z=L} + \Delta t_{sup}} \right)} \tag{302}$$

Combining these equation in the uncertainty of the superheated LMTD, (not including the individual terms)

$$\delta \vartheta_{m,sup} = \sqrt{\left(\frac{\partial \vartheta_{m,sup}}{\partial \Delta t_{sup}} \cdot \delta \Delta t_{sup} \right)^2 + \left(\frac{\partial \vartheta_{m,sup}}{\partial \Delta t_{z=L}} \cdot \delta \Delta t_{z=L} \right)^2 + \left(\frac{\partial \vartheta_{m,sup}}{\partial \Delta t_{brine,sup}} \cdot \delta \Delta t_{brine,sup} \right)^2} \tag{303}$$

The LMTD of the boiling section of the evaporator is calculated as

$$\vartheta_{m,evap} = \frac{\Delta t_{brine,evap}}{\ln\left(\frac{\Delta t_{z=0} + \Delta t_{brine,evap}}{\Delta t_{z=0}} \right)} \tag{304}$$

Thus, the corresponding uncertainty is

$$\delta \vartheta_{m,evap} = \vartheta_{m,evap} \sqrt{\left(\left(1 - \frac{\vartheta_{m,evap}}{\Delta t_{brine,evap} \cdot \left(\Delta t_{z=0} + \Delta t_{brine,evap} \right)} \right) \frac{\delta \Delta t_{brine,evap}}{\Delta t_{brine,evap}} \right)^2 + \left(\frac{\vartheta_{m,evap}}{\Delta t_{brine,evap}} \cdot \left(\frac{1}{\Delta t_{z=0}} - \Delta t_{z=0} - \Delta t_{brine,evap} \right) \delta \Delta t_{z=0} \right)^2} \tag{305}$$

Now, the uncertainty of the LMTD according to Dutto et al. (1991), eq. (290), may be calculated. Once this is done the uncertainty of the overall heat transfer

coefficient, eq. (281), may be calculated. When this has been done the total combined uncertainty of total area averaged refrigerant heat transfer coefficient, eq. (269), is readily calculated, and we have arrived at our goal, to express the uncertainty of the investigated heat transfer coefficient.

The heat transfer coefficient is often plotted against the heat flux, either by the boiling section area based heat flux or the total heat transfer area based heat flux. The heat flux may generally be expressed as

$$q'' = \frac{\dot{Q}}{A} \tag{306}$$

The corresponding uncertainty is

$$\delta q'' = \sqrt{\left(\frac{1}{A}\cdot\delta\dot{Q}\right)^2 + \left(-\frac{\dot{Q}}{A^2}\cdot\delta A\right)^2} \tag{307}$$

The transferred heat is calculated as

$$\dot{Q} = \dot{m}_R \cdot \left(h_{R_{out}} - h_{R_{in}}\right) \tag{308}$$

Thus, the uncertainty of the transferred heat is

$$\delta\dot{Q} = \sqrt{\left(\left(h_{R_{out}} - h_{R_{in}}\right)\cdot\delta\dot{m}_R\right)^2 + \left(\dot{m}_R\cdot\delta h_{R_{out}}\right)^2 + \left(-\dot{m}_R\cdot\delta h_{R_{in}}\right)^2} \tag{309}$$

which, inserted into eq. (307) gives an estimation of the uncertainty of the heat flux.

The resulting uncertainty of the measurements depend on the actual running conditions. A single representative value of each derived parameter, e.g. the heat transfer coefficient, is thus not meaningful. The uncertainty the experiments are instead indicated as error bars in the figures included in the thesis.

APPENDIX F CHRONOLOGICAL SUMMARY OF THE RESEARCH PROJECT

Plate heat exchangers may be used in many applications. In the present thesis, the application of plate heat exchangers operating as evaporators in domestic heat pumps has been considered. This implies certain running conditions of the evaporator. As stated, the thesis has been divided into three main parts, where the actual investigations are carried out. The chosen parts are by no means chronological, and it is the purpose of this section to brief the reader on the actual chronological order of the different investigations and the original motivation and questions asked.

The first investigation and measurements conducted was the investigations reported in chapter 20. The purpose was to evaluate the rather new technique of using Thermochromic Liquid Crystals in heat transfer experiments. I had already before starting this research project come in contact with this technique, as Colbein Oskarsson and Prof. Bengt Sundén at the Lund Institute of Technology conducted evaluation tests of TLC during the time I was conducting my Master of Science thesis work. However, the original idea to use TLC in plate heat exchangers was not mine, I inherited that from the previous project. However, it was decided that TLC was to be evaluated. A CCD-camera was bought together with a software to evaluate the obtained pictures.

TLC is rather easy to apply, you just paint it on the surface. However, if you really would like to take temperature readings, you have an enormous amount of calibration ahead of you. In this investigation, I did not really measure the actual temperature, merely made a distinction of “high” and “low” temperatures. For accurate temperature readings, you will need a perpendicular surface to the camera, truly white light and a calibration protocol, preferably on the actual tested surface.

In any case, the measurements were successful. The next step planned was to implement TLC inside the evaporator, using one of the CBE with transparent outer plate. However, I could never get the TLC to work with the refrigerant. I tried different covers in order to protect the TLC from the refrigerant, but none was successful. The purpose of the measurement was of course to measure the actual wall temperature. In retrospect, I do think that the proposed approach on the last chapter in the thesis is a better way. As is stated in the thesis, local wall temperature variations within each unitary cell is expected, and thus a rather fine spatial resolution is required to resolve that. It is my opinion that the unitary cell average heat transfer coefficient approach, as the proposed approach is, is easier and also more practically relevant. Using TLC measuring the wall temperature, through a transparent plate with poor light and on a wavy surface seems a bit unrealistic.

The next investigation conducted is presented in chapter 22. It turned out that SWEP International AB had carried out flow boiling experiments with plate heat exchangers having different chevron angles. It seemed that the people who conducted the experiment had left the company and there were no-one having the time to get into the measurements. It was decided to incorporate that experimental work in the research project I was working in. When the analysis was finished, a rather large scatter was observed at the higher heat flux range. It was only briefly discussed in the paper, but was investigated more thoroughly in the next investigation/paper, parts of chapter 23. In that paper several possible reasons for the observed scatter were discussed. Among them was the possibility of mist flow. This was ruled out based on reasoning. The idea was like this;

In the TLC measurements, a clear transition was observed from "cold" to "not-so-cold" region. In addition, from the numerical single phase investigation I carried out in my Master of Science thesis, together with other published CFD-simulations, a swirl flow is observed. It was thought that any droplets in the gas core would through the centrifugal force be thrown onto the walls, hence I would have observed that during the TLC measurements. As you may see in that chapter, mist flow is suggested as the main phenomenon responsible for the discrepancy observed. This change in view have emerged rather late in the research project. Why have I changed my mind. Well, even though several attempts have been carried out to explain this by some other means, trying to correlate it using strange parameters but nothing really worked. It eventually became clear to me that it may not be that complicated with an undiscovered mechanism; dry-out is known to occur in most other geometries, and if the droplets are small enough, perhaps they could travel with the gas flow and that the centrifugal force is not strong enough to throw them onto the surface?

The issue is still not resolved, since I do not have any hard evidence that mist flow does occur, however it seems to be the most likely explanation.

The next investigation was again initiated by Olivier Pelletier at SWEP International AB. They wanted to investigate how the evaporator perform with extremely low heat flux. This is experimentally difficult as a heat pump should be used. We slightly altered the investigation to instead investigate low total area averaged heat flux (but not extremely low) and low brine flow rate, obtaining low heat flux at the refrigerant inlet. The purpose was to see whether significant difference was observed as the "onset of nucleate boiling" come into play. We did not actually see that, but what we did see is reported in chapter 12.

During that time I conducted several investigations concerning the impact of refrigerant inlet flow geometry. A vast amount of experimental data had been produced. All of these were conducted with the water/brine flow rate controlled in such a way that the temperature drop on the water/brine side was 3 K. Would

I have got different results of the refrigerant side heat transfer coefficient using a different water/brine mass flow rate?

As I earlier had observed that heat flux seemed to be the dominating flow boiling mechanism, and I was not sure whether mist flow did occur or not, I asked myself, could co-current actually be more efficient as we would then obtain high wall superheat at the position with lots of liquid refrigerant, and small wall superheat at the position of high vapor quality, the region where mist flow may occur.

These two questions were asked almost at the same time, and the measurements conducted in these two measurements (chapter 13 and chapter 14) are very close together in time.

After realizing that the brine mass flow rate did affect the refrigerant side, and with the analysis done in those investigations, I asked myself: Can the LMTD method actually be used, since in flow boiling the heat transfer coefficient is not constant, as it should be according to the derivation of the LMTD. As my results indicated nucleate boiling to be the dominating boiling mechanism (even though there were a wild debate concerning this at the Jamaica conference), I decided to numerically investigate how much the appropriate temperature difference would deviate from the LMTD assuming the Cooper (1984) correlation to be valid locally as well as boiling area averaged. The results are reported in chapter 21. The analysis is not limited to CBE. However, the typical values used in the analysis are those found in a CBE.

At the same time, a question arose: Since the boiling section and superheated section shares the same heat transfer area, does this always add up to the total heat transfer area, i.e. is a mathematical solution always obtained or is the area distribution unsteady (pulsating back and forth)? I decided to numerically investigate this. In order not to rule out the possibility of convective evaporation, and as I came by the correlation by Donowski and Kandlikar (2000) developed for plate heat exchangers using the data by Yan & Lin (1999), I performed two different cases, nucleate boiling model and convective evaporation model. The original question was to answer if a solution always exists. The answer I got is found in chapter 15.

Finally the research project also aimed at finding out the local flow boiling and hydraulic performance of plate heat exchangers. The initial start of this was the construction of a pump circulation loop. One of the transparent plate heat exchangers was used to visualize and measure adiabatic two-phase flow. The tested heat exchanger had an inlet flow distribution device, even though the heat exchanger only had one refrigerant channel. The measured pressure drop was used to extract the frictional pressure drop. We obtained rather large values, and it could be suspected that the estimated distributor pressure drop was not

entirely correct. Thus, it was decided to redo these measurements using a plate heat exchanger not having an inlet flow distributor. The result is found in chapter 27. The last chapter deals with a novel technique, as far as I am aware, of measuring local flow boiling heat transfer coefficients in plate heat exchangers. However, a similar approach has been suggested for other geometries. Thome said in one of his presentations, I do not recall which one, that he suggests to use this method in measuring the water profile and wall profile during flow boiling in straight tubes. As discussed before, measuring the wall temperature in plate heat exchangers is a bit more challenging task than in straight tubes. Therefore I suggest to use the known single phase heat transfer coefficient and calculate the wall temperature rather than to measure it. The technique of drilling holes through an outer plate and inserting thermocouples into the flow stream is not new either, it was done by Haseler et al. (1992) for single phase flows. What is new is the combination of these during flow boiling tests. The results of the initial measurements is reported in chapter 28.

REFERENCES

Amooie-Foumeny M., 1977, Flow distribution in plate heat exchangers, Ph.D. thesis, Postgraduate School of Studies, in Chemical Engineering, University of Bradford, p. 240.

André H., 2001, Utveckling av beräkningsprogram för simulering av tvådimensionell strömning i värmeväxlare (Development of 2D flow field simulation program for plate heat exchangers, in Swedish), M.Sc. thesis, Div. Heat Transfer, Dept. Heat and Power Engineering, Lund Institute of Technology, Sweden, p. 28.

Bai X., Newell T.A., 2000, An investigation of two-phase flow characteristics in chevron-style flat plate heat exchangers, Proc. 8th Int. Refr. Conf. at Purdue University, West Lafayette, IN, USA – July 25-28, pp. 87-94.

Baker O., 1954, Simultaneous flow of oil and gas, Oil & Gas Journal, vol. 53, pp. 185 – 195.

Barnea D., Luninski Y., Taitel Y., 1983, Flow pattern in horizontal and vertical two-phase flow in small diameter pipes, The Canadian Journal of Chemical Engineering, vol. 61, Oct. 1983, pp. 617 – 620.

Blomerius H., Mitra N.K., 2000, Numerical investigation of convective heat transfer and pressure drop in wavy ducts, Numerical Heat Transfer, Part A, vol. 37, pp. 37-54.

Bogaert R., Bölcs A., 1995, Global performance of a prototype brazed plate heat exchanger in a large Reynolds number range, Experimental Heat Transfer, vol. 8, pp. 293 – 311.

Bond M.P. 1981, Plate heat exchangers for effective heat transfer, IChemE The Chemical Engineer, April 1981, pp. 162-167.

Buonopane R.A., Troupe R.A., Morgan J.C., 1963, Heat transfer design method for plate heat exchangers, Chemical Engineering Progress, vol. 59, no. 7, pp. 57-61.

Chato J.C., Wattalet J.P., Dobson M.K., Gaibel J.A., Ponchner M., Shimon R.L., Sweeney K.A., Villaneuva T.C., Rhines N.L., Allen D.G., Hershberger T.T., 1995, Prediction of the refrigerant-side heat transfer and pressure drop for the design of evaporators and condensers, Proc. 46th Annual Int. Appliance Techn. Conf., University of Illinois at Urbana-Champaign, May 15-17, 1995.

Chen J.C., 1966, Correlation for boiling heat transfer to saturated fluids in convective flow, I & EC Process Design and Development, vol. 5, no. 3, pp. 322-329.

Chen J.C., Tuzla K., 1995, Contributions of convective and boiling to convective flow boiling, in Proc. Convective Flow Boiling, ed. J.C. Chen, Banff, Alberta, Canada, April 30 – May 5, 1995, pp. 181-186.

Chisholm D., Laird A.D.K., 1958, Two-phase flow in rough tubes, Transaction of the ASME, vol. 80, Feb. 1958, pp. 276 – 286.

Chisholm D., 1967, A theoretical basis for the Lockhart-Martinelli correlation for two-phase flow, Int. J. Heat Mass Transfer, vol. 10, pp. 1767 – 1778.

Chisholm D., 1983, Two-phase flow in pipelines and heat exchangers, George Goodwin, London, p. 304.

Ciofalo M., Di Piazza I., Stasiek J.A., 2000, Investigation of flow and heat transfer in corrugated-undulated plate heat exchangers, Heat Mass Transfer, vol. 36, pp. 449-462.

Ciofalo M., Di Piazzo I., 2002, A computational approach to conjugate heat transfer between two fluids in plate heat exchangers of arbitrary geometry, International Journal of Heat Exchangers, vol. 3, pp. 1 – 32.

Claesson J., 1996, Numerisk simulering av värmeöverföring och strömning i plattvärmeväxlare med CFDS-FLOW3D 3.3, (Numerical simulation of heat transfer and fluid flow in a plate heat exchanger using CFDS-FLOW3D 3.3), in Swedish, Master of Science Thesis 96/2, Division of Heat Transfer, Lund Institute of Technology.

Claesson J., Palm B., 1999, Boiling mechanism in a small compact brazed plate heat exchanger (CBE) determined by using thermochromic liquid crystals (TLC), 20th Int. Congr. of Refrigeration, IIR/IIF, Sydney, 1999, paper 117.

Claesson J., Palm B., Pelletier O., 2001, "On the influence of geometry on evaporation in compact brazed plate heat exchangers", ICMF-2001 4th International Conference on Multiphase Flow, E.E. Michaelides ed., May 27 to June 1, 2001, New Orleans, Louisiana, USA, paper 156.

Claesson J., Forsén M., 2002, Capacity control of a domestic heat pump Part 1 – Performance of the heat pump and its components, Preprint of IIR/IIF Zero Leakage – Minimum Charge, Efficient Systems for Refrigeration, Air Conditioning and Heat Pumps, August 26-28, Stockholm, Sweden, pp. 367-376.

Claesson J., Palm B., 2002, Discrepancy between calculated and measured superheated area in an evaporator plate heat exchanger, HEFAT 2002, 1st Int. Conf. on Heat Transfer, Fluid Mechanics and Thermodynamics, 8-12 April, Kruger Park, South Africa, vol. 1, pt. 2, pp. 1079-1086.

Claesson J., Afghani M., Palm B., 2003, Influence of large temperature difference in a compact brazed plate evaporator with low overall heat flux, in Proc. Eurotherm no. 72: Thermodynamics, Heat and Mass Transfer of Refrigeration machines and heat pumps, eds. J.M. Corberán, R. Royo, Valencia, Spain, March 31 – April 2, pp. 33-37.

Claesson J., Simanic B., 2003, Pressure drop and visualization of adiabatic R134a two-phase flow inside a chevron type plate heat exchanger, 21st Int. Congr. of Refrigeration, IIR/IIF, Washington D.C., USA, paper 314.

Claesson J., Palm B., 2003, Performance of a compact brazed plate heat exchanger evaporator run in co-current and counter-current, in Proceeding 5th International Conference on Boiling Heat Transfer, Montego Bay, Jamaica, May 5 – May 8, Session VIII: Heat Transfer and Heater Characteristics, third paper.

Claesson J., 2004a, The influence of brine flow on the flow boiling refrigerant heat transfer coefficient in a compact brazed plate heat exchanger, Accepted for publication in International Journal of Heat Exchanger.

Claesson J., 2004b, Correction of Logarithmic Mean Temperature Difference in Compact Brazed Plate Heat Evaporator with Heat Flux Governed Flow Boiling Heat Transfer Coefficient, Accepted for publication in International Journal of Refrigeration, doi:10.1016/j.ijrefrig.2004.09.011.

Claesson J., 2004c, Theoretical study of a compact brazed plate heat exchanger operating as evaporator?, Submitted for publication in the International Journal of Refrigeration.

Claesson J., 2005, Thermal and Hydraulic Characteristics of Brazed Plate Heat Exchangers – Part I: Review of Single- and Two-Phase Adiabatic and Flow Boiling Characteristics, Accepted for presentation and publication at the ASHRAE Winter Meeting, Orlando, Fl., USA, Feb. 5 – 10, 2005.

Claesson J., 2005, Thermal and Hydraulic Characteristics of Brazed Plate Heat Exchangers – Part II: Current research on evaporators at KTH, Accepted for presentation and publication at the ASHRAE Winter Meeting, Orlando, Fl., USA, Feb. 5 – 10, 2005.

Cohen M., Carey V.P., 1989, A comparison of the flow boiling performance characteristics of partially-heated cross-ribbed channels with different rib geometries, International Journal of Heat and Mass Transfer, vol. 32, no. 12, pp. 2459-2474.

Collier J.G., Thome J.R., 1996, Convective Boiling and Condensation, 3rd ed., Oxford Science Publications, Oxford, p. 596

Cooper M.G., 1984, Heat flow rates in saturated nucleate pool boiling – A wide-ranging examination using reduced properties, Advances in Heat Transfer, vol. 16, eds. J.P. Harnett and T.F. Irvine Jr., Academic Press, Orlando, Florida, pp. 157 – 239.

Corberán J.M., de Córdoba P.F., Gonzálvez J., Alias F., 2001, Semiexplicit method for wall temperature linked equations (SEWTLE): A general finite-volume technique for the calculation of complex heat exchangers, Numerical Heat Transfer, Part B, vol. 40, pp. 37-59.

Croce G., D'Agaro P., 2002, Numerical analysis of forced convection in plate and frame heat exchangers, International Journal of Numerical Methods for Heat & Fluid Flow, vol. 12, no. 6, pp. 756 – 771.

Crozier R.D., Booth J.R., Steward J.E., 1964, Heat transfer in plate and frame heat exchangers, Chemical Engineering Progress, vol. 60, no. 8, pp. 43-45.

Damianides C.A., Westwater J.W., 1988, Two-phase flow patterns in a compact heat exchanger and in small tubes, 2nd UK Conference on Heat Transfer, London, IMechE, vol. 2, paper C128/88, pp. 1257 – 1268.

Donowski V.D., Kandlikar S.G., 2000, Correlating evaporation heat transfer coefficient of refrigerant R-134a in a plate heat exchanger, in Proc. Boiling 2000: Phenomena and Emerging Applications, Engineering Foundation, April 30 – May 5, Alaska, paper 154.

Dutto T., Blaise J.C., Benedic T., 1991, Mise en oeuvre et performances des echangeurs a plaques brassées dans une pompe a chalur, (Performance of brazed plate heat exchanger set in heat pump, In French), Proc. 18th Int. Congr. Refrigeration, vol. III, pp. 1284-1288, Montreal, Quebec, Canada, August 10-17.

Edwards M.F., Changal Vaie A.A., Parrot D.L., 1974, Heat Transfer and Pressure drop Characteristics of a Plate Heat Exchanger Using Newtonian and Non-Newtonian Liquids, The Chemical Engineer, May, pp. 286-288 & 293.

Engelhorn H.R., Reinhart A., 1989, Investigations in heat transfer at plate heat exchangers (in German), Kälte, no. 7-8, pp. 338-342.

Engelhorn H.R., Reinhart A.M., 1990, Investigation on heat transfer in a plate heat evaporator, Chem. Eng. Process., vol. 28, pp. 143-146.

Focke W.W., 1983, Turbulent convective transfer in plate heat exchangers, Int. Comm. Heat Mass Transfer, vol. 10, pp. 201-210.

Focke W.W., 1985, Asymmetrically corrugated plate heat exchanger plates, Int. Comm. Heat Transfer, vol. 12, pp. 67-77.

Focke W.W., Zachariades J., Oliver I., 1985, The effect of the corrugation inclination angle on the thermohydraulic performance of plate heat exchangers, International Journal of Heat and Mass Transfer, vol. 28, no. 8, pp. 1469-1479.

Focke W.W., 1986, Selecting optimum plate heat exchanger surface patterns, ASME Journal of Heat Transfer, vol. 108, February, pp. 153-160.

Focke W.W., Knibbe P.G., 1986, Flow visualization in parallel-plate ducts with corrugated walls, J. Fluid Mech., vol. 165, pp. 73-77.

Focke W.W., 1995, Heat transfer analogies for plate heat exchangers, S A J. Chemical Engineering, vol. 7, no. 1, pp. 1-5.

Forsén M., 2002, Personal Communication.

Forsén M., 2003, Personal communication, 2003-08-12.

Forsén M., 2004, Personal communication, 2004-02-23.

Friedel L., 1979, Improved friction pressure drop correlations for horizontal and vertical two phase pipe flow, 3R International, vol. 18, no. 7, pp. 485 – 491.

Gaiser G., Kottke V., 1998, Effects of wavelength and inclination angle on the homogeneity of local heat transfer coefficients in plate heat exchangers, in Proc. 11th Int. Heat Transfer Conf., Kyongju, Korea, vol. 6, pp. 203-208.

Gnielinski V., 1993, Heat transfer in concentric annulus, 1st English Edition, VDI Heat Atlas, VDI Verlag, ISBN 3-18-400915-7, section Gd.

Granryd E., Ekroth I., Lundqvist P., Melinder Å., Palm B., Rohlin P., 2003, Refrigerating Engineering, 4th ed., KTH, Dept. Energy Technology, Div. Applied Thermodynamics and Refrigeration, Stockholm, Sweden.

Gungor K.E., Winterton R.H.S., 1986, A general correlation for flow boiling in tubes and annuli, International Journal of Heat and Mass Transfer, vol. 29, no. 3, pp. 351-358.

Gungor K.E., Winterton R.H.S., 1987, Simplified general correlation for saturated flow boiling and comparisons of correlations with data, Chem Eng Res Des, vol. 65, no. March 1987, pp. 148-156.

Hallcrest, 1991, Handbook of thermochromic liquid crystal technology, Hallcrest Ltd, Stepnell Reach, 541 Blandford Road, Poole, Dorset, BH16 5BW, UK, p. 34

Han D.-H., Lee K.-J., Kim Y.-H., 2003, Experiments on the characteristics of evaporation of R410A in brazed plate heat exchangers with different geometric configurations, Applied Thermal Engineering, vol. 23, no. 10, pp. 1209–1225.

Haseler L.E., Wadekar V.V., Clarke R.H., 1992, Flow distribution effects in a plate and frame heat exchanger, in 1st European Thermal Sciences and 3rd UK National Heat Transfer Conf., September 1992, Birmingham, England, IChemE Symposium Series No. 129, pp. 361 – 367.

Haseler L.E., Butterworth D., 1995, Boiling in compact heat exchangers/Industrial practice and problems, in Convective Flow Boiling, ed. John C. Chen, Taylor & Francis, p. 391, pp. 57-70.

Heggs P.J., Ingham D.B., Sanderson P.D., 1996, Thermal performance of plate heat exchangers with flow maldistribution, looped configuration, in proc. 2nd European Thermal-Science and 14th UIT National Heat Transfer Conference, vol 3, pp. 1279 – 1286.

Heggs P.J., Sanderson P.D., Ingham D.B., 1993, Effectiveness-NTU relationship for plate heat exchangers where one stream undergoes a phase change, Chapter 15 in Heat Exchange Engineering: Advances in Design and Operation, E.A. Foumeny and P.J. Heggs, eds., pp. 213 – 262.

Holt A.J., Azzopardi B.J., 1995, Two-phase pressure drop and void fraction relevant to compact two-phase heat exchangers, in Proc. 4th UK National Conference on Heat Transfer, Manchester UK, IMechE, pp. 437 – 442.

Hsieh Y.Y., Lin T.F., 2002, Saturated flow boiling heat transfer and pressure drop of refrigerant R-410A in a vertical plate heat exchanger, International Journal of Heat and Mass Transfer, vol. 45, pp. 1033-1044.

Hsieh Y.Y., Lin T.F., 2003, Evaporation Heat Transfer and Pressure Drop of Refrigerant R-410A Flow in a Vertical Plate Heat Exchanger, ASME Journal of Heat Transfer, vol. 125, pp. 852-857.

Incropera F.P., DeWitt D.P., 1996, Fundamentals of heat and mass transfer, 4th ed., Wiley & Sons, New York, ISBN 0-471-30460-3, p. 886.

Jassim E., Chato J.C., Newell T.A., Infante Ferreira C.A., 2001, Two-phase pressure drop and flow visualization in chevron and bumpy plate heat exchangers, Proc. Thermophysical Properties and Transfer Processes of New Refrigerants, IIR/IIF Commission B1, Paderborn, Germany, October 3-5, 2001, pp. 234-241.

Jung D.S., Radermacher R., 1991, Prediction of heat transfer coefficients of various refrigerants during evaporation, ASHRAE Transactions, vol. 97, pt. 2, pp. 48 – 53.

Kandlikar S.G., 1990, A general correlation for saturated two-phase flow boiling heat transfer inside horizontal and vertical tubes, ASME Journal of Heat Transfer, vol. 112, pp. 219-228.

Kandlikar S., Steinke M.E., 2003, Predicting Heat Transfer During Flow Boiling in Minichannels and Microchannels, ASHRAE TRANSACTIONS 2003, Vol. 109, Pt. 1, paper CH-03-13-1.

Kandlikar S.G., Shah R.K., 1989a, Asymptotic effectiveness-NTU formulas for multipass plate heat exchangers, ASME Journal of Heat Transfer, vol. 111, pp. 314 – 321.

Kandlikar S.G., Shah R.K., 1989b, Multipass plate heat exchangers - Effectiveness-NTU results and guidelines for selecting pass arrangements, ASME Journal of Heat Transfer, vol. 111, pp. 300 – 313.

Katsaounis A., 1993, “Post-dryout heat transfer during forced convection”, 1st English Edition, VDI Heat Atlas, VDI Verlag, ISBN 3-18-400915-7, section Hbd.

Kew P.A., Cornwell K., 1994, Confined bubble flow and boiling in narrow channels, in Proc. 10th International Heat Transfer Conference, vol. 7, pp. 473-478.

Kline S.J., McClintock F.A., 1953, Describing uncertainties in single-sample experiments, Mechanical Engineering, vol. 75, pp. 3 – 8.

Kreissig G., Müller-Steinhagen H.M., 1992, Frictional pressure drop for gas/liquid two-phase flow in plate heat exchangers, Heat Transfer Engineering, vol. 13, no. 4, pp. 42-52.

Kumar H., 1992, The design of plate heat exchangers for refrigerants, Proc. Inst. R. 1991-92.5-1, Presented before Institute of Refrigeration at The Institute Marine Engineering.

Lazarek G.M., Black S.H., 1982, Evaporative heat transfer, pressure drop and critical heat flux in a small vertical tube with R-113, International Journal of Heat and Mass Transfer, vol. 25, no. 7, pp. 945-960.

Le Pellec C., Marvillet C., Clodic D., 1996, Experimental study of plate heat exchangers in ammonia refrigeration unit, IIF/IIR Commissions B1, B2, E1, E2, Aarhus (Denmark), Session 18, pp. 785-794.

Lee S.H., Cho Y.I., Bai C., Cho D.J., 2000, The effect of aspect ratio on turbulent flow heat transfer and pressure drop in a plate heat exchanger, International Journal of Heat Exchangers, vol. 1, pp. 113 – 124.

Liu Z., Winterton R.H.S., 1991, A general correlation for saturated and subcooled flow boiling in tubes and annuli, based on a nucleate pool boiling equation, International Journal of Heat and Mass Transfer, vol. 34, no. 11, pp. 2759-2766.

Lockhart R.W., Martinelli R.C., 1949, Proposed correlation of data for isothermal two-phase, two-component flow in pipes, Chem. Eng. Progress, vol. 45, no. 1, pp. 39-48.

Lowry B., Kawaji M., 1988, Adiabatic vertical two-phase flow in narrow flow channels, in Proc. Heat Transfer – Houston, 1988, AIChE Symposium Series 84(1988):263, pp. 133 – 139.

Manglik R.M., Ding J., 1997, Laminar flow heat transfer to viscous power-law fluids in double-sine ducts, International Journal of Heat and Mass Transfer, vol. 40, no. 6, pp. 1379 – 1390.

Margat L., Thonon B., Tadrist L., 1997, Heat transfer and two-phase flow characteristics during convective boiling in a corrugated channel, in Compact Heat Exchangers for the Process Industry, Begell House.

Martin H., 1996, A theoretical approach to predict the performance of chevron-type plate heat exchangers, Chemical Engineering and Processing, vol. 35, pp. 301 – 310.

Mehrabian M.A., 1996, Experimental, theoretical and computational modelling of flow in corrugated channels to investigate thermal and hydrodynamic characteristics of plate heat exchangers, Ph.D. thesis, Dept. Mechanical Engineering, University of Bristol, U.K., British Library number DX 209546, p. 151.

Mehrabian M.A., Poulter R., 2000, "Hydrodynamics and thermal characteristics of corrugated channels: computational approach", Applied Mathematical Modelling, Vol. 24, No. 5-6, pp. 343-364.

Melinder Å., 1997, Thermophysical properties of liquid secondary refrigerants, Tables and Diagrams for the Refrigeration Industry, Paris, IIF/IIR

Metwally H.M., Manglik R.M., 2004, Enhanced heat transfer due to curvature-induced lateral vortices in laminar flows in sinusoidal corrugated-plate channels, International Journal of Heat and Mass Transfer, vol. 47, no. 10 - 11, pp. 2283 – 2292, DOI:10.1016/j.ijheatmasstransfer.2003.11.019.

Moran M.J., Shapiro H.N., 1998, Fundamentals of Engineering Thermodynamics, 3rd ed., J. Wiley & Sons, Chichester.

Muley A., 1997, Heat transfer and pressure drop in plate heat exchangers, Ph.D. thesis, Dept. Mechanical, Industrial, and Nuclear Engineering, Div. Graduate Studies and Research, University of Cincinnati, UMI number: 9804592.

Muley A., Manglik R.M., 1999, Experimental study of turbulent flow heat transfer and pressure drop in a plate heat exchanger with chevron plates, ASME Journal of Heat Transfer, vol. 121, pp. 110 – 117.

Muley A., Manglik R.M., Metwally H.M., 1999, Enhanced Heat Transfer Characteristics of Viscous Liquid Flows in a Chevron Plate Heat Exchanger, ASME Journal of Heat Transfer, vol. 121, no. 4, pp. 1011-1017.

Müller-Steinhagen H., Heck K., 1986, A simple friction pressure drop correlation for two-phase flow in pipes, Chemical Engineering Process, vol. 20, pp. 297 – 308.

NIST, 1998, NIST standard reference database 23, REFPROP 6.01, The US National Institute of Standards and Technology, Refrigerant properties computer code.

Nuijens P.G.J.M., Focke W.W., Olivier I., 1991, Flow distribution in multi-compartment equipment with linear supply and discharge manifolds, South Africa Journal of Chemical Engineering, vol. 3, no. 2, pp. 26 – 50.

Osterberger R., Slipcevic B., 1990, Heat transfer during nucleate boiling within plate heat exchanger, (Wärmeübergang beim Blasenseiden in Plattenverdampfern, in German), Ki Klima –Kälte-Heizung, 11/1990, pp. 481 – 483.

Palm B., Granryd E., Reviewing two simple methods of calculating the length of adiabatic capillary tubes, Proc. 20th IIR/IIF Congr., Sydney.

Panchal C.B., Hillis D.L., Thomas A., 1983, "Convective boiling of ammonia and Freon 22 in plate heat exchangers, Proc. ASME/JSME Thermal Engineering Joint Conference, vol. 2, pp. 261-268.

Pelletier O., 1998, Propane as refrigerant in residential heat pumps, Licentiate Thesis, Dept. of Energy Technology, Div. Applied Thermodynamics and Refrigeration, Royal Institute of Technology, KTH, Trita REFR No 98/24 ISSN 1102-0245, p. 132.

Pelletier O., 1999, Personal Communications.

Pelletier O., 2002, Personal communication.

Råde L., Westergren B., 1990, BETA – Mathematics handbook, 2nd ed., Studentlitteratur, Lund, Sweden, ISBN 91-44-25052-5, p. 494.

Rao B.P., Kumar P.K., Das S.K., 2002, Effect of flow distribution to the channels on the thermal performance of a plate heat exchanger, Chemical Engineering and Processing, vol. 41., pp. 49 – 58.

Sadasivam R., Manglik R.M., Jog M.A., 1999, Fully developed forced convection through trapezoidal and hexagonal ducts, International Journal of Heat and Mass Transfer, vol. 42, pp. 4321 – 4331.

Sawyers D.R., Sen M., Chang H.-C., 1998, Heat transfer enhancement in three-dimensional corrugated channel flow, International Journal of Heat and Mass Transfer, vol. 41, pp. 3559 ─ 3573.

SCB, 2003, Energistatistik för småhus 2002, (Energy statistics for one- and two-dwelling buildings in 2002), Report EN 16 SM 0302, ISSN 1404-5869.

Shah M.M., 1976, A new correlation for heat transfer during boiling flow through pipes, ASHRAE Transactions, vol. 82, pt. 2, pp. 66-86.

Shah M.M., 1982, Chart Correlation for Saturated Boiling Heat Transfer: Equations and Further Study, ASHRAE Transactions, Vol. 88, pt. 1, pp. 185-196.

Shah R.K., Focke W.W., 1988, Plate heat exchangers and their design theory, in Heat Transfer Equipment Design, Hemisphere Publishing Corp., Washington D.C., pp. 227 – 254.

Shiomi Y., Nakanishi S., Uehara T., 2004, Characteristics of two-phase flow in a channel formed by chevron type plates, Experimental Thermal and Fluid Science, vol. 28, pp. 231 – 235.

Sieder E.N., Tate G.E., 1936, Heat transfer and pressure drop of liquids in tubes, Industrial and Engineering Chemistry, vol. 28, no. 12, pp. 1429 – 1435.

Spindler K., Müller-Steinhagen H., 2003, The influence of the thermophysical properties of the refrigerants on the performance of heat pump systems, in Proc. Eurotherm no. 72: Thermodynamics, Heat and Mass Transfer of Refrigeration machines and heat pumps, eds. J.M. Corberán, R. Royo, Valencia, Spain, March 31 – April 2, pp. 285 – 290.

Steiner D., Taborek J., 1992, Flow Boiling Heat Transfer in Vertical Tubes Correlated by an Asymptotic Model, Heat Transfer Engineering., vol. 13, no. 2, pp. 43-69.

Simanic B., 2003, Visualization of R134a two phase flow inside a compact brazed plate heat exchanger, M.Sc. Thesis, Royal Institute of Technology, Sweden, Nr 293/2003.

Sterner D., Sundén B., 1997, Performance of some plate-and-frame heat exchangers as evaporator in a refrigerating system, 5th UK National Conf. on Heat Transfer, Imperial College, London, September 17-18, 1997.

Sthapak B.K., Varma H.K., Gupta C.P., 1975, Mass vapour fraction at the onset of dryout in a horizontal tube evaporator, Progress in Refrigeration Science and Technology, 14th International Congress of Refrigeration, Moscow, 1975, published 1978, Vol. 2, paper B1.39, pp. 318-324.

Taborek J., 1998, Charts for mean temperature difference in industrial heat exchanger configurations, Section 1.5 in Heat Exchanger Design Handbook 1998, eds. G.F. Hewitt, Begell House, New York, ISBN 1-56700-098-3.

Talik A.C., Swanson L.W., Fletcher L.S., Anand N.K., 1995a, Heat transfer and pressure drop of a plate heat exchanger, ASME/JSME Thermal Engineering Conference, vol. 4, pp. 321-329.

Talik A.C., Swanson L.W:, Fletcher L.S., Anand N.K., Swanson L.W., 1995b, Heat transfer and pressure drop characteristics of a plate heat exchanger using a

propylene-glycol/water mixture as the working fluid, ASME HTD-Vol. 314, 1995 National Heat Transfer Conference, vol. 12, pp. 83-88.

Taitel Y., Bornea D., Dukler A.E., 1980, Modelling flow pattern transitions for steady upward gas-liquid flow in vertical tubes, AIChE Journal, vol. 26, no. 3, pp. 345 – 354.

Thonon B., Vidil R., Marvillet C., 1995, Recent research and developments in plate heat exchangers, Journal of Enhanced Heat Transfer, vol. 2, no. 1-2, pp. 149-155.

Thonon B., Feldman A., Margat L., Marvillet C., 1997, Transition from nucleate boiling to convective boiling in compact heat exchangers, International Journal of Refrigeration, vol. 20, no. 8, pp. 592-597.

Thonon B., Mercier P., 1996, "Plate heat exchangers : Ten years of research at GREThh – Part 2. Sizing and flow maldistribution" (in French), Rev Gén Therm, Vol. 35, pp. 561-568.

Tran T.N., 1999, Pressure drop and heat transfer study of two-phase flow in small channels, Doctoral Thesis, Texas Tech University, UMI Number 9912778, p. 226.

Tribbe C., 1998, Gas/Liquid flow in cylindrical and corrugated channels, Ph.D. Thesis, Dept. of Chemical & Process Engineering, University of Surrey, UK.

Tribbe C., Müller-Steinhagen H.M., 1997, The hydrodynamics of gas-liquid two-phase flow in a plate heat exchanger, The 1997 Jubilee Research Event, IChemE, University of Nottingham, UK, 8-9 April, pp. 357-360.

Tribbe C., Müller-Steinhagen H.M., 2001a, Gas/liquid flow in plate-and-frame heat exchangers – Part 1: Pressure drop measurements, Heat Transfer Engineering, vol. 22, pp. 5-11.

Tribbe C., Müller-Steinhagen H.M., 2001b, Gas/liquid flow in plate-and-frame heat exchangers – Part 2: Two-phase multiplier and flow pattern analysis, Heat Transfer Engineering, vol. 22, pp. 12-21.

Vlasogiannis P., Karagiannis G., Argyropoulos P., Bontozoglou V., 2002, Air-water two-phase flow and heat transfer in a plate heat exchanger, International Journal of Multiphase Flow, vol 28, pp. 757-772.

Wadekar V.V., 1995, An alternative model for flow boiling heat transfer, in Proc. 1st International Conference on Convective Flow Boiling, ed. J.C. Chen,

Banff, Canada, Taylor & Francis, Washington DC, USA, ISBN 1-56032-507-0, vol. 1, pp. 187 – 192.

Wagner W., Kruse A., Properties of Water and Steam - The Industrial Standard IAPWS-IF97 for the Thermodynamic Properties and Supplementary Equations for Other Properties, Springer-Verlag, Berlin, 1998.

Walton C., 2001, Flow and heat transfer in corrugated plate heat exchanger channels, Ph.D. thesis, Dept. Chemical Engineering, University of Manchester, UMIST, UK, p. 239.

Wambsganss W.M., Jendrzejczyk J.A., France D.M., 1992, Two-phase flow and pressure drop in flow passages of compact heat exchangers, SAE paper no. 920550, presented at Society of Automotive Engineers International Congress and Exposition, Detroit, USA, pp. 482 – 491.

Wambsganss W.M., Jendrzejczyk J.A., France D.M., Obot N.T., 1990a, Two-phase flow patterns and frictional pressure gradients in a small rectangular channel: A comparizon between two horizontal orientations, Argonne National Laboratory, report ANL—90/46.

Wambsganss W.M., Jendrzejczyk J.A., France D.M., Obot N.T., 1990b, Two-phase flow patterns and frictional pressure gradients in a small, horizontal, rectangular channel, Argonne National Laboratory, report ANL—90/19.

Wambsganss W.M., Jendrzejczyk J.A., France D.M., 1991, Two-phase flow patterns and frictional pressure gradients in a small, horizontal, rectangular channel, International Journal of Multiphase Flow, vol. 13, no. 3, pp. 327 – 342.

Wanniarachchi A.S., Ratnam U., Tilton B.E., Dutta-Roy K., 1995, Approximate correlations for chevron-type plate heat exchangers, ASME HTD-Vol. 314, 1995 National Heat Transfer Conference, Vol. 12, pp. 145-151.

Whalley P.B., 1987, Boiling, condensation, and gas-liquid flow, Oxford: Clarendon, ISBN 0-19-856181-4, p. 291.

Wilkinson, 1974, Flow distribution in plate heat exchangers, The Chemical Engineer, May, 1974, pp. 289 – 293.

Wilson E.E., 1915, A basis for rational design of heat transfer apparatus, Trans. ASME, vol. 37, pp. 47-70, discussion pp. 70-82.

Winkelmann D., Thonon B., Auracher H., Bontemps A., 1999, Two-phase flow characteristics of a corrugated channel, IIR/IIF 20th International Congress of Refrigeration, Sydney, vol. II, paper 426.

Yan Y.-Y., Lin T.-F., 1999, Evaporation heat transfer and pressure drop of refrigerant R-134a in a plate heat exchanger, ASME Journal of Heat Transfer, vol. 121, February 1999, pp. 118-127.

TRITA REFR Report No 04/44
ISSN 1102-0245
ISRN KTH/REFR/04/44-SE
ISBN 91-7283-931-7